

REPORT NO. 188/2003

Estimation of Biophysical Parameters in Boreal Forests
from ERS and JERS SAR Interferometry

Ph.D. Dissertation

MAURIZIO SANTORO

Faculty of Chemistry and Geosciences
Institute of Geography
Department of Geoinformatics
FRIEDRICH-SCHILLER-UNIVERSITY JENA
Jena, Germany

Department of Radio and Space Science
CHALMERS UNIVERSITY OF TECHNOLOGY
Göteborg, Sweden, 2003

Estimation of Biophysical Parameters in Boreal Forests
from ERS and JERS SAR Interferometry

Ph.D. Dissertation

MAURIZIO SANTORO

Faculty of Chemistry and Geosciences
Institute of Geography
Department of Geoinformatics
FRIEDRICH-SCHILLER-UNIVERSITY JENA
Jena, Germany

© MAURIZIO SANTORO, 2003.

Research Report No. 188/2003
Department of Radio and Space Science
Chalmers University of Technology
SE – 412 96 Göteborg
Sweden
Telephone +46 – (0) 31 – 772 1000

ISSN 1100-5564

Printed by Chalmers Reproservice
Göteborg, Sweden

**Estimation of Biophysical Parameters in Boreal Forests
from ERS and JERS SAR Interferometry**

Dissertation

Zur Erlangung des akademischen Grades doctor rerum naturalium
(Dr. rer. nat.)

vorgelegt dem Rat der Chemisch-Geowissenschaftlichen Fakultät der
Friedrich-Schiller-Universität Jena

von Dipl.-Ing. Maurizio Santoro

geboren am 15. Juli 1972 in Neapel, Italien

Gutachter:

1.

2.

Tag der öffentlichen Verteidigung:

Estimation of Biophysical Parameters in Boreal Forests from ERS and JERS SAR Interferometry

MAURIZIO SANTORO

Institute of Geography, Department of Geoinformatics
Friedrich-Schiller-University Jena

ABSTRACT

Due to their environmental and economic role, boreal forests need frequent and accurate monitoring. Spaceborne SAR imagery covers entire regions, is acquired on a roughly monthly basis and represents a data source for a broad spectrum of applications related to environmental monitoring. In this thesis SAR images and repeat-pass interferometric SAR images acquired during the ERS and JERS missions have been evaluated for retrieving biophysical parameters in boreal forests.

The availability of extensive data sets of images over several test sites located in Sweden, Finland and Siberia has allowed analysis of temporal dynamics of: 1) ERS backscatter, coherence and interferometric phase, 2) JERS backscatter and, to a lesser extent, coherence. Dielectric properties of the vegetation and the forest floor have strong influence on all signatures. Temporal interval between acquisitions affects the coherence and the interferometric phase. Concerning the one-day tandem ERS coherence, wind speed is the main source of decorrelation in dense forests. The ERS interferometric phase suffers from phase noise due to the temporal instability of the canopy and atmospheric artefacts.

Knowledge of the SAR and InSAR signatures characteristics is fundamental for modelling. In this thesis the Water Cloud Model, which relates forest backscatter to stem volume, and the Interferometric Water Cloud Model, which expresses the forest complex coherence as function of stem volume, have been considered. Since the models need to be trained using stem volume and remote sensing measurements, the validity of the results strongly depends on the training procedure and on the accuracy of ground-truth data and remote sensing quantities. Furthermore, in straightforward models such as those used in this work, the effect of the forest structure on the remote sensing quantities should not be neglected.

Model inversion has been carried out for stem volume retrieval using ERS coherence, ERS backscatter and JERS backscatter, whereas for tree height estimation the ERS interferometric phase has been used. Multi-temporal combination of ERS coherence images can provide stem volume estimates comparable to stand-wise ground-based measurements. The accuracy decreases at plot level and in large areas if the environmental conditions are different. JERS backscatter also shows a reasonable potential for stand-wise stem volume retrieval. Since the information content of the interferometric phase is strongly degraded by phase noise and uncorrected atmospheric artefacts, model-based tree height estimates generally show large errors.

Keywords: SAR, boreal forest, interferometry, ERS, JERS, backscatter, coherence, interferometric phase, stem volume, tree height.

Zusammenfassung

Als die Arbeit zu dieser Dissertation begann, setzte sich gerade die Einsicht durch, dass boreale Wälder nicht nur aus ökonomischer, sondern auch aus ökologischer Sicht von besonderer Bedeutung sind (siehe Kyoto-Protokoll 1997). Die große Ausdehnung des borealen Bioms (20% der Erdoberfläche) und der beschleunigte Wandel, dem die Wälder im letzten Jahrzehnt ausgesetzt waren, machen deutlich, dass neue Methoden der Überwachung, die die bisherigen Methoden in Form von Vorortmessungen und Photographie ergänzen oder teilweise ganz ersetzen, benötigt werden. Die Satelliten-Fernerkundung erwies sich hierfür als besonders gut geeignete Informationsquelle. Insbesondere der Satelliten-Fernerkundung mittels Radar-Sensoren wird ein großes Potential für das Monitoring des borealen Waldes eingeräumt. Synthetic Aperture Radar Sensoren (SAR) sind in der Lage, unabhängig von Wetter und Sonneneinstrahlung, großflächige Gebiete abzutasten. Diese Eigenschaften sind von grundlegender Bedeutung in den Breitengraden, in denen boreale Wälder zu finden sind, da hier häufige Bewölkung und lange Perioden der Dunkelheit die Einsatzmöglichkeiten optischer Fernerkundungssysteme erheblich einschränken. Weiterhin weisen SAR-Daten eine zeitliche und räumliche Auflösung auf, die ausreicht, um die Dynamik von intensiver Forstwirtschaft, Kahlschlägen, Brandschäden, usw. in kleineren Flächen von wenigen Hektar erfassen zu können.

Das Bildmaterial, das während der ERS¹- und JERS²-Missionen gewonnen wurde, wurde in zahlreichen Projekten auf seine Anwendbarkeit hin untersucht, einschließlich Wald-Monitoring und Ermittlung von Waldparametern mittels Radarrückstreuung. Aufgrund der höheren Empfindlichkeit des L-Bands an Bord des JERS-Satelliten für Waldstrukturen, erwies sich dieser als geeigneterer für Waldkartierung als das C-Band des ERS. Jedoch erreichten beide Systeme Genauigkeiten bei der Ermittlung von typischen Waldparametern, z. B. überirdischer Biomasse und Stammvolumen (Volumen der Stämme ohne Ästen, Zweige und Blätter), die meist deutlich hinter der Genauigkeit von Vorortmessungen zurückblieb.

Die kohärente Arbeitsweise von ERS und JERS ermöglichte bei beiden Systemen die interferometrische Verarbeitung von Bildpaaren, was den wohl größten Wert der

¹ *European Remote Sensing*

² *Japanese Earth Resource Satellite*

ERS-Mission und den teilweise unterschätzten Wert der JERS-Mission darstellt. Aus Interferogramme, außergewöhnliche Fortschritte konnten durch die Verwendung der interferometrischen Phase des ERS für die topographische Kartierung erreicht werden (BAMLER & HARTL, 1998; MASSONNET & FEIGL, 1998). Da Wälder von Radarsensoren als zusätzliche topographische Elemente erfasst werden, erschien auch die Bestimmung der Baumhöhe mittels Interferometrie, nach Aussage einiger Autoren, ein vielversprechendes Unterfangen zu sein (HAGBERG *et al.*, 1995; FLOURY *et al.*, 1996). Die interferometrische Kohärenz zeigte hingegen hohen Informationsgehalt hinsichtlich der Bestimmung von Landoberflächenparametern (ASKNE & HAGBERG, 1993; WEGMÜLLER & WERNER, 1995). Es konnte gezeigt werden, dass die Kohärenz besser für die Bestimmung von Waldparametern geeignet ist als die Radarrückstreuintensität (ASKNE *et al.*, 1997), da erste Analysen der Kohärenz hinsichtlich ihrer Aussagekraft über das Stammvolumen hervorragende Ergebnisse ergaben (FRANSSON *et al.*, 2001).

Obwohl die Rückstreueigenschaften borealer Wälder gut verstanden zu sein scheinen, so sind doch noch einige Fragestellungen betreffend des Verhältnisses von Radarrückstreuung und jahreszeitlichen Veränderungen in den verschiedenen Breitengraden und die räumliche Übertragbarkeit der Waldparameterbestimmung ungeklärt. Anders stellt sich die Situation der interferometrischen Datenverarbeitung dar. Die Mechanismen, die Kohärenz und interferometrische Phase beeinflussen, sind bisher noch nicht vollständig verstanden. Wenn dieses wie bei der Radarrückstreuung erreicht ist, kann die Analyse der jahreszeitlichen Dynamik und der übräumlichen Vergleichbarkeit der interferometrischen Messwerte, gefolgt von der Ermittlung des Einflusses auf die Bestimmung von Waldparametern, erfolgen.

Deshalb ist es das Ziel dieser Arbeit, das Wissen darüber zu erweitern, wie ERS- und JERS SAR und InSAR Signaturen von borealen Wäldern beeinflusst sind, und darauf basierend Verfahren und Werkzeuge zu entwickeln, die das Monitoring borealer Wälder ermöglichen.

Satellitendaten verschiedener Testgebiete in Schweden, Finnland und Sibirien stellten die Basis für die Untersuchung der zeitlichen und räumlichen Eigenschaften von ERS- und JERS-Rückstreuung sowie der interferometrischen Signatur borealer Wälder dar. Da die Mechanismen der Radarrückstreuung von der Standdichte abhängen, wurden die Untersuchungen in getrennten Gebieten mit dichter und spärlicher Vegetation durchgeführt. Im ersten Fall bedeckt der Wald fast den ganzen Untergrund, so dass die SAR und InSAR-Meßwerte mit Vegetationseigenschaften korrelieren. Im zweiten Fall sieht das SAR vor allem den Untergrund, so dass dessen Einfluss das Signal bestimmt.

Die Untersuchungen für das C-Band des ERS wurden in zwei Testgebieten durchgeführt: Kättböle (Schweden) und Tuusula (Finnland). Die Ergebnisse beider Testgebiete weisen eine gute Vergleichbarkeit auf. Die Rückstreueigenschaften beider Wälder weisen nur geringe Unterschiede auf, erstrecken sich aber über einen großen Wertebereich. Jahreszeitliche Veränderungen in Form von gefrorenem bzw. ungefrorenem Vegetation beeinflussen die Rückstreuung dichter Wälder,

wohingegen die Dielektrizität des Untergrundes (Bodenfeuchte, Schneebedeckung) die Rückstreueigenschaften der Wälder mit geringerer Staudichte bestimmt.

Aufgrund der für die ERS-Mission üblichen geringen Basislinien wird die Kohärenz der Wälder im wesentlichen von dem Zeitabstand zwischen den beiden Aufnahmezeitpunkten bestimmt. Im Falle des Abstandes von einem Tag während der ERS-Tandemmission ist die interferometrische Signatur empfindlich für verschiedene Wetterbedingungen. Die Kohärenz dichter Wälder ist viel niedriger als die wenig bewachsener Wälder, da der Wind den oberen Teil der Baumkrone bewegt, welcher für die Rückstreuung des Radarsignals verantwortlich ist. Für Bildpaare, die bei Frost aufgenommen wurden, scheint sich die Kohärenz zu erhöhen, was wohl auf die erhöhte Transparenz der Baumkrone aus Sicht des Radarsignals zurückzuführen ist. Der Untergrund weist in der Regel eine hohe Kohärenz auf, es sei denn, die dielektrischen Eigenschaften ändern sich, z. B. durch Niederschlag oder Schneebedeckung.

Für das L-Band des JERS wurden Bilder der Testgebiete Kättböle, Tuusula und Bolshe-Murtinski (Sibirien) analysiert. Die beiden Waldtypen zeigen hier sehr unterschiedliche Niveaus der Radarrückstreuung und nur sehr geringe Streuungen der Werte. Dies ist eine Folge des nun relevanten Eindringens der Radarwelle in die Baumkrone, weshalb das zurückgestreute Signal für Waldparameter empfindlich ist. Dichte Wälder weisen eine stärkere Beeinflussung durch die jahreszeitliche Dynamik auf. Wenn Frost auftritt, sinkt das Rückstreusignal deutlich um 4dB. Dieses Niveau bleibt dann konstant bis zum Einsetzen von Tauwetter im Frühjahr. Der hohe Korrelationsgrad zwischen Temperatur und der Rückstreuintensität von Wäldern bestätigt, dass dieser Parameter als Maß für jahreszeitliche Veränderungen in den Wäldern genutzt werden kann. Die Rückstreueigenschaften des Untergrundes werden wie im Falle des C-Bands, wenn auch nicht so deutlich, von den dielektrischen Eigenschaften des Waldbodens oder der Schneedecke bestimmt.

Die JERS-Kohärenz konnte nur für das Testgebiet in Kättböle untersucht werden. Selbst wenn die Basislinie ausreichende Werte aufwies, so führten doch die instabilen Wetterverhältnisse Skandinaviens und die niedrige Bildwiederholrate des JERS-Satelliten zu generell niedriger Kohärenz. Die Basislinien und der lange zeitliche Abstand zwischen der Aufnahme der Bildpaare beschränken das Potential der JERS-Kohärenz zur Nutzung für Wald-Monitoring.

Die Eigenschaften von Rückstreuintensität und Kohärenz bilden die Grundlage für Modellierungsversuche und die Bestimmung von Waldparametern. In dieser Dissertation werden zwei Modelle verwendet, die auf dem Strahlungstransfer durch eine homogene Schicht, welche eine Vegetationsschicht repräsentiert, basieren. Das Water Cloud Model (WCM) (ATTEMA & ULABY, 1978) und das Interferometric Water Cloud Model (IWCM) (ASKNE *et al.*, 1995; ASKNE, *et al.*, 1997) fassen die Rückstreuintensität und die komplexe Kohärenz als Summe der Beiträge einer Vegetations- und einer Waldbodenlage zusammen. Beide Modelle verknüpfen die Messwerte der Fernerkundung mit dem Stammvolumen. Da fünf Parameter der Modelle von vornherein unbekannt sind, müssen die Modelle mittels Regressionen

durch eine Reihe von Messungen der Rückstreuung oder der Kohärenz sowie der entsprechenden Stammvolumina trainiert werden.

Die Qualität der Modellanpassung hängt von der Qualität der Daten ab. Da die Rückstreuung des ERS-Signals stark streut und nur geringe Empfindlichkeit für Waldeigenschaften aufweist, unterliegen die Ergebnisse der Regression einem größeren Unsicherheitsfaktor. Die Kohärenz korreliert wesentlich besser mit dem Stammvolumen, weshalb sie auch besser zum Training der Modelle geeignet ist. Der Nachteil ist, dass aus einem Satz an Kohärenzmessungen, fünf Parameter gleichzeitig bestimmt werden müssen. In dieser Dissertation wird eine Kopplung der Regressionen des WCM und des IWCM vorgeschlagen. Auf diesem Wege werden nicht nur die Unwägbarkeiten der Rückstreuungsmessungen eingegrenzt, sondern auch die fünf unbekannt Parameter aus zwei Datensätzen, anstatt aus einem Datensatz, bestimmt. Im Falle des JERS wurde nur die Rückstreuintensität benutzt, da die Kohärenz unzureichende Qualität besaß.

Einem Iterationsschema folgend, wurde für alle verfügbaren Datensätze eine korrekte Anpassung erreicht. Um eine genaue Anpassung erreichen zu können, sind die Qualität der benutzten Daten und die Verteilung von Stammvolumina im Bereich, der von Interesse ist, von entscheidender Bedeutung. Allgemein kann gesagt werden, dass, solange keine Veränderung der Wetterbedingungen auftritt, die Schätzung der Modellparameter die hohe Kohärenz des Untergrundes, die niedrige Kohärenz der Vegetation, die steigende Strahlungsdurchlässigkeit des Waldes und die kaum zu unterscheidende Rückstreuung von Wald und Untergrund korrekt wiedergibt.

Bei der Anwendung des WCM-Modells auf die JERS-Rückstreuung blieben die Schätzungen der fünf Unbekannten zwar generell im realistischen Wertebereich, jedoch ergaben sich einige Unstimmigkeiten beim Vergleich der Strahlungsdurchlässigkeit der nord-europäischen und sibirischen Wälder, was auf die unterschiedliche Verteilung der Stammvolumenangaben und verschiedenen Forstverwaltungen zurückzuführen ist. Obwohl die Modellierung mittels ERS-Daten generell eine bessere räumliche Übertragbarkeit aufwies, so muss doch erwähnt werden, dass für Sibirien keine ERS-Daten zur Verfügung standen, weshalb diese Analysen auf Schweden und Finnland beschränkt blieben.

Mit den einmal trainierten Modellen kann durch Inversion eine Bestimmung des Stammvolumens an unabhängigen Standorten durchgeführt werden. Die Stammvolumenbestimmung aus Kohärenzdaten wurde auf die drei Grundeinheiten der Forstinventur bezogen: Bestand, Plot und regionale Ebene. Aufgrund des radartypischen *Speckle* wird die Rückstreuintensität nur auf dem Level des Bestands durchgeführt.

Im Bereich des Waldbestands ergibt das IWCM in Kombination mit der ERS-Kohärenz die besten Ergebnisse; insbesondere gilt dies für Bildpaare, die bei stabilen Winterbedingungen aufgenommen wurden. Die ERS-Rückstreuintensität ist generell unbrauchbar. Die Bestimmung des Stammvolumens mittels JERS-Rückstreuintensität führt hingegen bei trockenen und ungefrorenen Bedingungen zu

zuverlässigen und zeitlich konstanten Ergebnissen. Die multi-temporale Kombination der Ergebnisse führt zur Erhöhung der Bestimmungsgenauigkeit.

Abgesehen von der ERS-Rückstreuintensität, ist die Bestimmung des Stammvolumens stark abhängig vom jeweiligen Testgebiet. Die Übertragbarkeit der Ergebnisse auf andere Testgebiete ist gering. Zwei Gründe könnten hierfür angeführt werden:

- 1) Ungenauigkeit der Fernerkundungs- und Bodendaten, die für das Training der Modelle benutzt wurden
- 2) Arbeitsweise des Forstmanagements.

In Kättböle konnten, dank der qualitativ hochwertigen Kohärenz- und Bodendaten, mittels Inversion des IWCM und der multi-temporalen Kombination verschiedener Aufnahmen im Stammvolumenbereich zwischen 0 und 350 m³/ha Ergebnisse erreicht werden, die mit denen von Vorortmessungen vergleichbar sind (relativer RMSE von 7%). Die Inversion des WCM unter Verwendung der JERS-Rückstreuintensität ergab einen etwas schlechteren aber immer noch vergleichsweise geringen RMSE von 22%. Da diese Ergebnisse noch nicht in anderen Testgebieten erreicht werden konnten, wo vermutlich erhebliche Fehler entweder die Fernerkundungs- oder Bodendaten beeinflussen, ist es möglich für die Bestimmung des Stammvolumens im Beständen zu behaupten:

1. Die ERS-Tandem-Kohärenz ermöglicht die beste Ergebnisse.
2. Die JERS-Rückstreuintensität ermöglicht angemessene Schätzungen.
3. Die modell-basierte Herangehensweise und die multi-temporale Filterung stellen zuverlässige Verfahren dar.
4. Die Definition der Waldattribute und ihre Ermittlung vor Ort ist grundlegend für das Training der Modelle.

Die Bestimmungsgenauigkeit nimmt aufgrund der kleineren Fläche auf dem Plot-Level signifikant ab. Neben der Größe der betrachteten Waldfläche spielt auch die Variabilität der Umweltbedingungen eine wichtige Rolle. Für das in dieser Dissertation vorgestellte Verfahren müssen gleiche Umweltbedingungen im gesamten Testgebiet herrschen; diese Bedingung stellt gerade in Regionen mit häufigen Wetterwechseln einen beschränkenden Faktor dar. Dies gilt auch für die Stammvolumenbestimmung unter verschiedenen Umweltbedingungen auf regionaler Ebene. Ab einer Fläche von 1000 km² scheint es jedoch eine gute Übereinstimmung der Vorortmessungen und der geschätzten Werte zu geben.

Die zweite Größe, die im Rahmen dieser Arbeit hinsichtlich ihrer Anwendbarkeit für Forstanwendungen untersucht wird, ist die interferometrische Phase (in dieser Dissertation wird nur die Phaseninformation des ERS betrachtet). Diese Größe

korreliert direkt mit der Höhenlage, in der die Rückstreuung des Radarsignals geschieht. Deshalb kann aus der Phase die Baumhöhe bestimmt werden; vorausgesetzt, die Eindringtiefe der Welle in die Baumkrone ist bekannt. Da die interferometrische Phase starken Rauscheinflüssen unterliegt, verursacht durch die zeitliche Instabilität der Vegetation und atmosphärische Heterogenitäten, kann die Bestimmung der Baumhöhe erhebliche Fehler aufweisen. Obwohl der atmosphärische Einfluss theoretisch entfernbar ist, bleibt das Phasenrauschen eine Eigenschaft des Zielobjekts und verringert somit erheblich den Informationsgehalt der Messung. Die Technik des „*Permanent Scatterers*“ ist vielversprechend für Forstanwendungen in verstädterten Regionen; in borealen Wäldern werden jedoch für die Entfernung der atmosphärischen Artefakte Referenzinformationen von offenen Flächen benötigt, die ein „*phase-screen*“ ermöglichen. Da diese Anforderung selten gegeben ist, scheint es sinnvoller zu sein, Bildpaare zu wählen, zu denen auch meteorologische Messwerte zur Verfügung stehen. Bildpaare, die bei Nacht, im Winter oder stabilen Wetterverhältnissen aufgenommen wurden, sind am wenigsten durch Artefakte beeinflusst.

Die Inversion der interferometrischen Phase für die Testgebiete in Kättböle und Tuusula zeigt einen erheblichen Einfluss atmosphärischer Artefakte und des Phasenrauschens auf die Bestimmung der interferometrischen Baumhöhe. In den wenigen Bildpaaren, die nicht durch atmosphärische Artefakte beeinflusst sind, ist die interferometrische Baumhöhe sehr niedrig und korreliert aufgrund des Phasenrauschens wenig mit Parametern wie dem Stammvolumen. Da diese Bilder bei winterlichen Frostbedingungen aufgenommen wurden, kann die niedrige Baumhöhe mit dem tieferen Eindringen des Radarsignals in die Vegetation begründet werden. Mittels IWCM kann die interferometrische Baumhöhe um die Eindringtiefe und die volumetrische Dekorrelation des Signals korrigiert werden. Insgesamt unterliegt die Baumhöhenbestimmung großen Fehlereinflüssen. Trotz guter Ergebnisse bei kleinen Wäldern in Paris, scheint die Anwendbarkeit der interferometrischen Phase für die Baumhöhenbestimmung in borealen Wäldern begrenzt zu sein.

Zusammenfassend lässt sich sagen, dass es möglich ist mit SAR-Systemen im All zuverlässige und genaue Bestimmungen des Stammvolumens durchzuführen. Die C-Band-Kohärenz aus Tandemszenen aber auch die Rückstreuintensität des L-Bands ermöglichen im Größenbereich der Bestände Stammvolumenbestimmungen im Genauigkeitsbereich der Vorortmessungen. Hinsichtlich der Baumhöhenbestimmung konnte das Potential der interferometrischen Phase des C-Bands gezeigt werden, wobei das Phasenrauschen die erreichbaren Ergebnisse stark einschränkt. Die räumliche Übertragbarkeit der Fernerkundungsmessungen und Methoden zur Bestimmung von Waldparametern konnte bewiesen werden. Es bedarf allerdings einer klaren Definition der Wälderparameter, um Anwendungen in der borealen Zone ermöglichen zu können.

Referenzen

ASKNE, J., and HAGBERG, J. O., "Potential of interferometric SAR for classification of land surfaces," *Proceedings of IGARSS'93*, Tokyo, 18-21 August, pp. 985-987, 1993.

ASKNE, J., DAMMERT, P., FRANSSON, J., ISRAELSSON, H., and ULANDER, L. M. H., "Retrieval of forest parameters using intensity and repeat-pass interferometric SAR information," *Proceedings of Retrieval of Bio- and Geophysical Parameters from SAR Data for Land Applications*, Toulouse, 10-13 October, pp. 119-129, 1995.

ASKNE, J., DAMMERT, P. B. G., ULANDER, L. M. H., and SMITH, G., "C-band repeat-pass interferometric SAR observations of the forest," *IEEE Transactions on Geoscience and Remote Sensing*, vol. 35, 1, pp. 25-35, 1997.

ATTEMA, E. P. W., and ULABY, F. T., "Vegetation modeled as a water cloud," *Radio Science*, vol. 13, 2, pp. 357-364, 1978.

BAMLER, R., and HARTL, P., "Synthetic aperture radar interferometry," *Inverse Problems*, vol. 14, 4, pp. R1-R54, 1998.

FLOURY, N., LE TOAN, T., SOUYRIS, J.-C., SINGH, K., STUSSI, N., HSU, C. C., and KONG, J. A., "Interferometry for forest studies," *Proceedings of 'Fringe 96' Workshop on ERS SAR Interferometry*, Zürich, 30 September- 2 October, pp. 57-70, 1996.

FRANSSON, J. E. S., SMITH, G., ASKNE, J., and OLSSON, H., "Stem volume estimation in boreal forests using ERS-1/2 coherence and SPOT XS optical data," *International Journal of Remote Sensing*, vol. 22, 14, pp. 2777-2791, 2001.

HAGBERG, J. O., ULANDER, L. M. H., and ASKNE, J., "Repeat-pass SAR interferometry over forested terrain," *IEEE Transactions on Geoscience and Remote Sensing*, vol. 33, 2, pp. 331-340, 1995.

MASSONNET, D., and FEIGL, K. L., "Radar interferometry and its application to changes in the Earth's surface," *Reviews of Geophysics*, vol. 36, 4, pp. 441-500, 1998.

WEGMÜLLER, U., and WERNER, C. L., "SAR interferometric signatures of forest," *IEEE Transactions on Geoscience and Remote Sensing*, vol. 33, 5, pp. 1153-1161, 1995.

Table of contents

ABSTRACT.....	i
ZUSAMMENFASSUNG.....	iii
TABLE OF CONTENTS.....	xi
ACRONYMS AND SYMBOLS.....	xv
CHAPTER 1 – INTRODUCTION.....	1
1.1 ERS and JERS mission.....	2
1.2 Radar remote sensing of boreal forests.....	3
1.3 SAR interferometry in boreal forests.....	4
1.4 Scope of the thesis.....	5
1.5 Outline of the thesis.....	6
CHAPTER 2 – INSAR THEORY.....	9
2.1 SAR system overview.....	9
2.2 Radar scattering.....	10
2.3 SAR interferometry.....	12
2.4 InSAR processing.....	13
2.4.1 Pre-processing.....	14
2.4.2 InSAR estimation.....	14
2.4.2.1 Coherence estimation.....	15

2.4.2.2	Phase estimation.....	16
2.4.3	Post-processing.....	17
2.5	Coherence and interferometric phase.....	17
2.5.1	Coherence.....	18
2.5.2	Interferometric phase.....	20
CHAPTER 3 – BOREAL FORESTS.....		23
3.1	The boreal zone.....	23
3.2	Principles of forest inventory.....	24
3.2.1	Sweden and Finland.....	24
3.2.2	Swedish National Forest Inventory.....	26
3.2.3	Russia.....	27
3.3	Test sites.....	28
3.3.1	Kättböle.....	29
3.3.2	Swedish NFI area.....	29
3.3.3	Tuusula.....	29
3.3.4	Bolshe-Murtinsky.....	30
CHAPTER 4 – SAR AND INSAR IN BOREAL FORESTS.....		41
4.1	Forest scattering mechanisms.....	42
4.2	ERS backscatter.....	43
4.3	JERS backscatter.....	46
4.4	Forest decorrelation mechanism.....	48
4.5	ERS coherence.....	48
4.6	JERS coherence.....	50
4.7	Tree species identification.....	51
4.8	Conclusions.....	52
CHAPTER 5 – SAR AND INSAR FOREST MODELLING: THEORY.....		55
5.1	Forest backscatter modelling.....	55
5.2	Water Cloud Model.....	56
5.3	Interferometric Water Cloud Model.....	60
5.4	Properties of the IWCM.....	63

5.4.1	Graphic representation of the IWCM.....	63
5.4.2	Model-based tree height.....	66
CHAPTER 6 – SAR AND INSAR FOREST MODELLING: RESULTS.....		69
6.1	Model training procedures.....	69
6.2	Model training with ERS data.....	71
6.2.1	Training procedure.....	72
6.2.2	Model fitting.....	73
6.2.3	Model parameters estimates.....	73
6.2.4	Estimation of area-fill factor.....	80
6.2.5	Model sensitivity to the two-way tree attenuation.....	81
6.3	Model training with JERS data.....	85
6.3.1	Model fitting.....	87
6.3.2	Model parameters estimates.....	87
6.3.3	Estimation of penetration depth.....	90
6.4	Conclusions.....	90
CHAPTER 7 – STEM VOLUME RETRIEVAL.....		93
7.1	Retrieval procedure.....	93
7.2	Multi-temporal filtering.....	96
7.3	Stand-wise retrieval.....	97
7.3.1	ERS backscatter.....	97
7.3.2	ERS coherence.....	99
7.3.3	JERS backscatter.....	101
7.4	Plot-wise retrieval.....	104
7.5	Retrieval at regional level.....	110
7.6	Conclusions.....	113
CHAPTER 8 – TREE HEIGHT ESTIMATION.....		117
8.1	InSAR phase in forests.....	118
8.2	Interferometric tree height.....	119
8.3	Atmospheric artefacts.....	122
8.4	Filtering algorithms.....	123

8.4.1	Permanent Scatterers technique.....	124
8.4.2	Grid of open areas.....	128
8.4.3	Estimation of atmospheric path delay.....	131
8.4.4	Other methods.....	132
8.5	Interferometric tree height estimation.....	132
8.6	Model-based tree height.....	136
8.7	Conclusions.....	139
CHAPTER 9 – CONCLUSIONS.....		143
9.1	Summary of the thesis.....	143
9.2	Future outlook.....	145
CHAPTER 10 – ACKNOWLEDGEMENTS.....		147
CHAPTER 11 – REFERENCES.....		151
APPENDIX A.....		165
LIST OF PUBLICATIONS.....		167
SELBSTÄNDIGKEITSERKLÄRUNG		
TABELLARISCHER LEBENSLAUF		

Acronyms and Symbols

AIRSAR	Airplane Synthetic Aperture Radar
ALOS	Advanced Land Observing Satellite
APS	Atmospheric Phase Screen
AVHRR	Advanced Very High Resolution Radiometer
CNES	Centre National d'Études Spatiales
DEM	Digital Elevation Model
DInSAR	Differential Interferometric Synthetic Aperture Radar
DWD	Deutscher WetterDienst
EMISAR	ElectroMagnetic Institute Synthetic Aperture Radar
ENL	Equivalent Number of Looks
ENVISAT	ENVIronmental SATellite
ERS	European Remote Sensing
ESA	European Space Agency
EU	European Union
EUFORA	EUropean Forest Observations by Radar
FFT	Fast Forward Transform
GEC	Global Ellipsoid Corrected
GIS	Geographic Information System
GPS	Global Positioning System
GTC	Global Terrain Corrected
GTOPO30	Global TOPOgraphy (30 arc seconds grid space DEM)
HUTSCAT	Helsinki University of Technology SCATterometer
InSAR	Interferometric Synthetic Aperture Radar
IWCM	Interferometric Water Cloud Model
HH	Horizontal-Horizontal (polarisation)
HV	Horizontal-Vertical (polarisation)
kNN	k Nearest Neighbour
JERS-1	Japanese Earth Resource Satellite
MIMICS	MIchigan MIcrowave Canopy Scattering (model)
ML	Maximum Likelihood
NASDA	NATIONAL Space Development Agency (Japan)
NFI	National Forest Inventory
NOAA	National Oceanic and Atmospheric Administration

PALSAR	Phased Array type L-band Synthetic Aperture Radar
PCT	Principal Component Transformation
POLIMI	POLItecnico di Milano
PS	Permanent Scatterers
Radar	Radio Detection and Ranging
RCS	Radar Cross Section
SAR	Synthetic Aperture Radar
Seasat SAR	Seasat Synthetic Aperture Radar
SFA	State Forest Account
SIBERIA	SAR Imaging for Boreal Ecology and Radar Interferometry Applications
SIR	Shuttle Imaging Radar
SLC	Single Look Complex
SLU	Sveriges LantbruksUniversitet (Swedish University of Agricultural Sciences)
SMHI	Svenska Meteorologiska och Hydrologiska Institut (Swedish Meteorological and Hydrological Institute)
SRTM	Shuttle Radar Topography Mission
TM	Thematic Mapper
VHF	Very High Frequency
VV	Vertical-Vertical (polarisation)
WCM	Water Cloud Model

a	Amplitude of complex SAR image
arg	Argument of a complex quantity
f	Radar frequency
g	Complex SAR image
h	Tree height
$e^{-j\phi_i}, e^{-j\psi_i}$	Phase correction terms in coherence estimators
\hat{h}	Multi-temporal height estimate
\hat{h}_i	Height estimate from a single interferometric pair
h_{int}	Interferometric tree height
P	Percentage of correctly classified samples
r	Pearson's linear coefficient of correlation
s	Interferogram
W	Weighting coefficient
A_e	Effective area
A	Amplitude of the radar signal
B_n	Perpendicular component of the interferometric baseline
B_p	Parallel component of the interferometric baseline
$E\{\}$	Expected value
G	Antenna gain
L	Number of looks
L_c	Size of the resolution cell
L_{ind}	Number of independent looks

N	Number of samples
P_r	Received power
P_t	Transmitted power
R	Slant-range distance
R^2	Coefficient of determination
$RMSE$	Root Mean Square Error
SD	Snow depth
SE	Standard error
T_{for}	Two-way forest transmissivity
T_{tree}	Two-way tree transmissivity
V	Stem volume
WS	Wind speed
γ	Complex coherence
$ \gamma $	Coherence
$ \hat{\gamma} , \hat{\gamma}_{ML} $	Maximum Likelihood estimate of the coherence
$ \hat{\gamma}_{lin} $	Linear estimate of the coherence
α	Two-way tree attenuation
β	Two-way forest attenuation
γ_{for}	Forest complex coherence
$ \gamma_{for} $	Forest coherence
γ_{gr}	Temporal coherence of the ground
γ_{veg}	Temporal coherence of the vegetation
δ	Penetration depth
η	Area-fill factor
θ	Incidence angle
λ	Wavelength
σ	Radar cross section
σ_A^o	Sigma nought, backscatter coefficient
σ_{for}^o	Forest backscatter coefficient
σ_{gr}^o	Ground backscatter coefficient
σ_{veg}^o	Vegetation backscatter coefficient
σ_ϕ	Uncertainty of the InSAR phase
ϕ	SAR phase
$\hat{\phi}$	Estimate of SAR phase
ϕ_{for}	Forest InSAR phase
ϕ_{veg}	Vegetation InSAR phase
ω	InSAR system geometry coefficient
Γ_{gr}	Ground decorrelation term
Γ_{veg}	Vegetation decorrelation term
Δx_{atm}	Atmospheric path delay difference
Δz	Height difference
ΔR	Slant range difference
$\Delta \eta$	Terrain displacement

$\Delta\theta$	Incidence angle difference
$\Delta\rho$	Atmospheric path delay difference
$\Delta\varphi$	Difference of phase contributions due to scattering in a pixel
$\Delta\Phi$	InSAR phase difference between two points
$\Delta\Phi_{noise}$	Difference of phase noise between two points

Unit

cm	Centimetre
dB	Decibel
ha	Hectare
km	Kilometre
m	Metre
rad	Radians
tons	Ton
GHz	Gigahertz
MHz	Megahertz
°C	Degree Celsius

Wavelength

Frequency

X-band	3 cm	9.6 GHz
C-band	5.7 cm	5.3 GHz
L-band	23.5 cm	1.25 GHz
P-band	70 cm	440 MHz
VHF	3-15 m	20-90 MHz

La tesi di dottorato é come la pasta per le pizze: cresce sempre.

*Maurizio Santoro,
una notte di marzo nel 2003, davanti al computer*

Chapter 1

Introduction

Accurate assessment and planned exploitation of the Earth's natural resources represent key-issues in the current discussion concerning the status of the planet. Several areas are under rapid and partly uncontrolled transformation, one of the most endangered being the boreal biome and its forests. Boreal forests cover one fifth of the Earth surface. They represent a unique environment stretching all over the northern hemisphere, along the Arctic Circle. Despite their remote location and the fact that access is limited for long periods because of the prohibitive weather conditions, boreal forests have been acknowledged as being severely affected by human activities.

Boreal forests have both a fundamental economic and environmental role. On one hand timber products represent one of the main sources of income for several countries in the boreal zone (Sweden, Finland, Russia and Canada). On the other hand, boreal forests represent a significant carbon pool. Taking into account that Siberian forests contain roughly half of the world's growing stock volume of coniferous species, it is clear that boreal forests contribute to the carbon budget for the whole planet. The massive trade of wood, the intensive forest management, the considerable amount of illegal logging and damages due to fires, insects, pollution and storms put a severe requirement on quality and quantity of information needed to monitor the status of boreal forests.

Traditional forest survey methods can be considered reasonable when dealing with local investigations, which aim at an accurate estimation of forest properties, or with regional studies, finalized to provide a long lasting "picture" of the forest status. Taking into account the remoteness of most forests in the boreal belt and the continuous changes they are undergoing, traditional approaches are not satisfactory for the present requirements of large-scale forest mapping and periodic update of inventoried data. Ground-based surveys are too expensive, time consuming and restricted to too few and too small areas. Much effort has been recently put in

research and development of alternative sources of information, which should a) provide a global view of the whole boreal area, b) have high temporal resolution, c) provide reliable, consistent and accurate estimates of forest parameters.

Remote sensing, and in particular spaceborne remote sensing, certainly satisfies the first two points. The sensors carried onboard by the currently orbiting satellites provide full coverage of the globe, imaging areas of the order of several thousands of square kilometres. Typically the revisit period over an area is between a few days up to one or two months. However, at northern latitudes the amount of imagery obtained by optical sensors is severely limited for long periods of the year because of cloud cover, fog, mist, or darkness. To overcome these problems sensors active at wavelengths longer than the atmospheric elements size, such as radar, are needed. Radar is not sensitive to the fine elements that form clouds and fog, and does not depend on solar illumination; therefore, it can always provide an image, thus being suitable for observations in the boreal zone.

1.1 ERS and JERS mission

The main problem that limits the use of real aperture radar on flying platforms is the low spatial resolution in the along-track direction (see Chapter 2). Since this resolution is directly proportional to the distance between the sensor and the target, imagery acquired by spaceborne radar is characterised by an along-track resolution of the order of a few kilometres. Using the thousands of echoes scattered back by an object, synthetic aperture radar (SAR) improves the resolution, which is typically set below 10 m. It is not the intention of this thesis to provide a detailed description of all airborne and spaceborne SAR systems that have flown or are currently operating. This thesis focuses on applications based on imagery acquired by the SAR systems onboard the ERS and the JERS satellites; therefore, only for these two missions a description is reported. Table 1.1 summarises the principal aspects of both missions and illustrates some technical details of the SAR onboard the satellites.

The European Remote Sensing, ERS, mission consists of two satellites (ERS-1 and ERS-2) launched by the European Space Agency (ESA) in 1991 and 1995 respectively. Since ERS-2 was planned to give continuity to the data provided by ERS-1, the same orbit and the same design of the SAR system of ERS-1 were used for ERS-2. The ERS-1 mission ended in March 2000 whilst ERS-2 is still operating. Both satellites fly along a sun-synchronous orbit at 785 km altitude and complete a full coverage of the Earth in 35 days. For ERS-1 other repeat-pass cycles were used at the beginning of the mission for specific investigations (3 and 167 days). Between 1995 and 2000, the two satellites operated in the so-called “tandem” mode, during which the temporal interval between two acquisitions over an area was as short as one day. The satellites carry a side-looking antenna, with an incidence angle of 23° at mid-swath, active at C-band (5.7 cm, 5.3 GHz), sending and receiving vertically polarised waves (VV polarisation) and having a 100 km wide swath.

The Japanese Earth Resource Satellite JERS-1 was launched in 1992 by the National Space Development Agency (NASDA). The JERS-1 mission lasted more than six

years, until October 1998. The satellite flew at a height of 568 km with a repeat-pass cycle of 44 days. JERS-1 carried onboard an L-band (23.5 cm, 1.25 GHz) SAR system, which sent and received horizontally polarised waves (HH polarisation). The radar worked at a nominal incidence angle of 35° at mid-swath, illuminating a swath of approximately 75 km. Commonly, the JERS-1 mission is referred in the literature simply as JERS. Following this “tradition”, the shorter acronym will be used in the thesis.

1.2 Radar remote sensing of boreal forests

The first investigations of SAR imagery in forested areas aimed at understanding which factors govern the signal scattered back towards the radar (HENDERSON & LEWIS, 1998). Using experimental data and simulations based on behavioural models, the electromagnetic field received by the radar from a given forest was found to be dependent on frequency, polarisation and incidence angle. In particular, for increasing wavelength, the penetration of the electromagnetic wave into the forest canopy increases. At high frequencies (X- and C-band) the main interaction of the wave occurs within the canopy and the power scattered back to the radar (the “backscatter”) is primarily dependent on the properties of small branches, needles and twigs in the tree crown. At low frequencies (L- and P-band, and VHF) the microwaves are returned from large branches and stems, thus carrying information about parameters of major relevance in forest inventory (i.e. the trunk diameter, the volume of the tree trunks, the aboveground biomass, etc.).

In boreal forests, as well as in other types of forests, the correlation of X- and C-band backscatter with forest parameters has been shown to be small because of the shorter penetration of the waves through the forest canopy. The radar signal already saturates in sparse forests, thus explaining the poor results obtained when inverting the backscatter to estimate forest parameters. In multi-frequency investigations, substantially better results have been obtained at L- and P-band. The sensitivity of the L-band backscatter to forest attributes was higher than at C-band but still lower than at P-band, which made several authors conclude that P-band is most suitable for the estimation of forest parameters (DOBSON *et al.*, 1992; LE TOAN *et al.*, 1992; BEAUDOIN *et al.*, 1994; ISRAELSSON *et al.*, 1994; RANSON & SUN, 1994; RAUSTE *et al.*, 1994; RIGNOT *et al.*, 1994; DOBSON *et al.*, 1995; IMHOFF, 1995; RANSON *et al.*, 1997). An even stronger correlation to forest parameters has been found at VHF and virtually no saturation of the signal has been measured. For retrieval of biomass in dense forests the VHF band seems to be optimal. Nevertheless, in sparse forests the backscatter is close to the noise level, thus decreasing the total retrieval accuracy (FRANSSON *et al.*, 2000; SMITH & ULANDER, 2000).

Because of interferences with other microwave sources at P-band and absorption of VHF signals in the ionosphere, the lowest frequency used for spaceborne SAR systems has been L-band. Referring in particular to boreal forests, C-band ERS SAR backscatter was shown to provide interesting information for forest/non-forest mapping and regeneration analysis (KASISCHKE *et al.*, 1994), but it seemed almost useless for the estimation of biophysical parameters because of saturation of the

signal already at low biomass levels (PULLIAINEN *et al.*, 1996). L-band JERS backscatter has been considered more promising. Results indicated a clear relationship between backscatter and forest attributes, but yet inversion of remote sensing data and retrieval of the forest attributes were characterised by large errors in dense forests (HARRELL *et al.*, 1995; FRANSSON & ISRAELSSON, 1999; KURVONEN *et al.*, 1999; PULLIAINEN *et al.*, 1999; HYYPPÄ *et al.*, 2000).

1.3 SAR interferometry in boreal forests

Graham (GRAHAM, 1974) first showed that two SAR images acquired from slightly different positions can be combined to determine an image (the “interferogram”), which is directly related to the topography of the imaged area. This technique, called SAR interferometry (InSAR), has been initially investigated in airborne campaigns (ZEBKER & GOLDSTEIN, 1986; ZEBKER *et al.*, 1992), during the SIR-B (GABRIEL & GOLDSTEIN, 1988) and the Seasat (ZEBKER & VILLASENOR, 1992) missions, reaching its full maturity during the ERS mission.

ERS SAR interferometry has allowed the determination of the Earth topography with high accuracy and resolution (BAMLER & HARTL, 1998; MASSONNET & FEIGL, 1998). The strong sensitivity of the interferometric phase to the ground topography has been exploited for the generation of Digital Elevation Models (DEMs) (PRATI *et al.*, 1992; ZEBKER *et al.*, 1994b; RUFINO *et al.*, 1998; SANSOSTI *et al.*, 1999) and the detection of surface movements due to earthquakes (MASSONNET *et al.*, 1993; ZEBKER *et al.*, 1994a), elastic properties of land fast ice and ice sheet motion (GOLDSTEIN *et al.*, 1993; DAMMERT *et al.*, 1998), and subsidence (FERRETTI *et al.*, 2000). The little penetration of C-band waves through forest canopies has suggested the use of ERS interferometry for the determination of the additional “topography” introduced by forests in SAR images. Several studies have highlighted the possibility to obtain an insight on the scattering mechanisms within a forest at C-band and to determine an estimate of the tree height, which was in several investigations in good agreement with the ground-truth data in boreal (DAMMERT *et al.*, 1995; HAGBERG *et al.*, 1995; DAMMERT & ASKNE, 1998) as well as in temperate and tropical forest (FLOURY *et al.*, 1996b).

Since the two ERS images combined with the interferometric technique are acquired at different times, the interferogram is influenced by the temporal stability of the objects in the scene. This particular feature has suggested the use of ERS SAR interferometry for land-cover classification and forestry applications (ASKNE & HAGBERG, 1993; WEGMÜLLER & WERNER, 1995). The short repeat-pass between the acquisitions was found to be of extreme importance for the information content of the interferogram in forested areas. In boreal forests pairs formed by images acquired with a temporal baseline longer than one week showed increasing noise (SMITH *et al.*, 1996). Pairs with a temporal interval between acquisitions of at least the 35-days repeat-pass cycle appeared as totally decorrelated. Nevertheless cases of long-term pairs were shown to be useful for forestry applications even if the two acquisitions had been taken with more than one month of difference in temperate (FLOURY *et al.*, 1996a) and in tropical forests (RIBBES *et al.*, 1997).

Compared to the ERS backscatter, the amplitude of the interferogram (the “coherence”) has been showed to be more sensitive to forest properties (ASKNE *et al.*, 1995; BEAUDOIN *et al.*, 1996; FLOURY, *et al.*, 1996b; SMITH, *et al.*, 1996; ASKNE *et al.*, 1997a; ASKNE *et al.*, 1997b; RIBBES, *et al.*, 1997; CASTEL *et al.*, 2000; HYYPPÄ, *et al.*, 2000). In boreal forests coherence has been investigated for several monitoring applications such as forest mapping (ENGDAHL & HYYPPÄ, 1997; STROZZI *et al.*, 2000), identification of clear-cut areas (SMITH & ASKNE, 2001) and retrieval of biophysical quantities (SMITH *et al.*, 1998; HYYPPÄ, *et al.*, 2000; FRANSSON *et al.*, 2001).

Although the JERS mission was not conceived for interferometric applications, it has been shown that SAR interferometry is feasible for topographic mapping (ROSSI *et al.*, 1996). For forest monitoring, too few have been the studies. The potential of JERS repeat-pass coherence has been investigated in tropical forests by (LUCKMAN *et al.*, 2000), whereas in boreal forests an initial investigation has been carried out in (ASKNE *et al.*, 1999).

Mission	ERS-1/2	JERS-1
Duration	1991 – 2000 (ERS-1) 1995 – (ERS-2)	1992 – 1998
Height	785 km	568 km
Repeat-pass cycle	35 days (nominal) 3 days (ice phase) 167 days (geodetic phase) 1 day (“tandem” mission)	44 days
SAR frequency	C-band (5.3 GHz, 5.7 cm)	L-Band (1.25 GHz, 23.5 cm)
Incidence angle	23°	35°
Swath width	100 km	75 km
Spatial resolution	30 x 30 m	18 x 18 m
Polarisation	VV	HH

Table 1.1. Main features of the ERS and JERS-1 missions.

1.4 Scope of the thesis

The promising results obtained with ERS SAR interferometry in boreal forests were the trigger to further and deeper

- Understand which factors influence the interferometric signal,

- Understand the effect of temporal and spatial variations of the interferometric signal,
- Model the interferometric signal in terms of a few forest attributes,
- Investigate the potential of model-based approaches for the estimation of biophysical parameters. In particular, the focus has been put on:
 - Retrieval of stem volume using the coherence,
 - Estimation of tree height using the interferometric phase.

Since an analysis of the two interferometric parameters could not be considered independently of the underlying SAR signatures, these have been taken into account as a support to the interpretation of the properties of coherence and InSAR phase.

Although for forest applications the results provided by the JERS L-band backscatter have been promising, an answer had not been given to several questions, such as

- “Which applications are feasible with JERS backscatter in boreal forests?”
- “How strong is the effect of seasonal changes on the retrieval of biophysical parameters?”
- “Does the retrieval of forest parameters perform equally throughout the boreal zone?”
- “Can JERS interferometry provide substantial new information in boreal forests?”

thus suggesting the investigations reported in this thesis.

All these points express the aim behind the work carried out: **to increase the knowledge on how the ERS and JERS SAR and SAR interferometry “see” boreal forests and to provide methods and tools based on SAR and SAR interferometry for boreal forest monitoring.** The final goal would have been to present an answer to the third question posed at the beginning of the Chapter: **does spaceborne repeat-pass SAR interferometry represent a source of information from which reliable, consistent and accurate estimates of forest parameters can be determined?**

1.5 Outline of the thesis

At first a theoretical background on SAR interferometry and boreal forests is provided (Chapters 2 and 3). It is well known that before proceeding with any application that should make use of a set of measurements, it is essential to have an exhaustive knowledge of the measurements properties. Chapter 4 deals with this issue, focusing on the factors that affect the ERS and JERS backscatter and coherence in boreal forests. In particular, the effects on the remote sensing signatures

due to the SAR system, the environmental conditions and the type of forest are illustrated. The conclusions reported in this Chapter are of fundamental importance for the evaluation of the results presented in the remaining Chapters.

A key-point in this thesis is the definition and the use of simple and straightforward models that relate the SAR and the InSAR signatures to few forest attributes. The Water Cloud Model (WCM) (ATTEMA & ULABY, 1978) and the Interferometric Water Cloud Model (IWCM) (ASKNE, *et al.*, 1995; ASKNE, *et al.*, 1997b) are used to describe the total forest backscatter and coherence respectively, as function of stem volume. Chapter 5 illustrates the theoretical aspects of both models, whereas Chapter 6 presents results of model fitting to sets of backscatter, coherence and stem volume measurements.

Once the models have been fitted to reference SAR and InSAR data from well-known forest areas, they can be either used to predict values of SAR and InSAR signatures for a given forest or inverted to estimate forest parameters. Chapter 7 illustrates the stem volume retrieval procedure from measurements of backscatter and coherence at mensuration scales typical of boreal forests. Chapter 8 analyses the estimation of tree height using interferometric phase measurements. This Chapter discusses the properties of the interferometric phase in boreal forests, the disturbances due to atmospheric artefacts, their reduction and the potential for tree height retrieval using the Interferometric Water Cloud Model.

The results obtained are discussed within each Chapter and then summarised in Chapter 9, which consists of an overall conclusion and a future outlook, concerning unsolved problems, topics that need further investigation and scenarios of possible research.

Chapter 2

InSAR theory

This Chapter provides a comprehensive background on SAR and SAR interferometry to enable a clear understanding of the results presented in this thesis. An overview of a SAR system is given in Section 2.1, whereas a summary of radar scattering properties and mechanisms is included in Section 2.2. SAR interferometry is defined in Section 2.3. An important point in SAR interferometry is image processing, which is thoroughly presented and analysed in Section 2.4. The two outputs of SAR interferometry, the coherence and the interferometric phase, are described in Section 2.5. This last Section is extremely important for a full understanding of the chapters dealing with SAR interferometric applications in forests.

2.1 SAR system overview

An imaging real aperture radar is an active sensor mounted on a flying platform, such as an airplane or a satellite. The system alternatively sends out a pulse and records the echoes scattered back by the objects (called scatterers) seen by the radar. The receiving circuits are equipped to measure the time delay between the transmission of a pulse and the reception of the echo. This delay allows the distance to the scatterers to be measured, which is then converted to obtain an image of the swath. Pulses and echoes are characterised by several parameters: wavelength (or frequency), polarisation, pulse repetition frequency, etc. These are chosen depending on the purpose of the mission.

An imaging radar is arranged in a side-looking configuration. This improves the ground range resolution and avoids saturation of the signal, which can arise if the sensor is pointed straight down towards the ground surface. Independently of the configuration, the problem with radar, in particular spaceborne radar, is the along-track resolution, i.e. the resolution in the flight direction. The along-track resolution

is inversely proportional to the length of the antenna and directly proportional to the distance to the target. Since satellites cannot be equipped with very long antennas, the along-track resolution of a spaceborne radar image is extremely poor. Hence, an imaging real aperture radar does not have any application in space.

The along-track resolution can be tremendously improved when the echoes pulsed back by a scatterer towards the antenna are coherently summed together. In this way a long aperture antenna is synthesised, thus increasing the along-track resolution. This is the principle on which SAR is based. Compared to real aperture radar, the generation of SAR imagery is much more complex as many echoes from the same resolution cell have to be treated simultaneously. For each cell the time delay information and the Doppler history are required, as well as orbital information. This implies a heavy computational demand on the processing from raw data to a focused SAR image.

2.2 Radar scattering

Let us consider an object illuminated by an electromagnetic pulse transmitted by a radar. The signal scattered back to the sensor is a complex quantity, characterised by amplitude and phase. The amplitude expresses the strength of the scattering in the direction of the radar. Shape, orientation with respect to the line of sight of the radar and dielectric properties of the object determine the power scattered back. The phase is related to the two-way path length between the satellite and the scatterer.

The total power scattered back from an object is given by the radar equation:

$$P_r = \frac{P_t G A_e}{(4\pi R^2)^2} \sigma \quad (2.1)$$

in which the received power, P_r , is expressed as a function of the transmitted power, P_t , the distance between the radar and the target, R , the antenna gain, G , the antenna effective area, A_e , and the radar cross section (RCS) of the object, σ . Given a radar system, the received power depends on the radar cross section of the object. The radar cross section is the most important scattering property of an object and it is theoretically defined for point targets only. When dealing with distributed targets, the radar cross section is replaced by the backscatter coefficient, σ_A^o , which is defined as the radar cross section per unit area.

Depending on the target and the radar frequency, two scattering mechanisms can arise: surface and volume scattering. Surface scattering occurs for objects that do not allow the electromagnetic wave to penetrate its surface. In other words, the scattering from layers below the surface is negligible. When the wave hits the target, part of it is directly reflected at the air-target interface and the rest is strongly absorbed inside the medium, making the scattering from the volume negligible. The amplitude of the signal registered by the radar depends on the radiation pattern of the object. Surface scattering is common in built-up areas, for bare soils and water areas, and can be

considered the dominant mechanism in forested areas and snow packs at very high frequencies. Volume scattering takes place when the radar pulse gets transmitted through the target. The total signal echoed back to the radar comes from the volume below the surface. In media such as forests and snow layers, the percentage of power scattered from within the volume increases for decreasing radar frequency.

At the frequencies typically used for spaceborne SAR missions, there are generally hundreds of simple objects in an area of the size of a resolution cell. Each scatterer contributes with amplitude (A_i) and phase (φ_i). The signal scattered back to the radar is a coherent sum of the single scatterers contributions; therefore, it does not simply resemble the total scattering strength but it is related to the positions of the scatterers within the cell.

$$Ae^{j\varphi} = \sum_{i=1}^n A_i e^{j\varphi_i} \quad (2.2)$$

The phase in a cell has a deterministic contribution due to the two-way path of the wave, and a totally random internal contribution. If the slant range distance is R and the wavelength is λ , the phase is given by:

$$\varphi = \frac{4\pi}{\lambda} R + \varphi_{scatter} \quad (2.3)$$

where $\varphi_{scatter}$ includes phase effects due to the scatterers in the resolution cell. Path delays due to water vapour in the troposphere or clouds of electrons in the ionosphere cause phase shifts as well. However, because of the small size of the resolution cell with respect to the spatial variability of these effects, the atmospheric artefacts can be considered uniform within the cell.

Since the wavelength is generally much smaller than the size of the resolution cell, the total phase can have any value. This effect is known as speckle. Speckle shows as salt and pepper noise in the amplitude image and as pure noise in the phase image. Nevertheless, it is important to notice that speckle is not noise in the traditional meaning, i.e. something that does not contain any information about the observed scene. Speckle is an effect inherent to the scattering process and reflects properties of the imaged scene.

To reduce speckle effects, post-processing of SAR imagery is needed. The retrieval of the underlying RCS for a point target or the backscattered power for a distributed target can be performed either in the space or in the time domain. Spatial averaging is by far the simplest method, although it implies a loss in resolution, which depends on the number of pixels used. If the average is performed on L pixels, we speak of a L -look intensity image. The advantage of using an L -look image is the smaller variance in the measured intensity and the reduced memory needed for storing the image.

To keep the spatial resolution unchanged spatial and temporal filtering are used. Spatial filtering is adopted either to smoothen the image (LEE, 1981; FROST *et al.*, 1982), or to make edges and features more evident. In this case filtering algorithms are developed for the specific application (LOPES *et al.*, 1990; LOPES *et al.*, 1993; DEKKER, 1998). Temporal filtering can be performed if several images of an area are available. Temporal filtering does not alter the resolution (BRUNIQUEL & LOPES, 1997; QUEGAN *et al.*, 2000) but it is not suitable if there have been changes in the scattering, due for example to weather effects.

The coefficient commonly used to quantify the influence of speckle on the measured backscatter is the equivalent number of looks (ENL), defined as the ratio between the squared mean and the variance of the intensity for homogeneous surfaces without texture (OLIVER & QUEGAN, 1998). The ENL is equivalent to the independent number of intensity values averaged per pixel and is for example used to evaluate the smoothening effect of a speckle filter in comparison to the original data. A good filter should strongly increase the ENL.

2.3 SAR interferometry

In a SAR interferometric system two antennas observe an area from slightly different positions, the distance between them being referred to as the baseline (Figure 2.1). The component of the baseline in the along-track direction is generally negligible with respect to the across-track projection. In a Cartesian coordinate system on the across-track plane, this projection is commonly split in two components, respectively along the line of sight (so called parallel component of the baseline, B_p) and the direction perpendicular to it (so called perpendicular or normal component of the baseline, B_n). When it is clear that the normal component of the baseline is referred to in the discussion, simply the term “baseline” will be used.

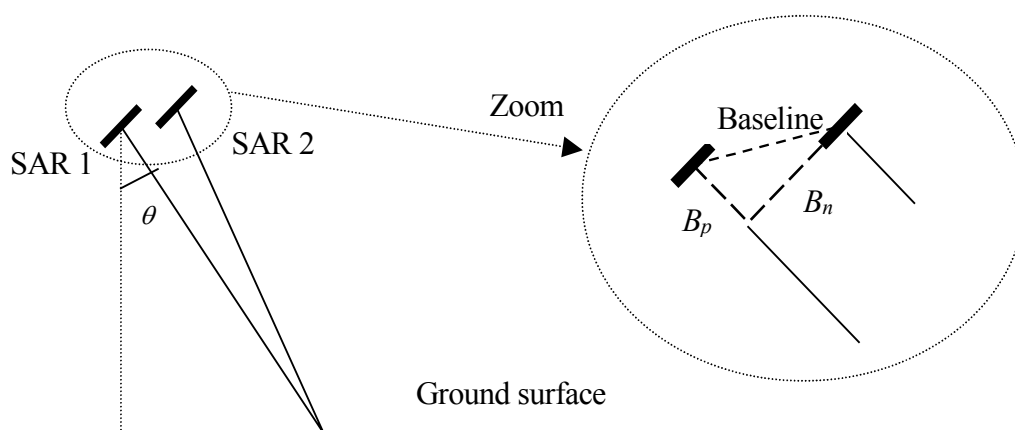


Figure 2.1. InSAR system geometry. SAR 1 and SAR 2 represent the two acquiring antennas, and θ is the incidence angle. In the zoomed part the baseline is represented by the two components in the direction parallel to the line of sight, B_p , and perpendicular to it, B_n .

Looking at SAR interferometry as a system (HAGBERG *et al.*, 1995), two SAR images, which express the ground reflectivity function of the scene, are processed to produce as output an interferogram. The interferogram is obtained from the Hermitian product of the two original complex SAR images, thus being a complex image as well. Given a pixel in the first SAR image, $g_{1,i}$, and the complex conjugate of the corresponding pixel in the second SAR image, $g_{2,i}^*$, the pixel in the interferogram can be written as:

$$\begin{aligned}
 s_i &= g_{1,i} g_{2,i}^* = \left(a_{1,i} e^{-j\varphi_{1,i}} e^{-j\frac{4\pi}{\lambda} R_{1,i}} \right) \left(a_{2,i} e^{-j\varphi_{2,i}} e^{-j\frac{4\pi}{\lambda} R_{2,i}} \right)^* = \\
 &= (a_{1,i} a_{2,i}) e^{j\Delta\varphi_i} e^{j\frac{4\pi}{\lambda} B_{p,i}}
 \end{aligned} \tag{2.4}$$

In Equation (2.4) the complex SAR pixels in the two images are written in terms of their amplitude, $a_{1,i}$ and $a_{2,i}$, and their phase. The recorded phase is a sum of the phase components related to the two-way travelling path ($R_{1,i}$ and $R_{2,i}$ are the slant range distances from the antenna to the pixel) and the specific target, $\varphi_{1,i}$ and $\varphi_{2,i}$. In Equation (2.4) the amplitude of the interferogram is given by the product of the two SAR amplitudes. The phase is related to the difference of phase contributions within the pixel, $\Delta\varphi_i$, and to the two-way path difference, i.e. the parallel component of the baseline, $B_{p,i}$. Although the phase is totally random in both SAR images, the phase difference is not because the random effects are cancelled out.

If the two SAR images are acquired simultaneously by two antennas we speak of single-pass interferometry. This configuration is considered mostly for airborne campaigns, but has been used during the Shuttle Radar Topography Mission (SRTM) as well. We speak instead of repeat-pass interferometry when the two images are acquired at different times. Repeat-pass interferometry is typical of spaceborne satellite systems, for which a simultaneous acquisition of two images has not been possible yet.

2.4 InSAR processing

The generation of an interferogram from two SAR images is divided in several processing steps. These can be grouped into three major blocks, which will be described in the following sub-sections:

1. Pre-processing (co-registration, band filtering).
2. Interferogram generation (InSAR estimation).
3. Post-processing (noise filtering, geocoding).

2.4.1 Pre-processing

The two SAR images do not usually overlap so that co-registration of one of them is needed in order to superimpose it on the other. Since all the information in the image to be resampled, in particular the phase, should be preserved, the accuracy in the co-registering operations must be exceptional. The misregistration error must be limited to few hundredths of a pixel, which requires complex interpolation filters. Theoretically one should use an ideal interpolator with a flat spectrum, i.e. an infinite sinc function. This is not possible because filters only have a finite length; nevertheless, as most of the SAR products are oversampled, the use of finite filters will not cause a loss of information (DAMMERT, 1996b).

The slightly different viewing positions cause loss of information in the interferogram; therefore pre-filtering is needed. If the SAR antennas have different squint angles at acquisition, the two images have a slight difference in the azimuth spectra. The shift between the two spectra is due to a Doppler centroid not equal to zero frequency. This is the case of ERS-1/2 pairs for example. To remove this effect, azimuth bandpass filtering is generally performed. At first the Doppler centroid frequency is estimated and then the bandpass filter is applied to fit the Doppler centroid (SCHWÄBISCH & GEUDTNER, 1995). When the baseline is not null, the slant range spectra of two images do not overlap completely so that the non-common parts in the slant range spectra must be filtered out. The filtering procedure, called wavenumber shift filtering, consists of several operations and requires accurate baseline estimation from orbital parameters and slope estimation (GATELLI *et al.*, 1994).

2.4.2 InSAR estimation

The generation of an interferogram according to Equation (2.4) is not feasible as it is. In practise an interferogram is computed using an ensemble average. The complex coherence, γ , which corresponds to s_i in (2.4), has been defined in (BORN & WOLF, 1980) as follows:

$$\gamma = \frac{E\{g_1 g_2^*\}}{\sqrt{E\{|g_1|^2\} \cdot E\{|g_2|^2\}}} \quad (2.5)$$

In (2.5) g_1 and g_2 denote the two complex SAR images and $E\{ \}$ represents the expected value. The magnitude and the phase of the complex interferogram are generally referred to as the coherence and the interferometric or InSAR phase respectively.

The coherence measures the degree of correlation between the two SAR images. In a repeat-pass configuration it can be as well said that it measures the temporal stability of the imaged scene. This definition, intuitively simple, will become clear in Section 2.5.1. The InSAR phase is related to the two-way path length difference and the scattering media. The coherence is a normalised quantity with values between 0 and

1. When the coherence is close to zero, total decorrelation has occurred. The phase image appears in a series of fringes and has values between 0 and 2π .

To compute the expected value in (2.5) the ensemble average has to be replaced by spatial averaging within a two-dimensional window. According to the principle that an estimate becomes more accurate for increasing number of samples, larger window should be preferred. The true coherence would be obtained in case of an infinite window size. In reality we can obtain only estimates of InSAR phase and coherence, which are therefore affected by bias and errors. Below an overview of the estimators used is reported (for an exhaustive description and technical details see (DAMMERT, 1996a)).

2.4.2.1 Coherence estimation

If a Maximum Likelihood, ML, estimation is performed, the coherence can be written as:

$$|\hat{\gamma}| = \frac{\left| \sum_{i=1}^N g_{1,i} g_{2,i}^* \right|}{\sqrt{\sum_{i=1}^N |g_{1,i}|^2 \sum_{i=1}^N |g_{2,i}|^2}} \quad (2.6)$$

where N is the number of pixels in the estimation window. The estimate shows decreasing bias and uncertainty for increasing window size, i.e. number of independent looks; only for asymptotically large data sets the estimate is unbiased (DAMMERT, 1996a; DAMMERT, 1996b; TOUZI *et al.*, 1999).

The number of independent looks represents the number of independent samples in the coherence estimation window. The computation of this coefficient is not straightforward and needs knowledge of several SAR parameters. As rule of thumb the following Equation relating it to the number of looks can be used (DAMMERT, 1999):

$$L_{ind} \approx 1 + \frac{L-1}{2} \quad (2.7)$$

Equation (2.6) is valid under the assumption that the ground does not induce a phase, i.e. for flat ground. Since the topography is rarely flat, the modified ML estimator with a topography-induced phase is preferable:

$$|\hat{\gamma}_{ML}| = \frac{\left| \sum_{i=1}^N g_{1,i} g_{2,i}^* e^{-j\phi_i} \right|}{\sqrt{\sum_{i=1}^N |g_{1,i}|^2 \sum_{i=1}^N |g_{2,i}|^2}} \quad (2.8)$$

where $e^{-j\varphi_i}$ is a correction term related to the local topography. When a DEM is available, it is possible to get to an accurate estimate of the coherence. Otherwise the correcting term can be approximated by constant, linear, quadratic or higher order functions over the estimation window. Depending on the chosen slope function, the correction changes the statistics of the estimator and influences the accuracy of the coherence estimates.

If a linear function is assumed, the estimator becomes (DAMMERT, 1996a):

$$|\hat{\gamma}_{lin}| = \frac{\max \left| \sum_{i=1}^N g_{1,i} g_{2,i}^* e^{-jvi} \right|}{\sqrt{\sum_{i=1}^N |g_{1,i}|^2 \sum_{i=1}^N |g_{2,i}|^2}} \quad (2.9)$$

where e^{-jvi} denotes the ground topography correction factor. In Equation (2.9) the numerator can be seen as a Fourier kernel, therefore the coherence corresponds to the highest peak in the FFT spectrum. Compared to the previous estimators, $|\hat{\gamma}_{lin}|$ is characterised by higher bias and longer error bars for low coherence (DAMMERT, 1996a; SANTORO *et al.*, 2000).

As a compromise between an accurate estimation and high spatial resolution, estimation algorithms with adaptive window size have been designed. The whole processing is divided in two steps. At first, a fixed and relatively small window size is used to give a rough estimate of the coherence level. Then the estimation is performed again with a window size that depends on the initial estimate of the coherence. In areas of low coherence, larger estimation windows are used (WEGMÜLLER *et al.*, 1998). Similar results have been obtained when computing the coherence according to Equation (2.8) and the adaptive estimation at the test site of Kättböle (see Chapter 3 for the description of the test site).

2.4.2.2 Phase estimation

The ML phase estimate, $\hat{\varphi}$, is simply the argument of the complex coherence estimate (SEYMOUR & CUMMING, 1994):

$$\hat{\varphi} = \arg \left(\sum_{i=1}^N g_{1,i} g_{2,i}^* \right) \quad (2.10)$$

The phase estimates are wrapped in the $[0, 2\pi[$ interval. As a consequence, for low coherence the mean of the estimate is biased because the variance of the estimate violates the Cramer-Rao lower bound (RODRIGUEZ & MARTIN, 1992; DAMMERT, 1999). To solve the problem the phase needs to be unwrapped. Phase unwrapping requires the knowledge of height for several points within the imaged area and is affected by errors in low coherent areas. If phase unwrapping is difficult, the phase

of the mean complex ML coherence can be computed instead of the mean of the phase. The bias is removed but phase unwrapping still needs to be performed.

2.4.3 Post-processing

Bias reduction is essential in areas of low coherence. Knowing the statistics of the estimator used, it is possible to reduce the uncertainty in the estimate due to the bias (DAMMERT, 1999; TOUZI, *et al.*, 1999). It is important to notice that, because of the uncertainty inherent in low coherence measurements, the corrected coherence does not coincide with the true value yet.

To increase the quality of coherence images, noise filtering is recommended. Simple mean or median filters can be used, with a window size fixed by the statistics of the estimator and the local variance in the window. The window size should be increased until the variance in the window is larger than the theoretical one (DAMMERT, 1999). Nevertheless, in order to keep the resolution at a reasonable level, sizes of the order of the estimation window can be used as well.

In a SAR image, each scattering cell is geometrically located with respect to the satellite position and velocity vectors and arranged in the across-along track geometry (so called Range-Doppler geometry). Commonly SAR and InSAR images need to be compared with digital maps in a given projection; therefore, it is necessary to perform a coordinate transformation. If the slope and the height information included in a Digital Elevation Model, DEM, are taken into account, the transformation is called geocoding. This operation is generally performed by means of a least-squares tiepoint fit between the SAR image and the simulated SAR image obtained from the DEM. The accuracy of satellite state position vectors and relative heights reported in the DEM determines the precision of a geocoded image.

Compared to the ERS mission, JERS-1 tracking was less accurate. JERS geocoded products are therefore affected by bigger positioning errors. In (SANTORO *et al.*, 2002b) a set of 18 ERS images was geocoded using the DIAPASON software by CNES. The relative positioning error was estimated to be one pixel (i.e. 25 m) in both directions. The same procedure was applied on a set of nine JERS images from the same area in (SANTORO *et al.*, 2002a). An absolute positioning error above one pixel was estimated and several warping effects could be easily noticed. Overlap of the geocoded images could be obtained only after co-registration using an additional set formed by many tiepoints.

2.5 Coherence and interferometric phase

Independently of how the estimation has been performed, for the repeat-pass configuration the normal component of the baseline and the temporal interval between acquisitions are the main factors that affect the quality of an interferogram.

The distance between the antennas can be increased until a certain limit, for which complete decorrelation occurs and the interferometric fringes disappear. The critical

value for the perpendicular component of the baseline can be written as (GOLDSTEIN *et al.*, 1988):

$$B_n \leq \frac{R\lambda}{2L_c \cos \theta} \quad (2.11)$$

where R represents the slant range distance, λ the wavelength, L_c the size of the resolution cell and θ the incidence angle. For most applications it is recommended to combine images with a normal component of the baseline well below the critical value reported in Equation (2.11). The ERS critical value is approximately 1100 m. Nevertheless, pairs with normal component of the baseline longer than 600 m are generally discarded. Because of the longer wavelength and the shallower incidence angle, the JERS critical baseline is longer than the ERS, being approximately 4 km. For topographic applications (ROSSI *et al.*, 1996) has suggested that even for a baseline of 5 km fringes can still be visible, whilst in (WIESMANN *et al.*, 1999) an upper bound of less than about 2 km is suggested for applications in low coherent areas, such as forests.

Between the two acquisitions, the scatterers in a resolution cell may move or their dielectric properties may change. Typical examples include water areas and tree canopies in the first case, and snow covered or wet surfaces in the second. In such cases, the two backscattered fields differ, thus being only partially correlated because of the temporal interval between the acquisitions. Taking into account that the number of scatterers in a resolution cell decreases for increasing wavelength and that the phase sensitivity to movements is lower at lower frequency, the temporal effects are stronger at C-band than at L-band.

2.5.1 Coherence

Based on (ZEBKER & VILLASENOR, 1992; ULANDER & HAGBERG, 1995), the coherence can be expressed as a product of five terms. Each term is related to a decorrelation source: the quality of the SAR processors used, the thermal noise in the receiver, the non-overlapping spectra in the along track direction, the baseline and the time interval between image acquisition. Therefore, coherence can be written as:

$$|\gamma| = |\gamma|_{processor} \cdot |\gamma|_{noise} \cdot |\gamma|_{azimuth} \cdot |\gamma|_{spatial} \cdot |\gamma|_{temporal} \quad (2.12)$$

The first two terms are independent of the viewed scene; the third and the fourth are related both to the scene and to the system; the last depends mostly on the target. SAR processing techniques preserve the coherence so that $|\gamma|_{processor}$ can be considered negligible. Negligible is also the noise decorrelation term $|\gamma|_{noise}$, caused by thermal noise in the receiver, as long as the target clutter to noise ratio is high (DAMMERT, 1996b). Since orbits do not have perfectly parallel orbits, the term $|\gamma|_{azimuth}$ includes the decorrelation due to a slight difference in the azimuth spectra of

the two SAR images. This decorrelation factor becomes negligible after azimuth band-pass filtering.

The spatial term $|\gamma|_{spatial}$ is strongly influenced by the normal component of the baseline, increasing for increasing baselines. By using the wavenumber shift filter, it is possible to reduce the effect of this term. Nevertheless, the problem persists if the normal to the surface plane has an azimuth component or there is volume scattering (DAMMERT, 1996b). According to (ASKNE *et al.*, 1997), in case of volume scattering the spatial decorrelation term can be split into two contributions under the assumption that the stable scattering function is only dependent on the height above the surface:

$$|\gamma|_{spatial} = |\gamma|_{slant-range} \cdot |\gamma|_{volume} \quad (2.13)$$

In Equation (2.13) the first term can be removed using the wavenumber shift technique as already mentioned, so that the spatial decorrelation can be interpreted simply in terms of volume decorrelation, $|\gamma|_{volume}$.

The temporal decorrelation factor $|\gamma|_{temporal}$ depends on changes occurring within the scene between the passes, i.e. if there has been a change of the ground reflectivity function. Several factors generally combine in determining the temporal decorrelation. A change in the geometry of the scatterers such as a change of position, shape, etc., is most likely to have the strongest effect on the short time scale (ZEBKER & VILLASENOR, 1992; CORR *et al.*, 1995; SMITH *et al.*, 1996; GAVEAU, 2002). These factors become even more important when the images in a pair have been acquired with an interval of several days or even several years. Changes in the dielectric properties of the imaged scene, mainly related to change in water content of the target, have more effect in pairs with long-time acquisition interval. However, it is not possible to conclude simply that the longer the time interval between acquisitions, the higher the temporal decorrelation (SMITH, *et al.*, 1996; USAI & KLEES, 1999).

With volume and temporal decorrelation as the only factors, coherence can be considered as the product of two terms:

$$|\gamma| = |\gamma|_{volume} \cdot |\gamma|_{temporal} \quad (2.14)$$

From Equation (2.14) it is evident that the coherence depends mainly on the imaged scene and only for long baselines and long radar wavelength on the InSAR system.

For forests, which are characterised by non-negligible volume decorrelation, both terms in Equation (2.14) should depend on the frequency. At lower frequencies (L- and P-band) the larger penetration of the wave within the media implies that the scattering comes from more stable elements. The backscatter is mainly due to twigs and leaves at C-band, and to branches at L-band. Since a resolution cell can contain

only few branches, which moreover are likely to remain in the same position, the temporal decorrelation will be higher at C-band. At C-band in fact the larger amount of scatterers and their high probability of moving within the resolution cell will cause a remarkably higher volumetric and temporal decorrelation. Unfortunately the ERS and JERS images do not allow a comparison because of the different repeat-pass period and viewing geometry.

2.5.2 Interferometric phase

The interferometric phase image comes out in a series of fringes obtained from the interference of the two SAR images. The visibility of the fringes is a function of the coherence. The lower the coherence, the larger the uncertainty in the phase estimates. Hence, the information provided by the phase over forests and water areas, where coherence is lowest, is more limited than in high-coherent areas such as cities or bare soils. The noise in the phase estimates can be expressed as (DÄNDLIKER, 1980):

$$\sigma_{\varphi} = \frac{1}{\sqrt{2L_{ind}}} \frac{\sqrt{1-|\gamma|^2}}{|\gamma|} \quad (2.15)$$

where L_{ind} represents the number of independent looks and $|\gamma|$ is the true coherence.

As shown in (BAMLER & JUST, 1993; JOUGHIN & WINEBRENNER, 1994; ZEBKER *et al.*, 1994), the accuracy of the phase estimates increases for increasing coherence and multi-looking factor. This implies that reduction of phase noise in low-coherent areas, such as forests, requires strong multi-looking factors, having as drawback, a decrease of spatial resolution.

Starting from Equation (2.4), it is possible to determine the variation of the interferometric phase between two points, by means of differentiation:

$$\Delta\Phi = \frac{4\pi}{\lambda} B_n \Delta\theta + \Delta\Phi_{noise} \quad (2.16)$$

where $\Delta\theta$ is the difference in incidence angle and the $\Delta\Phi_{noise}$ term is related to thermal noise, to the physical nature of the targets and to the uncertainty in the measured interferometric phase values. $\Delta\theta$ can be expressed in terms of several contributions: slant range and topographic differences, as well as possible atmospheric inhomogeneities and terrain movements. The phase difference between two pixels in an interferogram is finally given by:

$$\Delta\Phi = \frac{4\pi B_n}{\lambda R \tan \theta} \Delta R + \frac{4\pi B_n}{\lambda R \sin \theta} \Delta z + \frac{4\pi}{\lambda} \Delta\eta + \frac{4\pi}{\lambda} \Delta\rho + \Delta\Phi_{noise} + n \cdot 2\pi \quad (2.17)$$

The first term in Equation (2.17) includes the slant range difference between the pixels, ΔR , and is therefore related to the InSAR system geometry. It appears as

fringes in the across-track direction, which can be removed by applying “flat Earth compensation”. This expression is easily explained because these are the only fringes in an interferogram of a flat surface. The second term takes into account the topography of the imaged area since it expresses a phase difference between two points in terms of a difference in altitude, Δz . These two terms, together with the phase noise part, represent the contributions to the interferometric phase for static conditions and without any wave perturbation. This is a rather ideal case; therefore, Equation (2.17) includes two more contributions. Both appear in the repeat-pass case only.

The third term is related to coherent changes in the imaged scene. Ground movements between acquisitions, due for example to earthquakes, volcanic activity or ground subsidence, result in a coherent displacement of all the scatterers within a resolution cell. These coherent movements, expressed by $\Delta\eta$, introduce a phase difference, because the incidence angle has changed between acquisitions.

The fourth term expresses a phase difference due to different path delays in the atmosphere. If the atmosphere has different spatial properties at the two acquisitions (different electron density in the ionosphere, different water vapour content in the troposphere), radar pulses will not be equally delayed. Different path delays, $\Delta\rho$, can be seen as increase in slant range distances, thus causing the additional term. The atmospheric contribution can severely decrease the quality of an interferogram. A more detailed description on atmospheric artefacts, together with a summary on filtering algorithms, can be found in Chapter 8.

The last term expresses the phase ambiguity because phase is measured between 0 and 2π only (phase unwrapping term). Unwrapping the phase values means adding a correct multiple of 2π to the interferometric phase for each pixel. For the sake of the discussion, we will not consider the phase unwrapping term in this section.

With accurate orbital data, the flat Earth term can be completely removed. When these are not available, one can use blind estimates of the fringe frequency by finding the peak of the complex interferogram power spectrum. In this case, the phase difference includes residual uncompensated interferometric effects, which can introduce relevant errors when inverting phase measurements (LI & GOLDSTEIN, 1990; ZEBKER, *et al.*, 1994). Assuming correct removal of the systematic interferometric fringes and negligible effect of the atmosphere, Equation (2.17) can be inverted and used for height maps generation or terrain displacement analysis.

If there have not been geodetic events between the two acquisitions, the phase difference will be related only to topography and phase noise. The height resolution increases for increasing baseline, so that long baseline interferometric pairs should be preferred. Nevertheless, due to increasing speckle decorrelation, the perpendicular component of the baseline should not exceed an “optimum” range of values, generally estimated at around 200-300 m for the ERS case. For the JERS case, volume decorrelation is less dangerous and longer baselines can be used. The topographic accuracy depends on slopes as well. Simulations in (HAGBERG & ULANDER, 1993) have shown that in the ERS case for steep slopes towards the radar

the height estimation error increases for a perpendicular component of the baseline above 150 m.

Depending on the frequency, the “topography” to which radar is sensitive changes. For increasing frequency, the penetration of the electromagnetic wave in layered media decreases. Forests, cultivated areas and snow packs therefore introduce an additional topography that sums to the ground topography (DAMMERT *et al.*, 1995; ULANDER *et al.*, 1995; GUNERIUSSEN *et al.*, 1996). If the topography of the area is known, for example through a DEM, the second term in Equation (2.17) can be removed. In such case we speak of differential SAR interferometry, DInSAR (GABRIEL *et al.*, 1989). Besides the usual phase noise, the phase difference is related to coherent movements of the ground and residual topography not included in the DEM (due to forests or urban areas for example).

Chapter 3

Boreal forests

This Chapter has been designed to give a general overview of the boreal zone in Section 3.1 and a more detailed description of forests and forestry in the countries where the test sites of interest were located (Sweden, Finland and Russia) in Section 3.2. Section 3.3 reports a description of each test site in terms of the main forest attributes.

3.1 The boreal zone

The boreal zone stretches in northern hemisphere below the Arctic region along a belt interrupted only by oceans. The southern border is generally considered to be along the transition zone of the vegetation from the boreal cover type to the semi-boreal.

Boreal forests cover almost the entire land surfaces in the northern hemisphere between 70° N and 60° N, reaching 50° N in East Siberia and West Canada (Figure 3.1). The dominant species are coniferous, probably the most distinctive attribute of boreal forests. At the lowest latitudes, coniferous and broadleaf trees form a mixed type of forest, typical of the transition zone to a more temperate kind of vegetation.

Despite the common knowledge, the boreal region is far from being “just” a cold area. Temperatures below 0 °C and snow cover are not the rule for the whole year. Both along the North-South and the East-West direction the climate changes considerably. Independently of the longitude, the temperatures are generally lower at higher latitudes. Taking into account the Eurasian part only, a strong influence on the climate is due to oceanic currents of the Gulf Stream. Sweden and, to a lesser extent, Finland are characterised by rather mild winters and frequent precipitation. When moving towards Western and Eastern Siberia, the climate becomes more continental.

The monthly average winter temperatures decrease and the summer average increase. Precipitation is mainly in the form of snowfall but is remarkably less frequent. As a consequence the growing season for the vegetation is longer in Sweden and Finland, although the growth rate per year is bigger in Siberia.

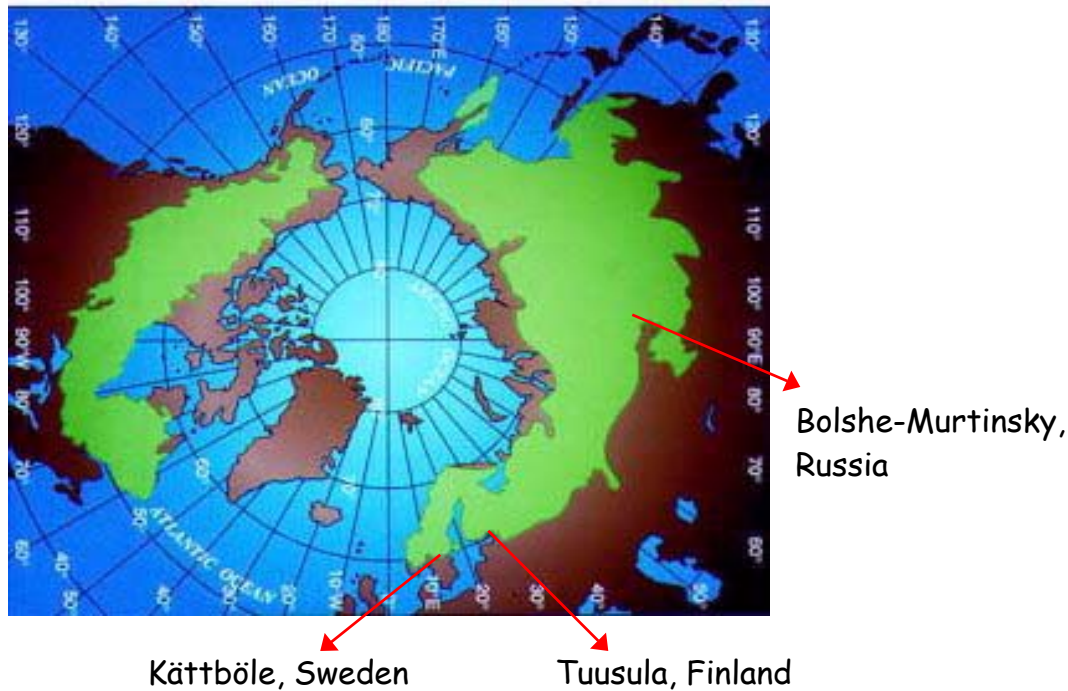


Figure 3.1. Extent of boreal forest (HARE & RITCHIE, 1972) and location of the test sites.

3.2 Principles of forest inventory

3.2.1 Sweden and Finland

The perception of forests in Sweden and Finland has greatly changed within the last two centuries. The rural economy of the 19th century considered forests both as a fundamental natural resource and a limit to agricultural production. Large vegetated areas were felled and the extent of forested areas enormously decreased. The rather uncontrolled use of forests started being regulated with laws in the last century. Forest management, supported by the legislation, is nowadays carried out according to long-term plans. Activities such as regeneration, periodical care (for example by means of thinning), reduction of over-mature forests are common practise.

Today, more than 50 % of the land surface is covered with forests, of which approximately 95% have been felled in the last 150 years. Forests are intensively and carefully managed to preserve them at the best possible conditions for the environment and for the users. For this purpose, accurate inventory and periodical update of forest information system are carried out. Traditional forest inventory is

based on local surveys; several measurements are collected with sampling techniques and accuracy that depend on the purpose of the survey. Diameter at breast height, tree species, tree height, number of trunks, etc. are measured in unit reference areas (plots). Parameters describing the soil are also measured (pH, type of soil, etc.).

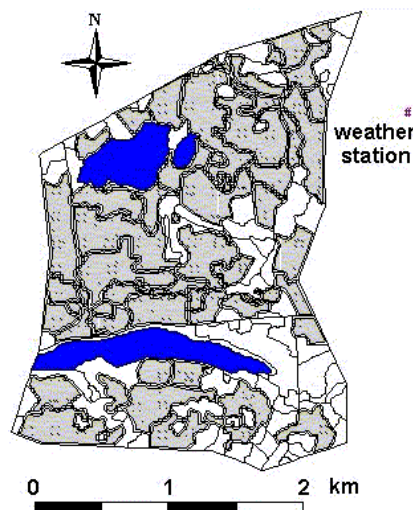


Figure 3.2. Example of stand-wise division of forests at the estate of Kättböle, Sweden, 5.5 km² (courtesy of Johan Fransson) The grey areas represent forest stands larger than 2 ha. The dark areas are lakes.

Forest mapping is commonly performed using stands, which are considered the primary inventory unit (Figure 3.2). A stand consists of relatively homogeneous forest in terms of tree cover and site conditions; however, stand boundaries can also be defined by technical obstacles, such as rivers, steep slopes, etc. The stand as a unit ranges from 0.5 ha to 20 ha and forest parameters can be collected using either objective or subjective methods. Objective methods are based on randomly distributed sample plots or relascope plots; subjective methods consider non-randomly distributed plots or visual estimation.

The most common measure used in forest inventory is stem volume. It is measured in m³/ha and represents the volume of tree trunks, including bark but excluding branches and stumps. Stem volume increases for decreasing latitude. In regions by the Arctic Circle, maximum values of 100-150 m³/ha are common. At 60° N, i.e. the latitude of Stockholm and Helsinki, it is not rare to measure stem volume of 400 m³/ha or even above. Stem volume is generally used as a synonym for aboveground dry biomass; in (HÄME *et al.*, 1992) it has been found that the dry aboveground biomass measured in tons per hectare can be converted to stem volume using a scaling factor of 0.6.

The computation of stem volume requires knowledge of diameter at breast height, tree height, tree species distribution and density of trees per hectare. In several forested areas located in Finland and Sweden, (ASKNE *et al.*, 1997; SANTORO *et al.*,

1999; SANTORO *et al.*, 2002) proved that a simple regression equation describes the relationship between stem volume and tree height reasonably well:

$$h = (aV)^b \quad (3.1)$$

In these investigations the empirically derived coefficients a and b were consistent, which should be a sign of the similar forest properties in the two countries. Figure 3.3 reports a scatterplot of tree heights versus stem volumes measured at one of the areas investigated and the regression curve obtained from Equation (3.1). The coefficient of determination equal to 0.89 indicates that a simple regression equation of the sort reported above can be used as alternative to allometric functions for the estimation of stem volume directly from tree height measurements and vice versa.

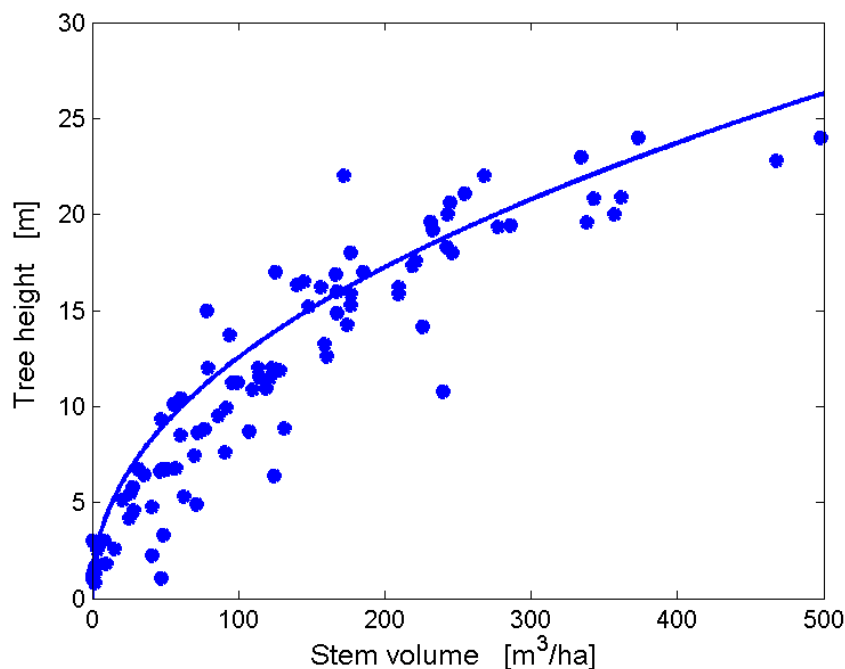


Figure 3.3. Tree height versus stem volume measurements at plot level in Kättböle, Sweden ($r = 0.91$; coefficient of determination based on Equation (3.1) = 0.89).

3.2.2 Swedish National Forest Inventory

The Swedish National Forest Inventory (NFI) consists of a large database of forest measurements at plot level. It started in 1923 with the aim of providing information to forest users. In order to adapt to new conditions and to describe forest properties in the most accurate way, the statistical design of sampling changed several times. In 1983 a last change was introduced; since then, forest planning has been carried out following rules that are described in (RANNEBY *et al.*, 1987).

The Swedish NFI statistical design is based on systematic cluster sampling, using plots arranged in tracts. A tract is a square having side length from 300 m up to 1800 m. Tracts are permanent or temporary; the first are revisited after some years, whilst the second are measured only once. A permanent tract commonly includes 8 plots with a radius of 10 m, located on the tract's perimeter. A temporary tract consists of 8 or 12 plots, with a radius of 7 m. Plots are positioned using differential GPS, with a nominal accuracy of about 5 m. Tracts are uniformly distributed over Sweden; being denser in the Southern regions. Measurements collected over several years (commonly five years) are combined for a complete characterisation of forests at county level. Sample measurements are aggregated to provide regional and national estimates of forest and ecological parameters with errors depending on the sampling technique used. For the 1983-1987 field survey, (LI & RANNEYBY, 1992) showed that the accuracy of forest variables differs depending on the region and is related to the interval of values considered.

3.2.3 Russia

Although the present conditions are rather similar, the evolution of Russian forests has strongly depended on the location, mainly because of their large extent and the different environmental conditions. In European Russia, after a long period of massive logging, intensive afforestation and reduction of fires have increased the forest cover. Despite the increased amount of wood, the quality has clearly decreased. A similar problem occurs in Siberia and the Far East. The harsh environmental conditions have limited the industrial and agricultural expansion so that forests are closer to their natural state. Nevertheless, the limited management and the increasing amount of fires and insect damages reduce the potential of these forests for economic and environmental exploitation. Nowadays, about 45% of the Russian Confederation is covered with forests, a high percentage of them being kept at natural status and not extensively managed as in Sweden and Finland. The management differs from region to region but it is common to skip the thinning making the forest consist more of a mix between thin and thick trees with a lot of undergrowth (FRANSSON, personal communication).

Russian forest inventory is either based on field measurements or on air-photo-interpretation. In the first case forest attributes are updated once per year within forest management units and then aggregated both at regional level (members of the Russian Federation) and for Russia as a whole. The inventoried data and the results of the aggregation are reported in the State Forest Account (SFA).

Each forest management unit in Russia is traditionally subdivided into forest districts. Each district is subdivided into compartments, and each compartment into evaluation strata. The evaluation strata correspond to stands in the Swedish and Finnish system. Forest inventory consists of measurements of several attributes (age, tree height, diameter at breast height, site class, increment, density, and layering) and computation of the growing stock volume. The growing stock volume is defined as the total volume of the trunks per hectare, thus being the same as stem volume. According to forestry definitions, growing stock volume estimation does not take into account stems having a diameter smaller than 8 cm. For the sake of clarity, from

now onwards, the term “stem volume” will be used independently of the region considered.

3.3 Test sites

The potential of SAR remote sensing for forestry applications was evaluated at stand level at three test sites located in Sweden, Finland and Siberia, and plot-wise in a large area in central Sweden. For this area, plot-wise measurements were also aggregated to provide estimates at coarser resolution. All sites were located at the southernmost edge of the boreal zone and stem volume locally reached values above 300 m³/ha. Topography was overall rather flat. To limit errors, the remote sensing measurements at stand level required a statistically sufficient number of pixels for averaging. Hence, only stands larger than a certain size were considered. As a general rule, stands consisting of less than 20 pixels were discarded.

In the following subsections a brief description of each test site is reported. Tables 3.1 and 3.2 list respectively the main attributes of the forests and the radar data available. Tables 3.3 and 3.4 give a synoptic view of acquisition date and weather conditions at the ERS and JERS acquisition respectively. For the ERS “tandem” pairs baselines are reported. Images were mainly acquired on a descending passes (10 a.m. and 10:30 a.m. local time respectively in for the ERS and the JERS case). In order to highlight which pairs have been acquired on an ascending pass (9 p.m. local time), a flag has been added next to the acquisition date. Because of the size the four tables have been included at the end of the Chapter. Table 3.5 below summarises the InSAR-based applications analysed in this thesis.

	<i>Stem volume</i>	<i>Tree height</i>
<i>C-band backscatter</i>	Kättböle Tuusula	-
<i>C-band coherence</i>	Kättböle NFI area Tuusula	-
<i>C-band InSAR phase</i>	-	Kättböle Tuusula
<i>L-band backscatter</i>	Kättböle Tuusula Bolshe-Murtinsky	-
<i>L-band coherence</i>	Kättböle	-

Table 3.5. Look-up table summarising which forest parameters were retrieved from the SAR and InSAR images available.

The images were all in Single Look Complex format (SLC). This type of imagery is commonly used for SAR interferometry and is characterised by a calibration error of 1-2 dB; therefore, SLCs are not the most suitable product for investigating the backscatter. If measurements are averaged for example at stand level, i.e. in areas containing a statistically sufficient number of pixels, speckle and uncertainty in the backscatter measurements sensibly decrease. Nevertheless, the absolute calibration error is still included. This aspect has been taken into account in the interpretation of the results, in particular when comparing with investigations that used different calibration procedures.

3.3.1 Kättböle

The forest estate of Kättböle (60° N, 17° E) is located northeast of Stockholm and Uppsala, Sweden, and covers 550 ha. Coniferous trees such as Scots pine (*Pinus sylvestris*) and Norway spruce (*Picea abies*) are the dominant species. Few stands of deciduous species, in particular birch (*Betula pendula*), can be found as well. In 1995 and 1996 the whole area, consisting of more than 100 forest stands, was very accurately inventoried (FRANSSON *et al.*, 2001). Measurements were collected at plot level and aggregated for each stand (see Figure 3.2). For application purposes only stands larger than 2 ha after edge erosion of a digital forest mask were retained. These stands included at least 128 pixels in the geocoded images. Because of the high accuracy of the ground-truth data, Kättböle will be considered throughout the thesis as a “reference” site for the evaluation of the investigations.

The extensive data set consisting of both ERS and JERS images (see Table 3.2) allowed the thorough investigation of C- and L-band backscatter and coherence dependency on weather conditions, and the potential for stem volume and tree height retrieval at plot and stand level. Since a plot roughly corresponded to a pixel, the backscatter measurements were used at stand level only because of speckle.

3.3.2 Swedish NFI area

The Swedish NFI area is located between the regions of Uppland and Västmanland, Sweden, and covers an area of 4235 km². The forest estate of Kättböle is approximately situated in the centre but it is not part of the NFI. In this large area, a set of 1004 plots measured between 1994 and 1998 was available. To decrease error sources, the analysis was restricted to plots that satisfied several criteria (position within the forest, stem volume and satellite coverage) (SANTORO, *et al.*, 2002).

In this area stem volume retrieval at plot and regional level have been investigated. As for the plot analysis carried out in Kättböle, only coherence images were considered.

3.3.3 Tuusula

The province of Tuusula is located 20 km north of Helsinki, Finland (60° N, 25° E). Forests and fields represent the main land-cover types (Figure 3.4). Forests comprise mainly coniferous tree species (Scots pine and Norway spruce), with few birch cases.

Forest measurements, with an estimation error above 20 % at stand level, were collected in more than 250 stands during the EUFORA project (European Forest Observations by Radar) in 1997 (HALLIKAINEN *et al.*, 1997). The average size of the stands was smaller than in Kättböle, which had an impact on the number of stands suitable for the investigations. After erosion, only 37 stands included more than 20 pixels, corresponding to an area larger than 1.25 ha. Less than 20 stands were larger than 2 ha, these being mainly at high stem volume. In order to uniformly represent the range of stem volumes typical of the area, the 37 stands were kept for the analysis.

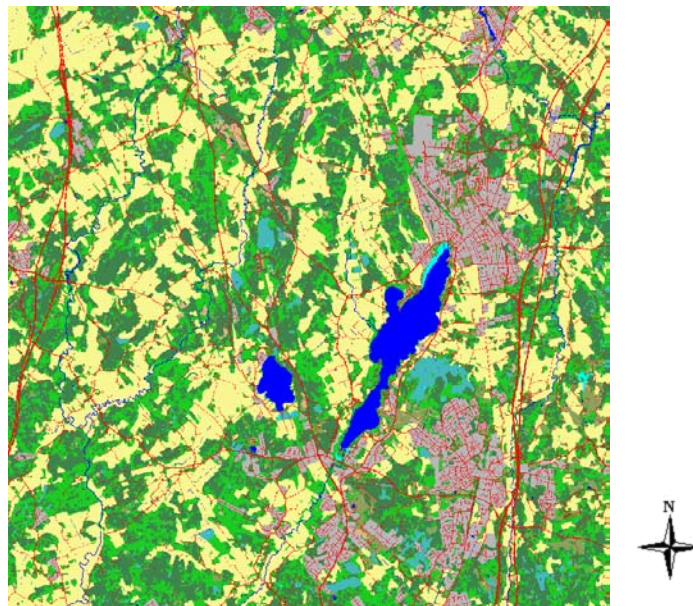


Figure 3.4. Land-cover map of the Tuusula region. The town of Tuusula on the right side of the picture neighbours the big lake. Forests in green and open fields in yellow represent the dominant land-cover classes. Area: 20 x 20 km.

Over Tuusula sixteen ERS images but only three uncalibrated JERS images were available. At C-band it was therefore possible to compare with results obtained in Kättböle, while at L-band the low quality data did not allow any significant evaluation.

Despite the similar geographical position of the two test sites, forests in Tuusula were characterised by a much larger interval of stem volumes and by different distribution of tree species within a stand. Pine and spruce dominated stands were the most frequent types of forest cover, whereas in Kättböle most stands were mixed pine and spruce.

3.3.4 Bolshe-Murtinsky

The territory of Bolshe-Murtinsky is located north of Krasnoyarsk along the river Yenisey in central Siberia (92° N, 57° E). Bolshe-Murtinsky comprises several forest

compartments, mostly covered with spruces, firs and birches with a percentage of cedar and aspen. Two compartments west of the Yenisey River are considered in this thesis. The distance between the centres of the two compartments is around 42 km. According to the numbering introduced within the SIBERIA (SAR Imaging for Boreal Ecology and Radar Interferometry Applications) project, of which Bolshe-Murtinsky was one of the test territories, the two test sites are labelled in this thesis as “Bolshe-2” and “Bolshe-4” [Schmullius, 2001 #600].

For both compartments an extensive GIS forest database, updated in 1998, was available. The data originates from the regular forest surveys performed by the Russian foresters. Based on information from the Russian forest inventory standards, growing stock volume is estimated with accuracy between 15% and 20%, depending on the age of the forest (SCHMULLIUS *et al.*, 2001; STOLBOVOI & MCCALLUM, 2002). Unfortunately exact figures for the two compartments were not available.

Compared to Kättböle and Tuusula, the area of the forest compartments is much bigger and the distribution of stem volume less uniform, this probably being a consequence of the different forest management practise in Sweden and Finland, and in Siberia. Besides mature and over-mature forests, both Kättböle and Tuusula included areas of regeneration, regrowth and thinning. In Bolshe-Murtinsky the very young and the dense forest types are dominant, whereas the intermediate growth stage is almost completely lacking (Figure 3.5).

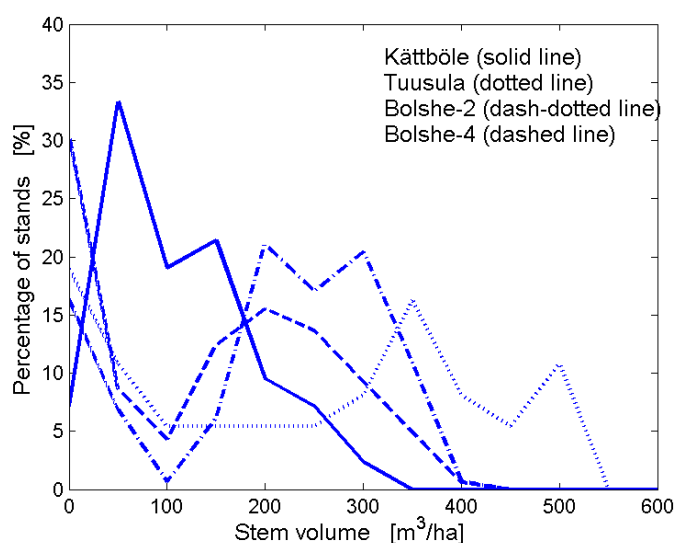


Figure 3.5. Stem volume distribution at the investigated test sites.

Although both ERS and JERS images have been acquired over Bolshe-Murtinsky, the JERS backscatter only has been considered in this thesis. The ERS data have been evaluated within the SIBERIA project (SCHMULLIUS, *et al.*, 2001), whereas the JERS coherence is currently under investigation (ERIKSSON *et al.*, 2003). As in Kättböle, the seasonal effects on the JERS backscatter were studied and the implications for stem volume retrieval were analysed.

Test sites						
	Kättböle	Kättböle	NFI area	Tuusula	Bolshe-2	Bolshe-4
Area [km ²]	5.5	5.5	4235	20	262	246
Unit area	Stands	Plots	Plots	Stands	Stands	Stands
Stem volume [m ³ /ha]	8 - 335	6 - 332	5 - 346	3 - 535	5 - 400	15 - 400
Mean – Standard deviation [m ³ /ha]	135 / 76	144 / 81	164 / 94	257 / 172	220 / 116	161 / 116
Standard error	18 %	-	-	> 20 %	NA	NA
Tree height [m]	2 - 22	-	-	0 - 26	-	-
Stands / plots	42	216	166	37	147	161
Stand size	2 – 14 ha (32 pixels)	< 314 m ²	< 314 m ²	1.25 – 7 ha (> 20 pixels)	> 8 ha (> 32 pixels)	> 8 ha (> 32 pixels)

Table 3.1. Characteristics of the investigated test sites. Stand size refers to the size of the stand after the erosion of one or two pixels along the perimeter. NA stands for “not available”.

	Kättböle / NFI area	Tuusula	Bolshe-Murtinsky
ERS imagery	Backscatter: 18 InSAR: 9 (June 1995 – April 1996)	Backscatter: 16 InSAR: 8 (September 1995 – July 1996)	-
JERS imagery	Backscatter: 9 InSAR: 6 (April 1997 – August 1998)	Backscatter: 3 - (February 1997 – June 1997)	Backscatter: 9 - (January 1994 – August 1998)

Table 3.2. Number of SAR and InSAR images available for each test site and period of acquisition.

Kättböle / NFI area		Tuusula	
11-12 June 1995	T≈10 °C, WS < 5 m/s, Rainfall	86 m	9-10 September 1995 T≈11 °C, WS < 6 m/s, Rainfall
16-17 July 1995	T≈15 °C, WS < 4 m/s, Rainfall	16 m	14-15 October 1995 T≈8 °C, WS < 6 m/s, Rainfall before first acquisition
20-21 August 1995	T≈15°C, WS < 3 m/s, Clouds at first acquisition	75 m	2-3 March 1996 T≈-5 °C, WS < 4 m/s, SD: 32 cm
24-25 September 1995	T≈10 °C, WS < 4 m/s, Rainfall before first acquisition	219 m	29-30 March 1996 (a) T≈-1 °C, WS < 4 m/s, SD: 36-40 cm, Snowfall
29-30 October 1995	T≈0 °C, WS < 2 m/s, Rainfall before first acquisition Clouds at second acquisition	18 m	6-7 April 1996 T≈5 °C, WS < 4 m/s, SD: 30 cm Melting snow, Refreezing
12-13 March 1996 (a)	T≈-5 °C, WS < 5 m/s, SD: 10 cm,	220 m	17-18 April 1996 (a) T≈4 °C, WS < 3 m/s, SD: 0 cm, Melted snow
17-18 March 1996	T≈-2 °C, WS < 2 m/s SD: 10 cm, Snowfall before first acquisition Clouds at first acquisition	66 m	15-16 June 1996 T≈15 °C, WS < 7 m/s Rainfall
16-17 April 1996 (a)	T≈8 °C, WS < 4 m/s Refreezing	74 m	20-21 July 1996 T≈15 °C, WS < 5 m/s, Rainfall
21-22 April 1996	T≈13 °C, WS < 4 m/s Little precipitation Clouds at first acquisition	55 m	

Table 3.3. Weather conditions at acquisition and normal component of the baseline for the ERS passes over the test sites. T: temperature, SD: snow depth, WS: wind speed. "Refreezing" indicates cases of temperature oscillating around 0 °C between the two acquisitions. "Precipitation" indicates either rainfall or snowfall. (a) stands for ascending orbit.

Kättböle		Bolshe-Murtinsky		Tuusula	
15 April 1997	T \approx 1°, SD: 9 cm Precipitation	6 January 1994	T \approx -17°, SD: 39 cm, Snowfall	17 February 1997	T \approx -9°, SD: 25 cm
29 May 1997	T \approx 7°, Rainfall	19 February 1994	T \approx -17°, SD: 45 cm, Snowfall	16 May 1997	T \approx 11°, Rainfall
12 July 1997	T \approx 18°	14 October 1996	T \approx -4°	29 June 1997	T \approx 17°
8 October 1997	T \approx 12°, Rainfall	27 November 1996	T \approx -21°, SD: 25 cm, Snowfall		
4 January 1998	T \approx 2°, SD: 5 cm Melting snow Precipitation	10 January 1997	T \approx -23°, SD: 45 cm		
17 February 1998	T \approx -2°, SD: 25 cm, Precipitation	23 February 1997	T \approx -16°, SD: 53 cm		
2 April 1998	T \approx 1°, SD: 0 cm, Precipitation before acquisition	8 April 1997	T \approx 10°, Probably snow melt		
16 May 1998	T \approx 19°	22 June 1998	T \approx 22°, Rainfall		
12 August 1998	T \approx 21°	5 August 1998	T \approx 19°, Rainfall		

Table 3.4. Weather conditions at the time of JERS acquisitions over the test sites. T: temperature, SD: snow depth, WS: wind speed “Precipitation” indicates either rainfall or snowfall.

Chapter 4

SAR and InSAR in boreal forests

The backscatter and the coherence of a forest depend on the properties of the SAR and on the environmental conditions of the imaged area. For environmental conditions we refer to weather conditions at acquisition and dielectric properties of the forest. Frequency, polarisation and incidence angle determine the type of scattering. The strength of the scattering is determined by the weather conditions and the dielectric properties of the forest. Being a combination of two SAR images, the repeat-pass coherence is very sensitive to the temporal interval between acquisitions and the environmental conditions at and between the two acquisitions. Finally, scattering and the way scattering changes in time should be directly influenced by the tree species specific structures.

This Chapter provides a background on radar scattering and InSAR decorrelation mechanisms in forests, followed in both cases by results illustrating the effect of weather conditions on the backscatter and the coherence. This Chapter does not deal with SAR and InSAR phase, to which Chapter 8 is dedicated. Section 4.1 introduces the fundamentals of radar scattering in a forest, focusing on the mechanisms dominant at C- and L-band for the ERS and JERS configurations respectively. The extensive set of SAR and InSAR images available over several test sites allowed a thorough description of the weather effects on ERS and JERS backscatter and a comparison of results (Section 4.2 and 4.3). Section 4.4 discusses the decorrelation mechanisms in a forest; particular emphasis is given to the effect of environmental conditions and temporal interval between acquisitions on ERS and JERS coherence in Sections 4.5 and 4.6 respectively. Finally, the effect of the tree species structure on the backscatter and the coherence is analysed in Section 4.7, where investigations concerning the identification of boreal tree species using ERS and JERS signatures are reported.

4.1 Forest scattering mechanisms

The total backscattered power from a forest is a sum of echoes returned towards the radar by a large number of various elements distributed within the tree canopy and on the ground. This complex system of contributions can be summarised in terms of scattering mechanisms occurring in a forest (see Figure 4.1):

- Direct scattering from the crown (tree canopy, branches and trunks)
- Direct scattering from the ground
- Double bounce crown-ground
- Double bounce trunk-ground

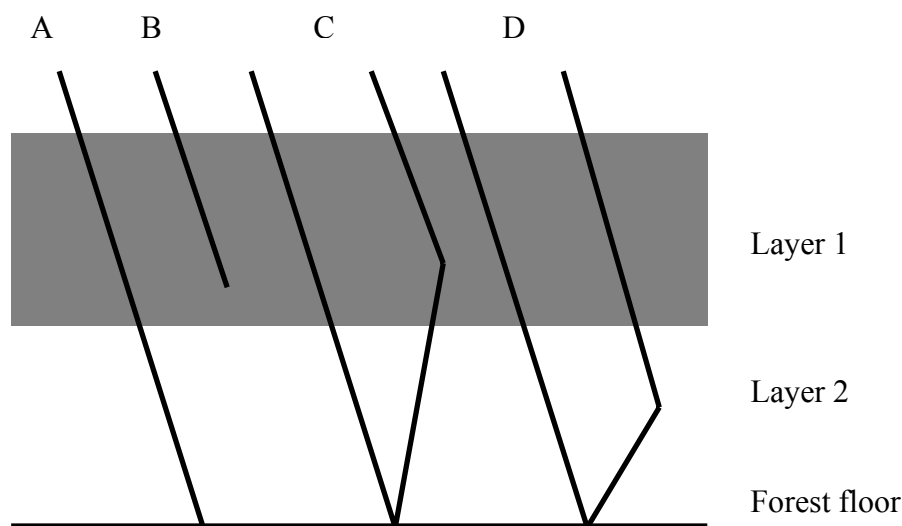


Figure 4.1. Backscatter in forested areas. A represents the backscatter from the ground, through the canopy, B is the direct reflection from the canopy. C and D represent the trunk-ground and canopy-ground reflections. At C-band, solutions A and B are dominant. At L-band, besides A and B, solutions C and D can be significant.

The dominance of one or few mechanisms depends primarily on the frequency used. At high frequency, the electromagnetic wave is strongly absorbed within the first layers of vegetation, thus making the contribution from branches and trunks as well as the direct contribution from the ground and the double bounces negligible. At lower frequencies, the deeper penetration of the wave into the canopy decreases the effect of surface scattering at the air-canopy interface on the total backscatter. Echoes from the main branches, from the ground and double-bounces canopy-ground and trunk-ground become more and more dominant.

The short wavelength of C-band (5.66 cm) is comparable to the size of the elements in the upper part of the tree canopy (needles, twigs, small branches and leaves). Hence, the backscatter can be considered mainly as surface scattering coming from the treetops. The strong attenuation of the wave in the upper layers of the canopy makes other scattering sources negligible. Ground contribution is related to gaps within the canopy. At L-band (23.5 cm) volume scattering and the ground contributions are more important. The wave partly penetrates the upper layers of the canopy, interacting with the main branches. It is not clear how much double-bounce effects between trunk and ground influence the total echo (see Chapter 5).

As mentioned in the Introduction, the main advantage of using SAR is its capability of acquiring data at any meteorological condition. Nevertheless, this property does not mean that the radiometry of the image is unaffected by the weather conditions at acquisition. It is well known that the SAR backscatter shows different patterns depending on whether the image has been acquired under dry conditions, at temperatures well above the freezing point or under thawing conditions. Just as an example, (WAY *et al.*, 1994) showed measurements of the dielectric constant real part in stems of different tree types. In correspondence of the plant fluid, the values were significantly lower under frozen conditions. A frozen medium is transparent to an incoming wave, thus affecting the backscatter. Obviously the effect of specific meteorological conditions depends on frequency used, polarisation and incidence angle.

So far the scattering properties have been presented for a dense forest, i.e. a fully grown forest, for which the canopy covers the ground so that the interaction with an incoming wave occurs within the canopy. In sparse forests, i.e. in forest where the forest canopy is characterised by large gaps, the backscatter is mainly related to the power echoed back to the radar by the forest floor. Dielectric properties and roughness of the ground determine the power of the backscattered signal. For increasing frequency the real part of the dielectric constant decreases so that the scattering strength decreases. A rougher ground surface is characterised by stronger scattering strength.

The backscatter of sparse and dense forests has been highlighted throughout the figures in this Chapter by two lines. Solid lines have been used for forests with stem volume below 50 m³/ha, i.e. for forests having a non-negligible ground-contribution. Dashed lines represent dense forests, i.e. forests with stem volume close to the biggest measured value. The threshold for the dense forest class is dynamic, depending on the stem volume distribution at each test site. For example in Kättböle, where the highest measured stem volume is 335 m³/ha, forest stands with stem volume above 250 m³/ha were included in the class. The same approach has been used for describing the run of coherence.

Both thresholds for the sparse and the dense forest represented a trade-off between having a statistically sufficient number of samples in each class but still the structure of the forest stands could be as similar as possible in order to remove the dependence of the backscatter/coherence from any biophysical parameters.

In particular, for sparse forests the choice of the threshold was crucial. Considering the strong dependence of both the backscatter and the coherence upon stem volume, the sparse forest class going from 0 to 50 m³/ha was not the optimal choice. In this interval there is a strong dependence of both parameters to stem volume (see Chapter 6). Rigorously speaking a slightly lower threshold should have been used (for example 20 m³/ha). Nonetheless the number of stands included in the class would have been too limited.

4.2 ERS backscatter

The ERS backscatter in boreal forests has been widely analysed in several publications, which showed the small dynamic range (i.e. the difference between sparse and dense forest backscatter), the effect of soil moisture on the ground backscatter and the changes in the vegetation backscatter at freeze and thaw events (see for example (KASISCHKE *et al.*, 1994; RIGNOT *et al.*, 1994a; HARRELL *et al.*, 1995; PULLIAINEN *et al.*, 1996; WAY *et al.*, 1997; DUGUAY *et al.*, 1999)). In this thesis the ERS backscatter images have been primarily considered as support to interpret the properties of forest coherence. Therefore, only those aspects necessary for the understanding of the coherence signatures have been reported.

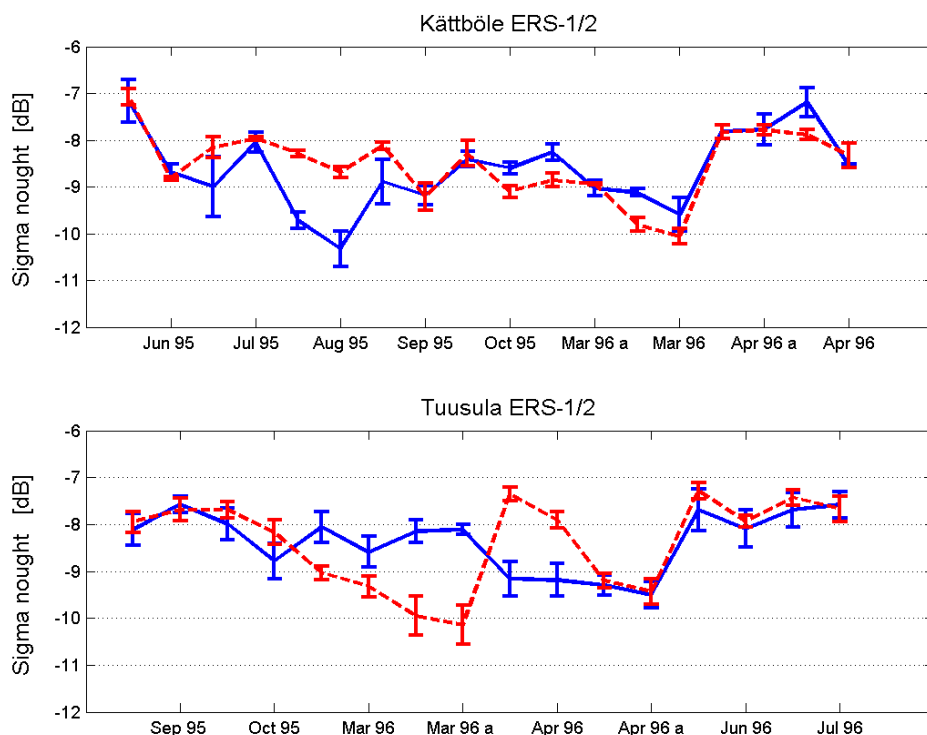


Figure 4.2. Run of ERS backscatter in sparse and dense forests between June 1995 and July 1996. The two types of forests are represented by the solid and the dashed line respectively. Sparse forests are forest stands with stem volume below 50 m³/ha. Dense forests are forest stands where stem volume is higher than 250 m³/ha in Kättböle and 450 m³/ha in Tuusula.

Figure 4.2 shows the changes in sparse and dense forests backscatter over a timeframe of approximately one year in Kättböle and Tuusula. As expected, the dynamic range is small. C-band waves interact with the treetop elements, thus having low sensitivity to forest attributes (see results presented in Chapter 6 and 7 as well). At the two test sites the dependence upon environmental conditions was similar and in line with previous investigations carried out in other areas. The backscatter in dense forests was mainly affected by the dielectric properties of the tree fluids (i.e. frozen or unfrozen state). The backscatter in sparse forests was indeed determined by the dielectric properties of the forest floor (snow cover and soil moisture). Since almost all images were acquired when the ground was either wet or covered with wet snow, it has not been possible to compare with backscatter values typical of dry-unfrozen conditions.

In dense forests the backscatter was rather constant, around -8 dB, and decreased when the temperature was below the freezing point (October 1995 in Kättböle and March 1996 at both sites). The drop of backscatter is explained in terms of the changed dielectric properties of leaves, needles and small branches. The water content determines the high dielectric constant of the scatterers. When the temperature is below 0 °C, the water freezes and the canopy becomes more transparent to the incoming wave. The transition from sub-zero to above-zero temperatures is clearly shown by the March and April images acquired over Kättböle, for which the backscatter increased with 2-3 dB. Similar results were obtained from a multi-temporal set of ERS-1 images acquired during freeze/thaw events in Alaskan taiga forest (RIGNOT, *et al.*, 1994a), in Finnish boreal forest (PULLIAINEN, *et al.*, 1996) and in sub-arctic forest (DUGUAY, *et al.*, 1999). In (WAY, *et al.*, 1997) the relationship between forest backscatter and thawed water in the stems was investigated. The backscatter rose when thaw started but did not drop when temperatures below 0 °C were measured in the stem. A second increase in backscatter occurred in spring but it was not clear whether it was caused by stem thaw. The backscatter in dense forest therefore seems to be an indicator of periods of tree activity.

In Tuusula, an interesting situation could be observed. Although in April, the temperature constantly rose from values around 0 °C (6-7 April) to $3-4$ °C (17-18 April), the first pair of images showed a backscatter typical of unfrozen conditions, whereas for the second pair the backscatter had returned to values observed during the winter. Since it is not possible that the plant fluid first thawed and then refroze, it can be argued that the high forest backscatter in the first pair was due to melting snow on the trees. Weather data report a strong decrease of the snow pack on the ground, which in turn made us assume that a similar situation occurred on trees. Hence, the high backscatter could be considered as a combined effect of melting snow and frozen vegetation dielectric properties.

Compared to the backscatter in dense forests, the backscatter in sparse forests shows larger variability and more pronounced dependence on the season. In case of rainfall or thaw, the moisture content of the soil increases and so does the dielectric constant. The backscatter is in such cases comparable to the dense forest backscatter or even

higher (PULLIAINEN, *et al.*, 1996). Snow can significantly affect the backscatter. At C-band, dry snow is transparent to the radar wave, which therefore interacts with the (frozen) ground, giving rise to a low backscatter. For wet snow the scattering occurs mainly at the air-snow interface and is influenced by the snow roughness. For increasing water content and surface roughness, the backscatter increases.

Several images acquired after or during rain precipitation were characterised by similar levels of backscatter in sparse and dense forests. When snow covered the ground, the backscatter was higher than in dense forests, which could be due either to partial snow wetness or snow roughness at the air-snow interface (see the March 1996 images at both sites). Cases of snowmelt (April 1996 at both test sites) were characterised by rather high backscatter, in particular in Kättböle, where probably the soil moisture content was higher than in Tuusula.

4.3 JERS backscatter

Since JERS operates at L-band and with a shallower incidence angle, the backscatter in forested areas is more sensitive to the forest structure and less to ground surface roughness, soil moisture and snow cover. Hence, the backscatter from dense forests is always stronger than from sparse forests and we can observe a larger dynamic range.

In this Section JERS observations from Kättböle, Bolshe-Murtinsky and Tuusula are discussed and compared. Over Kättböle and Tuusula the available images were mostly acquired between spring and fall, for dry-unfrozen conditions, whereas over Bolshe-Murtinsky more than half of the images available were acquired during the winter, at temperatures well below the freezing point. Furthermore, for each test site, several acquisitions were characterised by temperature around the freezing point, in conjunction with freeze or thaw events. In Figure 4.3 we report the run of JERS backscatter in Kättböle and Bolshe-Murtinsky. A graph for Tuusula is not included due to lack of calibrated data, which did not allow a full comparison with the other two test sites. Nevertheless, it has been possible to compare behaviours and trends due to seasonal dynamics.

Figure 4.3 shows the clear difference between the backscatter in sparse and mature forests, the little spread of measurements, expressed by the short error bars, and the weaker dependency of the ground backscatter upon several environmental conditions (for example snow cover and moisture content of the ground) in comparison to C-band. Similar results were reported in (HARRELL, *et al.*, 1995), where the influence of wet ground was stronger on the ERS than on the JERS backscatter, and in (BAKER & LUCKMAN, 1999), where multi-temporal EMISAR data acquired at 50° incidence angle was more consistent at L- than at C-band.

For dry-unfrozen conditions both in sparse and dense forests the backscatter was found to be higher than for winter-frozen conditions. A frozen canopy and a frozen ground scatter with less power because the dielectric constant is much smaller. Moreover, an incoming wave penetrates the canopy deeper and the percentage of

ground seen by the radar increases. Dry-unfrozen conditions occurred in Kättböle, between May and October 1997 and then again starting in May 1998. The backscatter in dense and sparse forests was at around -6 and -8 dB respectively. Winter-frozen conditions were observed in Bolshe-Murtinsky between January and February 1994 and between November 1996 and February 1997. The backscatter was clearly lower in both forest types, being at around -10 and -11 dB respectively, which shows that the dynamic range had decreased as well. Similar results were reported in (PULLIAINEN *et al.*, 1999) using a set of JERS images for a Finnish forest and in (RIGNOT *et al.*, 1994b) where 35° incidence angle AIRSAR data from Alaska showed an increase of 6 dB from winter-frozen to spring conditions.

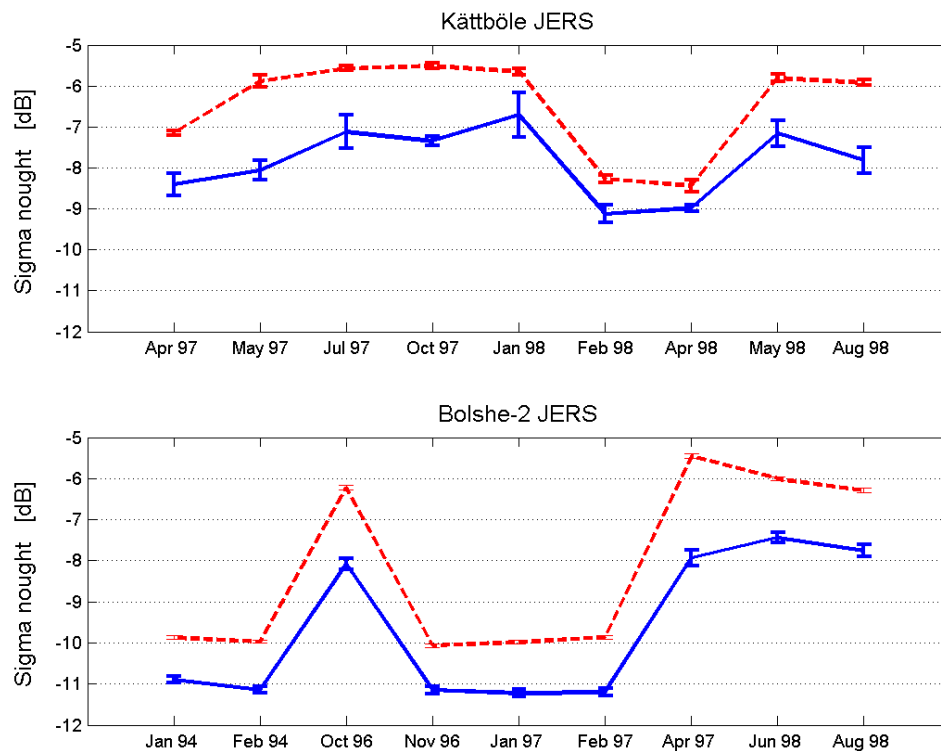


Figure 4.3. Run of JERS backscatter in sparse and dense forests. The two types of forests are represented by the solid and the dashed line respectively. Sparse forests are forest stands with stem volume below $50 \text{ m}^3/\text{ha}$. Dense forests are forest stands where stem volume is higher than $250 \text{ m}^3/\text{ha}$ in Kättböle and $350 \text{ m}^3/\text{ha}$ in Bolshe-Murtinsky

The only clear case of freezing was registered in Bolshe-Murtinsky (October 1996). The backscatter in sparse forests was similar to values measured for winter-frozen weather, whilst dense forests still showed a backscatter typical of unfrozen conditions. Probably the fluids in the trees were still active, whereas the moisture in the ground had already turned to the solid state.

Cases of thaw were reported both in Kättböle (April 1997, January, February and April 1998) and in Bolshe-Murtinsky (April 1997). Thaw events could be easily characterised in Bolshe-Murtinsky but not in Kättböle because several meteorological events occurred at the same time, influencing the backscatter. In Bolshe-Murtinsky the temperature had been above 0 °C for some days before the acquisition. Compared to the previous acquisition, the backscatter increased, reaching a level typical of unfrozen conditions. In Kättböle we could observe several behaviours. In April 1997 and January 1998 the temperature was around the freezing point, a thin snow layer covered the ground and precipitation occurred. The surprisingly high backscatter in both sparse and dense forests should be due to high dielectric constant of both ground and canopy, which could be explained in terms of very wet ground and tree activity. In February and April 1998, the backscatter was lower but not as low as for typically frozen conditions. A 25 cm thick snow layer together with fresh snow in the first case and a rather wet ground in the second case should explain the results.

4.4 Forest decorrelation mechanisms

At high frequencies the signal echoed by a forest towards the radar is likely to change on a short timescale, due to the typical temporal instability of the scatterers within the forest canopy. In a repeat-pass configuration, the correlation between two backscattered signals from a forest resolution cell should therefore be low. At C-band this assumption can be considered generally valid because of the high attenuation of the signal within the first few metres of the canopy. At L-band the signal will still be mainly returned by the canopy but the interaction with relatively more stable elements should result in a slightly higher degree of correlation. Besides the temporal decorrelation, it should not be forgotten that volume decorrelation becomes significant for increasing wavelength.

Movements of scatterers within a resolution cell in a vegetated area take a few seconds so that fully grown forests are commonly characterised by total decorrelation, whichever repeat-pass period characterises an InSAR system. For sparse forests the combined effect of vegetation and ground decorrelation becomes indeed crucial to understand the measured coherence.

If we interpret the decorrelation as a change in the scattering, ground is much more stable than vegetation. Changes can be due to movements of scatterers within the cell. In boreal forests shrubs and small trees form the understory, which is characterised by a limited temporal stability, thus causing partial ground decorrelation. Nevertheless, ground decorrelation is mostly related to changes in some of the properties of the scatterers within the ground resolution cell. An increase in snow water equivalent or soil moisture after precipitation causes a different arrangement of scatterers within the cell and alters the signal scattered towards the radar. In this case we commonly speak of decorrelation due to dielectric changes.

An important role on the total forest coherence is played by snow. At C-band the coherence of snow-covered surfaces is high if the properties of the snow have not

changed between the two acquisitions, independently of whether the snow is dry or wet. Changes of snow water equivalent or surface roughness alter the dielectric and geometric properties of the snow, causing decorrelation (STROZZI *et al.*, 1999). Compared to C-band the lower sensitivity of L-band to dry snow should imply that the coherence is determined by the underlying ground surface. Volume decorrelation has to be considered in wet snow covers. Temporal decorrelation can be expected in case of strong changes in the water content, because of changes in the scattering mechanisms within the snow volume.

4.5 ERS Coherence

The whole ERS mission has provided interferometric images with several acquisition intervals. During the five years long “tandem” mission, pairs could be formed with a temporal distance as short as one day. Besides the nominal 35-days interval, repeat-pass intervals of a few days were possible during the ERS-1 ice missions (3, 6, 9, 12 days, etc.).

In dense forests even the shortest ERS repeat-pass cycle is sufficient for observing an almost complete decorrelation of dense vegetated areas. Wind is considered the main source of decorrelation. In (CASTEL *et al.*, 2000; ASKNE *et al.*, 2001; ASKNE *et al.*, 2003) coherence and wind speed had a rather good correlation. In sparse forests the ERS one-day coherence is generally higher than in dense forests, unless meteorological events at and between the two acquisitions, due to rain, snowfall or snowmelt, have occurred. These cause partial or complete ground decorrelation. For stable weather conditions, coherence decreases for longer intervals, up to 10-15 days, because of increasing changes in the ground dielectric properties. For even longer intervals, of the order of one or more nominal repeat-pass cycles, commonly complete decorrelation of the scene occurs (SMITH *et al.*, 1996). Long-term coherence images from Kättböle and Tuusula confirmed previous results.

The relationship between dielectric properties of the trees and coherence is not as clear. During winter, when the temperature is constantly under the freezing point, trees are frozen; therefore, they are more transparent to the electromagnetic wave and should have high coherence. Periods of freeze/thaw events should coincide with changes in the tree physiology; hence, a relation between tree physiology and coherence seems to be reasonable. Nevertheless, these assumptions have not been supported by clear experimental evidence due to the noisiness in the observations.

Figure 4.4 illustrates how coherence changes throughout a year in Kättböle and Tuusula. As expected, dense forests were always more decorrelated than sparse. Coherence in sparse forests was around 0.7 unless meteorological events occurred. Heavy rainfall (June and July 1995 in Kättböle, September 1995 in Tuusula) and snowmelt (first April 1996 pair in Tuusula) were characterised by complete decorrelation. Rain precipitation occurred at the time of several acquisitions over Tuusula (October 1995, and the last three pairs from 1996) and Kättböle (September 1995) causing a partial change in the dielectric properties of the ground. As a consequence, sparse forests appeared partially decorrelated.

Coherence in dense forests was generally below 0.3 for unfrozen conditions. Higher coherence was measured when temperature was around or below the freezing point (October 1995 and first pair from April 1996 in Kättböle; first pair from March 1996 in Tuusula). Light winds were measured so that the only possible explanation for this behaviour is the larger penetration of the wave to more stable parts of the canopy. A similar behaviour was shown by (KOSKINEN *et al.*, 2001) at a test site located in southern Finland. The mean coherence in fully grown forests was equal to 0.5 in one pair acquired at sub-zero conditions. Despite the rather limited amount of examples available, these results show that the ERS one-day coherence can be used to infer the physiological state of a forest.

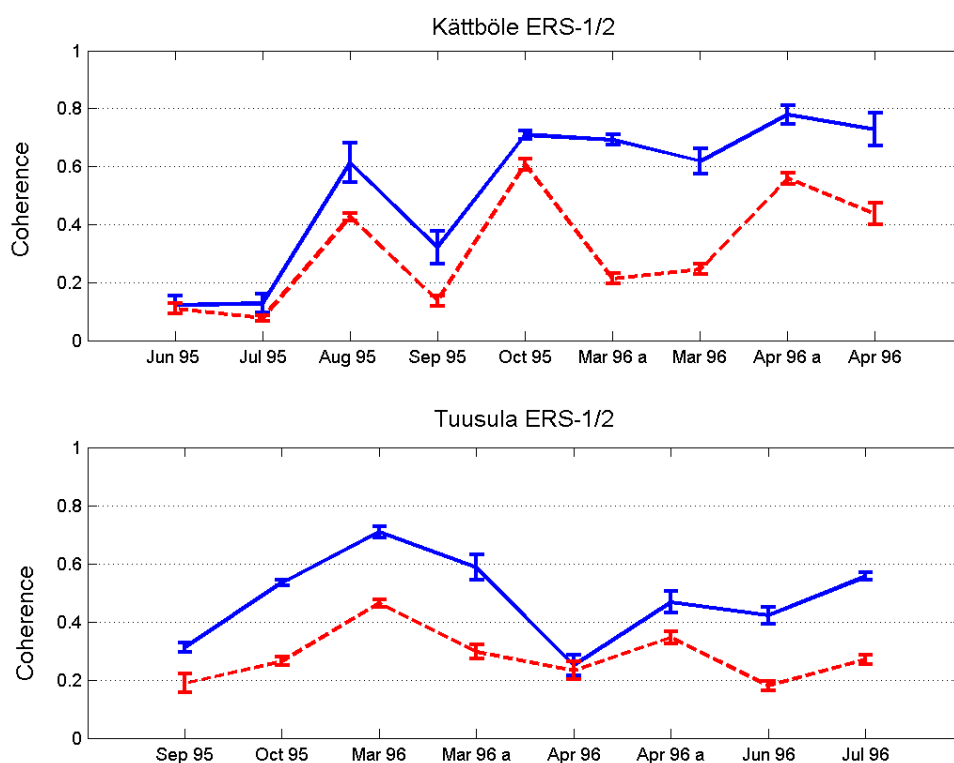


Figure 4.4. Run of coherence in sparse and dense forests. The two types of forests are represented by the solid and the dashed line respectively. For the definition of sparse and dense forest see Figure 4.2.

4.6 JERS coherence

The JERS mission was characterised by a long repeat-pass interval and by baselines that in most cases were too long for interferometric applications. Hence, JERS interferometric pairs suffer from both relevant temporal and volume decorrelation. These two factors have limited the investigations on JERS coherence in forested areas. A few studies have been carried out for tropical forest monitoring in Brazil (see (LUCKMAN *et al.*, 2000)). In Swedish and Finnish boreal forests (ASKNE *et al.*,

1999) has analysed the signatures of several land-covers, whereas in Siberia (ERIKSSON *et al.*, 2003) has shown a relatively higher coherence in regenerating forests than in dense forests, being consistently much higher in pairs acquired during winter.

JERS coherence was evaluated in Kättböle but the weather effects or too long baseline for an interferometric pair strongly affected all pairs that could be formed. Both dense and sparse forests were characterised by total decorrelation, except in one case when the coherence in sparse forests was measured at around 0.4 (ASKNE, *et al.*, 2003). These results were expected because of the frequent weather changes occurring in Sweden.

4.7 Tree species identification

Tree species discrimination using SAR data relies on the idea that each species has its own structural characteristics (distribution and amount of branches, twigs, needles and leaves), thus influencing the total backscattered signal.

Using a single SAR image, it has been proved that it is not possible to distinguish with reasonable accuracy between boreal tree species or even to separate broadleaf from coniferous covers. Only polarimetric data acquired at different frequencies seems to be accurate enough for biodiversity mapping. In (RANSON & SUN, 1994) Principal Component Transformation (PCT) has been used on quad-pol AIRSAR C-, L- and P-band data to reduce the amount of imagery and speckle effects. With a Maximum Likelihood Classifier softwood was separated from hardwood with high accuracy. Nevertheless it was not possible to distinguish between the two major hardwood species (hemlock and spruce). The same approach was used on SIR-C/XSAR data (polarimetric imagery acquired at X- C- and L-band) together with Landsat TM images in (RANSON *et al.*, 1997). The authors concluded the pine and aspen could be separated with an accuracy of approximately 95% whilst only 71.4 % of the spruce forests were correctly classified, probably because of stand size and site conditions. A set of SIR-C polarimetric images acquired at C- and L- band over the Western Sayani Mountains in Siberia was analysed in (RANSON *et al.*, 1999). Three methods were tested to classify the data, two of them being based on a reduction of images by means of PCT. Transformed imagery provided more accurate results, in line with the figures so far reported. ML classification of single images instead reached the best accuracy in the deciduous class and the mixed class with 61% of correctly identified stands. Using L-band data, HH polarised, acquired at several weather conditions over a Canadian boreal forest site, (RANSON & SUN, 2000) reported higher classification accuracy for pine, spruce and aspen class (between 68% and 95%). Nevertheless the results were not temporally consistent.

Coherence should be influenced by the tree species since each species should have a specific oscillation in response to wind forces. Moreover, in deciduous species leaves should be active agents in decorrelating a scene (WEGMÜLLER & WERNER, 1995; CASTEL, *et al.*, 2000; PROISY *et al.*, 2000), thus enabling the separation between coniferous and broadleaf forests. Using ERS backscatter and coherence (TÖRMÄ,

1999) identified pine and spruce stands with high accuracy. However, this study did not take into account that the two classes were characterised by different stem volume intervals.

An analysis of tree species discrimination was carried out in Kättböle and Tuusula using all types of images available. For the analysis stands with stem volume below 100 m³/ha were not considered. This threshold was a trade-off between having a sufficient number of stands for the investigation and a set of stands for which only the structural differences of the trees would have affected the backscatter and the coherence.

The limited number of stands allowed the creation of two classes only:

- Class 1: spruce with a percentage > 50%
- Class 2: spruce with a percentage < 50% (i.e. pine or birch or mixed forest types).

Other classes could not be determined because of too few stands with a percentage of a species above 50%. Results did not show a clear separation between the two classes, proving that that tree structures do not have any influence on the SAR and InSAR signatures and that tree species discrimination is not feasible using single ERS or JERS backscatter and coherence images.

4.8 Conclusions

The scope of this Chapter was to investigate the properties of the ERS C-band and the JERS L-band backscatter and repeat-pass coherence in boreal forests. Three test sites located in Sweden, Finland and Siberia were used for the purpose, which allowed a comparison of results in order to check for spatial consistency of the measurements. In order to give a full view of the factors affecting the values observed in boreal forests, two types of forests were considered: dense and sparse forests. Dense forests are characterized by fully developed tree crowns that cover almost completely the ground. Because of the strong attenuation within the canopy at C- and L-band, the backscatter and the coherence are mostly related to the scattering properties of the vegetation. In sparse forests instead the scattered signal is governed by the properties of the forest floor.

Because of the longer wavelength L-band backscatter has higher sensitivity to the forest structure and is less affected by the forest floor roughness. This explains the larger dynamic range of the JERS backscatter (2-3 dB in comparison to 1-2 dB difference for the ERS backscatter) and the consistent higher values in dense than in sparse forests. Nevertheless, the backscatter difference is not simply dependent on the sensor frequency but on the environmental conditions as well. These are fundamental to explain the signatures of the coherence, which is also affected by the temporal interval between the two acquisitions. Short repeat-passes, as the one-day interval during the ERS “tandem” mission, preserve the coherence at least in sparse forests. The 44-days interval between two JERS passes is instead too long for

observing any coherence, at least in Sweden and Finland because of the frequent changes in the weather patterns.

In dense forests both ERS and JERS backscatter are rather constant under unfrozen conditions and decrease when the temperature is below the freezing point because of the smaller dielectric constant of the vegetation. Because of the lower frequency, the JERS backscatter is stronger and shows a more marked difference between frozen and unfrozen conditions (approximately 3-4 dB difference). Hence, the L-band backscatter from dense forests seems to be a good indicator of freeze and thaw events.

The ERS coherence is influenced by the temporal stability of the canopy. The unstable nature of the upper part of the canopy, mainly due to wind-induced motions, causes low coherence. Nevertheless, for frozen conditions coherence increases, probably because of the deeper penetration into the canopy of the electromagnetic wave, which interacts with more stable scatterers. More investigations at sub-zero temperatures are needed in order to confirm the results obtained.

In sparse forests, the moisture content of the forest floor is the main variable affecting both the backscatter and the coherence. Images acquired when precipitation in form of rain occurred show the highest backscatter. At C-band it is even possible to observe higher backscatter than in dense forests. Because of the stable nature of the scatterers on the ground, the coherence is much higher than in dense forests. Changes in ground moisture cause decorrelation, which seems to increase for increasing amount of precipitation.

At the latitude of boreal forests an important role on backscatter and coherence properties is played by snow, which covers the ground for long periods of the year. Snow type and snow roughness strongly affect the power scattered back to the sensor and the decorrelation, although the behaviour is different at C- and L-band. The rather high ERS backscatter measured in Tuusula and Kättböle seems to indicate a rather rough surface and non-negligible water content. The high coherence (0.7-0.8) can be explained in terms of the high temporal stability of the snow cover and the negligible volumetric effects. Coherence does not seem to be a good measure for snow parameters estimation but rather for thaw monitoring, when total decorrelation occurs. At L-band the dielectric properties of the snow pack have less effect. Nevertheless it was possible to observe large backscatter differences (around 2-3 dB) between dry snow in Bolshe-Murtinsky and wet snow in Kättböle. Freeze and thaw could be easily characterised, in particular in Bolshe-Murtinsky, because of the respectively strong decrease and increase in the backscatter.

Boreal tree species, i.e. coniferous pine and spruce, did not affect in a different way either the backscatter or the coherence. Analysis of biodiversity does not seem to be feasible using a single SAR or repeat-pass InSAR image.

Chapter 5

SAR and InSAR forest modelling: theory

The following two Chapters focus on modelling of SAR backscatter and InSAR complex coherence as function of forest parameters. In this Chapter two models are introduced and the theoretical background is discussed. Results from model fitting to SAR and InSAR data will be thoroughly described in Chapter 6.

Section 5.1 summarises the fundamentals of radar scattering presented in the previous Chapter in order to comprehend the main approaches to radar backscatter modelling of forests. In Section 5.2 and 5.3 the Water Cloud Model for the backscatter and the Interferometric Water Cloud Model for the complex coherence are derived. Both models are expressed as function of the area-fill factor. Nevertheless, since the area-fill factor is not commonly used as forest parameter, an alternative formulation in terms of stem volume is reported. Section 5.4 describes the main properties of the Interferometric Water Cloud Model to provide a background for the understanding of the results and the discussion presented in Chapters 6 and 8.

5.1 Forest backscatter modelling

The complexity of SAR backscatter does not allow the definition of a detailed forest scattering model that would include the contributions from as many scattering sources as possible. Models require a number of assumptions concerning the scattering elements (type, amount, distribution and dielectric properties) and the dominant scattering mechanisms.

Several models treat forests as a multi-layered medium, in which scattering elements, characterised by few geometrically simple shapes, are distributed. The total intensity is computed either as a coherent sum of the electromagnetic fields scattered back by each element (CHAUHAN *et al.*, 1991; FUNG, 1994) or as an incoherent sum of

energies using the radiative transfer theory (ULABY *et al.*, 1990a; KARAM *et al.*, 1992; McDONALD & ULABY, 1993; SAATCHI & McDONALD, 1997). The forest volume is generally divided into two or three layers (tree-top, crown, trunk) with discs representing the foliage and cylinders representing branches and trunks. Size, dielectric properties and distribution of discs and cylinders are determined on the basis of statistical models, allometric relationships and observations. The forest floor is either treated as a plane surface or includes a term to account for surface roughness.

Another approach generally found in literature models the vegetation as one or more homogeneous layers within which size, shape and distribution of the scattering elements are not specifically taken into account (ATTEMA & ULABY, 1978; RICHARDS *et al.*, 1987; PULLIAINEN *et al.*, 1994; ASKNE *et al.*, 1995). The scattering elements are treated as particles, uniformly spread within a volume representing the vegetation slab. These particles idealize the tree elements and are characterised by an attenuation cross section related to the type of forest under investigation. Such models are based on radiative transfer. The incoming energy in one layer of infinitesimal thickness is partly reflected back to the radar and partly transmitted to the lower layer. The amount of energy transmitted depends on the attenuating properties of the forest. The total backscattered power is given by the incoherent sum of the single contributions coming from each layer. If each layer has the same properties, the integration is straightforward. In such models the total forest backscatter is described in terms of the main scattering mechanisms and expressed as a function of a few forest parameters.

Because of the large number of forest variables, the former type of models is commonly used for backscatter simulation. The rather simple formulation of the backscatter as a function of a few forest parameters make the second type of models suitable for inversion, i.e. to provide estimates of forest variables using backscatter measurements.

5.2 Water Cloud Model

A simple model describing the relationship between forest backscatter and forest parameters is the Water Cloud Model (ATTEMA & ULABY, 1978). In the WCM vegetation is treated as a homogeneous medium filled with water droplets, over a horizontal plane surface representing the ground. The water droplets scatter part of the incoming wave towards the radar, attenuating it along its path into the vegetated slab. Being a very simple and idealised model, the scatterers have all the same properties, i.e. the same total attenuation cross section and radar cross section. The total contribution from the vegetation is an incoherent sum of the energies scattered at each layer. The vegetation contribution adds up to the backscatter coming from the ground, which in turn depends on the density of the cloud. A high density of particles will strongly attenuate the wave along its path through the canopy, so that the ground backscatter represents a negligible contribution to the total backscatter.

Far from being a correct and exhaustive description of the reality, these are the main properties of the WCM.

- ↗ It explains the total forest backscatter in terms of two scattering mechanisms: direct contribution from the vegetation and from the ground.
- ↗ It takes into account the predominance of surface/volume scattering by means of an attenuating term.
- ↗ It weighs the contributions from the vegetated slab and from the ground as a function of canopy density.
- ↘ It neglects higher order scattering mechanisms such as double bounces between vegetation and ground.
- ↘ It does not include gaps between trees (horizontal inhomogeneity) and the varying structure of the canopy along the vertical profile of a forest (vertical inhomogeneity).

In a similar way to the WCM, a simple model based on radiative transfer through a horizontal scattering and attenuating layer with gaps has been considered in this thesis (ASKNE, *et al.*, 1995) (Figure 5.1):

$$\sigma_{for}^o = (1-\eta)\sigma_{gr}^o + \eta[\sigma_{gr}^o T_{tree} + \sigma_{veg}^o (1-T_{tree})] \quad (5.1)$$

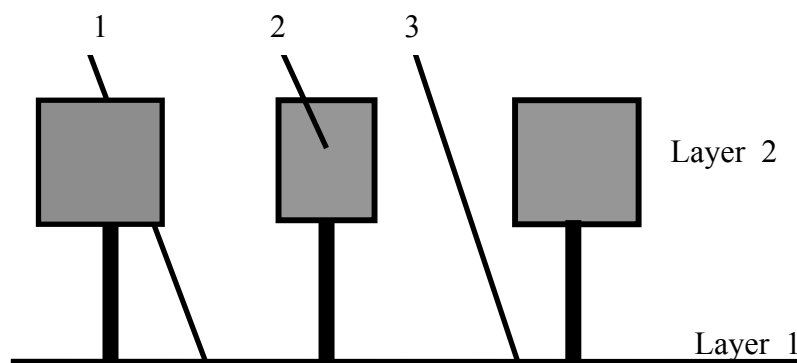


Figure 5.1. Scattering mechanisms in a forest with gaps: ground scattering attenuated by the tree (1), vegetation scattering (2), ground scattering through the gaps (3).

The forest backscatter, σ_{for}^o , is modelled as a sum of:

1. Direct scattering from the ground through the canopy gaps
2. Direct ground scattering attenuated by the canopy
3. Direct scattering from the forest canopy.

The first two terms form the ground contribution; the third expresses the vegetation contribution to the total forest backscatter. In order to take into account the gaps in the canopy, each term is weighted by the area-fill factor, η . This coefficient

represents the fraction of ground covered by tree crowns from the radar's perspective and is a forest property that should be independent from frequency and viewing angle. One method to measure area-fill factor is by thresholding photographs taken looking vertically upwards through the forest canopy (SMITH, 1998).

The coefficient T_{tree} represents the two-way transmissivity through the tree canopy. It expresses how much the incoming energy gets attenuated when it goes through the tree canopy. The two-way tree transmissivity can be written as $e^{-\alpha h}$, where α is the two-way attenuation per metre through the tree canopy and h is the thickness of the attenuating layer. In boreal forests, it can be assumed that thickness of the layer coincides with the tree height. The two-way attenuation per metre through the tree canopy can be easily related to the penetration depth, which is more commonly used to describe the attenuating properties of a medium. If α is given in dB/m, the two-way attenuation per metre can be converted into penetration depth, δ , by using the following equation:

$$\delta = \left(2 \cdot \ln 10^{\frac{\alpha}{10}} \right)^{-1} \quad (5.2)$$

The direct ground backscatter is given by the backscatter coefficient of the ground, σ_{gr}^o , weighted by the percentage of ground not covered by vegetation, $(1-\eta)$. The attenuated ground scattering is determined by the ground backscatter coefficient, attenuated by the vegetation layer, ηT_{tree} . The direct scattering from the vegetation is given by the backscatter coefficient of the vegetation layer, σ_{veg}^o , weighted by the area-fill factor.

In Equation (5.1) double-bounces and higher order reflections are not taken into account. This assumption is valid at C-band because of the strong attenuation of the wave within the first metres of the tree canopy. At L-band the larger penetration depth can involve a non-negligible effect of the trunk-ground double bounce on the total backscatter. Depending on polarisation, incidence angle and assumptions on the type of scatterers within the canopy and on the ground, different results have been obtained.

For eight coniferous stands imaged at 29.7°, (SUN & SIMONETT, 1988) conclude that the interaction of tree trunks and ground is fundamental for explaining the backscatter. Multi-angle simulations reported in (SAATCHI & McDONALD, 1997) show the dominance of branches and tree-ground double-bounces. Similar conclusions can be found in (SUN *et al.*, 1991), where the trunk-ground interaction in discontinuous coniferous forests is reported to increase for increasing incidence angle. Nevertheless, (SUN, *et al.*, 1991) and (KARAM, *et al.*, 1992) questioned how much the effect of a rough ground surface could alter the results. For loblolly pine forest (DOBSON *et al.*, 1992) observed that the backscatter is not dominated by the trunk-ground interaction. Using AIRSAR L-band data with an incidence angle between 40° and 50°, it was concluded that the main scattering comes from the branches.

The investigations reported in this thesis are based on the assumption that the double bounce is less important than the direct scattering from ground and vegetation. Previous investigations have showed the possibility of modelling L-band forest backscatter, considering these two contributions only (ASKNE, *et al.*, 1995; ISRAELSSON *et al.*, 1995; FRANSSON & ISRAELSSON, 1999). Although not fully correct, the assumption can be explained taking into account the coupled effect of the partial attenuation of the electromagnetic wave in the canopy and the non-perfectly flat ground in boreal forests. The rough topography of the ground can significantly deflect the double-bounce away from the radar while the thick and dense canopy can strongly attenuate the incoming wave. Support to the assumptions could be found in penetration depth values reported in (CHAUHAN, *et al.*, 1991; SHINOHARA *et al.*, 1992) (4 to 10 m). (FLEISCHMAN *et al.*, 1996) reported median two-way attenuation values for HH polarisation of 13 to 17 dB for mature forests at 30° to 45° depression angles. Similar values were obtained in (ULABY *et al.*, 1990b) where at an incidence angle of 40° one-way attenuation of approximately 10 dB was measured in mature pine forests with a 4 m thick crown. Concerning the effect of a rough ground on JERS double-bounce strength, (PULLIAINEN *et al.*, 1999) used a Water Cloud type of model in boreal forests. They found a double-bounce term in the model negligible, probably because of the rough ground. The combined effect of rough surface and strong attenuation in boreal coniferous and broadleaf types of forest explained the negligible double-bounces in AIRSAR data acquired at 35° incidence angle (RANSON & SUN, 1994). During freeze/thaw events, (WAY *et al.*, 1994) showed that the dominant scattering mechanism according to the MIMICS and the Van Zyl scattering models is the direct scattering from the crown for white and black spruce and balsam poplar.

Further support to the assumption was found in a study carried out in an area close to Kättböle. The importance of surface, volume and double-bounce scattering was investigated with polarimetric L-band imagery acquired by EMISAR. (BAKER & LUCKMAN, 1999) showed that volume scattering is predominant and double-bounces occur only in a few forests. The similar soil and forest type conditions at the two test sites were considered important to explain the “two-contributions” modelling approach used in Kättböle.

Both ground and vegetation backscatter coefficients are assumed to be constant in a forest. This is equivalent to saying that the variability of the scattering properties in a forest is neglected. At C-band the assumption is correct because only the upper part of the canopy contributes to the backscatter from the vegetation. At L-band we can interpret the vegetation backscatter as an “equivalent” vegetation coefficient obtained from the integration of the volume backscatter in the tree canopy.

In order to highlight the scattering components from the ground and the vegetation, Equation (5.1) can be rearranged as:

$$\sigma_{for}^o = \sigma_{gr}^o T_{for} + \sigma_{veg}^o (1 - T_{for}) \quad (5.3)$$

The two scattering components are weighted by the two-way transmissivity through the forest canopy, T_{for} . This coefficient expresses how much a wave penetrates into the vegetation considered as a uniform medium. Comparing Equations (5.1) and (5.3), the two-way forest transmissivity is given by:

$$T_{for} = [(1 - \eta) + \eta e^{-\alpha h}] \quad (5.4)$$

The first term takes into account the contribution due to the gaps between trees. The second term is related to the transmissivity through the single trees. At X- and C-band, microwaves get strongly attenuated within the first few metres of the tree canopy, thus making the term negligible (HENDERSON & LEWIS, 1998; ASKNE *et al.*, 1999; DAMMERT, 1999). In this case, Equation (5.4) can be simplified as follows:

$$T_{for} = 1 - \eta \quad (5.5)$$

The simple relationship between area-fill factor and two-way transmissivity measured from the helicopter borne scatterometer HUTSCAT has been illustrated in (ASKNE, *et al.*, 1999). Although long error bars characterised the measurements of both parameters, the two quantities clearly correlated.

Although the area-fill factor is a valid parameter for explaining the forest backscatter, it is not commonly measured and used in forest inventory. If the WCM is to be used for any inversion purpose, the model needs to be expressed in terms of a widely accepted forest parameter. Using HUTSCAT measurements, (PULLIAINEN, *et al.*, 1994) has expressed the two-way forest transmissivity as $e^{-\beta V}$, where V is the stem volume and β is an empirically defined coefficient. The total forest backscatter in Equation (5.3) can therefore be expressed as function of stem volume:

$$\sigma_{for}^o = \sigma_{veg}^o (1 - e^{-\beta V}) + \sigma_{gr}^o e^{-\beta V} \quad (5.6)$$

and Equation (5.4) can be rewritten as:

$$\eta = \frac{1 - e^{-\beta V}}{1 - e^{-\alpha h}} \quad (5.7)$$

Despite its more useful formulation for an application, the backscatter is only indirectly expressed in terms of the principal scattering agent, not taking into account that several forest structures can be characterised by the same stem volume. The reader can refer to Section 6.3.2 for a practical example.

5.3 Interferometric Water Cloud Model

The Interferometric Water Cloud Model was introduced in (ASKNE, *et al.*, 1995; ASKNE & SMITH, 1996; ASKNE *et al.*, 1997; ASKNE, *et al.*, 1999) and fully described in (DAMMERT, 1999; SANTORO *et al.*, 2002; ASKNE *et al.*, 2003). Similarly to the

Water Cloud Model, the IWCM expresses the total forest coherence as sum of two contributions coming from the vegetation and the ground:

$$\gamma_{for} = (1 - \eta) \gamma_{gr} \frac{\sigma_{gr}^o}{\sigma_{for}^o} + \eta \left[\gamma_{gr} \frac{\sigma_{gr}^o}{\sigma_{for}^o} T_{tree} + \gamma_{veg} \frac{\sigma_{veg}^o}{\sigma_{for}^o} \left(\frac{\alpha}{\alpha - j\omega} \right) (e^{-j\omega h} - T_{tree}) \right] \quad (5.8)$$

with σ_{for}^o being the forest backscatter given in Equation (5.1) and ω the InSAR system geometry coefficient:

$$\omega = \frac{4\pi B_n}{\lambda R \sin \theta} \quad (5.9)$$

where B_n represents the normal component of the baseline, R the slant range, λ the radar wavelength and θ the local incidence angle.

Despite its length and apparent complexity, the IWCM is a reasonably simple model. The IWCM explains the forest complex coherence using the straightforward approach presented in the WCM. It includes the vegetation contribution and the ground contribution for the parts of signal a) scattered from the forest floor directly seen through the gaps and b) attenuated by the tree canopy. Furthermore it takes into account volumetric decorrelation and InSAR geometry effects. Comparing with Equation (2.14), it is possible to observe that all decorrelation sources have been included in the model.

In order to get a clearer picture of the IWCM, the model is reported in terms of the ground and the vegetation components:

$$\Gamma_{gr} = (1 - \eta) \gamma_{gr} \frac{\sigma_{gr}^o}{\sigma_{for}^o} + \eta \gamma_{gr} \frac{\sigma_{gr}^o}{\sigma_{for}^o} T_{tree} \quad (5.10)$$

$$\Gamma_{veg} = \eta \gamma_{veg} \frac{\sigma_{veg}^o}{\sigma_{for}^o} \left(\frac{\alpha}{\alpha - j\omega} \right) (e^{-j\omega h} - T_{tree}) \quad (5.11)$$

The ground term is related to the temporal coherence of the ground, γ_{gr} , and the fraction of ground backscatter with respect to the total forest backscatter. The first term represents the coherence of the ground seen through the gaps; the second expresses the coherence of the signal scattered from the ground and attenuated by the canopy. The vegetation term in Equation (5.11) includes the three factors determining the total coherence due to vegetation: temporal effects, volume effects and InSAR geometry. The three components represent the coherence of the radar signal in a volume with a thickness equal to h and an attenuation given by α , seen from two positions separated by a baseline equal to B_n . The temporal component is given by the temporal coherence of the vegetation, γ_{veg} , weighted by the fraction of vegetation backscatter with respect to the total backscatter. As for the backscatter coefficient of the vegetation, γ_{veg} is assumed to be constant, i.e. independent from

horizontal and vertical heterogeneities. The volume decorrelation due to a scattering layer with attenuation α and height h is given by the first complex quantity in brackets (ASKNE, *et al.*, 1997). Finally, by analogy to topographic phase, the complex exponential in (5.11) includes the effect of InSAR system geometry, which is related to the fact that the radar is seeing a target characterised by a topography related to the forest height (see Chapter 8 for details).

The generalized formulation of the IWCM in Equation (5.8) can be simplified if the SAR frequency is high. As already mentioned, at high frequency the two-way attenuation per metre, α , is rather high so that the two-way tree transmissivity becomes negligible. In this case, the amplitude of the volume decorrelation is equal to 1 and Equation (5.8) becomes (see Appendix A):

$$\gamma_{for} = \gamma_{gr} \frac{\sigma_{gr}^o}{\sigma_{for}^o} (1 - \eta) + \eta \gamma_{veg} \frac{\sigma_{veg}^o}{\sigma_{for}^o} e^{-j\omega(h-\alpha^{-1})} \quad (5.12)$$

The first term represents the ground contribution, Γ_{gr} , whereas the second term expresses the vegetation contribution, Γ_{veg} . The approximation can be considered valid at C-band but not at L-band, for which the full IWCM must be used. At C-band however it must be noticed that for baselines at which $\alpha \cong \omega$ there is a non-negligible volume decorrelation and therefore it is not correct to use Equation (5.12).

The IWCM presented in Equation (5.8) describes the forest complex coherence as a function of area-fill factor. As for the Water Cloud Model, it is possible express the forest complex coherence and the two contributions in terms of stem volume by using the transformation given in Equation (5.7):

$$\gamma_{for}(V) = \gamma_{gr} \frac{\sigma_{gr}^o}{\sigma_{for}^o} e^{-\beta V} + \gamma_{veg} \frac{\sigma_{veg}^o}{\sigma_{for}^o} (1 - e^{-\beta V}) \left(\frac{\alpha}{\alpha - j\omega} \right) \left(\frac{e^{-j\omega h(V)} - T_{tree}}{1 - T_{tree}} \right) \quad (5.13)$$

$$\Gamma_{gr}(V) = \gamma_{gr} \frac{\sigma_{gr}^o}{\sigma_{for}^o} e^{-\beta V} \quad (5.14)$$

$$\Gamma_{veg}(V) = \gamma_{veg} \frac{\sigma_{veg}^o}{\sigma_{for}^o} (1 - e^{-\beta V}) \left(\frac{\alpha}{\alpha - j\omega} \right) \left(\frac{e^{-j\omega h(V)} - T_{tree}}{1 - T_{tree}} \right) \quad (5.15)$$

The simplified version of the model in Equation (5.12) becomes:

$$\gamma_{for}(V) = \gamma_{gr} \frac{\sigma_{gr}^o}{\sigma_{for}^o} e^{-\beta V} + \gamma_{veg} \frac{\sigma_{veg}^o}{\sigma_{for}^o} (1 - e^{-\beta V}) e^{-j\omega(h(V)-\alpha^{-1})} \quad (5.16)$$

In Equations (5.13), (5.15) and (5.16) the tree height has been expressed as function of stem volume, $h=h(V)$, in order to restrict the dependency of the total coherence on just one forest parameter. Equation (5.16) shows that for increasing stem volume, i.e. for a thicker canopy and a denser forest, the contribution from the ground decreases.

The vegetation term instead increases. The slope in both terms depends on the temporal coherence factors, on the backscatter ratios and on the two-way forest transmissivity coefficient, as well as on volumetric effects and InSAR geometry (see Section 5.4.1).

When $B_n \neq 0$, the complex exponential introduces a phase term related to height of the scattering centre of the vegetation, $(h - \alpha^{-1})$, i.e. the height of the forest, h , minus the penetration depth, α^{-1} . If the normal component of the baseline goes to zero, the volume decorrelation disappears and the forest coherence is determined by the coherence of the individual components weighted by their backscatter and the area-fill factor / stem volume. If $B_n = 0$ is assumed, the simplified version of the IWCM reduces to the empirical model presented in (KOSKINEN *et al.*, 2001). If one further assumes the independence of the forest backscatter from stem volume (i.e. $\sigma_{for}^o = \sigma_{gr}^o = \sigma_{veg}^o$), we obtain:

$$\gamma_{for}(V) = \gamma_{gr} e^{-\beta V} + \gamma_{veg} (1 - e^{-\beta V}) \quad (5.17)$$

Although these simplified models may well describe the relationship between stem volume and coherence, none of them take into account the baseline effects and the forest height. In such cases the model coefficients should not be interpreted as ground and vegetation coherence and backscatter but rather as regression parameters (SKINNER, 2002; WAGNER *et al.*, 2003). In Chapter 6 the importance of taking into account volume decorrelation and InSAR system geometry effects when fitting the model to experimental data will be shown.

5.4 Properties of the IWCM

5.4.1 Graphic representation of the IWCM

A simple way to describe the IWCM is to use a graphic representation in forms of vectors in the complex plane (Figure 5.2). For this purpose, let us start from the simplified version reported in Equation (5.16). The ground contribution, Γ_{gr} , is a real function of stem volume, and is directed along the horizontal axis. The length of this vector depends on ground coherence and backscatter, and decreases for increasing stem volume. The vegetation contribution, Γ_{veg} , includes both a real and an imaginary term. The amplitude of the vector is determined by the vegetation temporal coherence and the vegetation backscatter contribution, thus increasing for increasing stem volume. The phase of the vector depends on the topography seen by the radar at the frequency used. In other words, the forest introduces a topography given by the height of the tree scattering centre, which depends on the penetration of the wave into the tree canopy. As stem volume increases, the vector becomes longer and rotates with a rate determined, at a given frequency, by the baseline length and the tree attenuation.

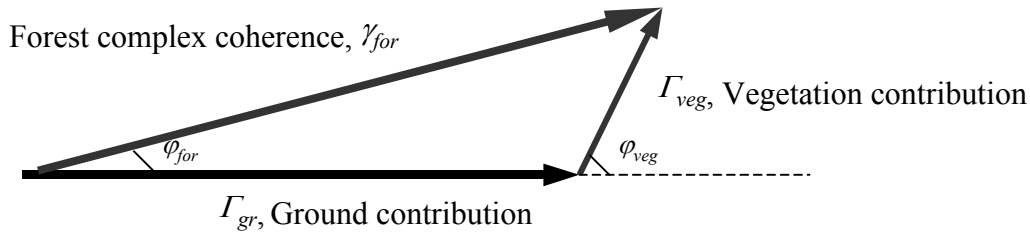


Figure 5.2. Representation of the total forest complex coherence in terms of a real vector (ground contribution) and a complex vector (vegetation contribution) that includes volume decorrelation and InSAR effects.

If the coefficient of the InSAR system geometry, ω , and the two-way tree attenuation, α , are of the same order, the approximation of Equation (5.16) is not valid anymore and the total vegetation contribution vector is represented by a sum of two vectors (see Equation (A.7)). This is commonly the case of ERS pairs with long baseline and JERS pairs, independently of the baseline length.

The sum of the ground and the vegetation vectors returns the forest complex coherence vector. As stem volume increases, the ground contribution vector decreases in size, whilst the vegetation vector increases and rotates. The vector of the ground contribution decreases quicker than the vegetation contribution vector increases, thus decreasing the length of the total forest coherence vector. The speed of the rotation is a function of the normal component of the baseline and the frequency. The amplitude, $|\gamma_{for}|$, represents the total forest coherence while the phase, φ_{for} , is the phase of the forest seen by the radar and is determined by the penetration of the wave into the canopy. The total forest phase φ_{for} returns the interferometric tree height (DAMMERT *et al.*, 1995). The true tree height is instead related to φ_{veg} , the phase difference between the forest and the ground level. The phase φ_{veg} would be the phase φ_{for} in case the forest allowed only surface scattering at its top and there had not been any penetration into it. For a theoretically full canopy without ground contributions, the total complex coherence vector, γ_{for} , would coincide with the vegetation term.

Figure 5.3 shows the trajectories described by the extremes of the ground decorrelation vector, the vegetation decorrelation vector and the total forest complex coherence, as function of sensor, i.e. radar frequency, and baseline. Since the ratio of the ERS and JERS critical baseline is equal to approximately one third, it was decided to adopt these criteria for the baseline values so that the InSAR effects could be considered as similar as possible. The upper plots simulate the forest behaviour in two ERS interferometric one-day pairs having normal components of the baseline equal to 70 and 200 m respectively. The lower plots illustrate the forest behaviour in two JERS pairs, with normal component of the baseline equal to 300 and 1000 m. Values for the five parameters were given according to previous observations and

expected values for dry-unfrozen conditions (see Chapter 6). For increasing stem volume, the length of the ground term decreases (i.e. the extreme of the ground vector moves along the Re axis towards the left), whereas the vegetation term increases in length and rotates (i.e. the extreme of the vegetation vector starts from the origin and describes the green trajectory clockwise). Hence, the total forest complex coherence vector describes the black trajectory clockwise and decreases in length. The impact of the rotation on the complex coherence becomes particularly significant at long baselines. In particular the rotation is stronger in an ERS than in a JERS pair. This is due to the smaller penetration of the wave into the canopy so that the percentage of ground seen is smaller. The total phase of the forest, ϕ_{for} , is therefore more sensitive to the stem volume.

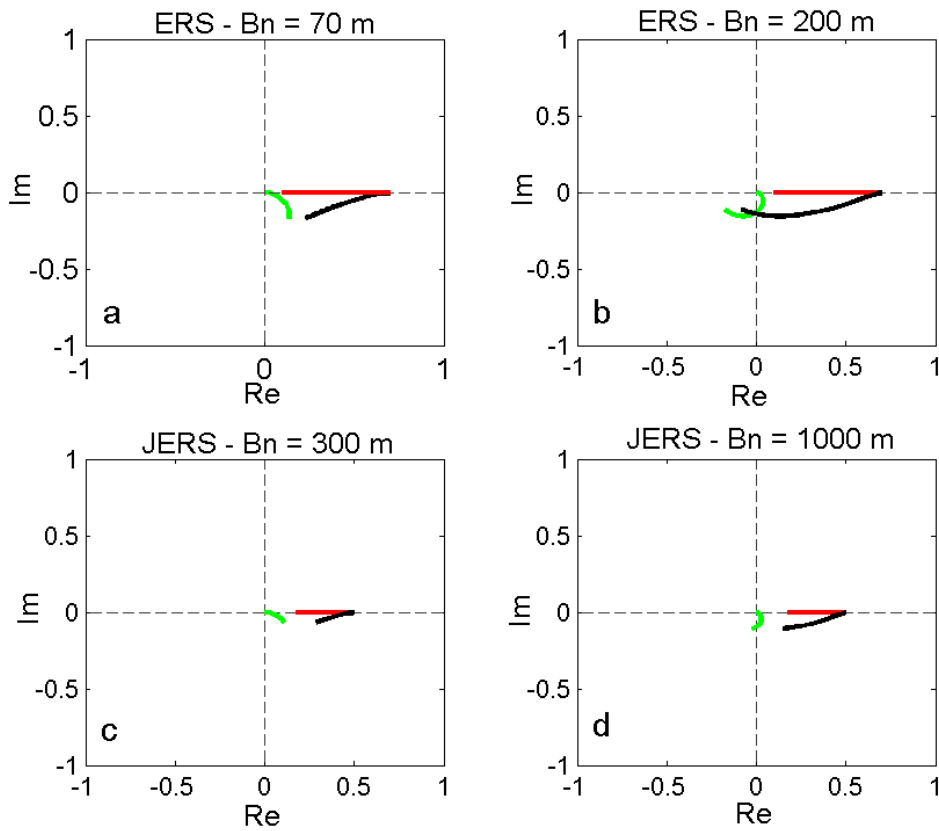


Figure 5.3. Trajectories described by the extremes of the ground decorrelation vector (red), the vegetation decorrelation vector (green) and the total forest coherence vector (black) for increasing stem volume. The ERS (a) and (b) cases were determined using $\gamma_{gr} = 0.7$, $\gamma_{veg} = 0.25$, $\beta = 0.006$ ha/m³, $\sigma_{gr}^o = -9$ dB, $\sigma_{veg}^o = -8$ dB and $\alpha = 2$ dB/m. The JERS (c) and (d) cases were determined using $\gamma_{gr} = 0.5$, $\gamma_{veg} = 0.2$, $\beta = 0.004$ ha/m³, $\sigma_{gr}^o = -10$ dB, $\sigma_{veg}^o = -6$ dB and $\alpha = 0.5$ dB/m. The interval of stem volume was $[0, 350]$ m³/ha.

For a given SAR system, the total forest phase should increase for increasing tree height, i.e. for increasing stem volume. According to the model, when the vegetation contribution vector has rotated 180° , the coherence reaches a minimum and then increases. Using the expression of the phase term in Equation (5.16) and the relation in Equation (3.1), the stem volume at which the IWCM predicts a minimum for coherence ($\varphi = \pi$) is (SANTORO, 2001):

$$V_{\min} = \frac{1}{a} \sqrt[3]{\frac{\lambda R \sin \theta}{4B_n}} \quad (5.18)$$

where we have assumed that the effect of the coefficient α is negligible. According to Equation (5.18), the stem volume at which the model predicts an oscillation in the coherence decreases for increasing normal component of the baseline. For the ERS mission, at B_n shorter than 150 m the oscillation occurs only if the range of stem volume interval exceeds $500 \text{ m}^3/\text{ha}$, a very rare situation in boreal forests. More realistic is the case for pairs with normal baselines around 200 m, when the oscillation occurs at around $300 \text{ m}^3/\text{ha}$, a value typical of dense boreal forests.

5.4.2 Model-based tree height

The interferometric tree height is always below the true tree height. It is determined by the radar frequency and by how much ground is covered by the vegetation. At high frequency and for a dense canopy, the interferometric height should be almost coincident with the true height. Although theoretically correct, in a repeat-pass configuration the scatterers within a resolution cell have time to move and change their position between two acquisitions. The unstable nature of the vegetation determines a remarkable decorrelation within the cell, thus preventing an accurate determination of the position of the scattering centre and limiting the use of the repeat-pass InSAR phase for tree height estimation (see Chapter 8).

Although the interferometric tree height only represents a scattering property of the forest but not the true height, Figure 5.2 shows that it is possible to use the IWCM to compensate the interferometric height to obtain the true height. Using the ‘‘Sine Rule’’, φ_{veg} can be expressed as follows:

$$\varphi_{veg} = \sin^{-1} \left[\frac{|\gamma_{for}|}{|\Gamma_{veg}|} \sin \varphi_{for} \right] \quad (5.19)$$

thus linking the phase of the vegetation slab to the measured coherence and InSAR phase. The phase φ_{veg} represents the phase of the vegetation decorrelation term, Γ_{veg} , and therefore is related to the true height. The estimation of the true tree height is governed by a complex expression (see Equation (5.11)) but becomes rather simple in case $\omega \ll \alpha$, i.e. for high frequency and not too long baseline, which is common for ERS pairs. Looking at Equation (5.16), the amplitude and the phase of the vegetation decorrelation term are given by:

$$|\Gamma_{veg}| = \gamma_{veg} \frac{\sigma_{veg}^o}{\sigma_{for}^o} (1 - e^{-\beta V}) \quad (5.20)$$

$$\varphi_{veg} = -\omega \left(h - \frac{1}{\alpha} \right) = -\omega h_{int} \quad (5.21)$$

where h_{int} represents the interferometric tree height, i.e. the true tree height minus the penetration depth. Rewriting Equation (5.21) in terms of interferometric tree height, we obtain:

$$h = h_{int} + \frac{1}{\alpha} = -\frac{\varphi_{veg}}{\omega} + \frac{1}{\alpha} = \quad (5.22)$$

from which, by inserting Equation (5.19), we can finally write:

$$h = -\frac{1}{\omega} \sin^{-1} \left[\frac{|\gamma_{for}|}{|\Gamma_{veg}|} \sin \varphi_{for} \right] + \frac{1}{\alpha} \quad (5.23)$$

This Equation relates the true tree height to measurements of coherence and InSAR phase, i.e. the interferometric tree height, thus performing a compensation using the penetration depth into the tree canopy.

Chapter 6

SAR and InSAR forest modelling: results

In the Water Cloud Model and the Interferometric Water Cloud Model several parameters are not known beforehand but must be estimated from a set of stem volume, backscatter and/or coherence measurements. This operation is referred to as “model training” or simply “training”, whereas the measurements used form the “training” set. Unless specified, at each test site training was performed using all the stands available.

Section 6.1 illustrates the methods that can be used depending whether InSAR data are available or not. WCM and IWCM training based on ERS SAR and InSAR is described in Section 6.2, whereas Section 6.3 focuses on the training of the WCM using the JERS SAR backscatter.

6.1 Model training procedures

In Equation (5.6) describing the WCM three parameters are unknown: the ground and vegetation backscatter coefficients (σ_{gr}^o and σ_{veg}^o) and the two-way forest transmissivity coefficient, β . The three parameters can be estimated with a simple non-linear regression using a least squares approach that minimises the sum of the squared differences between measured backscatter, $\sigma_{meas,i}^o$, and model-based backscatter, σ_i^o , for each training sample:

$$\sum_{i=1}^N [\sigma_{meas,i}^o - \sigma_i^o(\sigma_{gr}^o, \sigma_{veg}^o, \beta)]^2 = \min \quad (6.1)$$

In order to obtain a correct fit, the uncertainty in the backscatter measurements must be as small as possible. Because of speckle, training should not be carried out at pixel

level but rather use mean values of the backscatter in areas that contain a sufficient number of independent looks. Training at stand level is suitable because a reasonable amount of stands in boreal forests are big enough to satisfy the size requirement. Moreover, since stands by definition cover areas where trees have similar properties and are homogeneously distributed, the standard deviation of the backscatter should be small. The measured backscatter $\sigma^o_{meas,i}$ is therefore given by the mean intensity value within the i^{th} stand. Before averaging, the edges along the stand perimeter should be eroded in order to limit the effects of mismatches between backscatter images and the digital forest stand map used for extracting the backscatter signatures, the thickness of the buffer zone depending on the positional accuracy of the images.

The IWCM contains five unknowns (σ^o_{gr} , σ^o_{veg} , β , γ_{gr} and γ_{veg}). A simultaneous estimation of five unknown parameters from interferometric data would undoubtedly introduce relevant uncertainties in each factor. To overcome this problem, the backscatter measurements and the WCM can be used as well. Since the WCM already includes σ^o_{gr} , σ^o_{veg} and β , the ground and vegetation temporal coherence are the remaining unknowns in the IWCM. The determination of two parameters is certainly feasible, making a coupled WCM-IWCM training procedure more suitable.

Rigorously speaking, in the IWCM the two-way tree attenuation coefficient, α , should also be treated as unknown. Studies at C-band have shown that the penetration depth within coniferous forest canopies is of the order of a couple of metres, corresponding to a two-way tree attenuation of approximately 2 dB/m. These results support the assumption of using a constant α when modelling ERS coherence data (DAMMERT, 1999). At L-band, the penetration depth has been reported to vary between 4 and 10 m (see Chapter 5), corresponding to α values between 0.4 and 1 dB/m. The larger interval of possible values does not allow the same simplification adopted in the ERS case. Nevertheless, since the quality of the L-band coherence data available was poor, the IWCM could not be trained, thus leaving the topic open to future investigations.

A problem that can affect the estimation of the IWCM parameters is represented by the InSAR phase. The IWCM in Equation (5.13) expresses the complex coherence as function of stem volume, thus implying that both coherence and InSAR phase measurements can be used in the training. The correlation between coherence and stem volume is much bigger than between InSAR phase and stem volume (Figure 6.1), at least in the ERS case, because of the strong phase noise (see Chapter 8). Furthermore, the significant errors due to atmospheric artefacts make InSAR phase almost totally unreliable for correct model training. For these reasons, InSAR phase measurements have been discarded and coherence only has been used.

As for the backscatter, the set of unknown parameters can be estimated by means of a minimisation based on least squares:

$$\sum_{i=1}^N [\gamma_{meas,i} - \gamma_i(\gamma_{gr}, \gamma_{veg}, \beta, \sigma^o_{gr}, \sigma^o_{veg})]^2 = \min \quad (6.2)$$

where $\gamma_{meas,i}$ represents the measured coherence and γ_i the model-based coherence from Equation (5.13) for the i^{th} sample in the training set. In both cases we are referring to the amplitude of the complex coherence. If a coupled WCM-IWCM regression together with Equation (6.1) is performed, Equation (6.2) will contain two unknowns.

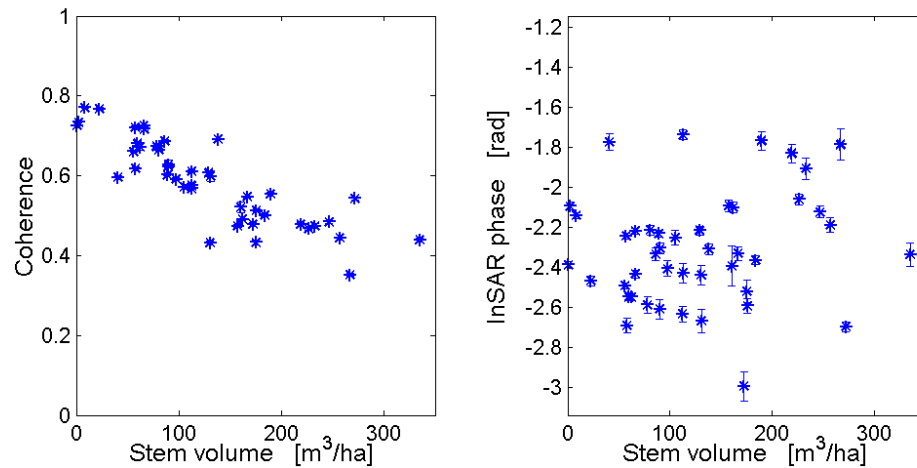


Figure 6.1. Coherence and InSAR phase versus stem volume (Pearson's correlation coefficient equal to -0.86 and 0.17 respectively). The data have been acquired over Kättböle on 21-22 April 1996. The uncertainty in the coherence estimates is negligible.

Independently of the procedure applied, the quality of the model fit depends on the accuracy of the coherence estimates. As illustrated in Chapter 2, the choice of the estimator is fundamental, especially in forested areas because of the typical low coherence. Assuming that the best possible estimate has been obtained, once again it is preferable to work at stand level rather than on a pixel basis. Averaging in areas of the size of a stand decreases the noise in the coherence estimates. The importance of edge-eroded stands is even more crucial than in the previous case because of border effects due to the window-based estimation of coherence.

6.2 Model training with ERS data

ERS backscatter and coherence modelling involves the following issues:

- WCM and IWCM training procedure.
- Properties of the WCM and IWCM parameters estimates.
- Estimation of area-fill factor.
- Sensitivity of the models to the two-way tree attenuation factor.

6.2.1 Training procedure

The availability of both backscatter and coherence measurements suggests a coupled regression using Equations (6.1) and (6.2). A major drawback of such approach is represented by the quality of the backscatter data. If the backscatter is affected by large spread, the three parameters σ_{gr}^o , σ_{veg}^o and β will suffer from remarkable uncertainty. When further training the IWCM, the uncertainty will propagate to the estimates of the remaining two parameters, introducing significant errors. In order to avoid error propagation, the model training procedure should take into account the different information content of the two types of data. The backscatter is generally spread out and has a small dynamic range. The coherence is in many cases not affected by spread of values and shows a clear decreasing trend for increasing stem volume. Coherence can therefore be considered more reliable for training, whereas the backscatter is used as support.

To confirm this assumption, the models were trained according to both a step-wise procedure and an iterative procedure. The step-wise method consisted of determining the three unknowns in the WCM using Equation (6.1). The estimates were then introduced in the IWCM and Equation (6.2) was used to obtain values for the remaining unknowns. In most cases, the training stopped at the first step because of the large spread of the backscatter and the little correlation between backscatter and stem volume. Estimates of σ_{gr}^o , σ_{veg}^o and β were either out of the range of realistic values or affected by large uncertainty.

The iterative procedure expressed the idea reported above, that the coherence should drive the training, whilst the backscatter refines it (SANTORO *et al.*, 1999; SANTORO *et al.*, 2000; SANTORO *et al.*, 2002). The procedure started with an initial estimation of β from coherence measurements using Equation (6.2), under the assumption that the two backscatter coefficients are equal. Such assumption is reasonable at C-band because of the small dynamic range. The initial estimate of β was then used in Equation (6.1) to determine σ_{gr}^o and σ_{veg}^o . Having already available an initial estimate of β obtained from training the IWCM, the number of unknowns in the WCM decreased to two, thus making the estimation of the two backscatter coefficients less noisy than in the previous approach. The estimates of the backscatter coefficients were finally introduced in Equation (6.2) to compute new values of β , γ_{gr} and γ_{veg} . At this stage the first iteration had finished. The refined estimate of β was used to provide refined estimates of the two backscatter coefficients, which in turn were introduced in the IWCM to refine the coherence parameters and β . The iteration was carried on until the values of all parameters did not show any remarkable change. With this procedure, the perturbation introduced by the backscatter measurements in the estimation was limited and a fit to the measurements included in the training set was obtained.

To prove the goodness of the fit, the results from the iterative procedure were compared to estimates provided by a more rigorous but time and memory demanding

approach. A five-dimensional matrix of possible values for each unknown was created and all possible combinations were used to train the IWCM. The combination for which the root mean square error of coherence reported in Equation (6.2) was smallest corresponded to the best fit. The best fit obtained with this procedure and the estimates obtained with the iterative approach were very similar and the IWCM curves perfectly overlapped, thus showing the reliability of the coupled iterative procedure.

6.2.2 Model fitting

Figures 6.2 and 6.4 illustrate the results of the regression between stem volume and coherence respectively in Kättböle and Tuusula, whereas Figures 6.3 and 6.5 show the results of the regression between stem volume and backscatter. The Figures show the ability of the two models to describe the relationship between the remote sensing quantities and stem volume, and their robustness for several environmental conditions (compare with Table 3.3).

For increasing stem volume the sign of the slope in the model-based backscatter curve depended on the dielectric properties of the ground (see Chapter 4). The curve either increased or decreased, reaching a constant level already at low stem volume. Saturation could be observed both in Kättböle and in Tuusula. In several cases the WCM returned an almost horizontal line. The coherence showed much higher sensitivity to stem volume than the backscatter. It decreased for increasing stem volume, with a slope that depended on the weather conditions, suffering from saturation only when environmental changes occurred during the period of acquisition.

One case of discrepancy between modelled and experimental data was found in Tuusula on the 29-30 March 1996, the discrepancy being clearer in the backscatter fit (Figures 6.4 and 6.5). The coherence was high for very sparse forest stands and significantly dropped in slightly denser forests, reaching a saturation level. To explain this behaviour it can be assumed that between acquisitions the dielectric properties of the snow had changed in forested areas (i.e. under the canopy) but not in clear cuts. The weather conditions reported snowfall, temperatures around the freezing point and snow on the ground. Unfortunately the data set of snow measurements could not confirm this assumption.

6.2.3 Model parameters estimates

Although we tried to limit the inaccuracy of the σ_{gr}^o and σ_{veg}^o estimates with the iterative procedure, the large spread of the data introduced significant uncertainties in both backscatter coefficients. The two-way forest transmissivity coefficient β also suffered from uncertainty because it was determined simultaneously from the backscatter and the coherence data. Since coherence measurements were commonly characterised by little spread, the uncertainty in the estimates of γ_{gr} and γ_{veg} was small. This was particularly the case in Kättböle, whereas in Tuusula a slightly larger dispersion of the coherence data was noticed. Possible reasons for the different

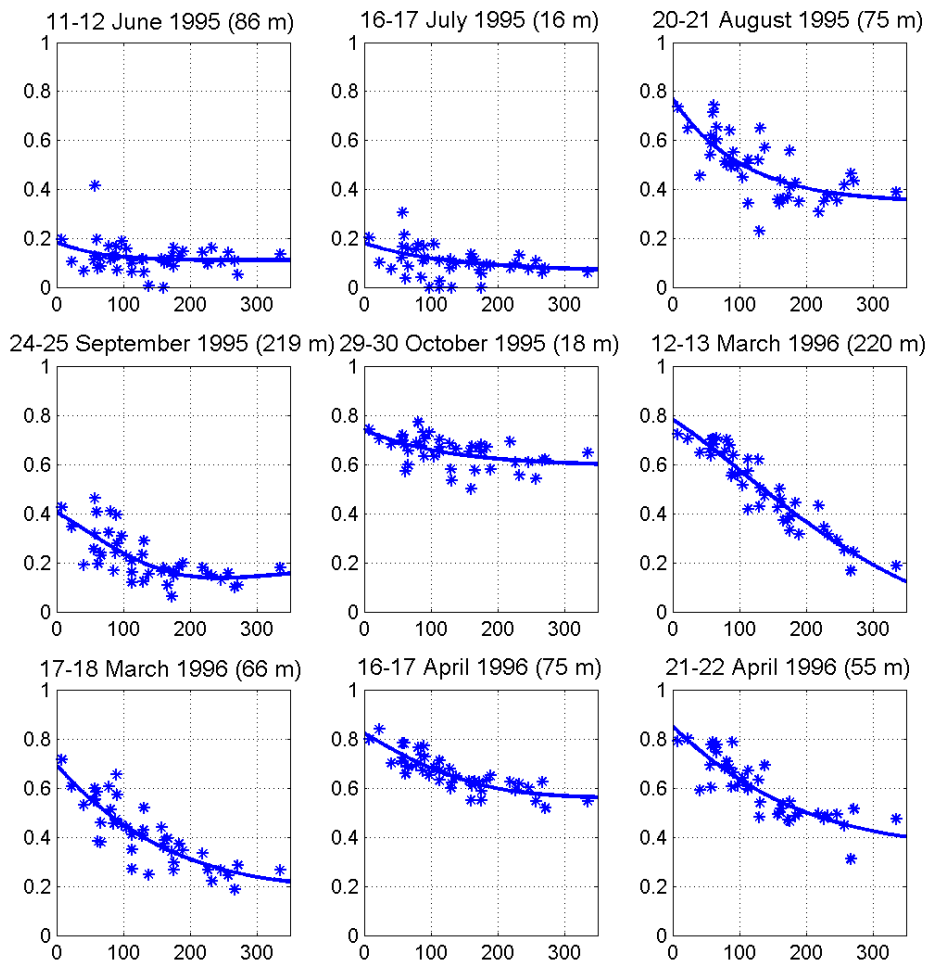


Figure 6.2. Coherence measurements and modelled coherence using the IWCM expressed as function of stem volume, between 0 and 350 m³/ha. Test site: Kättböle, 42 stands.

spread could be related either to the forest structure or to the accuracy of the measurements. Assuming that the forest management was carried out at the two test sites in a similar manner, the higher uncertainty in the ground-truth data at the Finnish test site could explain the larger dispersion of coherence and backscatter. Since the area under investigation in Tuusula is not much larger than in Kättböle, the effect of spatial variability of the environmental conditions on the two remote sensing quantities was considered negligible.

The IWCM is based on the assumption that the backscatter does not change between two acquisitions (ASKNE *et al.*, 1997). This did not seem to be the case in several pairs; therefore, the effect of temporally variable backscatter on the model was analysed. For each pair the training was performed first by using the ERS-1 and then the ERS-2 backscatter measurements. The values reported in Tables 6.1 and 6.2

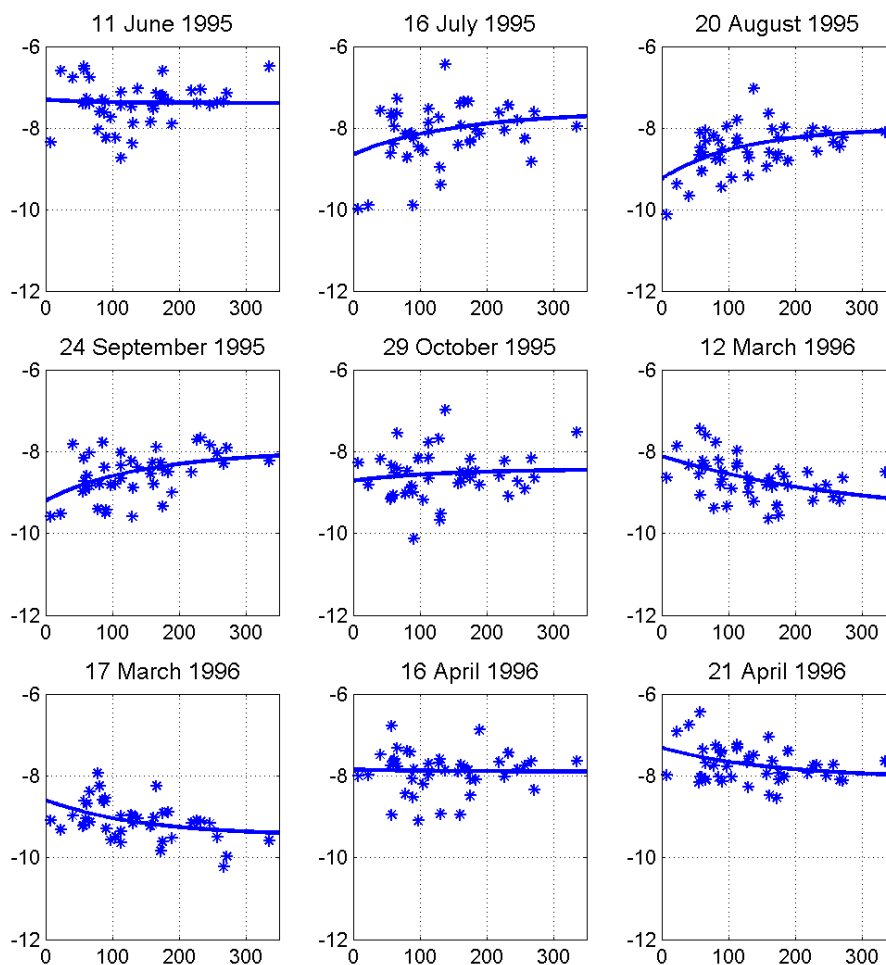


Figure 6.3. Backscatter measurements and modelled backscatter (in dB) using the WCM expressed as function of stem volume, between 0 and 350 m³/ha. Test site: Kättböle, 42 stands.

show that the estimated temporal coherence coefficients, γ_{gr} and γ_{veg} , were not affected by changes of the backscatter. In other words, the sensitivity of the IWCM to backscatter changes is minimal.

The rather large number of images over Kättböle and Tuusula allowed investigating the properties of the five unknown model parameters and their dependence upon meteorological conditions.

A significant interpretation of σ_{gr}^o and σ_{veg}^o estimates could not be carried out because of the dispersion of the data and the saturation. The analysis of the dynamics of both parameters is in line with the results reported in Chapter 4, to which the reader is referred.

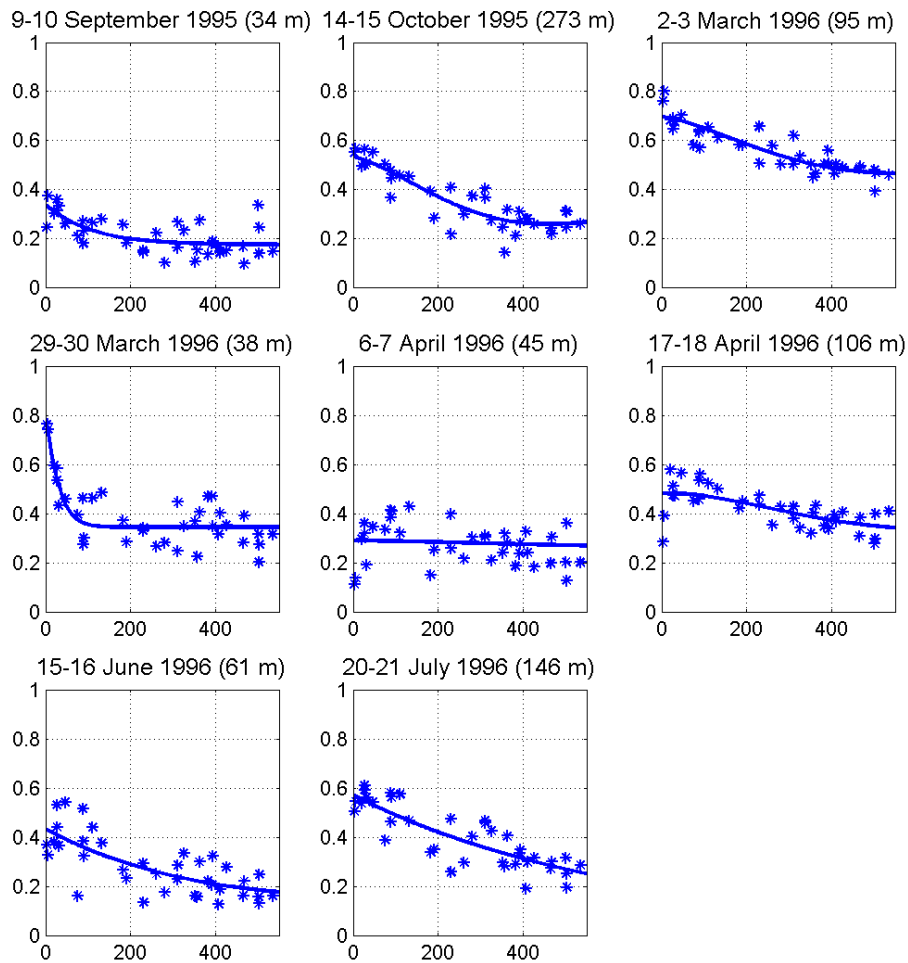


Figure 6.4. Coherence measurements and modelled coherence using the IWCN expressed as function of stem volume, between 0 and 550 m³/ha. Test site: Tuusula, 37 stands.

Meteorological events at or between acquisitions (namely rainfall, variation of soil moisture and snowmelt) partially or totally decorrelated the scene. Several cases were registered both in Kättböle (June, July and September 1995) and in Tuusula (September and October 1995, April, June and July 1996). For increasing stem volume, in some cases the slope became almost flat and the sensitivity of coherence to stem volume decreased or disappeared. The temporal coherence of the ground, γ_{gr} , which for stable conditions has values above 0.7, was always below this level. A correlation between ground coherence and changes of the moisture content on the forest floor could not be computed. Nevertheless from the meteorological data it could be inferred that γ_{gr} decreased for increasing amount of rain precipitation or snowmelt.

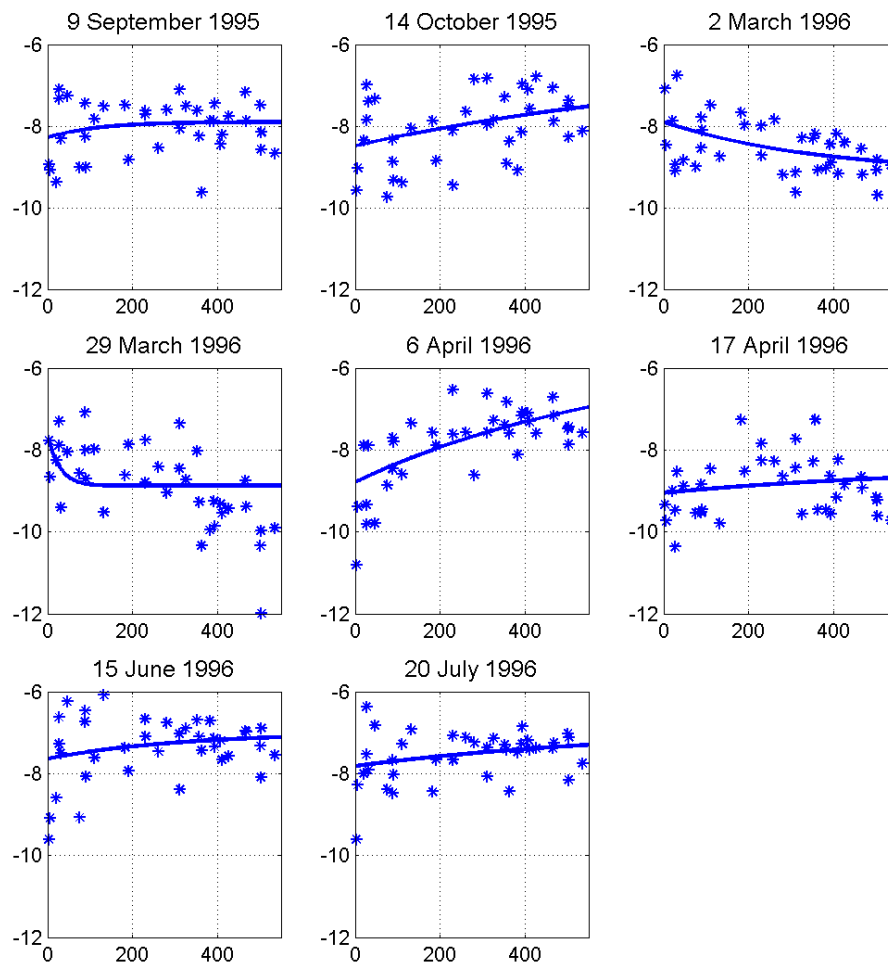


Figure 6.5. Backscatter measurements (in dB) and modelled backscatter using the WCM as a function of stem volume, between 0 and 550 m^3/ha . Test site: Tuusula, 37 stands.

Several pairs were acquired when the temperature was around or below the freezing point. An overall high coherence was observed under frozen conditions (October 1995 and 16-17 April in Kättböle and 2-3 March 1996 in Tuusula). This result could be explained in terms of an increased transparency of the canopy so that the scattering would have arisen at more stable parts of the vegetation. A similar situation did not occur for the 17-18 and 29-30 March 1996 pairs acquired over Kättböle and Tuusula respectively. In both cases the temperature was just below the freezing point, nevertheless the vegetation coherence was much lower. Since detailed measurements of snow parameters were not available, it was not possible to explain such results if not as a result of dielectric decorrelation due to snow on the canopy.

Image date	γ_{gr}	γ_{veg}	β [ha/m ³]	σ_{gr}^o [dB]	σ_{gr}^o [dB]
11-12 June 1995	0.18	0.11	0.0140	-7.3	-7.4
	0.18	0.11	0.0142	-8.6	-8.8
16-17 July 1995	0.18	0.06	0.0059	-8.6	-7.6
	0.18	0.06	0.0072	-8.0	-7.8
20-21 August 1995	0.77	0.35	0.0074	-9.3	-8.0
	0.77	0.35	0.0070	-9.9	-8.3
24-25 September 1995	0.40	0.22	0.0059	-9.2	-8.0
	0.40	0.21	0.0070	-9.0	-9.0
29-30 October 1995	0.74	0.59	0.0072	-8.7	-8.4
	0.74	0.59	0.0084	-8.7	-9.3
12-13 March 1996 (a)	0.78	0.18	0.0041	-8.1	-9.5
	0.78	0.22	0.0034	-8.9	-9.4
17-18 March 1996	0.69	0.19	0.0073	-8.6	-9.5
	0.69	0.18	0.0068	-9.4	-9.9
16-17 April 1996 (a)	0.82	0.57	0.0065	-7.9	-7.9
	0.82	0.57	0.0071	-7.6	-8.3
21-22 April 1996	0.85	0.36	0.0063	-7.3	-8.1
	0.85	0.34	0.0055	-8.1	-8.3

Table 6.1. Estimates of the five unknown parameters in the WCM and the IWCM in Kättböle. The training set consisted of 42 stands with stem volumes between 8 and 335 m³/ha. For each interferometric pair, the training has been performed using the ERS-1 and the ERS-2 backscatter separately, thus explaining the presence of two sets of estimates for each pair. (a) stands for ascending pass.

Image date	γ_{gr}	γ_{veg}	β [ha/m ³]	σ_{gr}^o [dB]	σ_{gr}^o [dB]
9-10 September 1995	0.34	0.17	0.0085	-8.3	-7.9
	0.34	0.17	0.0091	-7.6	-7.6
14-15 October 1995	0.53	0.23	0.0008	-8.5	-6.2
	0.53	0.22	0.0007	-9.2	-6.1
2-3 March 1996	0.70	0.56	0.0031	-7.9	-9.2
	0.70	0.56	0.0031	-8.4	-9.5
29-30 March 1996 (a)	0.80	0.34	0.0377	-7.7	-8.9
	0.80	0.34	0.0427	-7.3	-9.5
6-7 April 1996	0.29	0.29	0.0007	-8.8	-4.5
	0.29	0.29	0.0009	-9.0	-6.0
17-18 April 1996 (a)	0.48	0.54	0.0014	-9.0	-8.4
	0.48	0.54	0.0016	-9.3	-9.1
15-16 June 1996	0.43	0.15	0.0028	-7.6	-7.0
	0.43	0.15	0.0031	-8.3	-8.0
20-21 July 1996	0.57	0.00	0.0013	-7.8	-6.8
	0.57	0.00	0.0015	-7.7	-7.4

Table 6.2. Estimates of the five unknown parameters in the WCM and the IWCM in Tuusula. The training set consisted of 37 stands with stem volumes between 3 and 535 m³/ha. For each interferometric pair, the training has been performed using the ERS-1 and the ERS-2 backscatter separately, thus explaining the presence of two sets of estimates for each pair. (a) stands for ascending pass.

The estimates of the coefficient of the two-way forest transmissivity β were strictly related to the stability of the environmental conditions, i.e. to the level of ground coherence. When the two images were acquired under the same environmental conditions and no meteorological event occurred between acquisitions, the values obtained from the regression were rather constant between 0.005 and 0.008 ha/m³ (August and October 1995, 17-18 March 1996 and April 1996 in Kättböle). These values were furthermore in accordance with the regression values of approximately 0.005 ha/m³ found using HUTSCAT (PULLIAINEN *et al.*, 1994) and ERS data (KURVONEN *et al.*, 1999). The two-way forest transmissivity, $e^{-\beta V}$, rapidly increases, reaching a saturation value in forest with a thick canopy closure. The variability of the estimates was explained in terms of the spread of the training data, in particular the backscatter. For stable winter-frozen conditions (12-13 March 1996 for Kättböle and 2-3 March 1996 for Tuusula), the coefficient was slightly lower, 0.003 ha/m³, which could have been due to the frozen state of the trees that made the canopy more transparent to the incoming wave. In case of variations of the environmental conditions (rainfall before or between acquisitions, snowmelt, snowfall), according to the estimates the forest was mostly either almost completely transparent or impenetrable (all other pairs). It was possible to conclude that in such cases, although the models could fit the data, β had lost its physical meaning, becoming a mere regression factor.

In Chapter 5 the importance of the phase term related to the InSAR system geometry and the volumetric decorrelation has been presented. To analyse the effect of this term on the modelling, a comparison with results obtained using the zero-baseline version of the IWCM reported in Equation (5.17) has been carried out. For pairs with baseline below 100 m, the estimates of the five parameters did not show any remarkable difference, both in Tuusula and Kättböle. This result is consistent with the fact that short baseline pairs are characterised by negligible volume decorrelation and phase effects. For pairs with $B_n > 100$ m the simplified model was able to fit the data but the parameter values did not always have physical meaning. In Kättböle the two pairs with $B_n > 200$ m showed an unrealistic negative value for γ_{veg} , and a very low value of β , i.e. an almost transparent canopy, whereas in Tuusula the results for the three pairs with $B_n > 100$ m were not showing clear trends, probably because of the different weather conditions occurring at the time of the acquisitions and the stronger noise in the measurements. These results indicate the importance of the phase term in the IWCM on the modelling. Nevertheless more investigations should be performed on pairs with long baseline, acquired for stable weather conditions over forested areas with well-known forest properties.

6.2.4 Estimation of area-fill factor

In Chapter 5 it has been argued that it is better to express the WCM and the IWCM in terms of stem volume rather than as function of area-fill factor because of the more common use of the first parameter in forestry. Nevertheless, since the area-fill factor is a measure of the canopy closure, it represents a fundamental property for the explanation of the backscatter and the coherence measurements in forests. In our investigations, although area-fill could not be used for training the models because the measurements available at both test sites were too few and noisy, values collected

at 18 stands in Kättböle were considered as support to the fitting procedure. Once β was estimated, the area-fill factor was computed using Equation (5.7) and compared to the measurements to indicate whether the estimated β was reasonable.

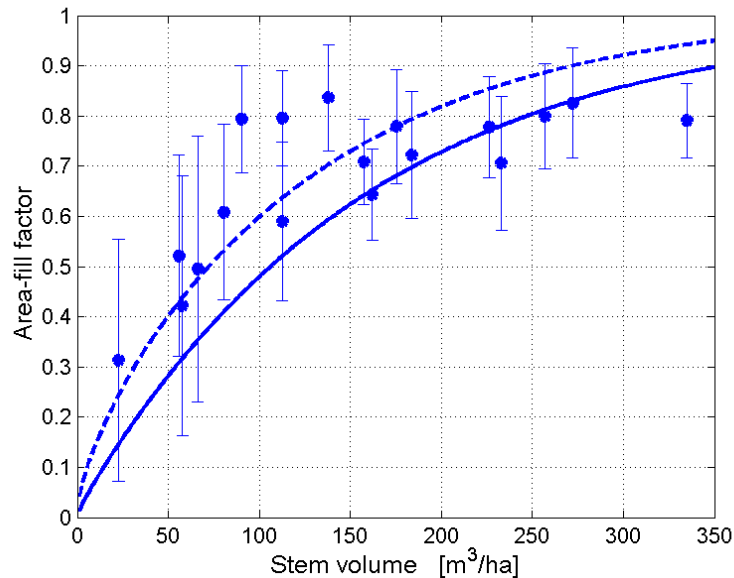


Figure 6.6. Measured area-fill factor, model-based area-fill factor (full line) and regression curve from Equation (5.7) (dashed line). The vertical bars represent the variability of the area-fill factor measurements in a stand. The length of each bar is equal to one standard deviation. The model-based curve was obtained from Equation (5.7) using $\alpha = 2$ dB/m and an average value for the estimates of β (0.0065 ha/m³). For the regression curve $\alpha = 0.62$ dB/m and $\beta = 0.0069$ ha/m³ were obtained.

Figure 6.6 reports the comparison between the model-based area-fill and the set of measurements collected in Kättböle. The dashed curve represents the result of a least squares regression to the area-fill measurements based on Equation (5.7) as function of α and β . Although the regression curve was characterised by a two-way tree attenuation lower than the values assumed so far (0.62 dB/m), the regression error was similar to the values obtained for $\alpha = 2$ dB/m and β between 0.005 and 0.008 ha/m³. In particular the curve obtained from Equation (5.7), in which the mean value of the realistic β estimates reported in Table 6.1 (0.0065 ha/m³) and $\alpha = 2$ dB/m were used, seemed to reasonably describe the relationship between area-fill and stem volume, thus confirming the validity of the estimates of β using the coupled iterative training procedure.

6.2.5 Model sensitivity to the two-way tree attenuation

So far it has been assumed that the two-way tree attenuation, α , is constant and equal to 2 dB/m. It is reasonable to believe though that the attenuation through the tree canopy can be different depending on the season. During winter, the frozen canopy

lets the incoming wave penetrate deeper; therefore, α should be smaller. To check the sensitivity of the IWCM to the two-way tree attenuation, the model was trained according to the iterative procedure, each time with a different value of α . This approach was preferred to a simultaneous regression involving six parameters in order to limit the uncertainty in the parameters estimates. The set of α used was in the range of realistic values for the penetration depth, i.e. between 0.2 and 2 dB/m, which corresponded to penetration depths between 2 and 20 m.

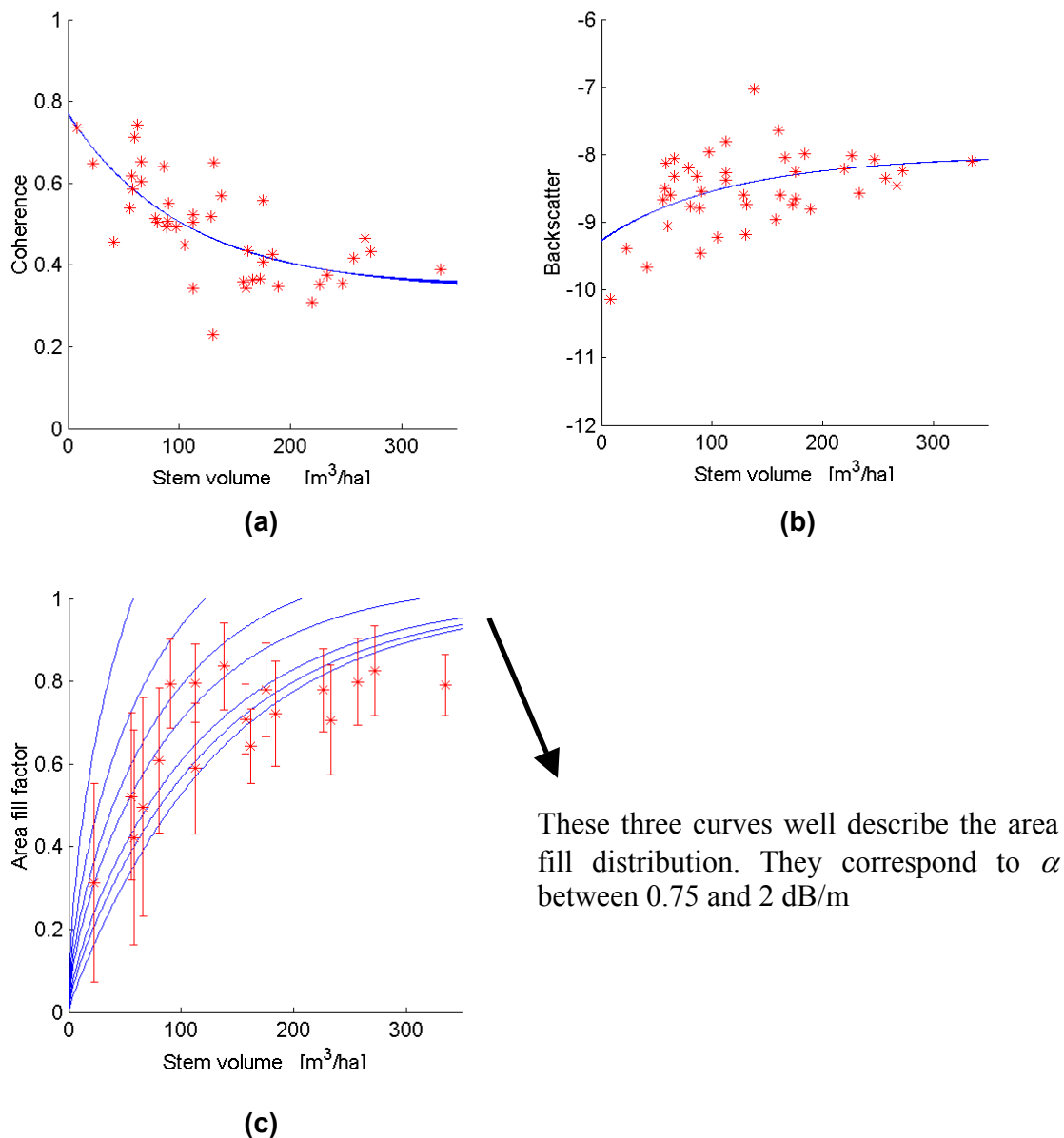


Figure 6.7. Coherence (a), backscatter (b) and area-fill factor (c) as function of stem volume, August 1995, Kättböle. In (a) and (b) all the curves overlap. In (c) the slope of the curves decreases for increasing α . The leftmost curve corresponds to 0.2 dB/m, the rightmost curve is obtained for $\alpha = 2$ dB/m.

To illustrate the effect of α on the backscatter and the coherence, Figures 6.7, 6.8 and 6.9 report the trend of the IWCM-based coherence curve, the WCM-based backscatter curve and the area-fill factor regression curve as function of α for three pairs acquired on August 1995, 12-13 March 1996 and 16-17 April 1996 over Kättböle. The analysis focuses on Kättböle because of the higher accuracy of the ground-truth and the small spread of coherence and backscatter. The three pairs have been chosen because they represented different seasonal conditions and baseline lengths.

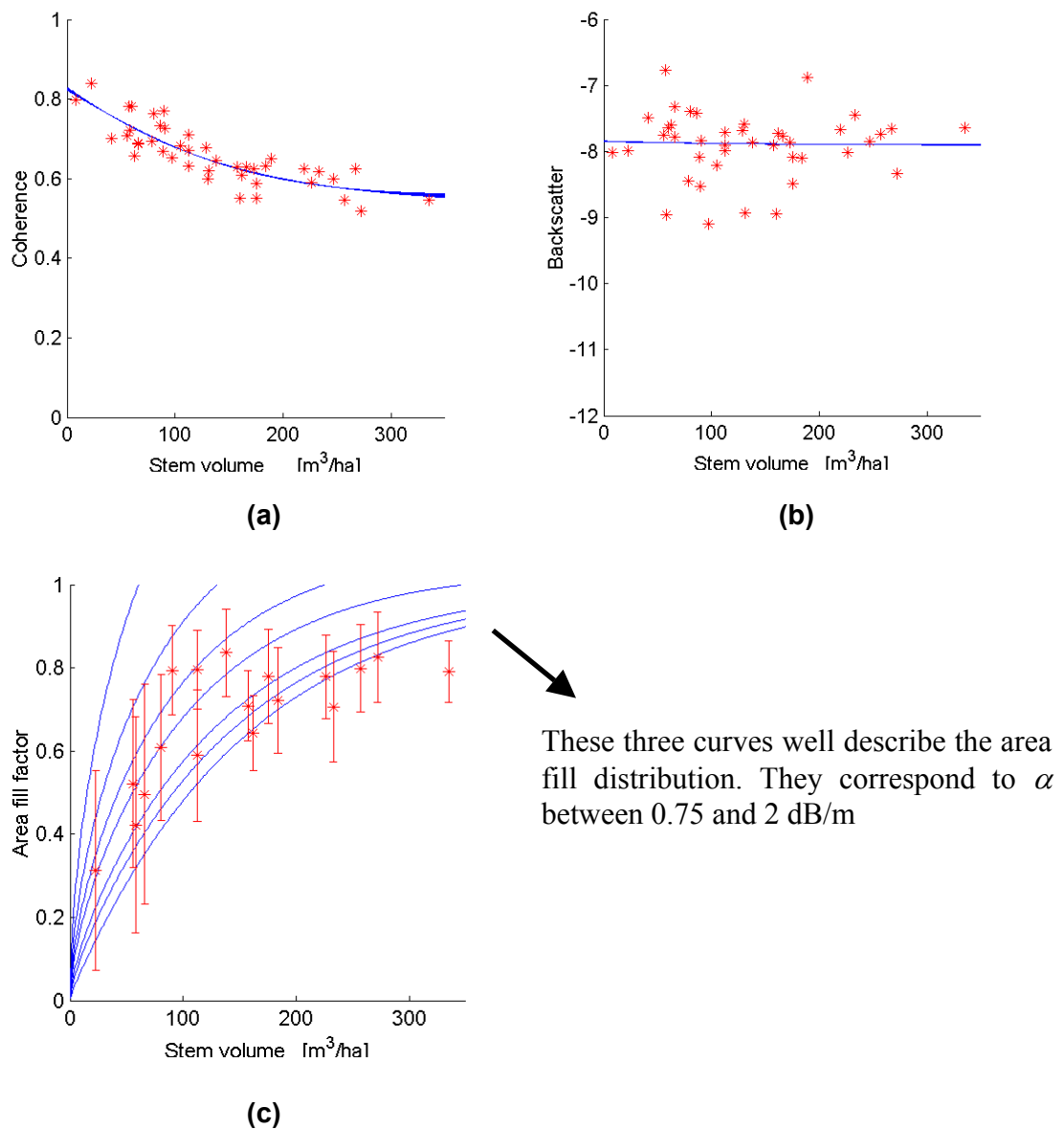


Figure 6.8. Coherence (a), backscatter (b) and area-fill factor (c) as function of stem volume, 16-17 April 1996, Kättböle. In (a) and (b) the curves overlap. In (c) the slope of the curves decreases for increasing α . The leftmost curve corresponds to 0.2 dB/m, the rightmost curve is obtained for $\alpha = 2$ dB/m.

For pairs with short baseline, summarised by the August and the April pairs, it is evident that model-based backscatter and coherence were independent of α . Volume decorrelation and InSAR system geometry effects were in these cases negligible because of the short baseline. The area-fill factor plots indicate reasonable values for α greater than 0.75 dB/m. Because of the relevant uncertainty in the area-fill factor, it was not possible to further evaluate the precision of α .

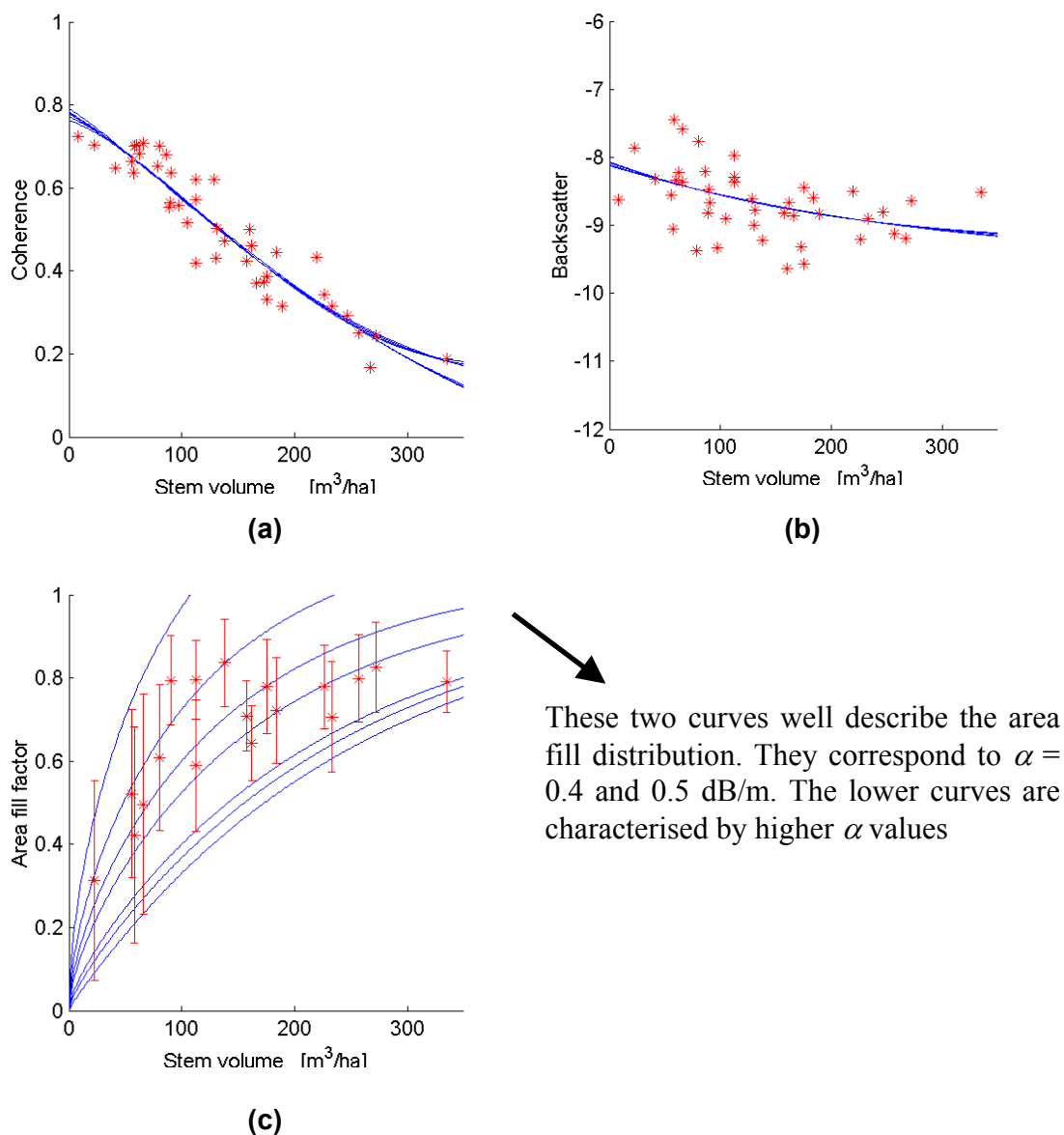


Figure 6.9. Coherence (a), backscatter (b) and area-fill factor (c) as function of stem volume, 12-13 March 1996, Kättböle. In (a) two sets of overlapping curves can be seen. In (b) all curves overlap. In (c) the slope of the curves decreases for increasing α . The leftmost curve corresponds to 0.2 dB/m, the rightmost curve is obtained for $\alpha = 2$ dB/m.

For pairs with long baseline, the volume decorrelation becomes relevant, i.e. the modelled coherence should depend on α . The pair acquired in March ($B_n = 220$ m, winter-frozen conditions) indicated that the modelled backscatter is independent of α , whilst for the modelled coherence two trends could be identified (Figure 6.9 a). For weak attenuation the model predicted a curve bending at the around the highest stem volumes measured in the forest estate, high vegetation coherence ($\gamma_{veg} \cong 0.5$) and values for β in accordance with previous observation ($0.005 \text{ m}^3/\text{ha}$). For α greater than 0.65 dB/m the model-based coherence did not oscillate, γ_{veg} was low ($\gamma_{veg} \cong 0.2$) whereas β was slightly below the value reported for small α .

From the coherence and the backscatter measurements it was not possible to conclude which solution is correct. Although the second seemed to be more in line with the theory, one could argue that the volume decorrelation summed up to the InSAR term and introduced an oscillation in the model-based curve, which then reached the asymptotic value given by the high γ_{veg} . High vegetation coherence has been registered in pairs acquired under similar environmental conditions, making the first solution reasonable. Unfortunately, the oscillation predicted by the model occurred outside the range of stem volumes available, therefore it was not possible to confirm the validity of such interpretation.

For further understanding, the regression to the area-fill factor was investigated. The plot reported in Figure 6.9 c shows that the trend in area-fill measurements was better described when α was smaller than 2 dB/m . A weaker attenuation is reasonable considering that the pair has been acquired in winter, during a period when the temperature was below 0°C , and the tree canopy should have been frozen. Although these results indicate the possibility of a certain seasonal variability for α , they were obtained in just one pair and were mainly supported by few and rather noisy area-fill factor measurements. Nevertheless, they suggest further investigations using long baseline pairs acquired in several seasons.

6.3 Model training with JERS data

Because of the limited amount and the poor quality of JERS coherence measurements available, only the backscatter was modelled using the WCM. In a similar manner to the ERS case, several points have been investigated:

- Properties of the WCM parameters estimates.
- Estimation of two-way tree attenuation and penetration depth.

Image date	σ_{gr}^o [dB]	σ_{veg}^o [dB]	β [ha/m ³] (x 10 ⁻⁴)	α [Np/m]	δ [m]
15 April 1997	-9.2	-6.2	35 [15 - 45]	0.28	8 [6 - 19]
29 May 1997	-8.7	-3.9	22 [5 - 30]	0.17	13 [9 - 60]
12 July 1997	-7.8	-4.9	46 [30 - 65]	0.4	5 [3 - 9]
8 October 1997	-8.2	-5.0	54 [40 - 65]	0.5	4 [3 - 7]
4 January 1998	-8.3	-5.6	191[150 - 200]	35.7	0 -
17 February 1998	-10.0	-7.0	20 [5 - 30]	0.15	14 [9 - 60]
2 April 1998	-9.6	-6.0	8 [5 - 10]	0.06	38 [30 - 60]
16 May 1998	-7.9	-5.1	38 [15 - 55]	0.31	7 [4 - 19]
12 August 1998	-8.7	-5.4	49 [30 - 65]	0.44	5 [3 - 9]

Table 6.3. Estimates of the three unknowns in the WCM, the two-way attenuation per metre and the penetration depth in Kättböle (JERS case). The first three parameters have been determined using 42 stands with stem volumes between 8 and 335 m³/ha. After sensitivity analysis, the intervals of acceptable β were included in brackets. The backscatter parameters did not show any variation. Two-way tree attenuation and penetration depth have been computed using Equation (5.7) from area-fill factor measurements at 18 stands.

Image date	σ_{gr}^o [dB]	σ_{veg}^o [dB]	β [ha/m ³] (x 10 ⁻⁴)
6 January 1994	-11.7	-10.0	98 [70 - 130]
19 February 1994	-11.9	-9.8	89 [70 - 115]
14 October 1996	-10.6	-6.3	129 [100 - 140]
27 November 1996	-11.2	-9.7	86 [55 - 120]
10 January 1997	-11.6	-9.9	90 [65 - 120]
23 February 1997	-11.8	-10.0	105 [80 - 140]
8 April 1997	-9.7	-5.5	111 [90 - 135]
22 June 1998	-10.1	-5.8	109 [90 - 130]
5 August 1998	-11.1	-6.6	97 [80 - 120]

Table 6.4. Estimates of the three unknowns in the WCM in Bolshe-4 (JERS case). The three parameters have been determined using 161 stands with stem volumes between 15 and 400 m³/ha. After sensitivity analysis, the intervals of acceptable β were included in brackets. The backscatter parameters did not show any variation.

6.3.1 Model fitting

The lack of coherence data simplified the fitting procedure. For all images available the optimisation procedure described in Equation (6.1) completed successfully and values for the three unknowns in the WCM (σ_{gr}^o , σ_{veg}^o and β) could be determined.

To quantify the uncertainty in the estimates of each parameter, a sensitivity analysis was carried out by varying β and performing the regression for the remaining two coefficients. For each β , the first member in Equation (6.1) was then compared with the value obtained from the three-parameters regression (i.e. the best fit to the data). Tables 6.3 and 6.4 show that the two backscatter coefficients did not vary, whereas even for a difference as small as 1%, the interval of acceptable β values was rather large, being larger in Bolshe-Murtinsky than in Kättböle. The spread of the backscatter and the limited number of stands in the “intermediate” interval of stem volumes, i.e. between 50 and 150 m³/ha, should explain the larger uncertainties in Bolshe-Murtinsky.

6.3.2 Model parameters estimates

Figure 6.10 illustrates in four plots the effect of weather conditions on the trend between backscatter and stem volume in Kättböle. Despite the small dynamic range (not more than 3-4 dB), under dry-unfrozen conditions the JERS backscatter constantly increased up to 350 m³/ha (Figure 6.10 a). When precipitation (rain or snow) occurred, the sensitivity to stem volume was lower. One case of saturation was found for rain precipitation and melting snow (Figure 6.10 b). In Bolshe-Murtinsky the dynamic range differed very much depending whether dry-frozen condition (Figures 6.11 a and b), thaw (Figure 6.11 c) or rainfall (Figure 6.11 d) occurred. Nevertheless, independently of the weather conditions, the backscatter saturated at around 150-200 m³/ha. Since we did not have available any image acquired under dry-unfrozen conditions, it was not possible to compare with the interesting results obtained in Kättböle.

The values of σ_{gr}^o and σ_{veg}^o in Tables 6.3 and 6.4 well corresponded to the average backscatter coefficients in sparse and dense forests reported in Section 4.3. Figure 6.12 shows the strong correlation between temperature on one side, and σ_{gr}^o and σ_{veg}^o on the other side. The Pearson’s linear coefficient of correlation was equal to 0.73 and 0.86 respectively. The vegetation backscatter showed larger variations than the ground backscatter, which was instead affected by few extreme cases (low right corner in Figure 6.12 a). These corresponded to images acquired when several simultaneous weather effects occurred (0° C, heavy rainfall, snowmelt, etc.).

For all the images acquired over Kättböle under dry-unfrozen conditions (May 1997 and 1998, August 1998) the estimates of β were in line with previous results and the theory (Table 6.3). In Finnish forests (KURVONEN, *et al.*, 1999) reported an approximate value of 0.003 m³/ha, which is consistent with the fact that the forest

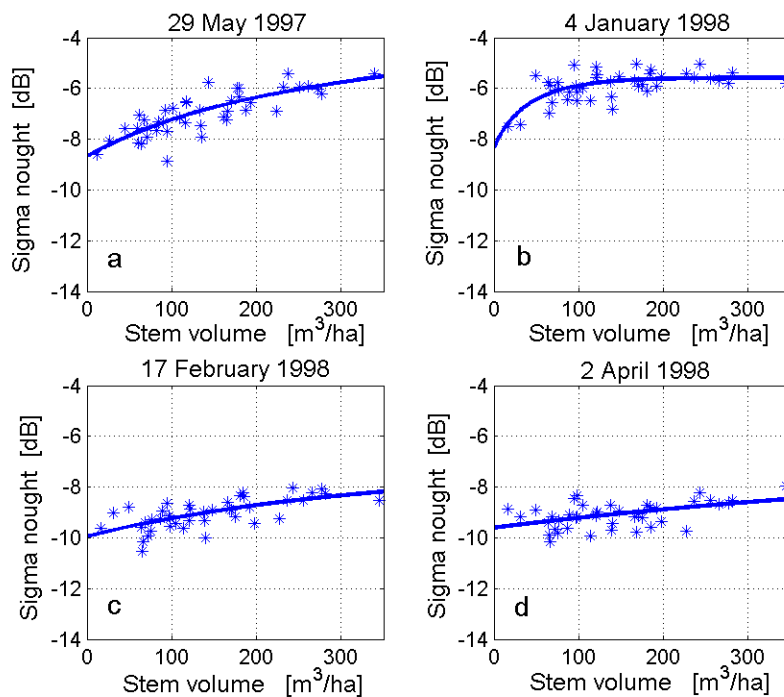


Figure 6.10. Backscatter versus stem volume measurements and regression curves in Kättböle (42 stands) for dry-unfrozen conditions (a), precipitation and melting snow (b), precipitation and snow cover (c), and temperature around freezing point and precipitation (d)

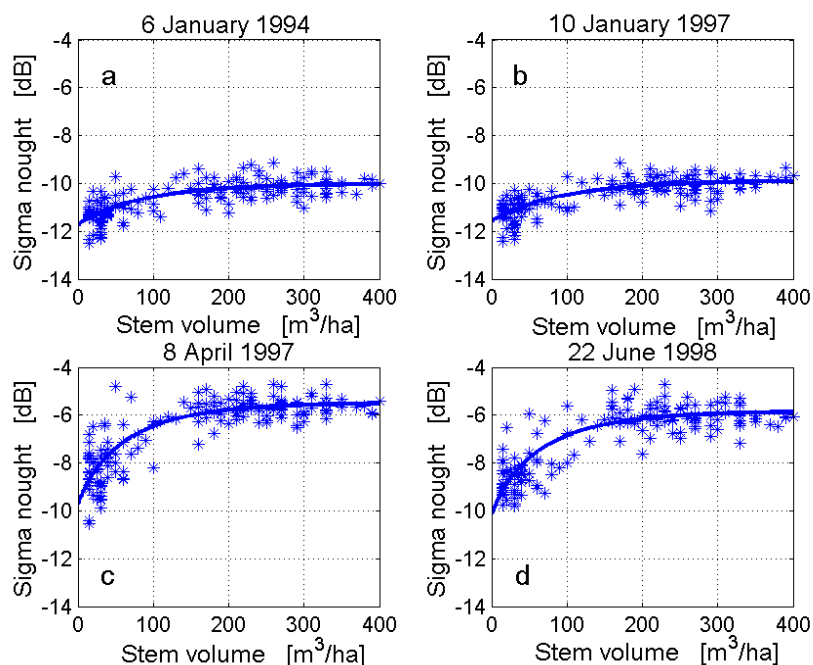


Figure 6.11. Backscatter versus stem volume measurements and regression curves in Bolshe-4 (161 stands) for dry-frozen conditions (a) and (b), thaw (c) and rainfall (d).

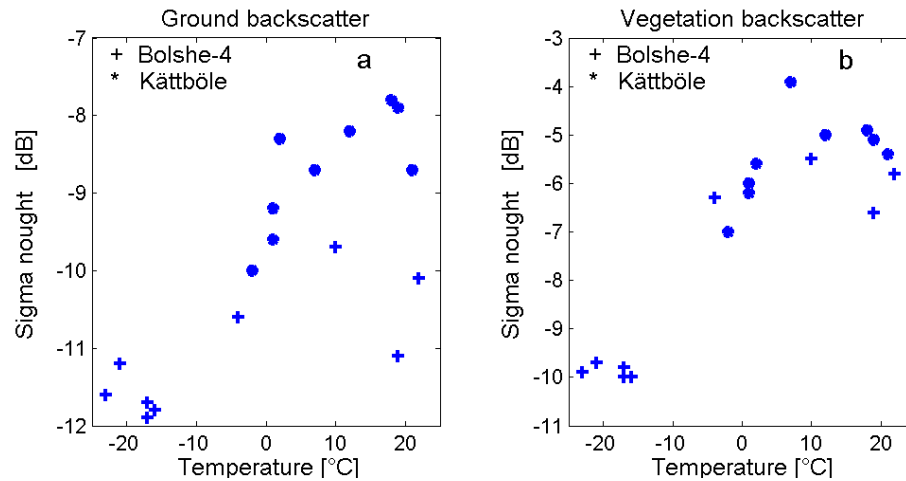


Figure 6.12. Scatterplots of temperature versus ground backscatter, σ_{gr}^o , (a) and versus vegetation backscatter, σ_{veg}^o , (b).

transmissivity at L-band should be higher than at C-band. Only during changing weather conditions were unrealistic values obtained (see for example the images acquired between January and April 1998). In Bolshe-Murtinsky the estimates were indeed consistently bigger (Table 6.4), thus meaning that the model had predicted an attenuation stronger than at C-band. This is an improbable situation, taking into account that many images had been acquired in winter at temperatures considerably below the freezing point.

These results were initially explained as a consequence of the lack of stands in the intermediate interval of stem volumes. Previous studies have shown that, for increasing stem volume, the JERS backscatter increases and reaches saturation slightly above $100 \text{ m}^3/\text{ha}$ (FRANSSON & ISRAELSSON, 1999; PULLIAINEN *et al.*, 1999). In order to determine the slope from the model as accurately as possible, it is therefore fundamental to have many samples in the range of volumes up to the saturation value. If there is a lack in such range, as for example in Bolshe-Murtinsky (see Figure 3.5), the slope, i.e. β , will be inaccurately estimated.

Although the high values of β could be related to an error in the regression due to the lack of stands with intermediate stem volumes, nonetheless this did not seem sufficient to explain the consistency of the high estimates. A possible further explanation was based on the different forest management practise in Sweden and in the Siberian region where Bolshe-Murtinsky is located. To explain this concept let us consider two forests (forest A and forest B). Forest A is characterised by thin trees and is very dense. Forest B instead includes fewer but thicker trees. Although the structure of the forests is different, they have the same stem volume. Since the backscatter of a forest is determined by the structural properties and only indirectly by the stem volume, it is reasonable to assume that in case of different forest management practise, the relationship between backscatter and stem volume differs, thus affecting the values of the model parameters estimates.

Unfortunately precise information concerning the management of the Bolshe-Murtinsky compartment was not available; therefore it was not possible to give any quantitative support to the assumption. Nevertheless, for the understanding of the backscatter signatures and for backscatter modelling throughout the boreal zone, the results stress the importance of the forest structural properties for the modelling and the knowledge of the relationship between these properties and forest attributes.

6.3.3 Estimation of penetration depth

The area-fill measurements collected in Kättböle were used to estimate the two-way tree attenuation from Equation (5.7). Although the measurements had been taken specifically for the ERS case, at an angle of 23° , it was reasonable to assume that the fraction of ground covered at a slightly different angle, such as the JERS incidence angle (35° - 40°), was similar. For realistic β values, which were obtained only for dry-unfrozen conditions, the estimated α and the corresponding penetration depth were in accordance with the values reported in the literature (4-10 m). These results should confirm the validity of the backscatter model, the negligibility of double-bounces and the assumption that the area-fill factor can be considered constant in the range of incidence angles of ERS and JERS.

6.4 Conclusions

This Chapter has devised a procedure for training:

- The Water Cloud Model and the Interferometric Water Cloud Model using ERS backscatter and coherence data.
- The Water Cloud Model with JERS backscatter data.

The IWCM was not considered at L-band because of the low quality of the JERS coherence data available.

Model training for the ERS case was based on the different information content of the relationship between backscatter and coherence on one side and the stem volume on the other. InSAR phase measurements were not considered because of the small correlation with stem volume.

The training algorithm consisted of a coupled iterative regression of the WCM and the IWCM, using as reference the coherence measurements. The iterative method was preferred to training the two models separately since the large spread of the backscatter data and its low sensitivity to stem volume would have introduced significant errors in the WCM (and the IWCM) parameters estimates.

With the coupled iterative training method accurate estimates of the coherence parameters γ_{gr} and γ_{veg} are obtained. Moreover, compared to results provided by a step-wise regression, the estimation error for the backscatter parameters σ_{gr}^o and

σ_{veg}^o , and the coefficient of the two-way forest transmissivity β are smaller. In order to keep the number of unknowns at a reasonable level, the IWCM can be trained assuming that the two-way tree transmissivity coefficient, α , is constant. Results from a sensitivity analysis show that model-based coherence and backscatter do not seem to depend on α . A weak indication of the coefficient seasonal dynamics is given by the modelled area-fill factor in one pair with long baseline acquired under winter-frozen conditions. This result suggests further analysis using more pairs with long baselines, acquired in several seasons.

The WCM and the IWCM well describe the dependence of respectively the backscatter and the coherence upon stem volume. The models were proven to be robust, being able to generate a correct fit for several environmental conditions. Very important is the quality of the data used for model training. Inaccurate data can strongly influence the model fit and the model parameters.

The low sensitivity of the ERS backscatter to stem volume is showed by the almost flat regression lines and the saturation reached already at small stem volume. The ERS coherence decreases for increasing stem volume, the slope depending on the meteorological conditions at the time of the acquisitions. Saturation does not occur unless the environmental conditions between the two acquisitions have changed. Model parameters are correctly estimated when at acquisitions stable weather conditions occur. In such cases the estimates of β predict reasonably well the area-fill factor. When environmental changes occur, e.g. precipitation or changes in the ground moisture content, it is still possible to fit a line to the data but β loses physical meaning, becoming a regression coefficient.

Concerning the complex term in the IWCM, for short baselines, the effect is negligible and the zero-baseline version of the model can be used. When the normal component of the baseline exceeds 100 m, both terms should be taken into account. Nevertheless the investigations carried out only partially showed the importance of the phase term, mostly because of the unsuitable environmental conditions for such an investigation and the errors in the ground-truth data in several images. Further investigations should analyse pairs with long baseline, acquired under stable weather conditions over forested areas with well-known forest properties.

Results obtained in Sweden, Finland and Siberia show that the WCM used for modelling JERS backscatter is robust. The dynamic range depends on the seasonal conditions, being largest under dry-unfrozen conditions. When precipitation occurs or for dry-frozen conditions, the signal saturates. Both the ground and the vegetation backscatter correlate strongly with the temperature. The uncertainty in the estimates of the coefficient β is much larger than for σ_{gr}^o and σ_{veg}^o . The estimation error is directly related to the spread of the backscatter measurements and the amount of training samples available in the non-saturated interval of stem volumes. The uniform distribution of accurately measured stem volumes in the training area is a crucial issue for correct and reliable model training.

Consistent differences were found in the two-way forest transmissivity at the investigated test sites. The estimates obtained in Kättböle are in line with previous results and with the traditional interpretation of forest transmissivity. Furthermore the penetration depth estimated from β is in agreement with typical L-band values. In Bolshe-Murtinsky the two-way forest transmissivity is too low even in young forest stands. Although the non-uniform distribution of stem volume can cause relevant errors in the regression, the consistent differences should be rather explained in terms of different forest management systems in the two areas. These results suggest that although the Water Cloud Model is able to describe the JERS backscatter in terms of a forest attribute, a few aspects concerning the physical meaning of the model need to be reconsidered if it is to be used for the whole boreal area.

To obtain a clearer picture concerning the forest transmissivity spatial inconsistency, it would be of extreme interest to:

- Observe the dependency of the backscatter upon a forest parameter directly related to its structure (e.g. area-fill factor, canopy closure, etc.).
- Model other types of remote sensing data, for which the underlying assumptions of the WCM are still valid. X- and C-band SAR backscatter could be investigated but the low sensitivity to stem volume does not let us expect striking new information. The use of the IWCM with C- and L-band repeat-pass coherence could probably be more suitable, but only in regions characterised by long periods of stable weather conditions.

Chapter 7

Stem volume retrieval

Once model training has been performed, it is possible to invert the model using a set of coherence and backscatter measurements independent from the training set in order to retrieve stem volume. The simple formulation of the WCM and the IWCM makes both models suitable for such operation. This Chapter starts with the description of the methodology adopted for stem volume retrieval from backscatter and coherence data (Section 7.1). When several images over the area of interest are available, multi-temporal combination of single-image estimates can be used to provide a new version of the stem volumes, characterised by an enhanced accuracy. The multi-temporal approach adopted in this work is described in Section 7.2. The remaining Sections report results of stem volume retrieval at three spatial scales of interest in forest inventory: stand level, plot level and regional level. Stand-wise retrieval using 1) ERS backscatter and coherence and 2) JERS backscatter is reported in Section 7.3, whereas at plot level the retrieval of stem volume using ERS coherence is described in Section 7.4. In both Sections the impact of meteorological conditions on the estimates accuracy is stressed. For large area estimates of forest properties, foresters commonly downscale plot-wise stem volume estimates. For the retrieval of the stem volume at regional level, Section 7.5 illustrates a similar approach, based on ERS coherence data and plot-wise InSAR-based stem volume estimates. Concluding remarks are included in Section 7.6.

7.1 Retrieval procedure

When only backscatter measurements are available, the retrieval of stem volume is straightforward. From Equation (5.6) it is possible to express stem volume as function of measured forest backscatter, σ_{for}^o :

$$V = -\frac{1}{\beta} \ln \left(\frac{\sigma_{veg}^o - \sigma_{for}^o}{\sigma_{veg}^o - \sigma_{gr}^o} \right) \quad (7.1)$$

Because of the complex exponential term, the inversion of the full IWCM expression reported in Equation (5.13) is more difficult and requires a numerical approach. Nevertheless, as shown in Chapter 5, for short baseline pairs the phase term can be neglected, thus facilitating the inversion of the IWCM. In a formulation similar to Equation (7.1), stem volume becomes a simple function of forest backscatter, σ_{for}^o , and coherence, γ_{for} , measurements:

$$V = -\frac{1}{\beta} \ln \left(\frac{\gamma_{veg} \sigma_{veg}^o - \gamma_{for} \sigma_{for}^o}{\gamma_{veg} \sigma_{veg}^o - \gamma_{gr} \sigma_{gr}^o} \right) \quad (7.2)$$

It is not rare that some measurements of either the backscatter or the coherence do not belong to the interval of modelled values. In Figure 7.1 ERS backscatter measurements included in a test set are shown together with the model-based curve obtained from training the WCM. Several stands are characterised by backscatter above the biggest value predicted by the WCM in the range of stem volumes found in the area. If the model had been trained on an infinite interval of stem volumes, it would have been possible to relate a retrieved stem volume to most of the stands.

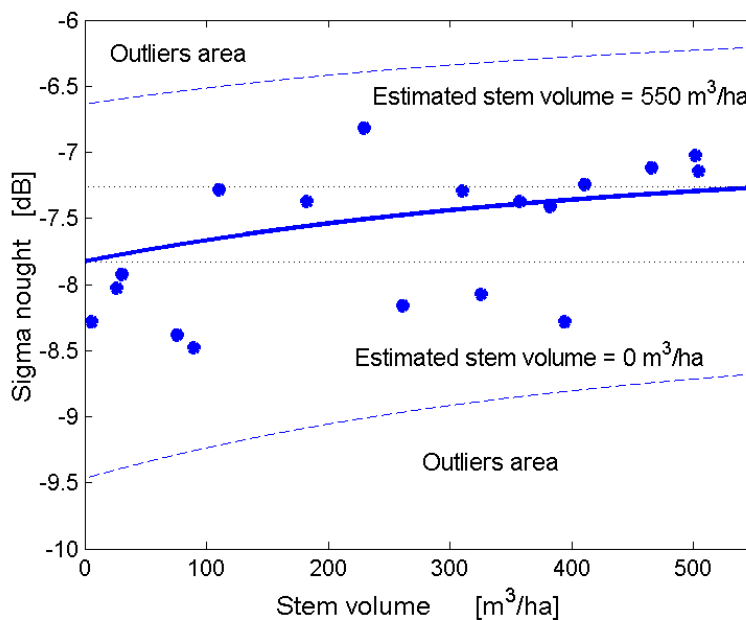


Figure 7.1. Stem volume retrieval possibilities. The solid line represents the regression curve obtained over Tuusula on 15 June 1996. The dashed lines are placed at two standard deviations from the model-based curve.

Nevertheless

1. These estimates would have been much bigger than the stem volumes typically measured in the region where the test site is located. Following the same reasoning, the stands with backscatter below the smallest value predicted by the WCM would have been characterised by a negative stem volume.
2. If there were measurements above the saturated backscatter, it would have been impossible to estimate the stem volume.
3. It is not correct to use a model outside the range of stem volumes used for training.

In order to associate a realistic stem volume to every sample included in the test set, some rules are therefore needed. A sensible way to proceed is to use the smallest and the biggest stem volume values measured in the region of interest. For example, since in Kättböle the stem volumes were measured between 0 and 350 m³/ha, these values were used as reference for the correction. In stands where the retrieval returned a negative stem volume, the corrected value was set to 0 m³/ha. In stands characterised by estimated stem volumes bigger than the maximum value measured, the corrected value was set to 350 m³/ha (SANTORO *et al.*, 2002a; SANTORO *et al.*, 2002b). When a sample was at least two standard deviations away from the range of modelled backscatter or coherence, it was labelled as outlier and no value was retrieved for it.

To describe the results of the retrieval the following statistical parameters are commonly considered: the coefficient of determination, R^2 , and the root mean square error (RMSE). Since the retrieval is influenced by inaccuracy in the ground-truth data used for training and testing, it is important that the sampling errors in the ground-truth are taken into account when computing the RMSE. At plot level the accuracy of the *in situ* measurements is high therefore the correction for sampling errors is not needed. At stand level the ground-truth estimates of stem volume include a 10-25 % error, depending on the methods used for the inventory. In (FRANSSON *et al.*, 2001; SANTORO, *et al.*, 2002a; SANTORO, *et al.*, 2002b) the following expression has been adopted to compute the retrieval error at stand level in Kättböle:

$$RMSE = \sqrt{\frac{1}{N_{test}} \sum_{i=1}^{N_{test}} (V_i - V_i^{gt})^2 - 0.5 \frac{1}{N_{test}} \sum_{i=1}^{N_{test}} (SE_i)^2} \quad (7.3)$$

where N_{test} represents the number of samples in the test set, V_i and V_i^{gt} are the retrieved stem volume and the stem volume estimated from the ground-truth for sample no. i . SE_i represents the standard error for stand no. i and the factor 0.5 is a correction due to systematic sampling design, in accordance with the empirical investigation by (LINDGREN, 1984). A similar correction was used in Tuusula.

When comparing the retrieval errors at more test sites it is necessary to take into account that the distribution of stem volumes can have different attributes. In such cases the relative RMSE, defined as ratio between the RMSE and the mean value of ground-truth stem volume, should be used.

7.2 Multi-temporal filtering

The advantage of spaceborne missions is the provision of several acquisitions over an area. For each sampling unit stem volume estimates from single backscatter and coherence images can be combined in a “multi-temporal” approach. Similarly to spatial averaging, a multi-temporal combination reduces the noise in the original data, with the advantage of keeping the resolution unchanged.

The easiest multi-temporal filter is to produce a mean value of the single-image estimates. Although simple and straightforward, this method does not take into account that the quality of the estimates may differ from image to image. Weighted averages are more suitable because for each combined image the retrieved stem volumes are multiplied by a factor related to the information content of the images. In this way images characterised by a low potential for stem volume retrieval will have less effect on the multi-temporal estimates.

The easiest multi-temporal combination of the stem volume estimates from M images can be written as:

$$V_{multi-temp,j} = \sum_{i=1}^M w_i \cdot V_{i,j} \quad (7.4)$$

where $V_{multi-temp,j}$ and $V_{i,j}$ represent the multi-temporal stem volume and the estimated stem volume from image no. i respectively, for the j^{th} sample in the test set. The weighting coefficients w_i are image dependent. For a multi-temporal combination of ERS and JERS backscatter images, (KURVONEN *et al.*, 1999) defined the weighting coefficients by means of least squares regression. In this study an alternative approach based on the ability of each image to retrieve stem volume has been considered (SANTORO *et al.*, 1999; SANTORO *et al.*, 2000; SANTORO, *et al.*, 2002b). Since the RMSE is a measure of estimation accuracy, it was considered to be a suitable weighting coefficient. The w_i coefficients in Equation (7.4) were therefore expressed as follows:

$$w_i = \frac{\left(\frac{P_{train,i} \cdot P_{test,i}}{RMSE_i^2} \right)}{\sum_{j=1}^M \left(\frac{P_{train,j} \cdot P_{test,j}}{RMSE_j^2} \right)} \quad (7.5)$$

The idea behind Equation (7.5) is that images with lower residuals, $RMSE_i$, should have more weight in the multi-temporal estimation. To further decrease the effect of images characterised by large dispersion of measurements, the percentages of samples between the maximum and the minimum modelled values both in the training and in the test set ($p_{train,i}$ and $p_{test,i}$) were included.

7.3 Stand-wise retrieval

Retrieval at stand level consists of training the models using a small subset of stands in the area of interest and to invert them in a test set, which had not been used during the training phase. In Kättböle and Tuusula the limited amount of stands forced to order them for increasing stem volume and divide them into two halves. Although not fully correct, this procedure ensured that in the two sets the distribution of stem volume would have been as similar as possible. Odd positioned stands formed one set; even positioned stands formed a second set. For the ERS case, the two sets were used for training and testing respectively, whereas both sets were used as training and test set in two different analyses when analysing the JERS backscatter. In this way it was tested whether small changes in the training set would have turned out in significant differences in the retrieval. In Bolshe-Murtinsky, a larger number of stands were available so that it was possible to proceed according to a statistically more correct approach. Each compartment was divided in four equal parts and training was performed in the one with the most uniform distribution of stem volume. As a consequence, 37 training stands in Bolshe-2 and 46 in Bolshe-4, corresponding respectively to 25% and 29% of the total amount of stands in each compartment were used.

7.3.1 ERS backscatter

Stem volume retrieval from ERS backscatter suffers from large errors because of saturation of the signal occurring already at low stem volumes. Several authors (PULLIAINEN *et al.*, 1994; PULLIAINEN *et al.*, 1996; HALLIKAINEN *et al.*, 1998; FRANSSON & ISRAELSSON, 1999) observed that the slope of backscatter measurements had flattened out in the interval between 50 and 100 m³/ha at several test sites located in Finland and Sweden. Similar results were reported in (DOBSON *et al.*, 1992) and in (IMHOFF, 1995), where C-band AIRSAR data acquired over coniferous forests in North America and Europe saturated at approximately 20 tons/ha.

The ERS backscatter seems to provide relevant information about stem volume only for sparse or very young forests, as pointed out for example in (KASISCHKE *et al.*, 1994), being irrelevant for mapping dense forests. In (PULLIAINEN, *et al.*, 1996) twelve ERS-1 images acquired over two test sites in Finland with stem volumes up to 400 m³/ha were combined in a multi-temporal approach. The estimation error was found to decrease compared to single images although the 90 m³/ha RMSE and the rather spread-out scatterplots presented show the low accuracy achievable from the inversion of ERS backscatter data. Besides the well-known low sensitivity of C-band backscatter to stem volume, the authors explained the poor results as an effect of speckle. For increasing stand size it was showed that the estimation error decreases. Similar conclusions were reported in (KURVONEN, *et al.*, 1999) where two ERS images were investigated in an 1800 km² large area in South Finland. The relative RMSE decreased for increasing forest block size, reaching a saturation level of approximately 30 % at stands larger than 20 ha. The authors analysed the implications of the number of images combined on the estimates accuracy as well,

reporting that, although the error decreases for increasing number of images, more important is the quality of the information contained in each image.

Results from retrieval carried out in Kättböle and Tuusula were consistent and confirmed the poor quality of stem volume estimates based on ERS backscatter. The RMSE was always greater than 100 m³/ha in Kättböle, except for one case when the error was 82 m³/ha. The situation was even worse in Tuusula where the RMSE was at least 200 m³/ha (Figure 7.2 and Table 7.1). The relative RMSE shows the higher inaccuracy of the estimates in Tuusula (Table 7.2). Low sensitivity to stem volume, i.e. small dynamic range, and large dispersion of the backscatter measurements equally characterised both test sites. Since most stands could not be classified in the inversion, the larger interval of stem volumes measured in Tuusula explains the higher error. The R^2 coefficient between ground-truth and SAR-based estimates was mostly below 0.1, reaching in a couple of acquisitions 0.36. This clearly shows that the two quantities do not correlate at all.

The multi-temporal combination decreased the noise but the result was still too poor to be acceptable (Tables 7.3 and 7.4). Results were in line with previous investigations for small sized stands and suggest that ERS backscatter is useless for stem volume retrieval, unless only large stands with low stem volume are investigated.

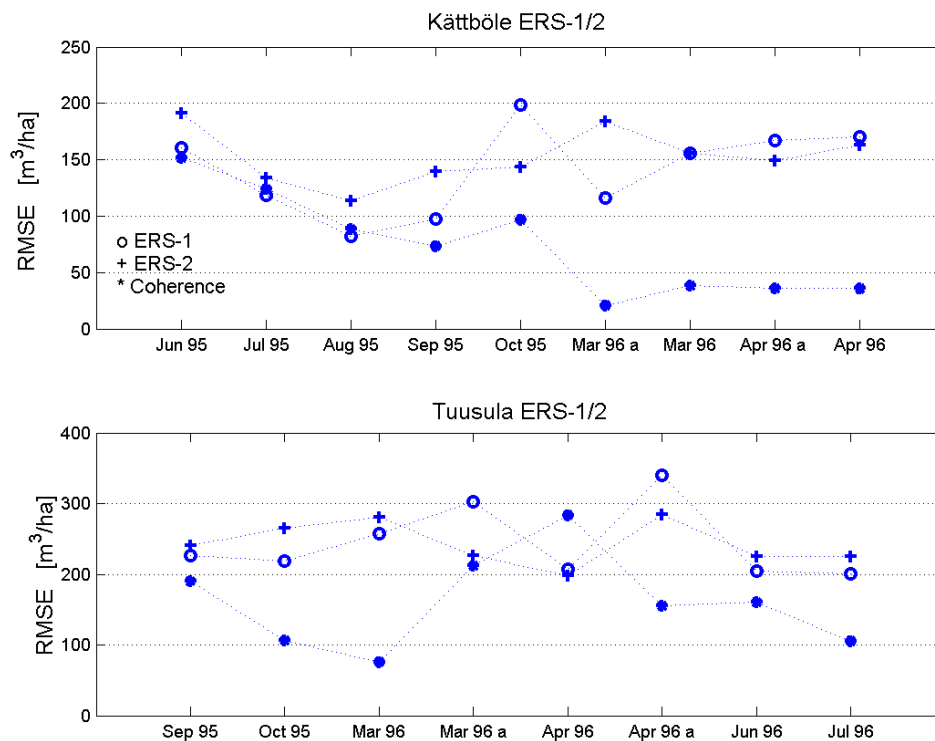


Figure 7.2. Stem volume retrieval accuracy, expressed in terms of RMSE, for ERS backscatter and coherence images in Kättböle and Tuusula.

7.3.2 ERS coherence

As pointed out in (ASKNE *et al.*, 1997), ERS coherence does not seem to suffer from saturation at low stem volumes, thus being more suitable for stem volume retrieval than the backscatter. The first investigations carried out on stem volume retrieval using coherence data were all based on linear regressions. For a subset of images acquired over Kättböle, (SMITH *et al.*, 1998) and (FRANSSON, *et al.*, 2001) obtained a RMSE of 31 m³/ha. The highest accuracy was achieved in pairs acquired during winter, under stable weather conditions at and between acquisitions. Similar conclusions were reported by (MANNINEN *et al.*, 2000), where the retrieval in forest stands larger than 2 ha located in South East Finland was characterised by a RMSE of 54 m³/ha for a range of stem volumes between 0 and 450 m³/ha. In a comparison of various remote sensing data types, (HYYPPÄ *et al.*, 2000) seems to contradict the good results reported in the previous studies. The standard error of 90.9 m³/ha should be interpreted as worst-case scenario since the images available were mostly acquired under changing environmental conditions. Poor results have been reported in (KOSKINEN *et al.*, 2001) as well. A subset of the images considered in this thesis over Tuusula was investigated by means of a semi-empirical model. Although a scatterplot showed agreement between the distribution of retrieved and ground-truth stem volume, the standard error of the estimate was 99 m³/ha. It is possible to argue that the result could have been even less accurate since the same data were used for training and testing the model.

Compared to the ERS backscatter, the plots reported in Chapter 6 have showed the higher sensitivity of the coherence to stem volume. These figures indicate that it is possible to obtain stem volume estimates much more accurately than from the two backscatter images forming the interferometric pair.

Figure 7.2 shows that both in Kättböle and in Tuusula stem volume could be predicted more accurately using coherence than backscatter. The most accurate estimates were achieved for pairs acquired in winter under stable weather conditions. In Kättböle the four pairs acquired in March and April 1996 showed consistent results, having errors between 21 and 38 m³/ha. In Tuusula only one of four pairs acquired in winter (2-3 March 1996) was characterised by stable weather and showed an RMSE of 76 m³/ha. Changes in the dielectric properties of the ground caused the decorrelation and, consequently, a significant error in the retrieval. Pairs acquired at the time of meteorological events or weather changes between passes did not provide any information.

Since these investigations had several images in common with the studies reported in (FRANSSON, *et al.*, 2001) and (KOSKINEN, *et al.*, 2001) respectively in Kättböle and Tuusula, it has been possible to compare results, although it must be mentioned that in Tuusula the test set used by the authors included many more stands. At both test sites the RMSE obtained from our model-based estimates was generally lower. Similar errors were mostly found in pairs showing saturation or low sensitivity of coherence to stem volume. Nevertheless, since the information content of such pairs is rather limited, it can be concluded that the IWCM fits the data better and should therefore be preferred to linear regression.

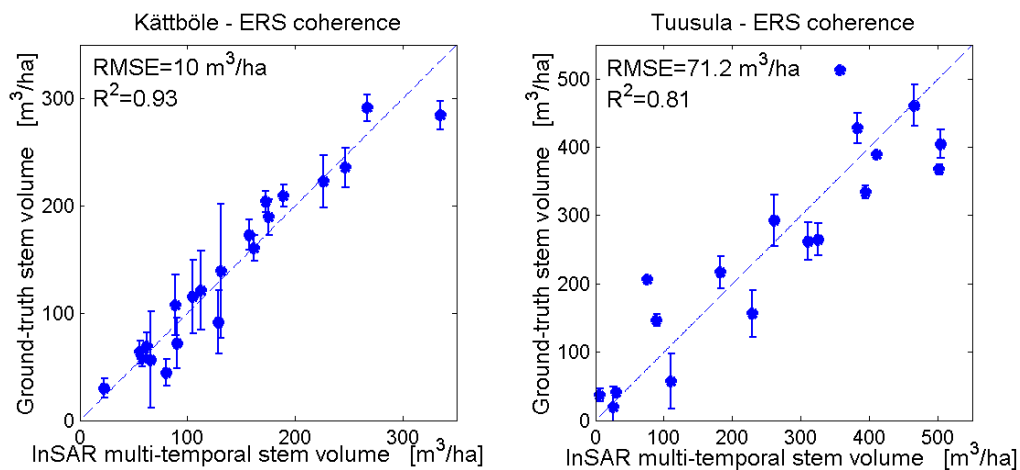


Figure 7.3. Comparison between multi-temporal estimates obtained from a combination of all coherence images available, and ground-truth stem volume, at stand level in Kättböle (21 stand) and Tuusula (18 stands). Error bars represent one standard error in the ground-truth estimates.

When several images were used in the multi-temporal approach, the error was lower than in each single image included in the combination (compare Tables 7.1 and 7.3). The RMSE did not always decrease for increasing number of images used but it mainly depended on which images were combined. Coherence-based estimates performed much better than those obtained from the backscatter (see Table 7.3). Adding intensity images to coherence images did not improve the accuracy. The best result was obtained in Kättböle when only winter-type pairs without meteorological changes between acquisitions were considered, reaching an error of $10 \text{ m}^3/\text{ha}$. Increasing the number of pairs combined did not further reduce the error. Using a multi-temporal combination of all interferometric pairs available, Figure 7.3 shows the extremely good results obtained in Kättböle, which are comparable to the ground-truth values, and the reasonable estimates achieved in Tuusula. Stem volume could be retrieved in the range of stem volume measured in the area without apparent signs of strong noise components or saturation.

The fundamental requirement for an accurate retrieval of stem volume is the big difference between ground and vegetation coherence. This is obtained in pairs acquired under stable weather conditions. Although there were more of such cases in Kättböle than in Tuusula, meteorological events cannot be considered entirely responsible for the consistently larger errors registered in Tuusula both in single-pairs and in the multi-temporal estimates. Reasons for such results were probably due to:

- Stand size. In Kättböle stand size and number of pixels within a stand for averaging were larger than in Tuusula. Hence, the coherence should have been less affected by uncertainty.
- Ground-truth accuracy. The estimation of forest parameters was more accurate in Kättböle than in Tuusula, as mentioned in Chapter 3.

If the coherence and the stem volume used for training are affected by errors, these propagate to the model-based curve and therefore to the estimates of stem volume, which include as well the error related to the fact that the coherence of the test stands does not entirely coincide with the true coherence. Finally, when computing the RMSE we would compare an estimate of stem volume affected by several sources of error to a stem volume that includes the inventory errors, leading to wrong conclusions. This digression stresses the importance of very accurate

1. Ground-truth data (for model training).
2. Coherence estimates (both for training and testing the model).
3. Backscatter measurements (since they are involved in the training process as well).

Yet another reason that was considered to explain the different retrieval accuracy was the effect of the forest structure on the coherence. Model training and inversion procedure are based on the fact that coherence is directly related to stem volume. As pointed out in (SMITH, 2000), it should rather be that the forest structure, i.e. the canopy closure to which stem volume is proportionally related, determines the coherence. This suggested to investigate whether there were differences in the structural properties of the forests such to influence the relationship between coherence and stem volume. Measurements of the area-fill factor taken in few dense forest stands at each test site were not characterised by significant differences. This result is not exactly in line with the initial assumption, which can either mean that the area-fill factor is not the correct parameter to be used for such type of investigation or the different retrieval errors are related to some other forest property not yet considered.

7.3.3 JERS backscatter

Compared to C-band, the higher sensitivity of L-band backscatter to forest attributes is clearly shown by the higher saturation level and correlation observed in several experiments, not only in boreal forests (DOBSON, *et al.*, 1992; LE TOAN *et al.*, 1992; ISRAELSSON *et al.*, 1994; RIGNOT *et al.*, 1994; IMHOFF, 1995; HALLIKAINEN, *et al.*, 1998). Using EMISAR data at two test sites located in Britain and in Sweden close to Kättböle, (BAKER & LUCKMAN, 1999) reported a higher dynamic range at L-band, although the Swedish test site showed saturation at lower stem volumes probably because of the rougher and wetter conditions of the ground. In (ISRAELSSON *et al.*, 1995; FRANSSON & ISRAELSSON, 1999; KURVONEN, *et al.*, 1999) it has been shown that the JERS backscatter in Swedish and Finnish boreal forests saturates between 150 and 225 m³/ha, thus being more suitable than ERS C-band for stem volume retrieval. In particular (FRANSSON & ISRAELSSON, 1999) reported an interesting correlation between ground-truth and retrieved stem volume ($r=0.781$). Similar conclusions were presented by (HARRELL *et al.*, 1995), who investigated ERS and JERS backscatter with implications for biomass estimation in Alaskan forests. The retrieval of stem volume from JERS backscatter was investigated in (KURVONEN, *et al.*, 1999). Compared to the ERS backscatter, the use of JERS data improved the accuracy but reasonable estimates could be obtained only when stands larger than 10

ha and at least two images were combined in a multi-temporal fashion. For stands larger than 20 ha, there did not seem to be any difference in accuracy between ERS- and JERS-based estimates. A combination of six ERS and JERS backscatter images was found to decrease the relative estimation uncertainty to 25% with a correlation coefficient of 0.73. In their evaluation of several remote sensing data sources (HYYPPÄ, *et al.*, 2000) showed that for forest parameters estimation the JERS backscatter is more promising than ERS backscatter but still inferior to the ERS coherence.

The plots reported in Chapter 6 clearly showed that in Kättböle the JERS backscatter is more suitable for stem volume retrieval than in Siberia. In Tuusula the small dynamic range and the spread of the backscatter data suggested that the accuracy of the stem volume estimates would have been poor.

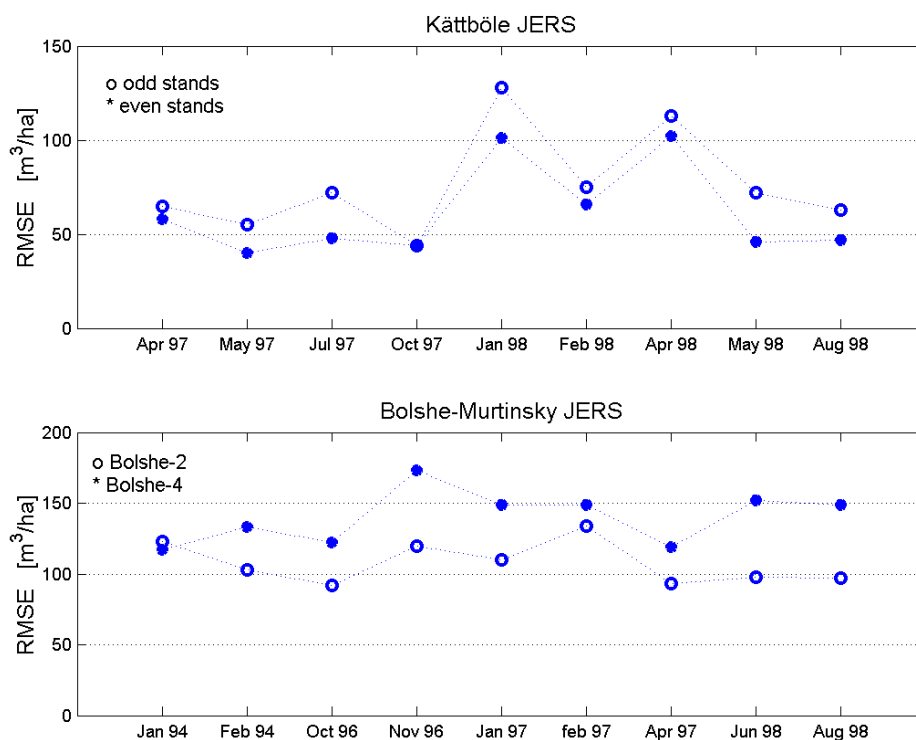


Figure 7.4. Stem volume retrieval accuracy, expressed in terms of RMSE, for JERS backscatter images in Kättböle and Bolshe-Murtinsky.

Retrieval of stem volume performed more accurately in Kättböle, where several images had consistent RMS errors between 40 and 50 m³/ha in the test set formed by even positioned stands (Table 7.1 and 7.3, Figure 7.4). These were all cases acquired under dry-unfrozen conditions. When thaw or winter-frozen conditions occurred, the accuracy decreased. In Bolshe-Murtinsky, worse results were found at Bolshe-2, where stem volume was generally higher than at Bolshe-4. All images were characterised by winter-frozen conditions, freeze/thaw events or precipitation. These

results suggest that the retrieval of stem volume from JERS backscatter data should be avoided in winter periods and in case of strong precipitation. The worst absolute RMSE was registered in Tuusula, although in terms of relative RMS errors, Bolshe-Murtinsky and Tuusula behaved quite similarly. Not only the less suitable weather conditions for retrieval encountered in Siberia and Finland, but also the different stem volume distributions, which particularly in Bolshe-Murtinsky might have strongly affected the model training, and the ground-truth errors were considered responsible for the discrepancy of accuracy between Kättböle and the other test sites.

Looking at Table 7.1 it is possible to notice that JERS backscatter performs better than the ERS backscatter but worse than the ERS coherence, thus confirming the evaluation reported in (HYYPÄ, *et al.*, 2000). When training and test set were switched, the results changed, thus showing that training and test set should be as similar as possible (Figure 7.4).

With a multi-temporal combination the error decreased significantly except for Bolshe-4. In Kättböle the RMSE showed very promising results for the application of JERS backscatter for stem volume retrieval (Figure 7.5 and Table 7.3). Very different was the situation at the other test sites, where the rather high relative RMSE, between 40% and 50%, limits the previous conclusions to Kättböle. Both in Kättböle and Bolshe-Murtinsky, the combination of images acquired during the leaf-on period gave the most accurate results. These did not improve when other images were considered in the combination. From Figures 7.5 and 7.6, it can be seen that reliable estimation can be provided for the whole range of stem volumes in Kättböle, whilst in Bolshe-Murtinsky a value of 200 m³/ha seems to be the uppermost limit for the use of JERS backscatter. Above this level, the stem volume is mostly spread out and underestimated, because saturation of the backscatter has occurred in the interval of intermediate stem volumes.

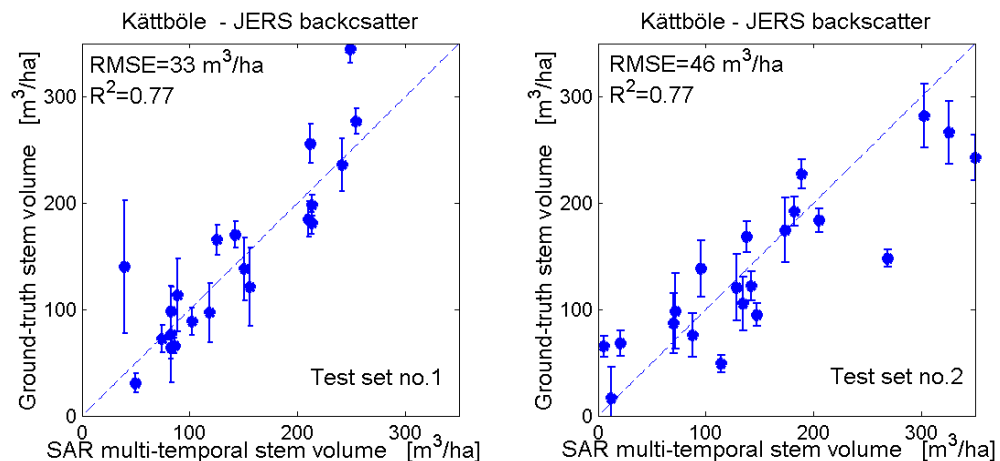


Figure 7.5. Comparison between multi-temporal estimates obtained from a combination of all JERS backscatter images available, and ground-truth stem volume, at stand level in Kättböle. Test set no.1 refers to even positioned stands. Test set no.2 includes odd positioned stands. Both sets include 21 stands. Error bars represent one standard error in the ground-truth estimates.

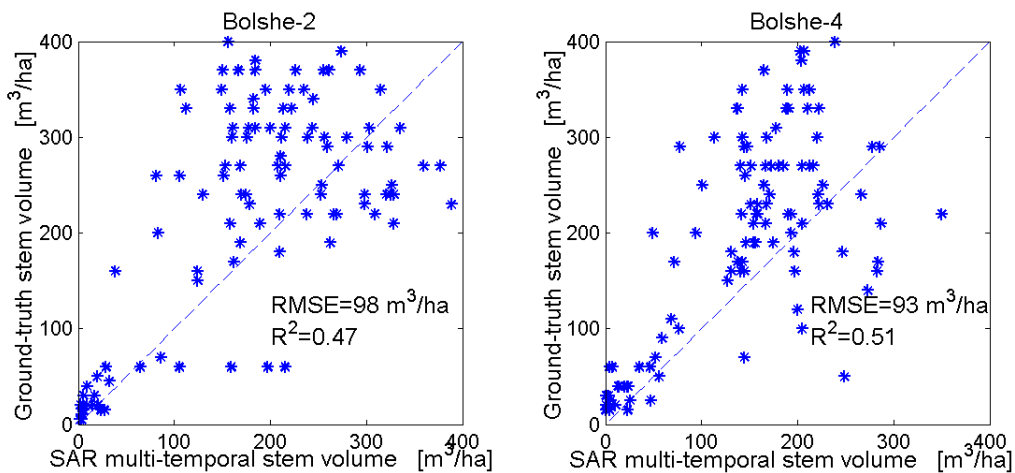


Figure 7.6. Comparison between multi-temporal estimates obtained from a combination of all JERS backscatter images available, and ground-truth stem volume, at stand level in Bolshe-Murtinsky. The test set at the two compartments included 110 and 115 stands respectively.

7.4 Plot-wise retrieval

The very promising results obtained with ERS coherence at stand level suggested that stem volume could be estimated with a relatively good accuracy at scales finer than a stand. Areas smaller than stands and of interest to forest inventory are plots, i.e. the basic sampling units.

Retrieval at plot level means that stem volume is estimated from one or few pixels. Plots have a diameter between 15 and 20 m, while the pixel size of SAR and InSAR images is generally about 20 by 20 m after multi-looking and geocoding. Due to speckle, the retrieval using backscatter data is not feasible. Coherence instead should be less affected by noise, although filtering of the image is recommended before retrieving stem volume. Because of the small size of the sample, the coherence-based retrieval at plot level is limited by two factors: the accuracy of the coherence estimate at pixel level and the geometric mismatch between the plot and the corresponding pixel.

It was previously mentioned that the measured coherence is only an estimate of the true coherence. Contrarily to stand-wise retrieval, at plot level we must count on the values of just the pixel; therefore, it is fundamental that the coherence of the pixel is as accurate as possible. In areas of low coherence, as forests, the coherence is affected by large uncertainty. A large window would improve the accuracy of the estimate but at the same time decrease the resolution so that the value found at pixel level would be influenced by the properties of the neighbouring pixels. In the end, the required accuracy might not be reached, which in turn will show its effects on the retrieved stem volume.

	ERS backscatter		ERS coherence		JERS backscatter	
	RMSE	R ²	RMSE	R ²	RMSE	R ²
Kättböle	82.4	.19	20.9	.92	40.0	.77
Kättböle (plot-level)	-	-	62.9	.50	-	-
Swedish NFI (plot-level)	-	-	77.8	.36	-	-
Tuusula	198.1	.15	76.0	.80	125.6	.61
Bolshe-2	-	-	-	-	117.0	.43
Bolshe-4	-	-	-	-	92.0	.43

Table 7.1. Best RMSE (in m³/ha) and corresponding R² for retrieval using single images.

	ERS backscatter	ERS coherence	JERS backscatter
Kättböle	61.0	15.0	29.6
Kättböle (plot-level)	-	43.7	-
Swedish NFI (plot-level)	-	47.4	-
Tuusula	77.1	29.6	48.9
Bolshe-2	-	-	53.6
Bolshe-4	-	-	49.3

Table 7.2. Best relative RMSE (%) for retrieval using single images

To determine the position of a plot, traditional surveys make use of GPS measurements, which in dense forested areas are typically characterised by a 5 to 10 m absolute positioning error. Since geocoded images might suffer from misplacements, a plot and the corresponding pixel in the coherence images might not coincide. Coherence images and plot maps would therefore not perfectly overlap so that the coherence used would probably not coincide with the coherence of the plot of interest. A filter, such as a mean or a median filter can reduce the effect of the geometric mismatch (SANTORO, *et al.*, 2002b). Nevertheless, the window size should be small in order not to decrease the resolution.

	ERS backscatter		ERS coherence		JERS backscatter	
	RMSE	R ²	RMSE	R ²	RMSE	R ²
Kättböle	74.2	.13	10.4	.93	33	.77
Kättböle (plot-level)	-	-	55.0	.56	-	-
Swedish NFI (plot-level)	-	-	71.2	.43	-	-
Tuusula	155.5	.25	71.2	.81	103.4	.72
Bolshe-2	-	-	-	-	98.0	.47
Bolshe-4	-	-	-	-	93.0	.51

Table 7.3. RMSE (in m³/ha) and R² for multi-temporal combination of single images estimates.

	ERS backscatter	ERS coherence	JERS backscatter
Kättböle	53.4	7.5	22.0
Kättböle (plot-level)	-	39.6	-
Swedish NFI (plot-level)	-	43.4	-
Tuusula	60.0	27.5	40.1
Bolshe-2	-	-	44.9
Bolshe-4	-	-	49.8

Table 7.4. Relative RMSE (%) for multi-temporal combination of single images estimates.

The retrieval of stem volume at plot level puts strong requirements on the correctness of the model training and on the images to be used. On one hand, stand-wise measurements of coherence and stem volume should be preferred to plot-wise values because of the higher accuracy of both types of data. On the other hand, since the accuracy of the plot-wise InSAR stem volume estimates is expected to be lower than at stand level, pairs known to provide inaccurate results already at stand level should be discarded.

In Kättböle plot measurements in those stands previously considered for the evaluation of stand-wise stem volume retrieval were used as test samples. The retrieval was carried out for the four pairs that performed best in the stand-wise analysis (i.e. the pairs acquired in March and April 1996). For each plot the corresponding pixel in the coherence images were extracted and the IWCM was inverted. The RMS errors and R² values obtained at stand and at plot level can be

compared in Table 7.5. Plot-wise retrieval followed the patterns seen at stand level but showed bigger errors, which were partially corrected for with the multi-temporal combination. Nevertheless, the filtered estimates did not have the high accuracy reached at stand level.

	Kättböle (stand)		Kättböle (plot)		Swedish NFI (plot)	
	RMSE	R ²	RMSE	R ²	RMSE	R ²
12-13 March 1996	20.9	.92	62.9	.50	77.8	.36
17-18 March 1996	38.4	.74	80.4	.25	114.3	.12
16-17 April 1996	35.8	.77	81.5	.21	111.3	.16
21-22 April 1996	35.6	.74	77.7	.35	100.3	.21
Combination of the four images	10.0	.94	55.0	.56	71.2	.43

Table 7.5. RMSE (in m³/ha) and R² for retrieval based on ERS coherence images. The test set consisted of 21 stands and 216 plots in Kättböle, and of 166 plots in the Swedish NFI area.

The scatterplot on the left in Figure 7.7 illustrates the level of agreement between ground-truth and InSAR multi-temporal stem volume estimates. The large spread and the tendency to underestimation at very high stem volumes could be explained as a consequence of positioning errors and inaccuracies in the coherence values. These factors are stronger at plot level than at stand level, where averaging is performed and therefore noise is partly filtered out.

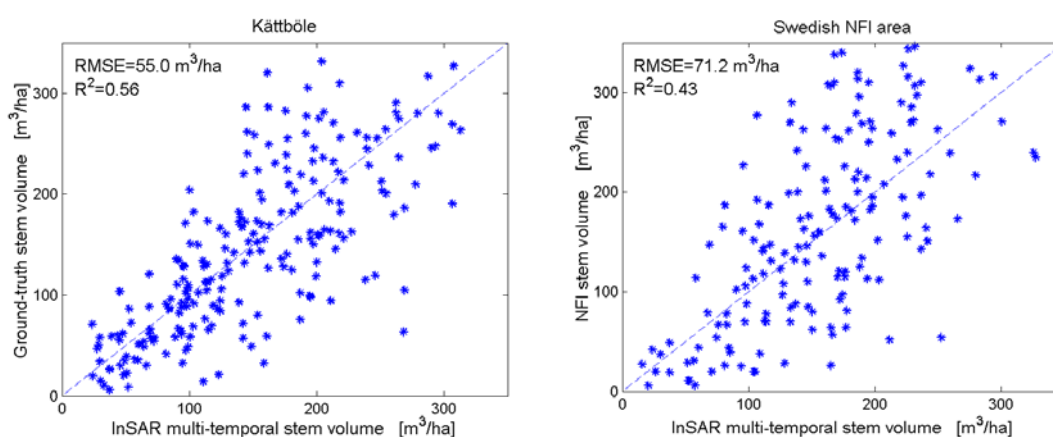
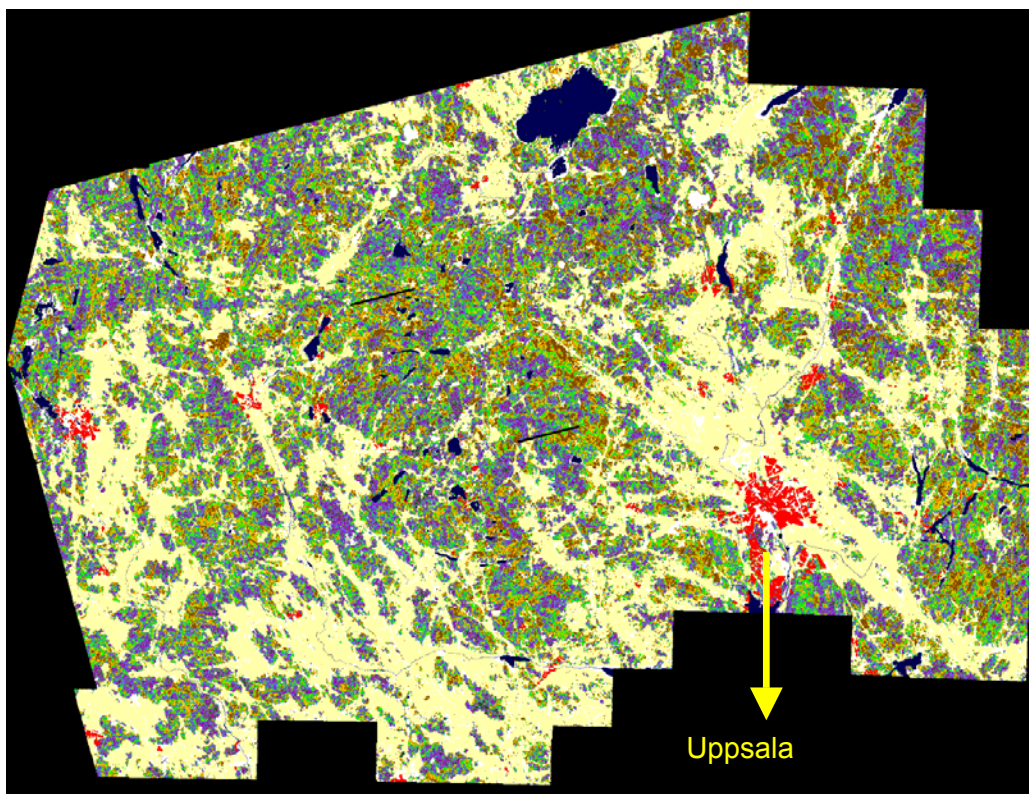


Figure 7.7. Comparison between multi-temporal estimates obtained from a combination of four coherence images and ground-truth stem volume at plot level in Kättböle (216 plots) and in the NFI area (166 plots) Before estimation the coherence images had been median filtered in a 3 by 3 window.

The inversion of coherence on a pixel basis was not only used for the evaluation of plot-wise retrieval in Kättböle but also to produce stem volume forest maps. Taking into account that forest inventory in large areas is carried out at a limited number of plots distributed on a large territory, theoretically a forest stem volume map covering areas of thousands of square kilometres with a resolution equal to the plot size would be an extremely desirable product. For this purpose it is fundamental to train the model at stand level in areas where very accurate ground-truth and coherence measurements are available (the forest estate of Kättböle for example). The inversion of coherence is then performed at pixel level in forested areas surrounding the training area and covered by the images (SANTORO, *et al.*, 2002b).




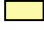



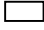





Stem volume	$0 \div 50 \text{ m}^3/\text{ha}$		Cultivated areas	
Stem volume	$51 \div 100 \text{ m}^3/\text{ha}$		Urban areas	
Stem volume	$101 \div 150 \text{ m}^3/\text{ha}$		Open areas	
Stem volume	$151 \div 200 \text{ m}^3/\text{ha}$		Water areas	
Stem volume	$201 \div 250 \text{ m}^3/\text{ha}$			
Stem volume	$251 \div 300 \text{ m}^3/\text{ha}$			
Stem volume	$301 \div 350 \text{ m}^3/\text{ha}$			

Figure 7.8. Forest stem volume map of a 4235 km² large area centred in the forest estate of Kättböle (SANTORO, *et al.*, 2002b). Stem volume has been estimated from four coherence images acquired in March and April 1996. The map has been superimposed onto a digital land-cover map. For displaying reasons, stem volumes have been grouped into intervals of 50 m³/ha each.

The fundamental assumption underlying this procedure is that the environmental conditions must be the same all over the scene. A difference in the weather or in the ground properties within the imaged area would alter the relationship between coherence and stem volume, thus leading to wrong stem volume estimates. This aspect has been considered in the SIBERIA project, where a forest map over an approximately 1 million km² large area was produced from ERS coherence data (SCHMULLIUS & ROSENQUIST, 1997; SCHMULLIUS *et al.*, 2001). In particular (WAGNER *et al.*, 2003) correctly pointed out that, in order to obtain spatially consistent estimates of stem volume in very large areas, the retrieval method should be independent of the properties characterising a local training set.

In Figure 7.8 the forest stem volume map for an area of 4235 km², surrounding the forest estate of Kättböle is reported. For each pixel defined as productive forest land in a land-cover map provided by the Swedish National Land Survey, stem volume was estimated. Once again, only the four coherence images that performed best at stand level in Kättböle were used. The forest map represents a multi-temporal combination of the four channels.

In order to verify the accuracy of the map, a set of plots provided by the Swedish National Forest Inventory was used. These were the only measurements easily obtainable, which stresses a common problem when assessing the accuracy of a remote sensing product: the insufficient amount of reference data. For each NFI plot, the stem volume estimates were compared to the measured ground-truth value. Compared to Kättböle, Figure 7.7 and Table 7.5 show larger errors, which are probably due to heterogeneities of the environmental conditions in the area. The spatial variability of the environmental conditions became relevant especially in pairs characterised by temperatures around the freezing point during the period of acquisition and by changing snow conditions (17-18 March and 16-17 April).

To confirm these assumptions, in (SANTORO, *et al.*, 2002b) scatterplots comparing retrieved stem volumes from each of the four pairs were reported. The scatterplots for 12-13 March and 21-22 April (Figure 7.9) showed an agreement between retrieved stem volumes up to about 200 m³/ha, proving that both pairs were suitable for retrieval in the large area. The comparison with the 17-18 March pair clearly showed the spatial inconsistency of the estimates (Figure 7.10), whereas the 16-17 April pair showed consistent but underestimated stem volumes.

These results show the limits of SAR interferometry for mapping of large areas at plot level. Nevertheless a comparison with results obtained in (FAZAKAS *et al.*, 1999) from Landsat data in Kättböle and part of the large area, showed the higher potential of ERS coherence for stem volume retrieval at plot level.

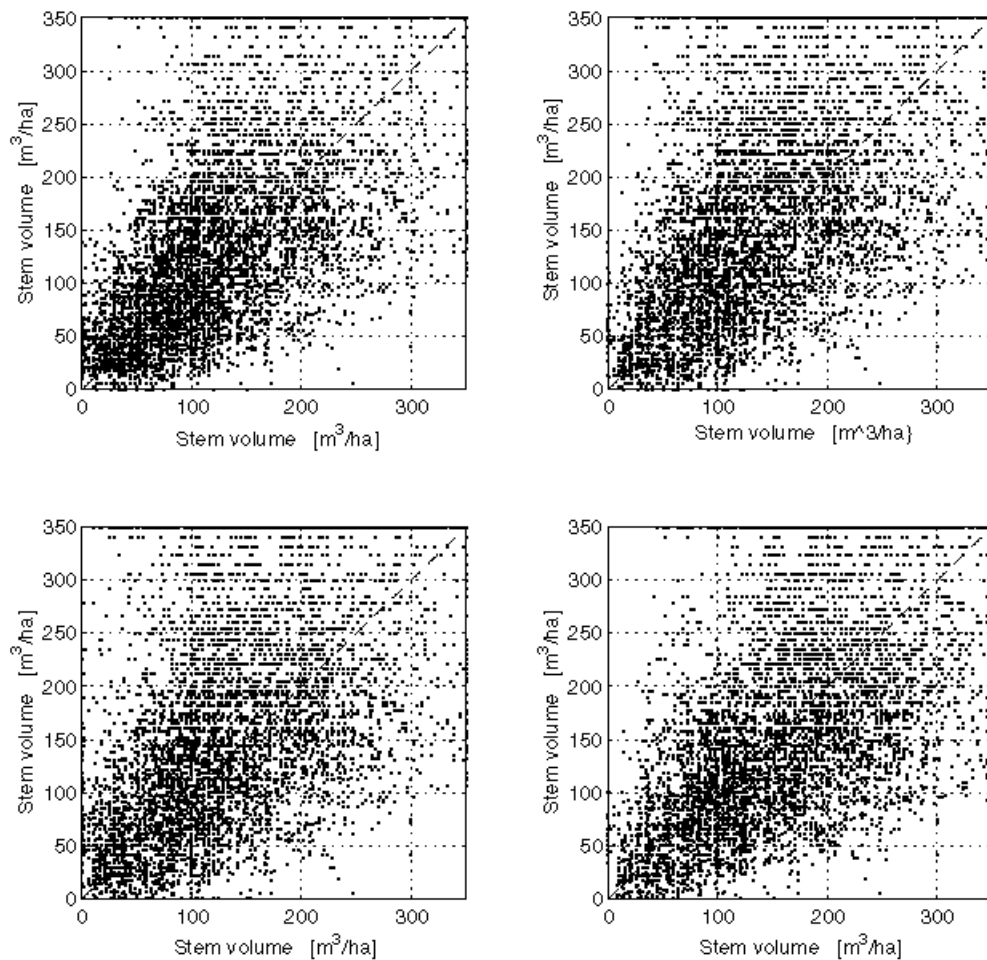


Figure 7.9. Scatterplots of pixel-wise retrieved stem volume in four squares randomly located in the large area. The x- and y- axis respectively report the estimates from the 12-13 March and the 21-22 April 1996 pairs (SANTORO, *et al.*, 2002b).

7.5 Retrieval at regional level

Plot measurements in the Swedish NFI database are used to infer the properties of forests at regional and national level. The statistical design of the sampling procedure has been under investigation in the last two decades and several changes have been made in order to increase the accuracy of forest parameters estimates (RANNEBY *et al.*, 1987). (NILSSON, 1997) and (FAZAKAS, *et al.*, 1999) reported that the present sampling technique gives estimates with a relative RMSE below 10 % for areas of at least 25000 ha (i.e. 250 km²), whereas at a higher resolution the traditional inventory based on ground-based surveys is not able to provide accurate estimates of the forest properties. Even at regional level (LI & RANNEBY, 1992) presented coefficients of variation with a high uncertainty, depending on region and class of the forest attribute.

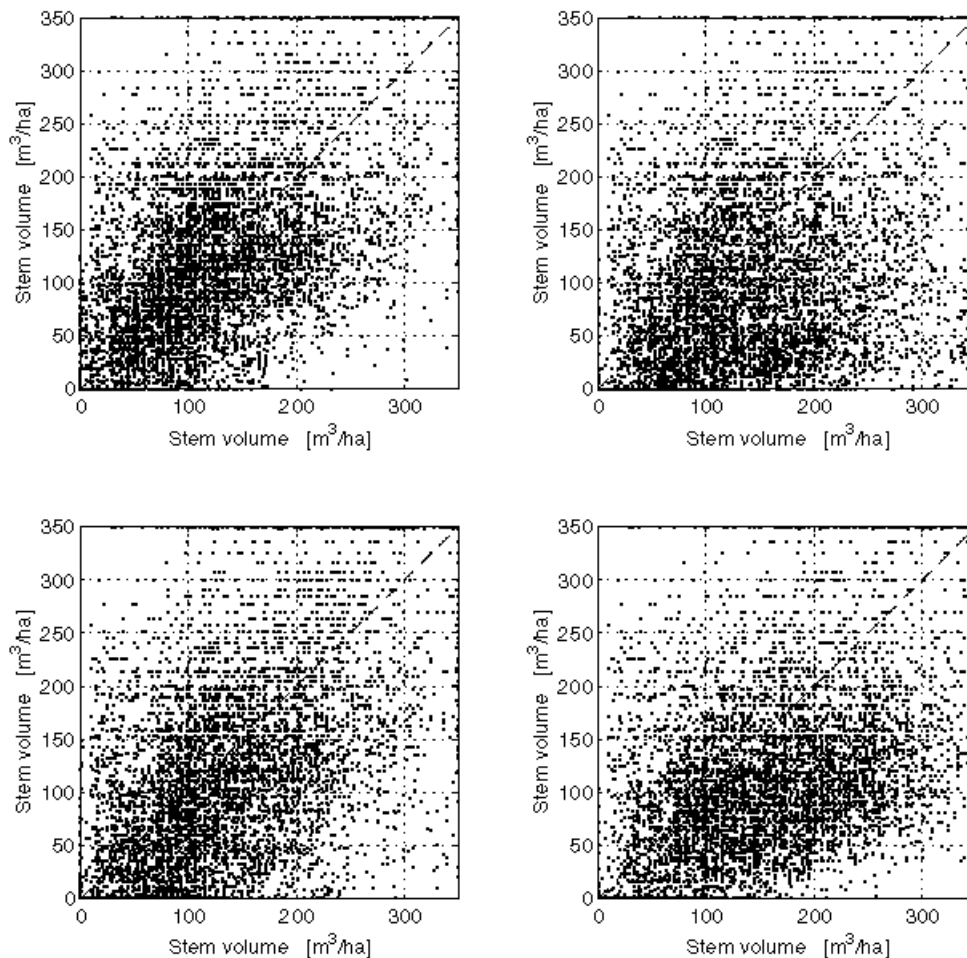


Figure 7.10. Scatterplots of pixel-wise retrieved stem volume in the same four squares described in Figure 7.9. The x- and y- axis respectively report the estimates from the 12-13 March and the 17-18 March 1996 pairs (SANTORO, *et al.*, 2002b).

In order to improve regional and national inventory of forest resources, (NILSSON, 1997) and (FAZAKAS, *et al.*, 1999) evaluated the possibilities offered by optical remote sensing as data source alternative to local surveys. Although estimates of stem volume at pixel level were affected by significant errors, their spatial average provided new estimates with accuracy increasing for increasing size of the area in which averaging was performed. The authors concluded that a procedure based on Landsat data and the *kNN* (Nearest Neighbour) method provides reliable estimates already in 100 ha large areas.

Using SAR interferometry, a similar approach was considered (see also (SANTORO, 2001) and (ASKNE *et al.*, 2001)). Starting from the stem volume map reported in Figure 7.8, the NFI and the multi-temporal estimates of stem volume have been aggregated in areas of increasing size and then compared. For each block size in which averaging was performed, mean and standard deviation of stem volume were computed. The results are reported in the two upper plots in Figure 7.11 for the

aggregated InSAR-based estimates (left) and the NFI plots (right). These plots show that the InSAR mean stem volume is smaller, because of the underestimation due to the low sensitivity of coherence at high stem volumes. Nevertheless, the absolute errors in the ground-truth estimates should be taken into account. The uncertainty affecting the ground-truth estimates is much larger because of the fewer points available in each block for computing the averages.

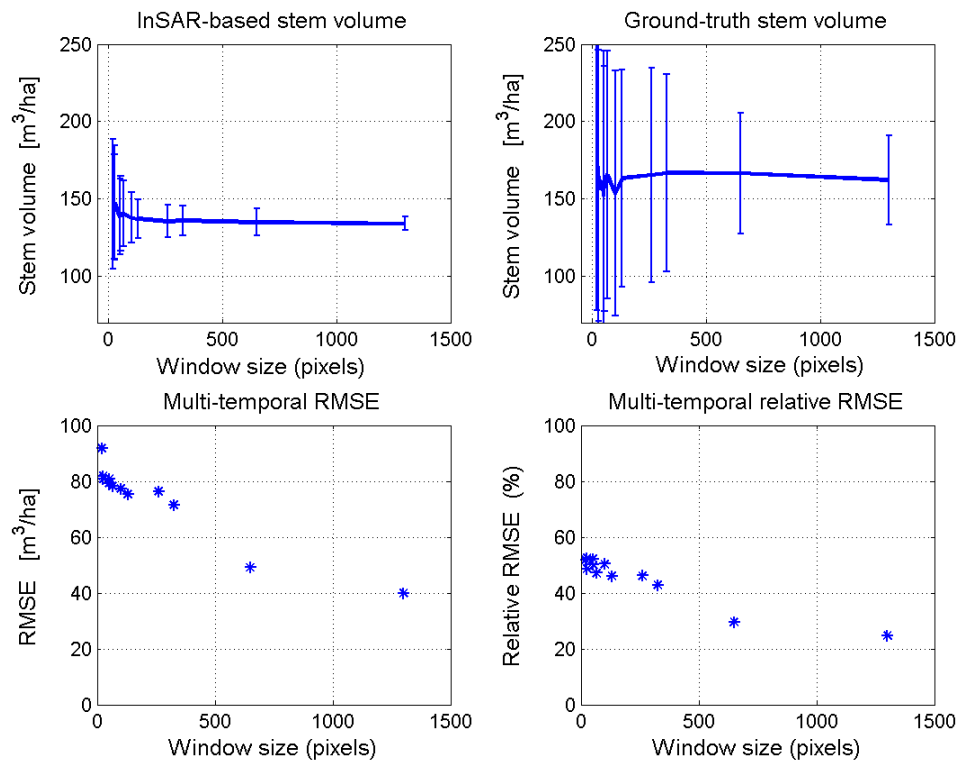


Figure 7.11. For increasing averaging areas, mean value and standard deviation of multi-temporal retrieved stem volume (top left), NFI ground-truth stem volume (top right), RMSE (bottom left) and relative RMSE (bottom right). The area size is reported in terms of the averaging window size. A 500 by 500 window corresponds to 156 km², a 1000 by 1000 window to 625 km², a 1500 by 1500 window to 1406 km² (SANTORO, 2001).

The lower plots in Figure 7.11 show that for increasing block size the relative RMSE between the two types of stem volume estimates decreases reaching a level of around 20 % for areas of the order of 1400 km². This result should be interpreted taking into account that the errors of the NFI-based regional level estimates decrease for increasing area and the averaged retrieved stem volumes might still suffer from errors introduced by the spatial variations of the environmental conditions in the coherence estimates. Since in small areas the NFI mean cannot be considered a totally reliable reference, the RMSE provides only an approximate measure of the regional-wise InSAR stem volume accuracy. For increasing size the inherent errors in the NFI source decreases, thus improving the information content of the RMSE. In

very large areas, of the order of 1000 km² the NFI plots should be accurate enough to be used as reference. The small relative error shows that regional estimates of stem volume can be obtained from SAR interferometry, although averaging in very large areas is needed in order to filter out as much noise as possible.

Compared to optical data the results are nonetheless slightly poorer, probably because the spatial variations of the environmental conditions were too irregular compared to the window size used for averaging and could therefore not be completely filtered out.

7.6 Conclusions

In this Chapter stem volume retrieval using ERS and JERS backscatter, and ERS coherence has been investigated at the three inventory units commonly used in forestry. The inversion of the WCM and the IWCM in a test set formed by samples independent from those used for training has been carried out at several test sites and results have been compared. An important point concerned the procedure to be adopted in case test samples could not be automatically classified in the inversion and the definition of outliers. These aspects are relevant, especially when working with ERS and JERS backscatter because of the small dynamic range and the signal saturation at already low stem volumes. Typically for each image a few samples might not be classified by the model but only according to subjective rules, which in turn makes comparisons more difficult to be carried out.

The accuracy of stem volume retrieval depends on the sensitivity of the remote sensing parameter to the forest attribute and on the weather conditions at acquisition. When more backscatter and coherence measurements are available for a forest sampling unit, typically the corresponding estimates are affected by different noise components, which are related to the ability of the each specific image to retrieve stem volume. This information, for example expressed by the RMSE between ground-truth and retrieved stem volume, can be used in a multi-temporal combination of single-image estimates to improve the quality of the retrieval. For the multi-temporal filtering the type of images combined is more important than their number.

For stem volume retrieval coherence is by far the most suitable parameter, since it is highly sensitive to forest properties and seldom suffers from saturation. Furthermore, it can be used for both stand-wise and plot-wise estimation. Speckle does not allow backscatter measurements to be used for inversion at plot level. Saturation at low stem volumes and relevant spread of the measurements make in particular the ERS backscatter almost useless.

At stand level coherence is able to predict stem volume with reasonable accuracy when winter conditions without meteorological events characterise the interferometric pair. Results were consistent in Kättböle, and generally more accurate than in Tuusula. When weather changes occur, the accuracy decreases. In case of precipitation and snowmelt the inversion does not provide any information. To

explain the differences in relative RMSE at the two test sites under investigation, the less suitable weather conditions in Tuusula were not considered sufficient. The lower accuracy of both the coherence estimates and the *in situ* measurements in Tuusula can be addressed as possible reasons, whereas nothing can be concluded concerning the effects of the forest structure since the area-fill factor measurements were at the two test sites very similar.

With a multi-temporal combination of several coherence images the retrieval error significantly decreases. Intensity images do not provide any additional information and can be neglected for further investigations. The four pairs acquired over Kättböle in winter, under stable conditions, predicted stem volume with the highest accuracy (RMSE= 10 m³/ha). When other images were added to the multi-temporal set, the accuracy did not increase. Although in Tuusula the relative RMSE was higher, we could observe a strong agreement between measured and retrieved stem volumes. The results obtained in Tuusula are even more important if we take into account that no apparent saturation occurred in the range of stem volumes up to 550 m³/ha.

These results show that the procedure based on 1) ERS coherence, 2) inversion of the IWCM and 3) multi-temporal filtering is able to predict stand-wise stem volume in boreal forests up to 550 m³/ha with high correlation. Furthermore, with very accurate ground-truth and coherence measurements it is possible to reach accuracy comparable to traditional forest inventory methods in an interval of stem volumes between 0 and 350 m³/ha.

Retrieval of stem volume using JERS-backscatter is mainly affected by weather conditions. Images acquired under dry-unfrozen conditions perform best, with a consistent accuracy of 40-50 m³/ha, whereas the error strongly increases for winter-frozen conditions or when environmental changes occur. The exchange of train and test set shows the importance of having the same distribution of stem volumes for a correct evaluation of the retrieval.

Although the stem volume estimates are less accurate in comparison to ERS coherence, the temporal consistency of the retrieval over several images and the reasonable RMSE make the JERS-type of backscatter an interesting data source. The final relative RMSE of 22% registered in a multi-temporal combination of the images acquired under dry-unfrozen conditions stresses even more the importance of spaceborne L-band backscatter for inventory applications in boreal forests.

Compared to stand-wise retrieval, at plot level the estimation performs worse. The 44% relative RMSE shows that retrieval at plot level is not feasible using coherence because of positioning errors and uncertainties in the coherence estimates due to the small size of the plots. An even higher error of 47% registered in the large NFI area was due to spatial variations of the environmental conditions. This not only confirms that at plot level spaceborne imagery is not able to provide estimates with the necessary accuracy but also stresses the problems connected with mapping in large areas. For the methodology presented in this thesis, stable weather and homogeneous environmental conditions are fundamental requirements to obtain reasonable accuracy in areas larger than a forest estate.

Estimation of stem volume at regional level is less affected by the spatial variability of the coherence signatures although this cannot be completely suppressed not even in very large averaging windows. Reasonable estimates with a 20% relative error are obtained in areas larger than 1400 km². Although optical remote sensing seems to be more appropriate than SAR as alternative source of information at large scales, problems related to full coverage limits the application of optical imagery in areas characterised by frequent cloud cover, such as Sweden. For practical reasons SAR interferometric data could therefore be preferred, in particular for estimates of region- and nation-wide stem volume.

Chapter 8

Tree height estimation

Another application of SAR interferometry in forested areas is the determination of the tree height. In this case, the parameter to be inverted is the interferometric phase. The InSAR phase provides information about the “topography” seen by an InSAR system. Since forests let an incoming wave propagate through the canopy, the topography seen is not related to the true tree height but gives information about the scattering height of the forest. In this case we speak of interferometric tree height. Theoretically, this measurement can be compensated for obtain the true tree height by taking into account the penetration of the electromagnetic wave into the canopy and volumetric decorrelation effects.

This Chapter is organised in order to provide the reader with a background on the properties of the InSAR phase in forests (Section 8.1) and the InSAR height (Section 8.2). The characterisation of the InSAR phase will be given in particular for the repeat-pass case. When two images are acquired at different times, the phase noise due to the unstable nature of the forest canopy dominates the InSAR phase. Nevertheless, the major error source when dealing with spaceborne repeat-pass InSAR phase is represented by atmospheric path delays. Section 8.3 gives a summary on atmospheric perturbations, followed by a description of filtering algorithms with particular regard to their application in the boreal zone (Section 8.4). In Section 8.5 interferometric tree height estimates are evaluated and compared to tree height measurements. The results showed in this Section are very important to understand the discussion presented in Section 8.6, where the ability of the IWCM to model the InSAR phase and the possibility to derive the true tree height from the interferometric height are presented. As usual, concluding remarks and a summary are included in Section 8.7. Since the quality of JERS interferograms was too low, the Chapter focuses on the ERS interferometric phase only.

8.1 InSAR phase in forests

It has been mentioned in previous Chapters that, because of the short wavelength, C-band waves mainly interact with the top layers of the forest canopy and the return from big branches, trunks as well as double bounces are negligible. Because of gaps in the forest canopy, part of the signal returned to the radar comes from the ground. Due to the strong tree attenuation, the ground contribution transmitted through the canopy can be considered of minor importance.

This combination of surface and volume scattering does not allow exactly locating a point that can be considered the origin of the backscattered signal. The scattering origin can be rather considered to be spread out from the top of the canopy to the ground around one point (the scattering centre) (HAGBERG *et al.*, 1995; FLOURY *et al.*, 1996b; ASKNE *et al.*, 1997b; SARABANDI & LIN, 2000) (Figure 8.1). The position of the scattering centre and the spread depend on the fraction of ground seen by the radar and on the spatial distribution and the strength of the scatterers within the tree crown. In dense forests, the scattering centre is located a few metres under the treetops. Young or sparse forests let the incoming wave penetrate more to the ground so that the scattering centre should be located closer to the forest floor.

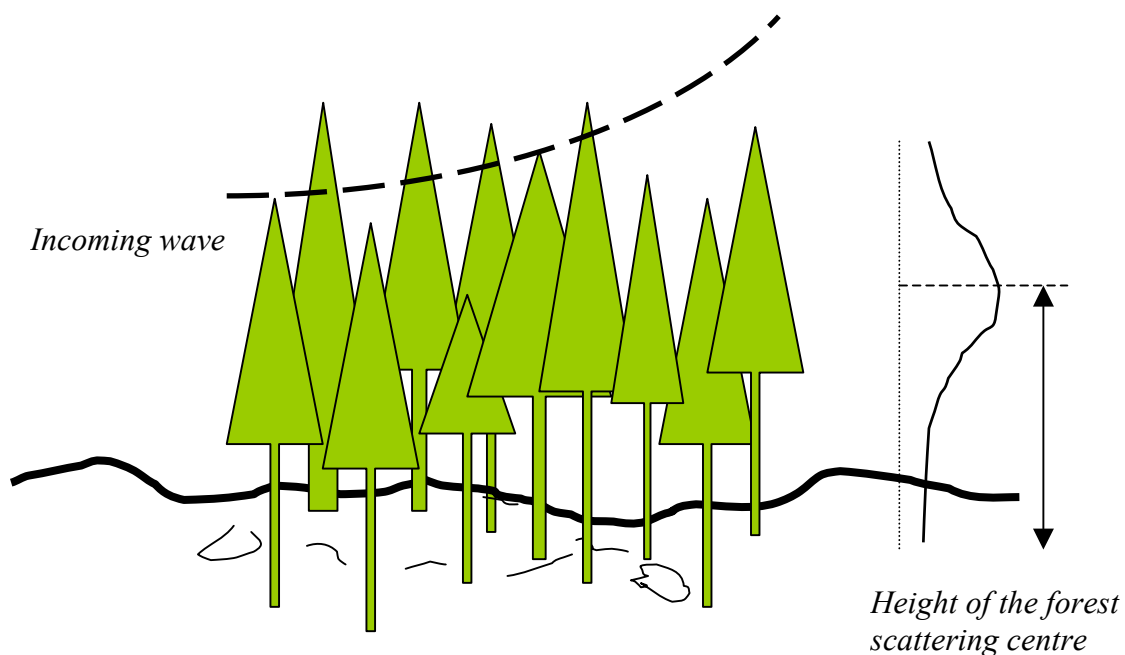


Figure 8.1. Scattering mechanism in a forest with regard to penetration properties and scattering strength along the forest vertical profile.

A forest is therefore seen by C-band SAR as a topographic feature, with a height related to the position of the scattering centre above the ground reference level. Since SAR interferometry can detect topography, the InSAR phase from two SAR images of the forest can be used to infer the height of the scattering centre. It has to be noticed that with SAR interferometry only the height of the scattering centre can be

determined and not the true tree height. This last parameter can be estimated from the height of the scattering centre, by means of a compensation for the attenuation through the tree canopy.

In a repeat-pass configuration, the total SAR phase in a resolution cell is likely to change between two acquisitions because of the unstable nature of the forest canopy. Considering a whole forest, not only the scattering centres will have changed position within the canopy but also the distribution of the scattering around them will be probably characterized by different properties. In other words, the forest topography seen by the SAR and the corresponding uncertainty is different at the two acquisitions. The InSAR phase includes therefore a significant noise component that dominates the topographic information. In sparse or young forests, where the ground contribution to the signal echoed back to the radar is relevant, the forest topography seen by the radar should be less affected by the temporal variability of the scattering so that the position of scattering centre should be estimated with a higher accuracy.

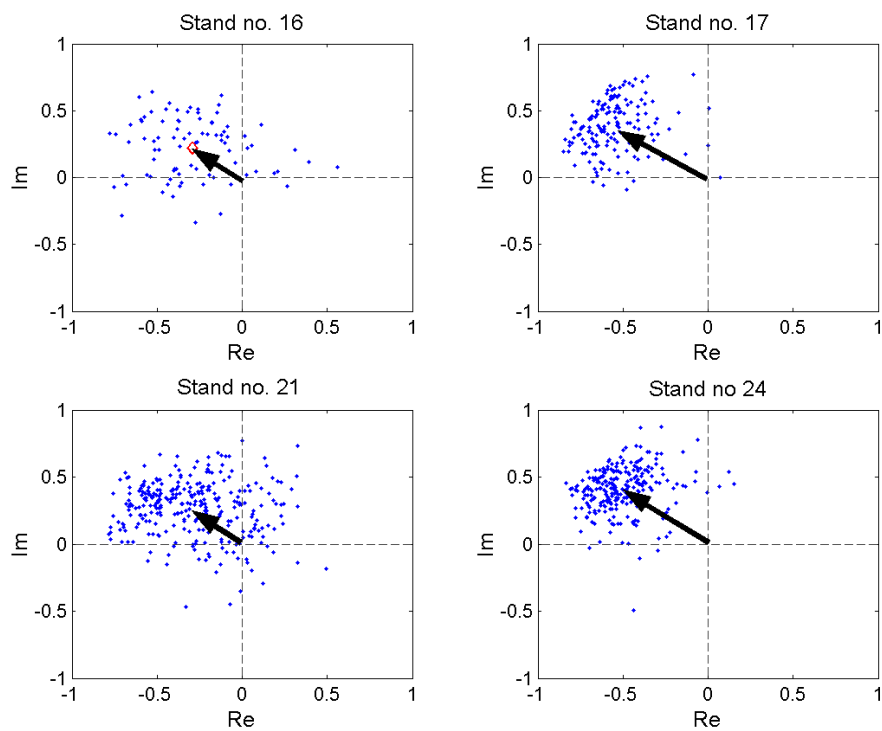
In Figure 8.2 the distribution of the ERS “tandem” complex coherence has been reported for a dense stand, a young stand and two clear-cuts in Kättböle. Forests show a diffuse cloud of measurements and a rather spread out histogram, whereas in open areas the InSAR phase is more concentrated. Similar results have been reported in (FLOURY *et al.*, 1996a) over intensively managed coniferous forests in South France. Although these results tend to indicate that the InSAR phase should be sensitive to forest attributes, the correlation with stem volume was in several pairs between ± 0.3 , probably because of the strong noise component in the phase values.

8.2 Interferometric tree height

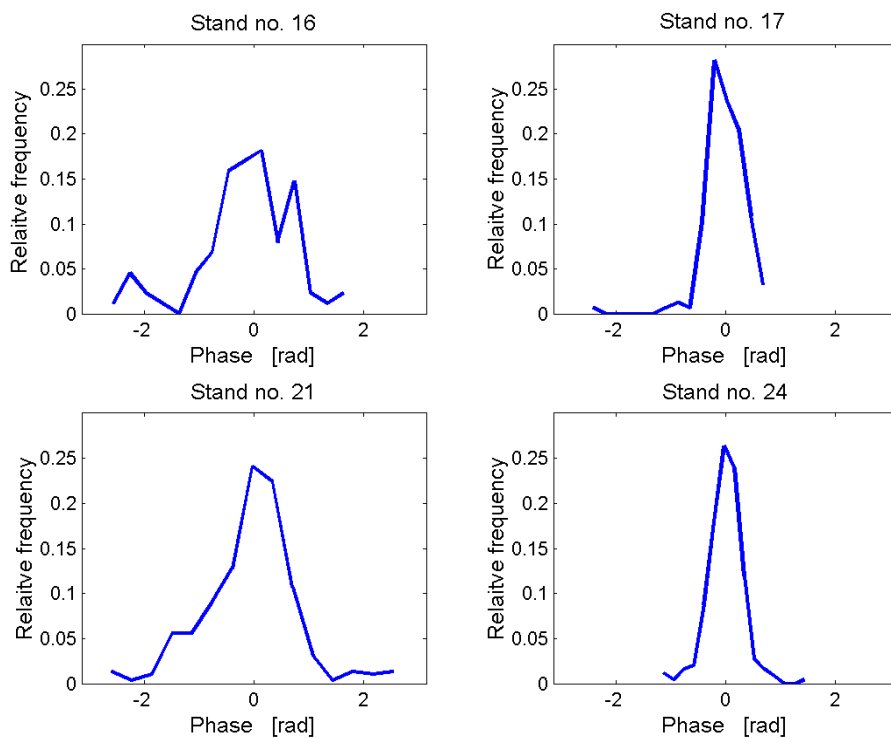
The difference of InSAR phase between two points has been expressed in Section 2.5.2. If the compensation for flat Earth has been applied and the topography included in a DEM of the bold Earth has been removed, the difference is related to residual height differences not included in the DEM (for example the height difference between a forest and a field), atmospheric path delays and phase noise:

$$\Delta\Phi = \frac{4\pi B_n}{\lambda R \sin \theta} \cdot \Delta z + \frac{4\pi}{\lambda} \Delta x_{atm} + \Delta\Phi_{noise} \quad (8.1)$$

Phase noise is a “property” of the target and therefore cannot be removed. On the other hand the identification and the correction of atmospheric artefacts is possible but represents a very delicate matter. In Equation (8.1) the phase unwrapping term has not been included because in boreal forests the tree height is commonly smaller than the ERS ambiguity height. To avoid a significant volume decorrelation, the normal component of the baseline should not be longer than 300 m. For such baseline, the ambiguity height is around 30 m, which is more than the tree height typically measured in boreal forests.



(a)



(b)

Figure 8.2. Distribution of the complex coherence (a) histogram of phase (b) in two forested areas (Stand no. 16, $V = 160 \text{ m}^3/\text{ha}$ and Stand no. 21, $V = 105 \text{ m}^3/\text{ha}$) and in two clear-cuts (Stands no. 17 and 24). Kättböle, 17-18 March 1996.

Equation (8.1) can be inverted and from the phase difference between a forest and a neighbouring flat area (such as an open field), it is possible to determine the interferometric tree height, i.e. the height of the scattering centre of the forest, also referred to as effective tree height:

$$h_{\text{int}} = \frac{\lambda R \sin \theta}{4\pi B_n} \Delta\Phi_{\text{meas}} \quad (8.2)$$

where $\Delta\Phi_{\text{meas}}$ represents the phase difference between the two areas and h_{int} the corresponding height jump. If the atmospheric contributions are negligible or have been correctly removed, the interferometric tree height will suffer from the noise in the phase estimates only.

The uncertainty in the height estimate, corresponding to the uncertainty in the InSAR phase can be expressed as (LI & GOLDSTEIN, 1990; HAGBERG, *et al.*, 1995):

$$\sigma_h = \frac{\lambda R \sin \theta}{4\pi B_n} \sigma_\phi \quad (8.3)$$

The uncertainty can be decreased by averaging over larger areas and by using pairs with a long baseline. Long baselines have the drawback that volume decorrelation will affect the coherence, increasing the phase noise.

Equation (8.3) would be sufficient in case the reference area for the height had coherence close to 1. As this is not the case, the uncertainty in the phase estimate over the reference flat area must be taken into account as well, so that the total height uncertainty is expressed as:

$$\sigma_{h,\text{tot}} = \sqrt{\sigma_{h,\text{forest}}^2 + \sigma_{h,\text{field}}^2} \quad (8.4)$$

with $\sigma_{h,\text{forest}}^2$ and $\sigma_{h,\text{field}}^2$ representing the uncertainty of the forest and the field height estimates respectively.

If several estimates are available, they can be combined in a multi-temporal approach. For interferometric tree height estimation this is a crucial aspect because of the noisy phase in forested areas. Besides the simple mean value of single-image estimates, weighted averages can be performed in order to take into account the properties of each image included in the combination. For example in (FERRETTI *et al.*, 1999a) the refinement of a DEM has been performed by means of a Maximum Likelihood Gaussian estimation:

$$\hat{h} = \frac{\sum_{i=1}^N \frac{\hat{h}_i}{\sigma_{hi}^2}}{\sum_{i=1}^N \frac{1}{\sigma_{hi}^2}} \quad (8.5)$$

where \hat{h} represents the multi-temporal estimate of single-pair height estimates, \hat{h}_i (i represents the pair number with N pairs available). The weights are given by the noise variance associated to the height estimates, given by Equation (8.4).

8.3 Atmospheric artefacts

Because of the strong phase noise occurring in forests, the computation of the interferometric tree height requires that the external error sources are minimal for any interpretation or further application to take place. Assuming that the flat Earth compensation has been correctly carried out, i.e. the baseline has been accurately estimated, and the DEM used for removing the topography is accurate enough, the spatial and temporal variability of the atmosphere represent the major source of error affecting the InSAR phase.

The wave transmitted by a spaceborne SAR does not propagate undisturbed through the atmosphere but is perturbed both in the ionosphere and the troposphere. When passing through the ionosphere the wave gets delayed depending on the electron density of the medium. Although not completely predictable, the effect of the ionosphere is related to the day-night cycle. The electron density is higher during the day and decreases at night. Ionospheric effects are therefore less noticeable in SAR imagery acquired at night, which makes ascending passes preferable. In the troposphere, the water vapour concentration affects the refractive properties of the medium, thus causing delays in the propagation of the electromagnetic wave (wet path delay) (HANSSEN, 1998; HANSSEN *et al.*, 1999). The spatial distribution of water vapour is related to meteorological conditions, i.e. wind speed and direction, pressure, temperature and relative humidity. In (GOLDSTEIN, 1995) tropospheric turbulence and water vapour mixing were indicated as causes of path delays. The importance of cloud formation was addressed in (MASSONNET & FEIGL, 1995) and (TARAYRE & MASSONNET, 1996). These observations put a strong limitation on the usefulness of SAR and InSAR phase in regions characterised by frequent changes of the weather conditions, as for example in Scandinavia. Nevertheless, it was pointed out in (HANSSEN, 1998) that tropospheric turbulences decrease at night and water vapour concentration is lower during winter, thus suggesting that winter pairs acquired on an ascending orbit can be more suitable for an application of the InSAR phase.

Path delays are visible in an InSAR image because the spatial and temporal variability of the water vapour in the troposphere and the electron density in the ionosphere differently delay the waves at the two acquisitions, thus creating additional fringes in the interferogram. In (GOLDSTEIN, 1995) propagation delays were estimated from atmospheric artefacts on SIR-C interferograms and compared to results from water vapour radiometer data taken at the time of image acquisition, showing a clear agreement. GPS measurements were used in (MASSONNET & FEIGL, 1995; WILLIAMS *et al.*, 1998; HANSSEN, *et al.*, 1999; VAN DER HOEVEN *et al.*, 2002)

to characterise both ionospheric and tropospheric delays observed in interferometric fringes.

Figure 8.3 illustrates two differential interferograms acquired over the area of Kättböle. The accurate orbital data and the small uncertainty in the DEM let us assume that atmospheric heterogeneities caused the fringes. The upper image was acquired on 21-22 August 1995 while a front of clouds was moving above Sweden (as shown by NOAA-AVHRR data). Many blobs caused probably by an inhomogeneous concentration of water vapour are visible. The rather small size, of the order of 1 km, and the irregular patterns completely altered the topographic information contained in the image. The lower image was acquired on 29-30 October 1995, clearly showing a fringe with a constant phase slope along the East-West direction. Weather data reported variable relative humidity throughout the two days whereas NOAA-AVHRR images showed cloud cover at the second acquisition.

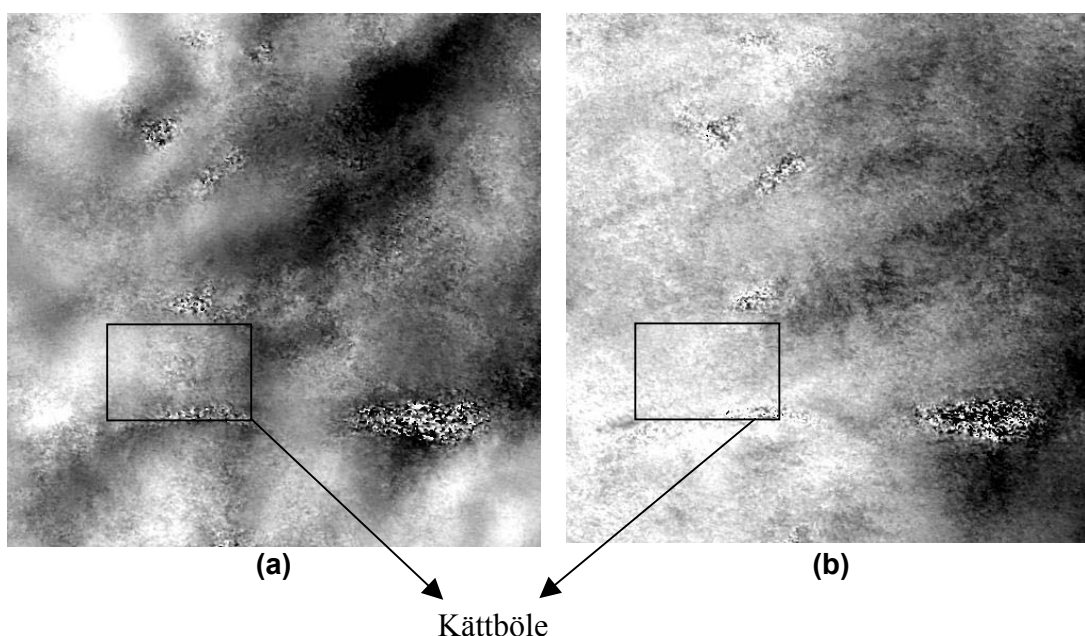


Figure 8.3. InSAR phase imagery affected by atmospheric artefacts acquired over Kättböle on 21-22 August 1995 (a) and 29-30 October 1995 (b). Area: 6 x 6 km.

8.4 Filtering algorithms

Because of the unpredictable spatial and temporal distribution of atmospheric artefacts in interferograms, their compensation is not a trivial task. Corrections can be either performed by exploiting the scattering properties of objects within a scene or requires the knowledge of several atmospheric parameters at the time of acquisition. The first approach aims at determining a reference grid of targets for which the phase is sufficiently reliable to be used for compensating the phase of the whole scene (see Sections 8.4.1 and 8.4.2). In the second approach the atmospheric

path delay is estimated from accurate measurements of temperature, pressure, relative humidity, wind speed, etc. and the corresponding phase factor is then added to the InSAR phase. Other filtering approaches exploit specific properties of the atmospheric fringes. They are commonly used for land dynamics detection; therefore, only a brief summary is given in this thesis.

8.4.1 Permanent Scatterers technique

The Permanent Scatterers (PS) technique developed at POLIMI is based on scatterers (the Permanent Scatterers) of the size of a pixel, or even less, that show a coherent behaviour in time throughout a set of $N+1$ SAR images (FERRETTI *et al.*, 1999b; FERRETTI *et al.*, 2001). The phase stability allows visual identification of Permanent Scatterers because a coherent summation of the $N+1$ images returns very bright points, where the scattering has been stable and strong throughout time, on a rather dark background, where the phase has changed in time. Figure 8.4 illustrates this concept from a vectorial point of view. The coherent sum of the electromagnetic fields over several acquisitions returns a very long vector for a stable scatterer, otherwise fading occurs.

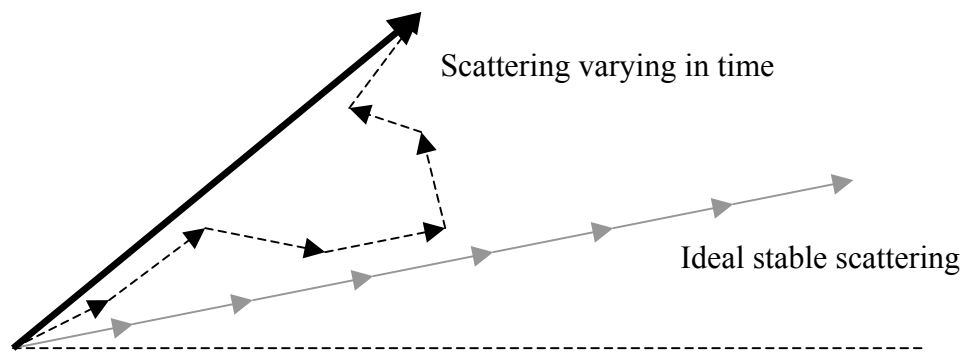


Figure 8.4. Coherent addition in phase for two resolution cells characterised by stable scattering and temporally variable scattering. Grey arrows represent the ideal stable scattering condition. The second case is described by dashed components and the thick black resultant. All vectors have the same length and represent unity vectors. The coherent addition does not take into account the amplitude of the scattering but purely the phase (SANTORO, 2001).

The definition of a target as Permanent Scatterer is based on the N interferometric pairs that can be produced, using the remaining image as common master. Commonly almost total decorrelation and a completely noisy InSAR phase are observed in these interferograms. Only the Permanent Scatterers show high coherence and contain phase information, because they have a very strong scattering, are stable in time and do not suffer from baseline decorrelation. PS are selected from the inversion of a set of equations of the sort in Equation (2.17) (FERRETTI, *et al.*, 2001) and from their phase an atmospheric phase screen (APS) is estimated. SAR imagery filtered with the APS is used for interferometric processing. The

requirements for a correct estimation of the APS are a large set of SAR images (approximately 40) and a very dense grid of PS (above 20 per square kilometre). These very stringent conditions are met mostly in urban areas and, in general, in areas where stable scattering occurs. In large forested areas this approach is not recommended because of the scarcity of targets identifiable as Permanent Scatterers.

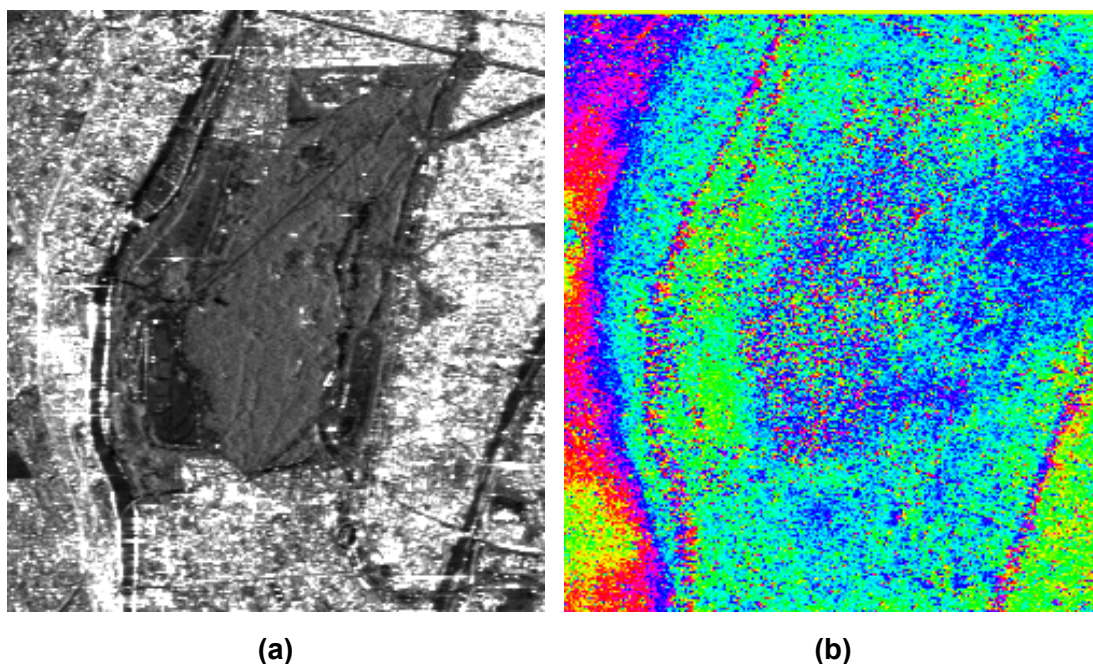


Figure 8.5. Mean backscatter amplitude of 64 ERS SAR images of the Bois de Boulogne (courtesy of POLIMI) (a), wrapped topographic InSAR phase acquired on February 1996 ($B_n = 78.09$ m) (b). On the left side of the Bois, the two horse racecourses appear as dark areas in (a) and as uniform green in (b).

The potential for tree height estimation of atmosphere-corrected SAR images using the PS technique was evaluated in the forested area of the Bois de Boulogne, Paris, France (SANTORO, 2001). Nine one-day ERS pairs acquired between June 1995 and April 1996, and a reference master ERS SAR image acquired on 8 March 1997 were available. Both one-day and long-term pairs were produced. The latter were then discarded in the analysis because they appeared completely decorrelated. The Bois de Boulogne is a wood surrounded by extremely dense urban areas, covers 865 ha (approximately 3.7 km in the North-South direction and 2.4 km in the East-West direction) and houses two horse racecourses that were used as reference fields for the tree height estimation (they are referred to as Field 10 and Field 11). Figure 8.5 shows the Bois in a mean backscatter amplitude image and in a topographic InSAR image. The two racecourses are clearly visible because of the low backscatter and the uniform phase. Forests appear brighter in the backscatter image and very noisy in the InSAR phase image. Trees mostly belonged to temperate broadleaf species and densely covered the whole area. At the end of December 1999 a storm damaged

around 40% of the forests. Since the wood was surveyed and several forest attributes were measured two years later, the collected measurements might have not represented with high accuracy the properties of the forests when the images were acquired. Five areas with homogeneous forest cover were identified (Forest 1, 2, 3, 6 and 9). Stands were between 16 and 30 ha large in order to minimize the uncertainty of the corresponding phase estimates. Additionally an area with sparse vegetation was considered (Area 12). The InSAR phase difference between the five forest stands and the closest reference field was inverted to determine the interferometric tree height.

The coherence showed the typical patterns for forests and open areas reported in Chapter 4. In forested areas the coherence was mostly below 0.3, being above this level, up to 0.46, in three winter pairs. The two fields showed a higher coherence (between 0.4 and 0.64) except when rainfall occurred at the time of acquisition. The coherence of Area 12 depended on the season, being lower in summer pairs (0.25-0.33) and higher in winter pairs (0.46-0.63). These results should be due to the fact that the area was not a homogeneous open field but was covered with a 1-2 m thick vegetation layer.

The estimated interferometric tree height showed a large variability (Figure 8.6). Four forest-field areas were always characterised by values ranging from slightly above the ground level up to some metres above the canopy. The oscillations of the estimates could be due to the rather high phase noise, as shown by the coherence values. Despite the large number of looks, the instability of the scattering between two acquisitions seemed to dominate the estimated interferometric tree height. Nevertheless it can not be excluded that residual atmospheric artefacts still affected the images since the PS give only an estimate of the atmospheric phase screen (FERRETTI, *et al.*, 2001) and within the Bois the density of PS was low. Furthermore slight errors were found in the flat Earth compensation, which might have caused additional noise. The fifth forest-field area showed interferometric tree heights both above and below the ground level, because the InSAR phase of the reference area (Area 12) was characterised by a variable uncertainty, dependent on the state of the vegetation throughout the year.

The estimated interferometric height was generally around or above the measured height in Forests 1 and 2. When surveyed, both forests appeared to have had a dense canopy and a uniform vegetation cover at the time of acquisition. Forests 3 and 6 were instead characterised by larger openings between trees and thick understory (between 0.5 and 2 m high) forming a second vegetation layer. Furthermore, Forest 6 included both tall and short trees, being less homogeneous than other stands. In both areas the height estimates were consistently below the measured tree heights, which was due to the fact that the SAR saw a larger portion of ground.

Having available several pairs acquired during the leaf-off period (November 1995 - March 1996), the dynamics of the scattering height throughout a year were investigated. In broadleaf forests the interferometric tree height should be higher in summer and lower in winter because of larger gaps in the crown. Unfortunately the values reported in Figure 8.6 did not clearly support this assumption.

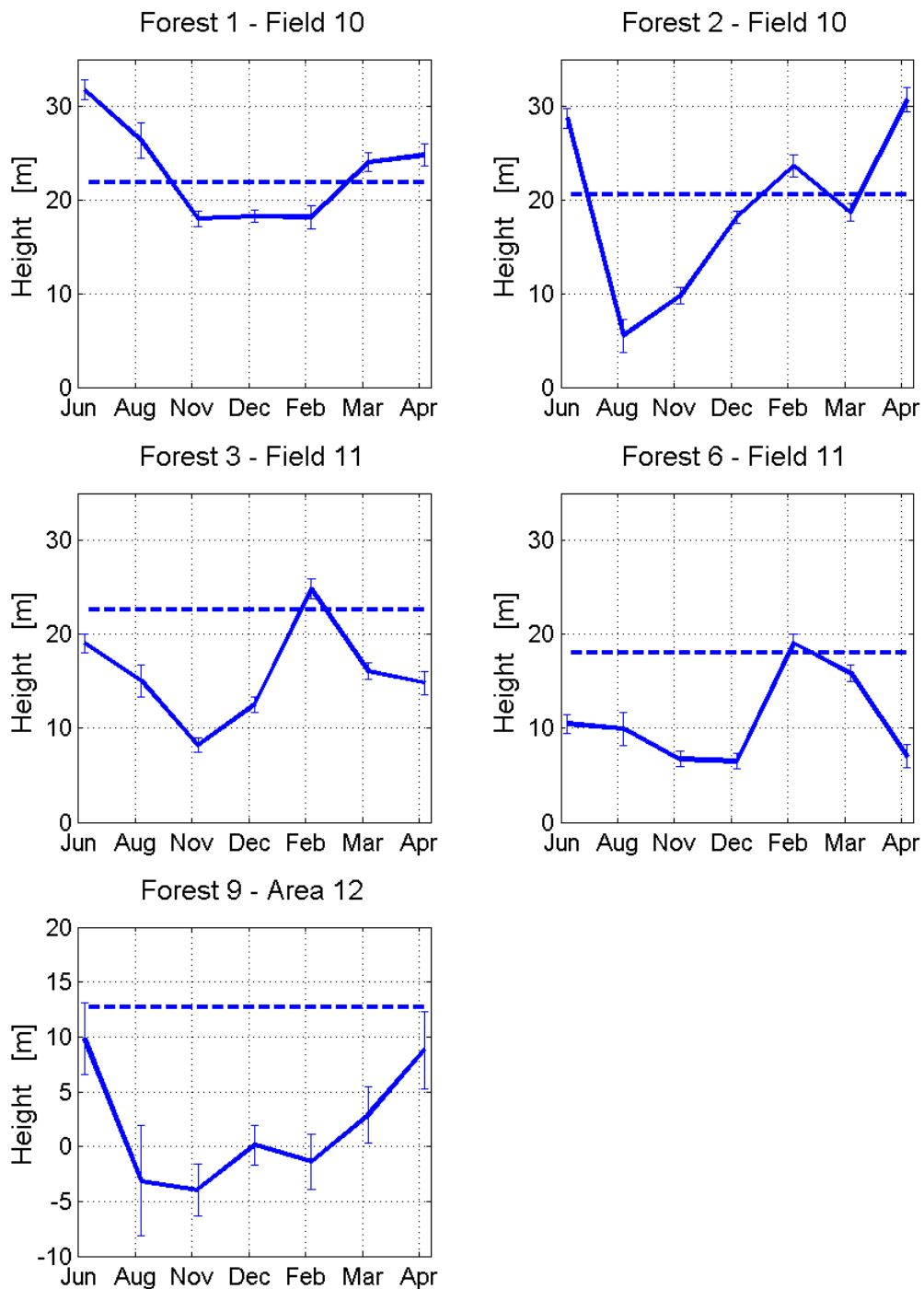


Figure 8.6. InSAR tree height estimates for five forest-field pairs. The error bars represent one standard deviation, computed according to Equation (8.5).

With a multi-temporal combination of single-pair interferometric heights, errors could be partially removed (Figure 8.7). Weighted averaging according to Equation (8.5) did not perform differently than a simple average. In the rather dense and

homogeneous forests (Forests 1 and 2) the interferometric height was close to the measured tree height. In Forests 3 (forest with wide openings) and 6 (sparse forest) the interferometric height underestimated the true height as one might have expected. Hence, the combination of estimates from several pairs had a strong effect in reducing the noise in the estimates and highlighted the scattering properties of the forests under investigation.

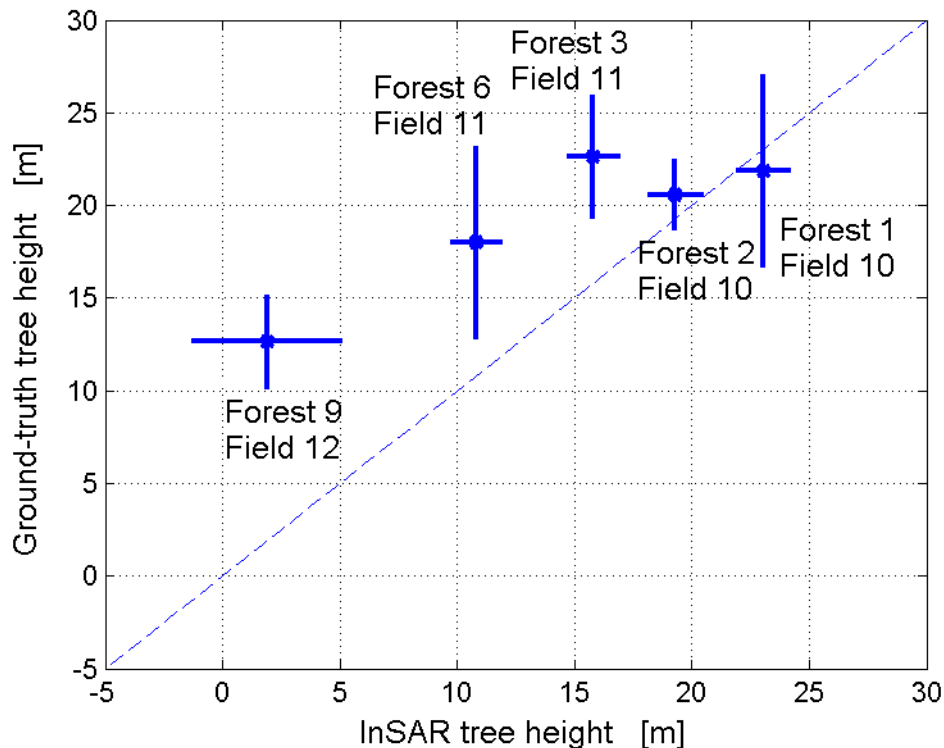


Figure 8.7. Comparison between a simple average of InSAR heights from seven one-day pairs and in situ measurements. The vertical bars represent one standard deviation in the estimate of the InSAR height between the forest and the field (from Equation (8.5)). The horizontal bars represent one standard deviation in the in situ measurements.

8.4.2 Grid of open areas

Alternatively to the PS technique, large open areas with high coherence (bare soils, fields, clear cuts) can be used as reference “grid”. In a differential interferogram, open areas have the same height, equal to the ground reference level. Moreover, the error in the phase estimate is small because of the high coherence and the large number of pixels used to compute the estimate. Therefore, if there are phase differences among fields, they should indicate that the image is affected by atmospheric artefacts. Similarly to the approach presented in the previous subsection, the InSAR phase from a grid of open areas can be used to determine an

atmospheric phase screen. The phase is interpolated over the whole image and the phase screen is then removed from the differential interferogram (DAMMERT, 1999). As in the PS technique, a dense grid of reference fields is needed to obtain a reasonable correction. Compared to the PS approach, the phase compensation using reference fields is more feasible in forested areas. However, if a field is only partially affected by atmospheric artefacts, the phase screen might include errors, thus leading to a wrong correction. The size of the reference areas is therefore based on a trade-off between having as many pixels as possible for a correct estimate of the phase and limiting the effects of the spatial variability of the artefacts within the open area.

This approach was applied in Kättböle and Tuusula. Since forests covered in both cases most of the area and only a few farms were scattered around, the number of Permanent Scatterers would have been totally insufficient for phase correction. In Tuusula the density and the size of reference fields was considered sufficient to obtain a reliable estimate of the phase screen. To prove whether the correction had correctly worked, the height differences of four fields with respect to a “master” field were computed.

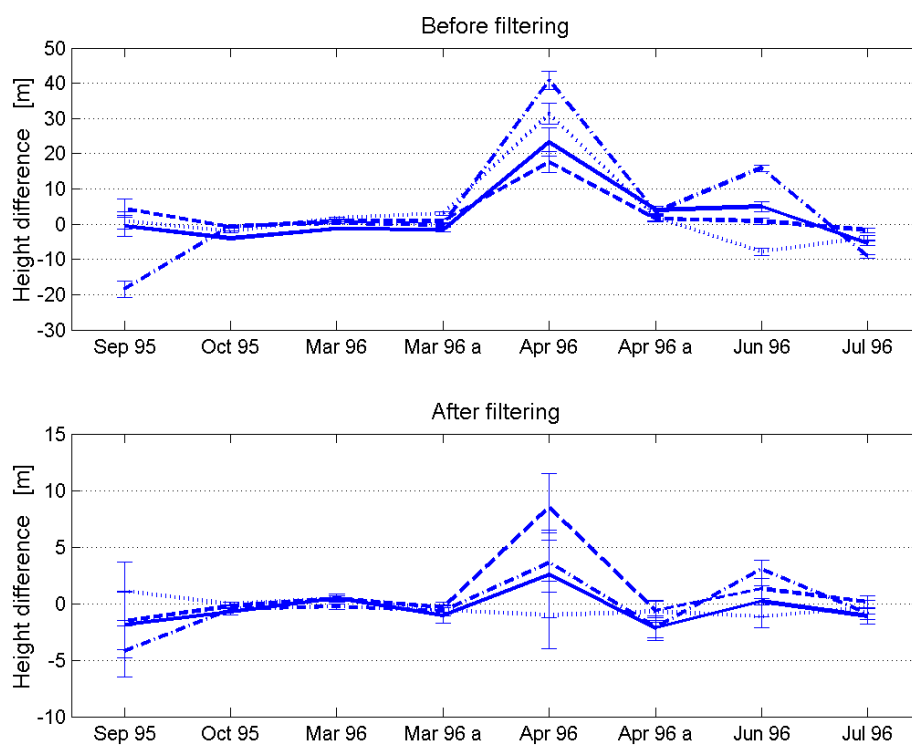


Figure 8.8. Height difference between four fields and a “master” open area in the Tuusula region. The field size was between 11 and 33 ha. The “master” field size was 33 ha. The error bars represent the uncertainty expressed in terms of one standard deviation from Equation (8.5).

Figure 8.8 reports the height differences before and after the phase compensation for each pair available. Overall, the filtering algorithm could strongly reduce the atmospheric artefacts. These were correctly compensated for when weather was stable at the time of acquisition, whereas residual errors still affected the InSAR phase when the environmental conditions had changed at the time of the acquisitions. The low coherence introduced large errors in the phase values and a strong uncertainty in the InSAR phase, thus affecting the interpolation. For heavy rainfall or snowmelt (September 1995 and first April 1996 pair) the errors decreased only partly. In other pairs where partial decorrelation of the ground occurred (October 1995, second pair April 1996, June and July 1996), the filter could remove almost all artefacts. The effect of path delay differences within a reference area was not taken into account. The rather small height differences after correction suggested that this aspect is of minor importance, at least when the spatial variability of the atmospheric properties is limited.

The forest estate of Kättböle is located in the centre of a forested area of approximately 20 km diameter. At the perimeter few fields are scattered, but most of them are too little to obtain the sufficiently accurate phase estimates required by the procedure. Only five open areas could be identified as reference, a number that was considered too small for filtering. Because of this limitation the atmospheric effects could not be corrected. Nevertheless, the phase measurements from each reference area were used to quantify the phase distortions caused by atmospheric artefacts in a pair in order to decide whether it should have been kept or rather discarded.

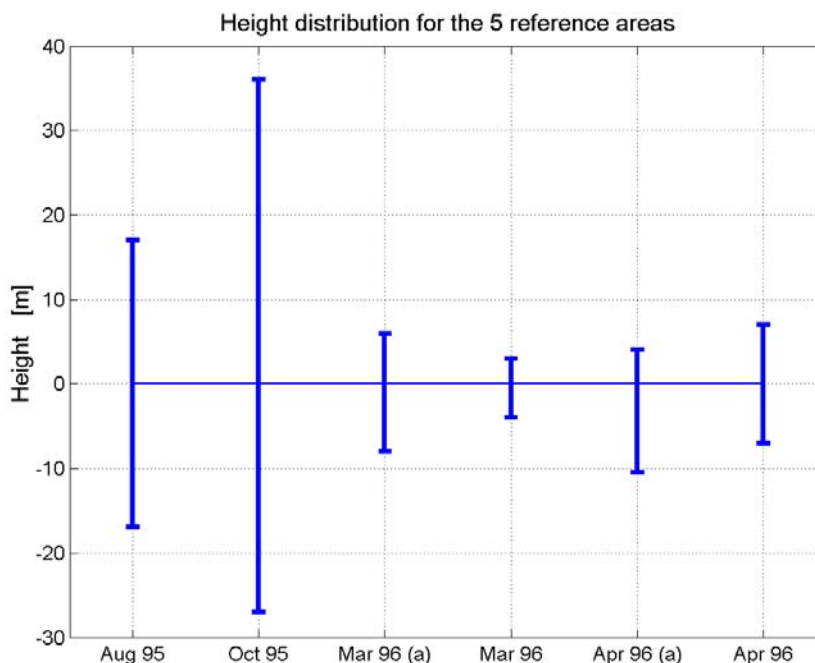


Figure 8.9. Distribution of height for the five reference open areas located around Kättböle. The (a) stands for “ascending” pass.

For six pairs Figure 8.9 shows the deviation of height from a reference ground level. The pairs reported in Figure 8.3 were characterised by the largest deviations. Smaller height differences were found in pairs acquired during the winter, at rather stable weather and atmospheric conditions. Similar results were given by the height jump measured between two neighbouring clear-cuts within the test-site. Pairs acquired under stable weather conditions, without large atmospheric changes (i.e. constant and low relative humidity) showed the smallest difference (between -1 and 4 m). In other cases, differences above 10 m were obtained.

8.4.3 Estimation of atmospheric path delay

Several authors have reported a remarkable agreement between the path delays estimated from InSAR phase imagery and the values predicted by behavioural models of the ionosphere and the troposphere, suggesting that the distortions in the InSAR phase can be corrected if measurements of the propagation delay are available (TARAYRE & MASSONNET, 1996; ZEBKER *et al.*, 1997; DELACOURT *et al.*, 1998; WILLIAMS, *et al.*, 1998). The derivation of the propagation delay is generally obtained from ground-based measurements of meteorological variables, GPS and water vapour radiometer observations. For an accurate correction of the atmospheric artefacts, a spatially dense set of measurements, taken at the time of the satellite acquisitions, is needed. SAR images are seldom acquired simultaneously to GPS and radiometer measurements. Moreover, the highly spatial and temporal resolution required for an accurate compensation makes such approach feasible only in dedicated experiments.

Because of the limited meteorological data available at the test sites, a phase mask of tropospheric disturbances could not be obtained. Nevertheless, this procedure was investigated to determine an approximate measure of the variability of the tropospheric delays in order to judge whether the InSAR phase of a pair was suitable for any application. The analysis was carried out only in Kättböle, where meteorological data were available at more than one weather station.

The model presented in (ZEBKER, *et al.*, 1997) was used to give a rough estimate of the tropospheric delays over an area close to the test site. The model required the knowledge of the temperature and the relative humidity at acquisition. Data were available at two weather stations only, located 2 and 40 km from Kättböle; therefore, the results could be used only to indicate whether a pair was “clean” from artefacts. The path length at the two stations was first estimated and then the path difference was computed. From Table 8.1 the ascending pair acquired in March 1996 did not seem to be affected by atmospheric artefacts. The delays estimated for the descending March pair and the ascending April pair should have been due to the very rough approach rather than to atmospheric perturbations. These were indeed clearly affecting the pairs acquired in August 1995, and the descending pair from April 1996. This pair in particular was the only case that showed a result in partial disagreement with the height jumps obtained using the previous approach. Little precipitation registered at several weather stations and thick clouds over the area visible in NOAA-AVHRR imagery suggested that atmospheric artefacts affected the pair.

August 1995	October 1995	March 1996 (a)	March 1996	April 1996 (a)	April 1996
176 m	NA	2 m	-14 m	10 m	63 m

Table 8.1. Height difference due to atmospheric path delay estimated according to (ZEBKER, *et al.*, 1997) at two weather stations located 2 and 40 km from Kättböle. (a) and (d) stand for “ascending.

The two filtering approaches applied in boreal forests show that images acquired at night, i.e. on ascending orbits, were the most suitable for phase exploitation, confirming the indications reported in (HANSSEN, 1998). When working with descending passes, cloud cover and changes in the water vapour content strongly altered in most cases the phase information, making such pairs unsuitable for any application.

8.4.4 Other methods

Because of the non-systematic nature of atmospheric artefacts, (SANDWELL & PRICE, 1998) stacked several differential interferograms to minimize them. Although the procedure provided accurate results, this method cannot be used for topographic interferograms because the accuracy of the inversion of phase to height is strictly related to the baseline (ZEBKER, *et al.*, 1997). The use of two or more interferograms and an *ad hoc* algorithm were found to successfully detect and suppress atmospheric artefacts (SARTI *et al.*, 1999; FRUNEAU & SARTI, 2000; CROSETTO *et al.*, 2002). None of the methods were found to be suitable in forested areas though.

8.5 Interferometric tree height estimation

As previously mentioned and then showed with the results in the Bois de Boulogne, the interferometric tree height is referred to the height of the scattering centre within the forest canopy, thus being smaller than the true tree height. For the mostly coniferous forest estate of Landes, Southwestern France, (FLOURY, *et al.*, 1996b) and (FLOURY, *et al.*, 1996a) showed that the interferometric height depends on the age, i.e. on the structure, of the forest. For older forests, the penetration depth decreases and therefore the interferometric height tends towards the true height. At the managed pine forest at Thetford, United Kingdom, (SKINNER *et al.*, 2002) illustrated that the mean InSAR height and the top height were almost uncorrelated. In boreal forests investigations have been carried out mostly during winter, when the ground was covered with snow. This condition guaranteed the highest ground coherence and the smallest uncertainty in the phase estimate of the ground reference level. The three-day repeat-pass cycle of the ERS-1 mission in 1992 allowed the formation of several pairs over Hökmark, a forested area in North Sweden. In a dense 15 m tall forest (HAGBERG, *et al.*, 1995) obtained interferometric tree heights a few metres below the true level for in pairs with baselines longer than 200 m. Very small values were estimated in pairs with baselines below 100 m as well as in a sparse 10 m tall

forest. On the same area, several other studies showed instead heights varying between 0 and 7 m (DAMMERT *et al.*, 1995; ASKNE *et al.*, 1997a). Similar results were obtained in three forest stands within the same test site by (DAMMERT & ASKNE, 1998), where the effective height was found to represent up to 60% of the true height, and in (HYYPÄ & ENGDAL, 2000), where forests in InSAR ERS “tandem” DEMs were characterised by offsets of a few metres with respect to the ground level. Unfortunately pairs acquired in other seasons were always affected by atmospheric artefacts at acquisition, which did not allow the determination of accurate estimates and the possibility of a comparison with the winter-type interferometric tree height.

The estimation of interferometric tree height should depend strongly on the number of pixels used for averaging. Although large forest stands already have a size sufficient to obtain relatively good estimates, groups of stands with similar characteristics in terms of stem volume and height include many more samples, thus decreasing the uncertainty of the stand-wise InSAR phase. The drawback of grouping stands is that stands might not have all the same properties and structure, causing an inevitable dispersion of values.

In Kättböle the interferometric tree height for the 42 forest stands has been estimated using as reference ground level the two clear-cuts in the forest estate. Only pairs characterised by stable weather conditions were considered. To increase the amount of plots and pixels for more accurate tree height and InSAR phase estimates, neighbouring stands were grouped according to similar forest properties. Eleven large stands with a size between 2 and 66 ha, uniformly covering the range of stem volumes measured in the area, were obtained. The two clear-cuts were grouped together and became the reference ground level. In Tuusula the rather small size of the stands suggested to carry out the study directly on grouped stands. Six large groups of stands were formed, having a size between 11 and 30 ha (DAMMERT, 1999). Two groups consisted of rather young stands. The remaining four areas consisted of clusters of neighbouring mature stands with similar forest properties.

From Equations (8.2) and (8.4) the interferometric height and the corresponding uncertainty were estimated. For each pair considered in Kättböle, Figures 8.10 and 8.11 illustrate the relationship between the interferometric and the measured tree height at stand level and for grouped stands, respectively. Interferometric tree height estimates from Tuusula have already been thoroughly discussed in (DAMMERT, 1999), therefore they are considered in this Section as means of comparison.

The pairs acquired in August and October 1995 did not show any relationship between the true and the interferometric tree height. This confirmed the strong effect of the atmospheric artefacts, proving that the methods based on the evaluation of height differences in open areas represent a valid tool for a preliminary evaluation of an interferogram. In October 1995, the estimates were worsened by the short normal component of the baseline, which had the effect of increasing the uncertainty in tree height estimates.

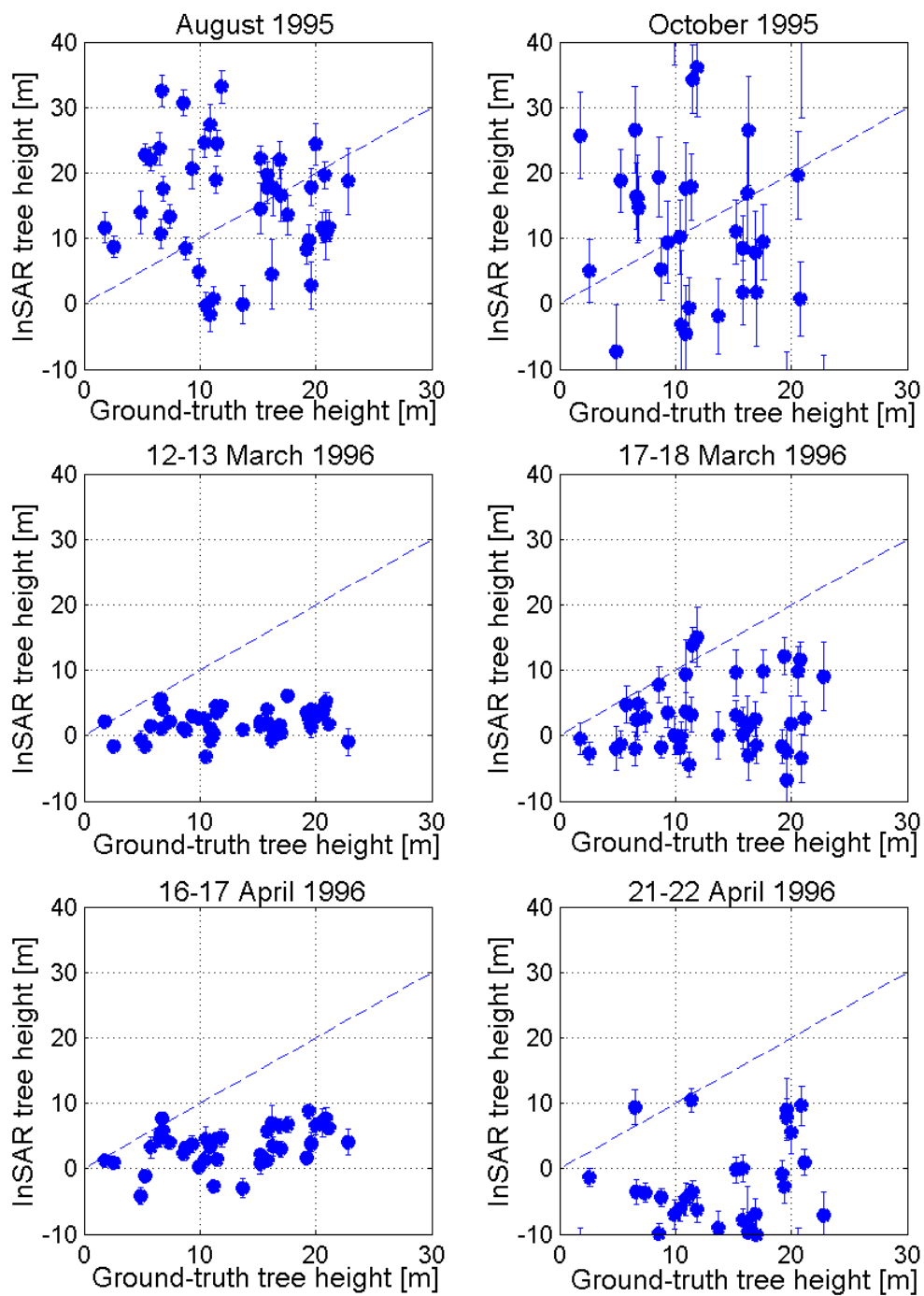


Figure 8.10. InSAR versus measured tree height at stand level in Kättböle (42 stands). The error bars represent one standard deviation in the InSAR tree height estimates.

The pairs acquired in March and April 1996 clearly underestimated the tree height. However, two different trends could be spotted. The pairs acquired on an ascending orbit (12-13 March and 16-17 April) showed interferometric heights closer to the

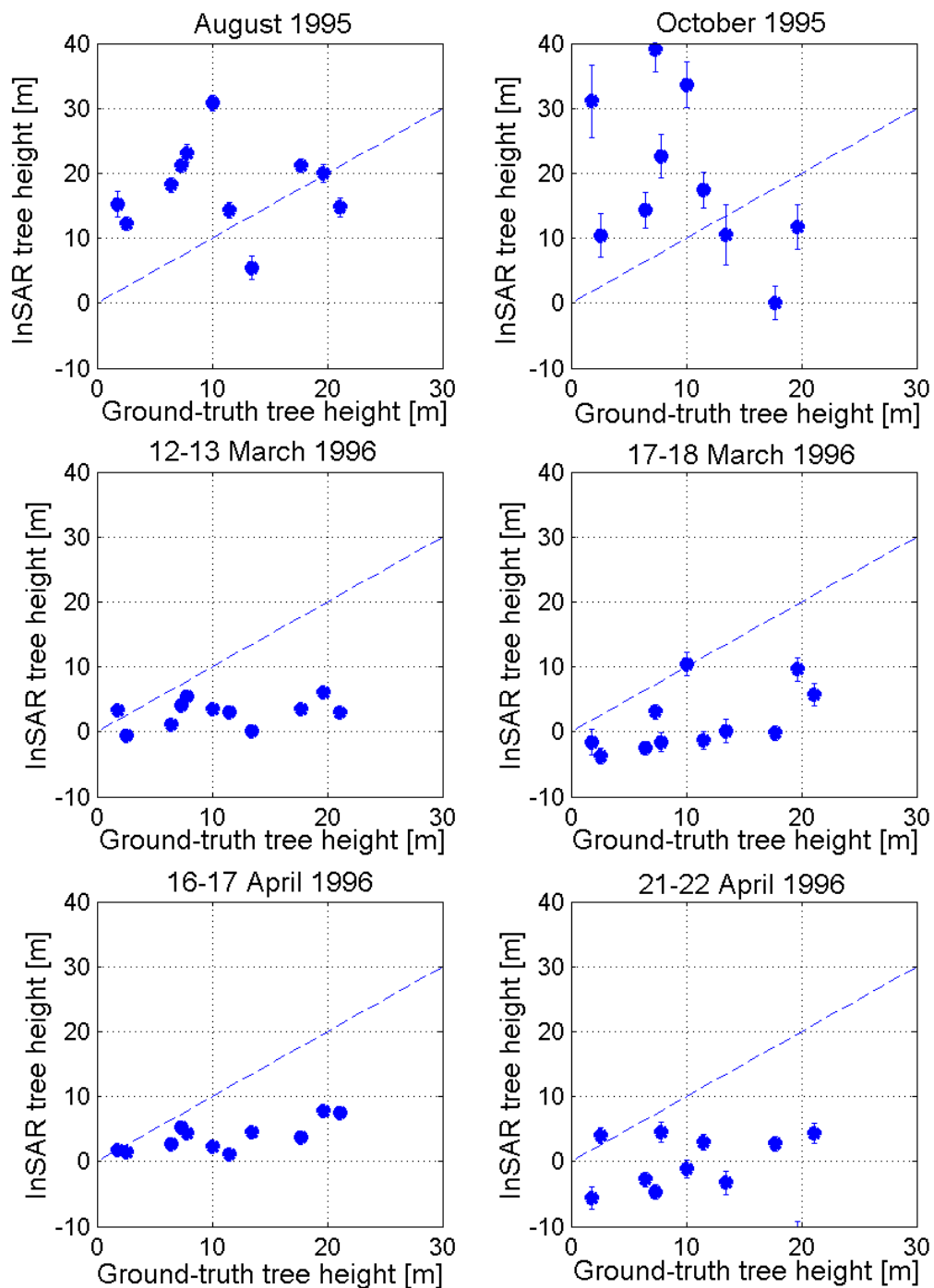


Figure 8.11. InSAR versus measured tree height for 11 grouped stands in Kättböle. The large amount of pixels has decreased the uncertainty of the InSAR tree height estimates so that the error bars are not clearly visible.

ground level than to the true height. Furthermore, these did not seem to depend on forest properties, being always below 6 m. A similar behaviour was observed in Tuusula for winter-frozen conditions. The pairs acquired on a descending orbit (17-18 March and 21-22 April) showed noisier height estimates, being between a few

metres below the true height and slightly negative values. These pairs had probably been affected by atmospheric artefacts, as shown in particular in the April pair, or by the heterogeneous properties of the snow covering the ground at the time of acquisition. This assumption finds support in Tuusula where the noisy values obtained from several filtered interferograms were interpreted as being affected by the dielectric properties of the snow cover. A snow layer introduces volume scattering where the wave has reached the ground passing through the gaps. Therefore the total phase returned to the SAR consists of two volumetric terms, which should introduce an even larger absolute and relative uncertainty in the measured phase. Unfortunately a detailed description of the snow cover within each stand was not available, thus not allowing any further investigation on how snow cover affects the interferometric height.

When stands were averaged over larger areas, the slightly shorter error bars show that part of the uncertainty was filtered out. Nevertheless the trends observed at stand level did not change (Figures 8.10 and 8.11). This proves that interferometric tree height can be determined already at stand level and that averaging over large areas only decreases the uncertainty in the estimates, but does not alter the value of the estimate.

Based on these results, the scattering centre of the forests should be well below the top of the canopy. This is somehow in contrast not only with the theory for which the scattering centre is located almost at the top of the forest canopy, but also with the results obtained at the Bois de Boulogne and in some of the cases reported by (HAGBERG, *et al.*, 1995) in North Sweden. Taking into account that the images were acquired during winter, the larger penetration of the electromagnetic wave into the canopy as a consequence of the frozen state of the trees could explain the low height. This interpretation is in accordance with the explanations reported in Chapter 4 and 6 concerning the unusual high coherence observed in these pairs in dense forests. Since stands mainly include coniferous tree species, the high coherence can definitely not be explained in terms of an increased number of gaps in the canopy because of leafless tree crowns.

8.6 Model-based tree height

Once the IWCM has been trained it is possible to:

- Determine the model-based interferometric tree height and compare it to the measurements obtained from InSAR phase estimates.
- Compensate the interferometric tree height estimates using the model to retrieve the total tree height.

As shown in Section 5.4.2, the inversion of the phase of the IWCM complex coherence by means of Equation (8.2) returns the model-based interferometric tree height. Figure 8.12 illustrates the interferometric tree height predicted by the IWCM as function of stem volume in Kättböle. The tree height derived from Equation (3.1)

is included for reference. The plots show that the interferometric tree height was always below the true tree height. The difference between the two curves decreased for increasing stem volume, because the wave attenuation increased in denser forests.

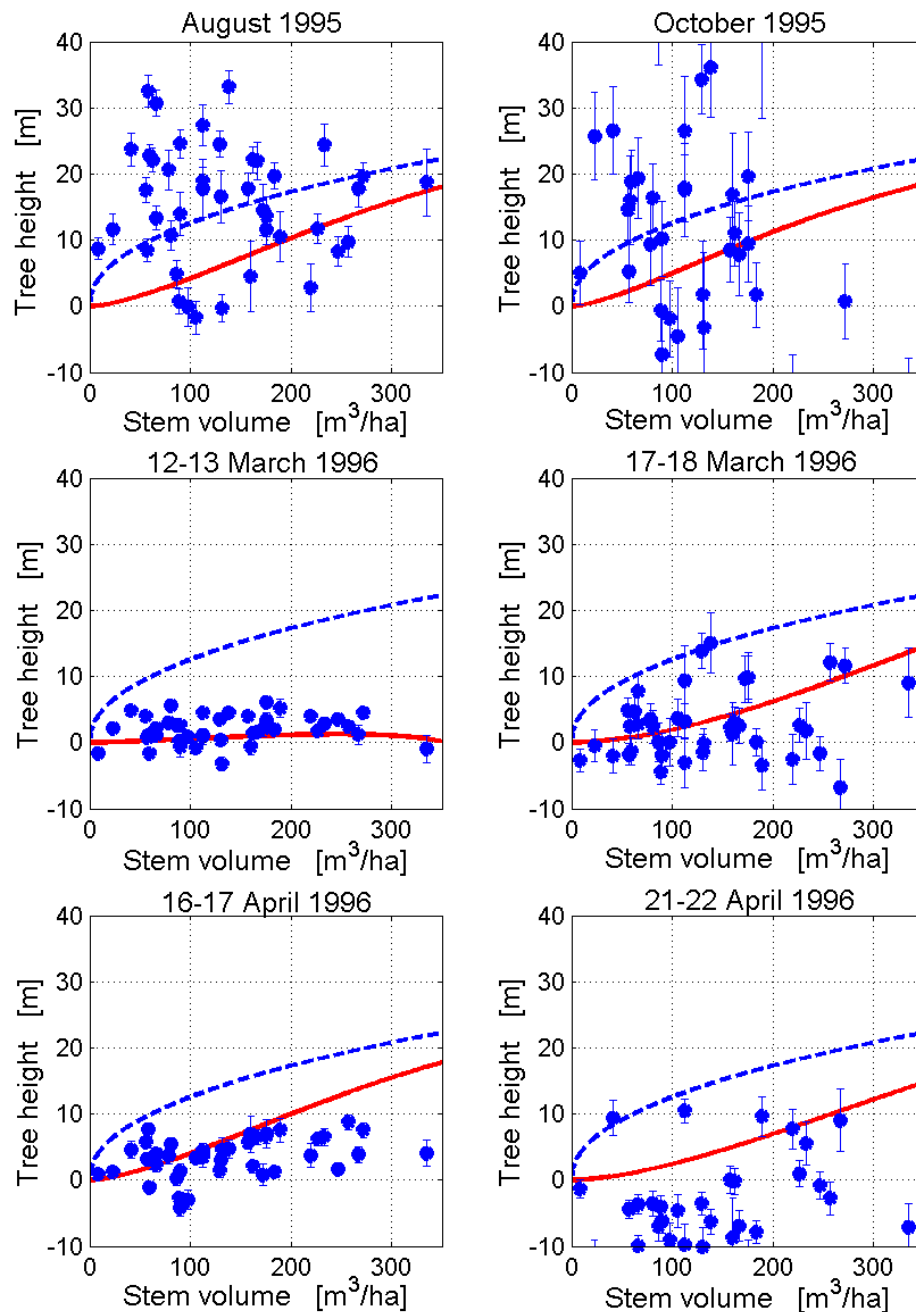


Figure 8.12. Measured tree height according to Equation (3.1) (dashed line) and model-based InSAR tree height (solid line) versus stem volume at stand level. Test site: Kättböle. The error bars represent one standard deviation in the InSAR height estimates.

Due to the atmospheric artefacts, there was no accordance between measured and modelled interferometric tree height in the first two pairs and, to a lesser extent, in the second pair acquired in April 1996. For the remaining pairs, the model seemed to describe well the trend between the interferometric tree height and stem volume. Nevertheless, at high stem volumes, the experimental interferometric tree height was in two cases smaller than the value predicted by the model. Taking into account that the pairs were acquired during winter, this result was initially interpreted in terms of a weaker attenuation of the electromagnetic wave in the tree crown. In order to verify this assumption, model training was performed with a set of two-way tree attenuation values between 0.4 and 1 dB/m. The model-based interferometric tree height decreased but only slightly and in dense forests the predicted height was still bigger than the experimental.

Although the IWCM seemed to describe the relationship between stem volume and interferometric tree height, the errors and the large uncertainty in InSAR phase measurements did not allow an accurate compensation for tree height retrieval. Tree height was estimated in Kättböle from single pairs and then using a multi-temporal combination based on a weighted average as defined in Equation (7.5). As for stem volume retrieval at stand level, the model was trained on 21 stands and tested on the remaining 21. The single-image retrieval did not provide any significant result. The multi-temporal combination of tree height estimates only slightly decreased the root mean square error, this being at around 7 m, but still the correlation between retrieved and true tree height was close to zero (Figure 8.13).

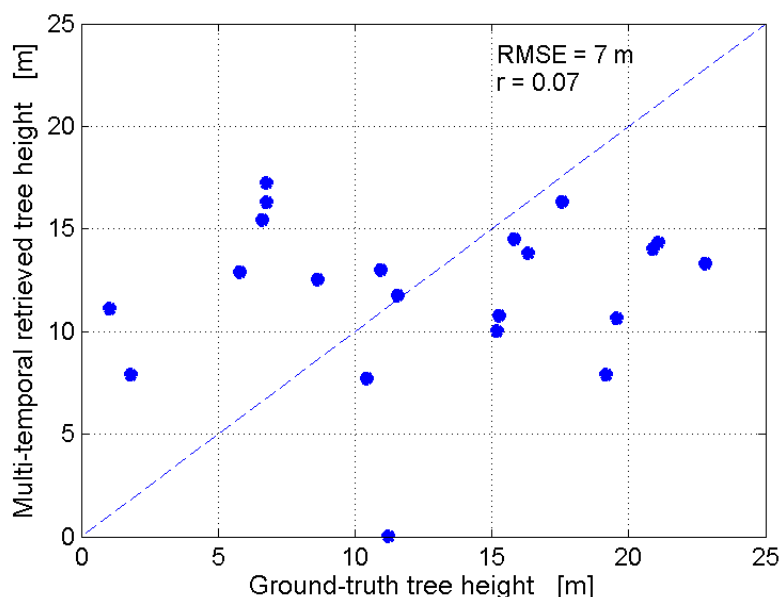


Figure 8.13. Model-based tree height obtained from a combination of three ERS InSAR pairs (12-13, 17-18 March and 16-17 April 1996) over Kättböle. The test set consisted of 21 stands.

In order to understand why stem volume retrieval from coherence is much more accurate than tree height estimation from InSAR phase, let us consider the vectorial representation of the IWCM introduced in Chapter 5. Given a stand with stem volume V , in Figure 8.14 we report the complex coherence vector measured in the interferometric image and the corresponding modelled complex coherence vector obtained after training the IWCM. The two complex coherence vectors have the same length but different angles with respect to the horizontal reference line. The two vectors have the same length because the coherence predicted by the IWCM is commonly close to the value measured in the image. The strong noise component in the phase estimates explains the different angles. Because of this difference, the stem volume, V' , at which the IWCM predicts the observed total forest complex coherence, does not coincide with the true value. In case of short baselines, even for small discrepancies between the phases of the two vectors, the experimental data can only be fitted at unrealistic stem volumes (too high for the area of interest or negative), thus explaining why tree height is determined with significant errors.

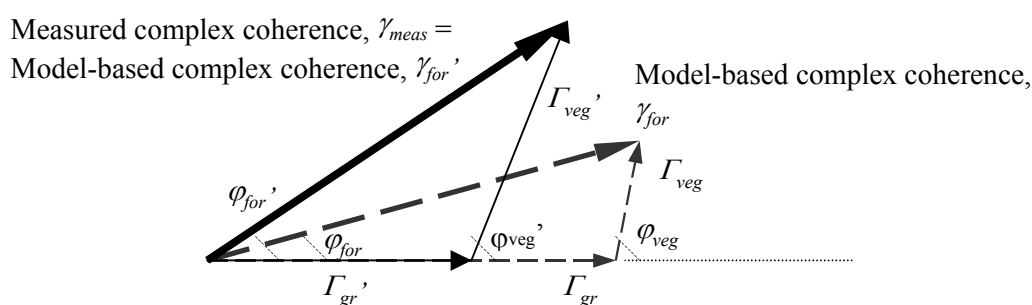


Figure 8.14. Comparison between model-based and experimental forest complex coherence. Although the two vectors have the same length, i.e. the same coherence, the different interferometric phase will make the model fit the measurement at a stem volume V' which does not correspond to the true value V .

8.7 Conclusions

The possibility of deriving the topographic feature of forests using the ERS InSAR phase has been analysed in this Chapter. Because of the strong attenuation of the wave in the upper layers of the forest canopy, the SAR sees a forest as topography, which is not related to the true height but to the height of the scattering centre of the forest. This is located between the treetop and the forest floor depending on amount and size of gaps in the crown. Because of the temporal instability of the canopy, the forest topography seen by the radar changes between acquisitions so that the InSAR phase is characterised by a strong noise component and suffers from large spread.

A major problem affecting the InSAR phase is the presence of atmospheric artefacts. In order to remove them, several filtering methods found in the literature were tested. After correction with the PS technique, the height of the scattering centre in the Bois de Boulogne, Paris, oscillated around the true height in dense forests, whereas it was

constantly below the true height in sparse forests. The low coherence in dense forests and the fact that the phase correction might have not worked properly in the Bois, are two valid explanations for the temporal variations of the height in dense forests. A multi-temporal combination of single pairs interferometric tree heights filtered part of the noise out. The height of the scattering centre was determined a few metres below the tree top in dense forests and further down in sparse forests, being in good agreement with the theory. The main drawback of the PS technique is that it requires a dense grid of stable scatterers, a condition impossible to be met in boreal forests.

In boreal forests the method based on a grid of open areas seems to be the only reasonable filtering approach. Nevertheless the requirement of a dense grid of open areas limits the application in areas largely dominated by forests.

The results obtained with this procedure and the one based on the estimation of the atmospheric path delay suggest that it is more sensible to choose pairs acquired at well-defined times and weather conditions rather than to apply a phase correcting algorithm to the interferogram. Pairs acquired at stable weather and atmospheric conditions, at night, possibly with a long baseline, seem to provide the most reliable phase estimates. This represents a major limitation to the use of the InSAR phase in particular in Scandinavia. The quite variable weather conditions severely affect the phase, thus strongly decreasing the amount of interferometric pairs with reliable phase values.

The interferometric tree height can be retrieved only from pairs that have an interval between acquisitions as short as one day. For longer intervals, the coherence of the reference open field drops to the noise level and the phase does not provide any information. For the same reason, “tandem” pairs acquired at any weather event (precipitation, freeze/thaw) should be discarded.

In the few pairs not affected by major atmospheric disturbances the interferometric height was estimated well below the level expected. These pairs were all acquired in winter. A larger penetration due to the frozen state of the trees can explain the low height of the forest scattering centre. Unfortunately, the lack of pairs acquired during the summer, without major atmospheric artefacts, limits the conclusions regarding the behaviour of the interferometric height to winter conditions.

From the IWCM the model-based interferometric tree height has been determined and compared with the estimated stand-wise values. For pairs not affected by atmospheric artefacts, the model seems to describe well the relationship between stem volume and the interferometric tree height. Unfortunately, the large number of pairs with some type of disturbances (ground decorrelation and atmospheric events) limits the evaluation of the results to a few cases. Nevertheless, it has been clearly shown that in forests phase effects occur and therefore they must be taken into account when modelling the relationship between coherence and InSAR phase on one side and stem volume on the other.

Using the IWCM it is theoretically possible to compensate the interferometric height for attenuation and volumetric decorrelation in order to retrieve the true tree height.

Ideally pairs with long baselines, which are more sensitive to height variations, are preferable but they would suffer from volumetric decorrelation that causes errors in the estimates. Moreover, the vegetation decorrelation term would in such case be very short so that the InSAR phase is almost insensitive to stem volume, whereas the model-based interferometric height curve is almost horizontal. Hence, pairs with an intermediate baseline length and a high temporal coherence of the vegetation give the most suitable conditions for tree height retrieval. In the investigations, the pairs not affected by atmospheric noise were not the most suitable for the compensation: either the vegetation decorrelation was too strong or the baseline was too short. Furthermore, the rather large errors affecting the interferometric height explain the poor estimates of the total tree height. In such cases a multi-temporal combination of tree height estimates improves results only partially.

Considering that in Scandinavia the weather conditions are very variable and that the ideal conditions just reported appear quite improbable, tree height estimation from InSAR phase in this region does not seem to be feasible. Investigations of pairs acquired in East Canada and Siberia are suggested because of the much more stable meteorological conditions. In particular images acquired in winter, at night should be considered. Such investigations would set an important benchmark for the estimation of tree height using C-band repeat-pass InSAR phase in boreal forests.

Chapter 9

Conclusions

9.1 Summary of the thesis

As reported in the Introduction, the aim of the work reported in this thesis has been “to increase knowledge on how the ERS and JERS SAR and SAR interferometry see boreal forests and provide methods and tools based on SAR and SAR interferometry for boreal forest monitoring”. The extensive data set of satellite images acquired over several test sites located in Sweden, Finland and Siberia has been fundamental for analysing the spatial and temporal properties of ERS and JERS backscatter, coherence and InSAR phase in boreal forests. Furthermore, it has allowed development of model-based procedures for the retrieval of forest attributes, having as input one or more SAR and InSAR quantities.

The ERS backscatter suffers from large spread of values and low sensitivity to forest properties, whereas the JERS backscatter is characterised by higher sensitivity to forest attributes and larger dynamic range, in particular for dry-unfrozen conditions. At both frequencies seasonal dependence in terms of frozen/unfrozen conditions affect the backscatter in dense forests, whereas the dielectric properties of the ground (wetness, snow cover, soil moisture) determine the values registered in sparse forests. The influence of seasonal dynamics is stronger at L-band than at C-band. In particular, the strong correlation between temperature and JERS backscatter suggests that L-band backscatter can be used as an index to follow tree activity.

At the test sites investigated, the ERS coherence contained information only for short repeat-pass cycles. The one-day coherence is significantly related to forest properties, being lower in dense than in sparse forests. Wind is the main agent decorrelating the vegetation, unless frozen conditions occur, whereas in sparse forests the commonly high coherence decreases due to changes of the dielectric properties of the forest floor. Long baselines and repeat-pass cycles limit the

exploitation of JERS coherence for forest studies, although promising results have been obtained in other studies.

Knowledge of backscatter and coherence properties provides the background for modelling approaches and retrieval of forest parameters. In this thesis, the Water Cloud Model and the Interferometric Cloud Model have been used for modelling the backscatter and the coherence respectively, as function of stem volume. Model training needs a reliable procedure and an accurate set of remote sensing data and stem volume measurements. These must be uniformly distributed in the range of stem volumes typical of the area investigated.

Using a coupled iterative method, in which two regressions are considered simultaneously, the models have been proved to fit ERS backscatter and coherence data acquired under several environmental conditions. Estimates of the five unknown model parameters are realistic, showing the physical consistency of the WCM and the IWCM. When environmental changes at acquisitions occur, there can be some discrepancies in the coefficient of the two-way forest transmissivity, β , which need further investigation. JERS backscatter modelling is well performed by means of the WCM under several weather conditions. The estimates of the two backscatter coefficients are physically valid for dry-unfrozen weather conditions. Discrepancies can occur for β both temporally, in case of precipitation or frozen conditions, and spatially, depending on the location of the test site. In this second case, not only unequal distribution of stem volumes but also the management system can cause such differences. The spatial inconsistency of β suggests the need for further investigations throughout the boreal zone, in order to prove how strong the dependence of the WCM upon the local conditions of the forest is. Although it could not be proved in this thesis whether such dependency occurs for ERS data, it is theoretically possible that the modelling of ERS backscatter and coherence by means of the WCM and the IWCM presents the same problems.

Stem volume retrieval is most feasible using one-day interval ERS coherence. The procedure based on the inversion of the IWCM and a multi-temporal combination of images acquired under winter stable conditions can provide estimates comparable to values measured in local surveys. The inversion of the WCM using JERS backscatter is suggested under dry-unfrozen conditions. Although the estimates are slightly worse than in the previous case, the temporal consistency of the estimates and the multi-temporal combination return rather accurate results, indicating that the JERS backscatter is a possible candidate for stem volume retrieval in boreal forests. However, the different retrieval accuracy obtained in both cases at the test sites under investigation clearly stresses the importance of the ground-truth measurements and the remote sensing data quality for accurate stem volume retrieval.

The retrieval procedure presented in this thesis requires similar environmental conditions all over the test area, which can be a limiting factor in regions characterised by frequent weather changes. At plot level and, to a lesser extent at regional scale, it has been shown how the weather conditions can introduce significant errors in the estimates. If there are spatial differences in the environmental

conditions, spaceborne repeat-pass InSAR can be considered suitable for mapping of large areas only when averaging over many pixels.

The interferometric phase (in this thesis only the ERS case was considered) includes strong noise components due to the temporal instability of the canopy and to atmospheric heterogeneities. Although the atmospheric contribution is theoretically removable, the phase noise is a property of the target and strongly decreases the information content of the measurements. Images filtered with the Permanent Scatterers technique are promising for forestry studies but only in semi-urban areas, because of the high number of stable scatterers required. In boreal forests the reduction of atmospheric artefacts is feasible only with a dense reference grid of open areas. Since this requirement is seldom met, it is more sensible to choose beforehand the pairs to be used on the basis of meteorological information rather than post-processing the data. Pairs acquired at night, during winter, under stable weather conditions are more suitable because less affected by artefacts.

The inversion of the interferometric phase in Kättböle and Tuusula shows the strong influence of atmospheric artefacts and phase noise on the estimation of the interferometric tree height. For the few pairs not affected by the irregular properties of the atmosphere, the interferometric height was very low and almost uncorrelated with forest properties, such as stem volume. Since these images were acquired under winter-frozen conditions, the larger penetration of the wave through the canopy can explain the low height. By means of the IWCM, the interferometric tree height can be compensated for attenuation and volumetric effects. Nevertheless, the tree height estimates suffer from large errors due to phase noise. Of great interest would be a comparison with summer acquisitions under stable atmospheric conditions, possibly characterised by a baseline between 100 and 200 m.

Summarising the results, it is possible to assert that spaceborne repeat-pass SAR interferometry is a data source from which reliable and accurate estimates of forest stem volume can be obtained. C-band one-day coherence and, to a lesser extent, L-band backscatter can provide estimates comparable to ground-based inventories at stand level. For tree height estimation the potential of the IWCM-based approach using C-band interferometric phase has been shown. Nevertheless, phase noise and atmospheric artefacts strongly limit the results achievable. Independently of the application considered, the applicability of the model-based methods for forest attributes estimation in the boreal zone need stable weather conditions, both spatially and temporally, and clear definitions of the forests under investigation.

9.2 Future outlook

With the end of the ERS-1 mission, C-band repeat-pass SAR interferometry in forests has lost its big appeal because of the 35-days repeat-pass cycle characterising the ERS-2 and the ENVISAT missions. For forestry applications the use of C-band long-term coherence does not seem to be feasible in the whole boreal zone. Very stable weather conditions on a rather long time period are required for stem volume retrieval. Such conditions are more likely to be met during the winter in North

Scandinavia, the Eastern regions of Russia and East Canada, when snow covers the ground and the temperature is constantly below the freezing point. Nevertheless, based on the results obtained for winter-frozen conditions, larger penetration of the electromagnetic wave can be foreseen, which could decrease the sensitivity of the coherence to the forest attributes.

The situation is even more critical for the InSAR phase because atmospheric changes are very likely in the timeframe of one month. Hence, for several years investigations on interferometric tree height will not be possible.

The future of L-band spaceborne SAR and SAR interferometry appears much more promising, considering the launch of the ALOS satellite in 2005, which will carry onboard the fully polarimetric L-band system PALSAR. The interesting results described in this thesis and those achieved in several airborne and spaceborne L-band missions, indicate a strong potential of the L-band backscatter in many forestry-oriented applications, including the estimation of forest attributes, in the whole boreal zone. The repeat-pass coherence of ALOS should in principle behave as the JERS coherence, since the revisit period will be only two days longer (46 days). If the launch of ALOS is successful, it will be theoretically possible to investigate the dynamics of forests over at least two decades using spaceborne backscatter and repeat-pass coherence.

Chapter 10

Acknowledgements

This thesis reports four years of work carried out at the Remote Sensing Group of the Chalmers University of Technology in Göteborg and the Remote Sensing Unit of the Friedrich-Schiller-University in Jena. During these years I have learnt how to do research, I have acquired skills, I have had the opportunity to meet people that had the same enthusiasm and the same worries while doing research, and I learnt how it feels to be “on the other side” (i.e. to teach).

I am extremely thankful to the two people that supported me throughout the Ph.D. studies: Prof. Jan Askne and Prof. Christiane Schmullius. I think they have believed in me from the beginning, although I never understood why they did it! I was surprised when Jan offered me the chance of staying at Chalmers and pushed me to the Licentiate. I was surprised when Christiane said after 11 minutes (I counted them!) that there would have not been any problem to continue the Ph.D. in Jena. What I have learnt from Jan and Christiane was not only how to do research but also how to find the motivations and that I should always look beyond the horizon to see if there is something else and new to be discovered.

Following an order that is only chronological, I want to thank Patrik Dammert and Gary Smith (I am really not able to call them Dr.!) for the true friendship and the fruitful work on SAR interferometry. I remember days full of discussions that not only focused on why “is the coherence so difficult to understand?” but also on “why has Sweden never won any football World Cup?” and “which are the quality factors for pizza?” These and other similar questions were the rule in a very dynamic group that consisted of the three of us, Elaine, Sverre, Xianyun, Carlos, Patrick and Donal. Still today we keep up the old topics and not just because Sweden has not won the World Cup yet! Special thanks go to Britt-Marie, who always helped me and explained how administrative things I had no idea about, worked at Chalmers.

Chalmers was not only the “work-container” for almost three years but also the place where I met several interesting researchers and most of my friends. We all belonged to the so-called “cervelli in fuga”: escaping brains from Italy in search of reasonable conditions for researching. Chalmers was in several occasions our home, for example when we prepared the “celebration” for a new Doctor or wanted to play table tennis. In such moments I felt as having close friends and at the end of my experience in Sweden it was extremely hard for me to say good-bye. I hope to see Mauri, Silvia, Fede, Dem, Giusy, Danieladaniela, Daniela C. and Bobo on the day of the thesis defence in order to get the treatment I deserve from them! And I wish that we could always be as close as we are.

When speaking of three years spent in Sweden I cannot forget all the time spent with Serena, Christophe, Attilio and Anette. Translating from Italian I could define them as “where you put them, there you find them”, which means that our friendship has not changed throughout time. In particular, since I moved to Germany I miss Serena and those never-ending talks about Italy and Sweden.

Moving to Jena has been much easier of what I thought. For all this I need to thank Leif Eriksson. While we had much to learn from each other, we have also been able of things that only two people that understand each other very well can do. Singing the Lucia song at 6 a.m. after a sleepless night in front of a computer screen because of an important deadline is a clear sign of the time spent together and the efforts done to achieve the best results in our work.

From a wonderful idea of Christiane, the Siberia-II room was created, in which together with me and Leif Christian Beer is “living”. Although three people in one office sound as a difficult working environment, I cannot be more satisfied. We have a unique group feeling, which expands outside of the room to all the Remote Sensing Group: Sören, Tanja, Daniela and Dmitri. The feeling that we are not just colleagues applies for all the “Geoinformatiker” as well, in particular for Bettina Hoffi, Manfred and Peter, with whom I have shared important experiences that made me discover the persons sitting behind a desk.

Although Jena means to me the maturity of the Ph.D. studies and a lot of work, it also means Francesca, Martin, Sandy, Silvia, Lucia and Ronny. They represent a wonderful group of friends, always ready to cheer me up and sustain me when something is not working as it should. And although they do not live in Jena (but at least they came here!), I want to thank Eliana, Marianschla and Giuliana for being so close to me, all the time.

I left the last part for special thanks to people that represent a reference point. I start with Attilio Fanelli, a unique example of unbeatable colleague and friend, and continue with Prof. Pasquale Murino, to whom the thesis is dedicated. If I am writing this thesis, is because he made me love remote sensing. Thank you Gośka for always understanding me and for making fun of me every time I suspiciously looked at the treetops while we walked in a forest. *Dulcis in fundo*, the biggest and deepest acknowledgment goes to my parents, for whom I cannot really find words to say how

grateful I am for everything they have done for me during these years away from home.

Further acknowledgements go to Dr Johan Fransson at the Swedish University of Agricultural Sciences, SLU, for the ground-truth measurements collected in Kätthöle, as well as for being a kind advisor on forestry issues and an unbeatable proof-reader of papers. Dr Mats Nilsson, SLU, is acknowledged for providing the NFI plot data. ERS interferograms from Tuusula were processed by Dr Patrik Dammert and Gamma Remote Sensing. All JERS images, except those acquired in 1998 over Bolshe-Murtinsky, were provided through NASDA's Global Boreal Forest Mapping project and processed to SLC by Gamma Remote Sensing and Dr. Masanobu Shimada, NASDA. The interferometric processing of the images was performed with the ISAR toolbox from ESA, the DIAPASON software from CNES, the Gamma software and coherence estimation software provided by Dr Patrik Dammert. Preparation of Bolshe-Murtinsky ground database and processing of the images acquired in 1998 was done within the EU project SIBERIA (Contract No. ENV4-CT97-0743-SIBERIA). The PS-based atmosphere-filtered images from Pairs were kindly provided by POLIMI. NOAA-AVHRR imagery has been downloaded from the Dundee Satellite Receiving Station web site (<http://www.sat.dundee.ac.uk>). I am very thankful to the Swedish Hydrological and Meteorological Institute, SMHI, and to the Deutscher Wetterdienst, DWD, for the meteorological data from the Swedish NFI area and Bolshe-Murtinsky respectively. Additional measurements were downloaded at <http://www.wunderground.com/>.

Chapter 11

References

ASKNE, J., and HAGBERG, J. O., "Potential of interferometric SAR for classification of land surfaces," *Proceedings of IGARSS'93*, Tokyo, 18-21 August, pp. 985-987, 1993.

ASKNE, J., DAMMERT, P., FRANSSON, J., ISRAELSSON, H., and ULANDER, L. M. H., "Retrieval of forest parameters using intensity and repeat-pass interferometric SAR information," *Proceedings of Retrieval of Bio- and Geophysical Parameters from SAR Data for Land Applications*, Toulouse, 10-13 October, pp. 119-129, 1995.

ASKNE, J., and SMITH, G., "Forest INSAR decorrelation and classification properties," *Proceedings of 'Fringe 96' Workshop: ERS SAR Interferometry*, Zürich, 30 September-2 October 1996, pp. 95-103, 1996.

ASKNE, J., DAMMERT, P. B. G., and SMITH, G., "Interferometric SAR observations of forested areas," *Proceedings of Third ERS Symposium on Space at the service of our Environment*, Florence, 14-21 March, pp. 337-344, 1997a.

ASKNE, J., DAMMERT, P. B. G., ULANDER, L. M. H., and SMITH, G., "C-band repeat-pass interferometric SAR observations of the forest," *IEEE Transactions on Geoscience and Remote Sensing*, vol. 35, 1, pp. 25-35, 1997b.

ASKNE, J., DAMMERT, P. B. G., and SMITH, G., "Understanding ERS InSAR coherence of boreal forests," *Proceedings of IGARSS'99*, Hamburg, 28 June - 2 July, pp. 2111-2114, 1999a.

ASKNE, J., WEGMÜLLER, U., SMITH, G., SANTORO, M., and DAMMERT, P., "JERS-1 interferometry of boreal forest," in *JERS-1 Science Program '99 PI Reports*, Shimada, M., Ed.: EORC, National Space Development Agency of Japan, pp. 144-148, 1999b.

ASKNE, J., SANTORO, M., SMITH, G., and FRANSSON, J. E. S., "Large area boreal forest investigations using ERS InSAR," *Proceedings of Third International*

Symposium on Retrieval of Bio- and Geophysical Parameters from SAR Data for Land Applications, Sheffield, 11-14 September, pp. 39-44, 2001.

ASKNE, J., SANTORO, M., SMITH, G., and FRANSSON, J. E. S., "Multi-temporal repeat pass SAR interferometry of boreal forests," *IEEE Transactions on Geoscience and Remote Sensing*, vol. 41, 7, pp. 1540-1550, 2003.

ATTEMA, E. P. W., and ULABY, F. T., "Vegetation modeled as a water cloud," *Radio Science*, vol. 13, 2, pp. 357-364, 1978.

BAKER, J. R., and LUCKMAN, A. J., "Microwave observations of boreal forests in the NOPEX area of Sweden and a comparison with observations of a temperate plantation in the United Kingdom," *Agricultural and Forest Meteorology*, vol. 98-99, pp. 389-416, 1999.

BAMLER, R., and JUST, D., "Phase statistics and decorrelation in SAR interferograms," *Proceedings of IGARSS'93*, Tokyo, 18-21 August, pp. 980-984, 1993.

BAMLER, R., and HARTL, P., "Synthetic aperture radar interferometry," *Inverse Problems*, vol. 14, 4, pp. R1-R54, 1998.

BEAUDOIN, A., LE TOAN, T., GOZE, S., NEZRY, E., LOPES, A., MOUGIN, E., HSU, C. C., HAN, H. C., KONG, J. A., and SHIN, R. T., "Retrieval of forest biomass from SAR data," *International Journal of Remote Sensing*, vol. 15, 14, pp. 2777-2796, 1994.

BEAUDOIN, A., CASTEL, T., and RABAUTE, T., "Forest monitoring over hilly terrain using ERS INSAR data," *Proceedings of 'Fringe 96' Workshop on ERS SAR Interferometry*, Zürich, 30 September - 2 October, pp. 105-115, 1996.

BORN, M., and WOLF, E., *Principles of Optics*, 6 ed: Pergamon Press, 1980.

BRUNIQUEL, J., and LOPES, A., "Multi-variate optimal speckle reduction in SAR imagery," *International Journal of Remote Sensing*, vol. 18, 3, pp. 603-627, 1997.

CASTEL, T., MARTINEZ, J.-M., BEAUDOIN, A., WEGMÜLLER, U., and STROZZI, T., "ERS INSAR data for remote sensing hilly forested areas," *Remote Sensing of Environment*, vol. 73, pp. 73-86, 2000.

CHAUHAN, N. S., LANG, R. H., and RANSON, K. J., "Radar modeling of a boreal forest," *IEEE Transactions on Geoscience and Remote Sensing*, vol. 29, 4, pp. 627-638, 1991.

CORR, D. G., KEYTE, G. E., and WHITEHOUSE, S., "Studies of Decorrelation in Multi-Temporal SAR Imagery," *Proceedings of IGARSS'95*, Florence, 10-14 July 1995, pp. 1026-1028, 1995.

CROSETTO, M., TSCHERNING, C. C., CRIPPA, B., and CASTILLO, M., "Subsidence monitoring using SAR interferometry: Reduction of the atmospheric effects using stochastic filtering," *Geophysical Research Letters*, vol. 29, 9, pp. 26-1,26-4, 2002.

DAMMERT, P. B. G., ULANDER, L. M. H., and ASKNE, J., "SAR interferometry for detecting forest stands and tree heights," in *Synthetic Aperture Radar and Passive Microwave Sensing*, Franceschetti, G., Oliver, C. J., Shiue, J. C., and Tajbakhsh, S., Eds.: Proc. SPIE 2584, pp. 384-390, 1995.

- DAMMERT, P. B. G., "Accuracy of INSAR measurements in forested areas," *Proceedings of 'Fringe 96' Workshop on ERS SAR Interferometry*, Zürich, 30 September - 2 October, pp. 37-49, 1996a.
- DAMMERT, P. B. G., "Applications of spaceborne SAR interferometry," Department of Radio and Space Science, Chalmers University of Technology, Göteborg, Sweden, Technical Report 254L, 1996b.
- DAMMERT, P. B. G., and ASKNE, J., "Interferometric tree height observations in boreal forests with SAR interferometry," *Proceedings of IGARSS'98*, Seattle, 6-10 July, pp. 1363-1366, 1998.
- DAMMERT, P. B. G., LEPPÄRANTA, M., and ASKNE, J., "SAR interferometry over Baltic Sea ice," *International Journal of Remote Sensing*, vol. 19, 16, pp. 3019-3037, 1998.
- DAMMERT, P. B. G., "Interferometric Tree Heights - Measurements and Modeling," Department of Radio and Space Science, Chalmers University of Technology, Göteborg, Sweden, Research Report 183, 1999a.
- DAMMERT, P. B. G., "Spaceborne SAR Interferometry: Theory and Applications," Department of Radio and Space Science, Chalmers University of Technology, Göteborg, Sweden, Ph.D. thesis, Technical Report, 382, 1999b.
- DÄNDLIKER, R., "Heterodyne Holographic Interferometry," in *Progress in Optics*, vol. XVII, Wolf, E., Ed.: North-Holland Publishing Company, pp. 3-84, 1980.
- DEKKER, R. J., "Speckle filtering in satellite SAR change detection imagery," *International Journal of Remote Sensing*, vol. 19, 6, pp. 1133-1146, 1998.
- DELACOURT, C., BRIOLE, P., and ACHACHE, J., "Tropospheric corrections of SAR interferograms with strong topography. Application to Etna," *Geophysical Research Letters*, vol. 25, 15, pp. 2849-2852, 1998.
- DOBSON, M. C., ULABY, F. T., LE TOAN, T., BEAUDOIN, A., KASICHKE, E. S., and CHRISTENSEN, N., "Dependence of radar backscatter on coniferous forest biomass," *IEEE Transactions on Geoscience and Remote Sensing*, vol. 30, pp. 412-416, 1992.
- DOBSON, M. C., ULABY, F. T., PIERCE, L. E., SHARIK, T. L., BERGEN, K. M., KELLNDORFER, J., KENDRA, J. R., LI, E., LIN, Y. C., NASHASHIBI, A., SARABANDI, K., and SIQUEIRA, P., "Estimation of forest biophysical characteristics in Northern Michigan with SIR-C/X-SAR," *IEEE Transactions on Geoscience and Remote Sensing*, vol. 33, 4, pp. 877-895, 1995.
- DUGUAY, C. R., ROUSE, W. R., LAFLEUR, P. M., BOUDREAU, L. D., CREVIER, Y., and PULTZ, T. J., "Analysis of multi-temporal ERS-1 SAR data of subarctic tundra and forest in the Northern Hudson Bay lowland and implications for climate studies," *Canadian Journal of Remote Sensing*, vol. 25, 1, pp. 21-33, 1999.
- ENGDAHL, M., and HYYPPÄ, J., "Forest inventory using interferometric SAR techniques," *Proceedings of Third ERS Symposium on Space at the service of our Environment*, Florence, 14-21 March, pp. 345-350, 1997.
- ERIKSSON, L. E. B., SANTORO, M., WIESMANN, A., and SCHMULLIUS, C., "Multi-temporal JERS repeat-pass coherence for growing stock volume estimation of

- Siberian forest," *IEEE Transactions on Geoscience and Remote Sensing*, vol. 41, 7, pp. 1561-1570, 2003.
- FAZAKAS, Z., NILSSON, M., and OLSSON, H., "Regional forest biomass and wood volume estimation using satellite data and ancillary data," *Agricultural and Forest Meteorology*, vol. 98-99, pp. 417-425, 1999.
- FERRETTI, A., PRATI, C., and ROCCA, F., "Multibaseline InSAR DEM reconstruction: the wavelet approach," *IEEE Transactions on Geoscience and Remote Sensing*, vol. 37, 2, pp. 705-715, 1999a.
- FERRETTI, A., PRATI, C., and ROCCA, F., "Permanent Scatterers in SAR interferometry," *Proceedings of IGARSS'99*, Hamburg, 28 June-2 July, pp. 1528-1530, 1999b.
- FERRETTI, A., PRATI, C., and ROCCA, F., "Nonlinear subsidence rate estimation using Permanent Scatterers in differential SAR interferometry," *IEEE Transactions on Geoscience and Remote Sensing*, vol. 38, 5, pp. 2202-2212, 2000.
- FERRETTI, A., PRATI, C., and ROCCA, F., "Permanent Scatterers in SAR interferometry," *IEEE Transactions on Geoscience and Remote Sensing*, vol. 39, 1, pp. 8-20, 2001.
- FLEISCHMAN, J. G., AYASLI, S., ADAMS, E. M., and GOSSELIN, D. R., "Foliage penetration experiment Part I: Foliage attenuation and backscatter analysis of SAR imagery," *IEEE Transactions on Aerospace and Electronic Systems*, vol. 32, 1, pp. 135-144, 1996.
- FLOURY, N., LE TOAN, L., and SOUYRIS, J. C., "Relating forest parameters to interferometric data," *Proceedings of IGARSS'96*, Lincoln, 27-31 May, pp. 975-977, 1996a.
- FLOURY, N., LE TOAN, T., SOUYRIS, J.-C., SINGH, K., STUSSI, N., HSU, C. C., and KONG, J. A., "Interferometry for forest studies," *Proceedings of 'Fringe 96' Workshop on ERS SAR Interferometry*, Zürich, 30 September- 2 October, pp. 57-70, 1996b.
- FRANSSON, J. E. S., Personal communication.
- FRANSSON, J. E. S., and ISRAELSSON, H., "Estimation of stem volume in boreal forests using ERS-1 C- and JERS-1 L-band SAR data," *International Journal of Remote Sensing*, vol. 20, 1, pp. 123-137, 1999.
- FRANSSON, J. E. S., WALTER, F., and ULANDER, L. M. H., "Estimation of forest parameters using VHF SAR data," *IEEE Transactions on Geoscience and Remote Sensing*, vol. 38, 1, pp. 720-727, 2000.
- FRANSSON, J. E. S., SMITH, G., ASKNE, J., and OLSSON, H., "Stem volume estimation in boreal forests using ERS-1/2 coherence and SPOT XS optical data," *International Journal of Remote Sensing*, vol. 22, 14, pp. 2777-2791, 2001.
- FROST, V. S., STILES, J. A., SHANMUGAN, K. S., and HOLTZMAN, J. C., "A model for radar images and its application to adaptive digital filtering of multiplicative noise," *IEEE Transactions on Pattern Analysis and Machine Intelligence*, vol. 4, 2, pp. 157-166, 1982.

- FRUNEAU, B., and SARTI, F., "Detection of ground subsidence in the city of Paris using radar interferometry: isolation of deformation from atmospheric artifacts using correlation," *Geophysical Research Letters*, vol. 27, 24, pp. 3981-3984, 2000.
- FUNG, A. K., *Microwave Scattering and Emission Models and Their Applications*. Norwood, MA: Artech House, 1994.
- GABRIEL, A. K., and GOLDSTEIN, R. M., "Crossed orbit interferometry: theory and experimental results from SIR-B," *International Journal of Remote Sensing*, vol. 9, 5, pp. 857-872, 1988.
- GABRIEL, A. K., GOLDSTEIN, R. M., and ZEBKER, H. A., "Mapping small elevation changes over large areas: differential radar interferometry," *Journal of Geophysical Research*, vol. 94, B7, pp. 9183-9191, 1989.
- GATELLI, F., MONTI GUARNIERI, A., PARIZZI, F., PASQUALI, P., PRATI, C., and ROCCA, F., "The wavenumber shift in SAR interferometry," *IEEE Transactions on Geoscience and Remote Sensing*, vol. 32, 4, pp. 855-865, 1994.
- GAVEAU, D. L. A., "Modelling the dynamics of ERS-1/2 coherence with increasing woody biomass over boreal forests," *International Journal of Remote Sensing*, vol. 23, 18, pp. 3879-3885, 2002.
- GOLDSTEIN, R., "Atmospheric limitations to repeat-track radar interferometry," *Geophysical Research Letters*, vol. 22, 18, pp. 2517-2520, 1995.
- GOLDSTEIN, R. M., ZEBKER, H. A., and WERNER, C. L., "Satellite radar interferometry: Two-dimensional phase unwrapping," *Radio Science*, vol. 23, 4, pp. 713-720, 1988.
- GOLDSTEIN, R. M., ENGELHARDT, H., KAMB, B., and FROLICH, R. M., "Satellite radar interferometry for monitoring ice sheet motion: application to an Antarctic ice stream," *Science*, vol. 262, pp. 1525-1530, 1993.
- GRAHAM, L. C., "Synthetic interferometer radar for topographic mapping," *Proceedings of the IEEE*, vol. 62, 6, pp. 763-768, 1974.
- GUNERIUSSEN, T., JOHNSEN, H., and SAND, K., "DEM corrected ERS-1 SAR data for snow monitoring," *International Journal of Remote Sensing*, vol. 17, 1, pp. 181-195, 1996.
- HAGBERG, J. O., and ULANDER, L. M. H., "On the optimization of interferometric SAR for topographic mapping," *IEEE Transactions on Geoscience and Remote Sensing*, vol. 31, 1, pp. 303-306, 1993.
- HAGBERG, J. O., ULANDER, L. M. H., and ASKNE, J., "Repeat-pass SAR interferometry over forested terrain," *IEEE Transactions on Geoscience and Remote Sensing*, vol. 33, 2, pp. 331-340, 1995.
- HALLIKAINEN, M., HYYPPÄ, J., KOSKINEN, J., ROSCHIER, M., and AHOLA, P., "EUFORA Campaign plan, Version 2," Laboratory of Space Technology, Helsinki University of Technology, Helsinki, Finland, 1997.
- HALLIKAINEN, M., MÄKYNEN, M., LAAKSO, S., RANTALA, A., TARES, T., UUSITALO, J., KOSKINEN, J., PULLIAINEN, J., HYYPPÄ, J., and HYYPPÄ, H., "Experimental results on radar response to boreal forests," *Proceedings of Second International Workshop*

- on Retrieval of Bio- and Geo-physical Parameters from SAR data for Land Applications, ESTEC Noordwijk, 21-23 October, pp. 325-332, 1998.
- HÄME, T., SALLI, A., and LAHTI, K., "Estimation of carbon storage in boreal forests using remote sensing data," in *Pilot study. In The Finnish Research Program on Climate Change, Progress Report*, vol. 3, Kanninen, M., and Anttila, P., Eds. Helsinki, Finland: Academy of Finland, pp. 250-255, 1992.
- HANSEN, R., "Atmospheric heterogeneities in ERS tandem SAR interferometry," Delft University of Technology, Delft, The Netherlands, DEOS Report 98.1, 1998.
- HANSEN, R. F., WECKWERTH, T. M., ZEBKER, H. A., and KLEES, R., "High-resolution water vapor mapping from interferometric radar measurements," *Science*, vol. 283, pp. 1297-1299, 1999.
- HARE, F. K., and RITCHIE, J. C., "The boreal bioclimates," *Geographical Review*, vol. 62, pp. 333-365, 1972.
- HARRELL, P. A., BOURGEOU-CHAVEZ, L. L., KASISCHKE, E. S., FRENCH, N. H. F., and CHRISTENSEN JR., N. L., "Sensitivity of ERS-1 and JERS-1 radar data to biomass and stand structure in Alaskan boreal forest," *Remote Sensing of Environment*, vol. 54, pp. 247-260, 1995.
- HENDERSON, F. M., and LEWIS, A. J., "Principles and Applications of Imaging Radar," in *Manual of Remote Sensing*, vol. 2, Ryerson, R. A., Ed., 3rd ed. New York: John Wiley & Sons, 1998.
- HYYPPÄ, J., and ENGDAHL, M., "Verification of the capability of repeat-pass SAR interferometry to provide tree height information in boreal forest zone," *Proceedings of IGARSS 2000*, Honolulu, 24-28 July, pp. 402-404, 2000.
- HYYPPÄ, J., HYYPPÄ, H., INKINEN, M., ENGDAHL, M., LINKO, S., and ZHU, Y.-H., "Accuracy comparison of various remote sensing data sources in the retrieval of forest stand attributes," *Forest Ecology and Management*, vol. 128, 1-2, pp. 109-120, 2000.
- IMHOFF, M. L., "Radar backscatter and biomass saturation: ramifications for global biomass inventory," *IEEE Transactions on Geoscience and Remote Sensing*, vol. 33, 2, pp. 511-518, 1995.
- ISRAELSSON, H., ASKNE, J., and SYLVANDER, R., "Potential of SAR for forest bole volume estimation," *International Journal of Remote Sensing*, vol. 15, 14, pp. 2809-2826, 1994.
- ISRAELSSON, H., ASKNE, J., FRANSSON, J., and SYLVANDER, R., "JERS-1 SAR analysis of boreal forest biomass," Ministry of International Trade and Industry, National Space Development Agency of Japan, Tokyo, Volume II, 1995.
- JOUGHIN, I. R., and WINEBRENNER, D. P., "Effective number of looks for a multilook interferometric phase distribution," *Proceedings of IGARSS'94*, Pasadena, 8-12 August, pp. 2276-2278, 1994.
- KARAM, M. A., FUNG, A. K., LANG, R. H., and CHAUHAN, N. S., "A microwave scattering model for layered vegetation," *IEEE Transactions on Geoscience and Remote Sensing*, vol. 30, 4, pp. 767-784, 1992.

- KASISCHKE, E. S., BOURGEOU-CHAVEZ, L. L., CHRISTENSEN JR., N. L., and HANEY, E., "Observations on the sensitivity of ERS-1 SAR image intensity to changes in aboveground biomass in young loblolly pine forests," *International Journal of Remote Sensing*, vol. 15, 1, pp. 3-16, 1994.
- KOSKINEN, J. T., PULLIAINEN, J. T., HYYPPÄ, J. M., ENGDAHL, M. E., and HALLIKAINEN, M. T., "The seasonal behavior of interferometric coherence in boreal forest," *IEEE Transactions on Geoscience and Remote Sensing*, vol. 39, 4, pp. 820-829, 2001.
- KURVONEN, L., PULLIAINEN, J., and HALLIKAINEN, M., "Retrieval of biomass in boreal forests from multitemporal ERS-1 and JERS-1 SAR images," *IEEE Transactions on Geoscience and Remote Sensing*, vol. 37, 1, pp. 198-205, 1999.
- LE TOAN, T., BEAUDOIN, A., RIOM, J., and GUYON, D., "Relating forest biomass to SAR data," *IEEE Transactions on Geoscience and Remote Sensing*, vol. 30, 2, pp. 403-411, 1992.
- LEE, J.-S., "Speckle analysis and smoothing of synthetic aperture radar images," *Computer Graphics and Image Processing*, vol. 17, 1, pp. 24-32, 1981.
- LI, C.-Z., and RANNEBY, B., "The Precision of the Estimated Forest Data from the National Forest Survey 1983-1987," Department of Forest Survey, Swedish University of Agricultural Sciences, Report 54, 1992.
- LI, F. K., and GOLDSTEIN, R. M., "Studies of multibaseline spaceborne interferometric synthetic aperture radars," *IEEE Transactions on Geoscience and Remote Sensing*, vol. 28, 1, pp. 88-97, 1990.
- LINDGREN, O., "A study on circular plot sampling of Swedish forest compartments," Department of Biometry and Forest Management, Swedish University of Agricultural Sciences, Umeå, Sweden, Report 11, 1984.
- LOPES, A., NEZRY, E., and TOUZI, R., "Adaptive filters and scene heterogeneity," *IEEE Transactions on Geoscience and Remote Sensing*, vol. 28, 6, pp. 992-1000, 1990.
- LOPES, A., NEZRY, E., TOUZI, R., and LAUR, H., "Structure detection and statistical adaptive speckle filtering in SAR images," *International Journal of Remote Sensing*, vol. 14, 9, pp. 1735-1758, 1993.
- LUCKMAN, A., BAKER, J., and WEGMÜLLER, U., "Repeat-pass interferometric coherence measurements of disturbed tropical forest from JERS and ERS satellites," *Remote Sensing of Environment*, vol. 73, pp. 350-360, 2000.
- MANNINEN, T., PARMES, E., HÄME, T., SEPHTON, A., BACH, H., and BERGEAUD, M., "ERS coherence and SLC images in forest characterisation," *Proceedings of ERS-Envisat Symposium*, Gothenburg, 16-20 October, CD-ROM, 2000.
- MASSONNET, D., ROSSI, M., CARMONA, C., ADRAGNA, F., PELTZER, G., FEIGL, K., and RABAUTE, T., "The displacement field of the Landers earthquake mapped by radar interferometry," *Nature*, vol. 364, 6433, pp. 138-142, 1993.
- MASSONNET, D., and FEIGL, K. L., "Discrimination of geophysical phenomena in satellite radar interferograms," *Geophysical Research Letters*, vol. 22, 12, pp. 1537-1540, 1995.

- MASSONNET, D., and FEIGL, K. L., "Radar interferometry and its application to changes in the Earth's surface," *Reviews of Geophysics*, vol. 36, 4, pp. 441-500, 1998.
- MCDONALD, K. C., and ULABY, F. T., "Radiative transfer modelling of discontinuous tree canopies at microwave frequencies," *International Journal of Remote Sensing*, vol. 14, 11, pp. 2097-2128, 1993.
- NILSSON, M., "Estimation of Forest Variables Using Satellite Image Data and Airborne Lidar," Department of Forest Resource Management and Geomatics, Swedish University of Agricultural Sciences, Umeå, Sweden, Ph.D. thesis, Report 17, 1997.
- OLIVER, C., and QUEGAN, S., *Understanding Synthetic Aperture Radar Images*. Boston: Artech House, 1998.
- PRATI, C., ROCCA, F., and MONTI GUARNIERI, A., "SAR interferometry experiments with ERS-1," *Proceedings of First ERS-1 Symposium - Space at the Service of our Environment*, Cannes, 4-6 November, pp. 211-218, 1992.
- PROISY, C., MOUGIN, E., DUFRÊNE, E., and LE DANTEC, V., "Monitoring seasonal changes of a mixed temperate forest using ERS SAR observations," *IEEE Transactions on Geoscience and Remote Sensing*, vol. 38, 1, pp. 540-552, 2000.
- PULLIAINEN, J. T., HEISKA, K., HYYPPÄ, J., and HALLIKAINEN, M. T., "Backscattering properties of boreal forests at the C- and X-bands," *IEEE Transactions on Geoscience and Remote Sensing*, vol. 32, 5, pp. 1041-1050, 1994.
- PULLIAINEN, J. T., MIKKELÄ, P. J., HALLIKAINEN, M. T., and IKONEN, J.-P., "Seasonal dynamics of C-band backscatter of boreal forests with applications to biomass and soil moisture estimation," *IEEE Transactions on Geoscience and Remote Sensing*, vol. 34, 3, pp. 758-770, 1996.
- PULLIAINEN, J. T., KURVONEN, L., and HALLIKAINEN, M. T., "Multitemporal behavior of L- and C-band SAR observations of boreal forests," *IEEE Transactions on Geoscience and Remote Sensing*, vol. 37, 2, pp. 927-937, 1999.
- QUEGAN, S., LE TOAN, T., YU, J. J., RIBBES, F., and FLOURY, N., "Multitemporal ERS SAR analysis applied to forest mapping," *IEEE Transactions on Geoscience and Remote Sensing*, vol. 38, 2, pp. 741-753, 2000.
- RANNEBY, B., CRUSE, T., HÄGGLUND, B., JONASSON, H., and SWÄRD, J., "Designing a new national forest survey for Sweden," Faculty of Forestry, Swedish University of Agricultural Sciences, Uppsala, Sweden, *Studia Forestalia Suecica* 177, 1987.
- RANSON, K. J., and SUN, G., "Northern forest classification using temporal multifrequency and multipolarimetric SAR images," *Remote Sensing of Environment*, vol. 47, pp. 142-153, 1994a.
- RANSON, K. J., and SUN, G., "Mapping biomass of a northern forest using multifrequency SAR data," *IEEE Transactions on Geoscience and Remote Sensing*, vol. 32, 2, pp. 388-396, 1994b.
- RANSON, K. J., SUN, G., LANG, R. H., CHAUHAN, N. S., CACCIOLA, R. J., and KILIC, O., "Mapping of boreal forest biomass from spaceborne synthetic aperture radar," *Journal of Geophysical Research*, vol. 102, D24, pp. 29,599-29,610, 1997.

- RANSON, K. J., SUN, G., KHARUK, V. I., and KOVACS, K., "Characterization of Forests in Western Sayani Mountains, Siberia from SAR data," *Proceedings of IGARSS'99*, Hamburg, 28 June - 2 July, pp. 747-749, 1999.
- RANSON, K. J., and SUN, G., "Effects of environmental conditions on boreal forest classification and biomass estimates with SAR," *IEEE Transactions on Geoscience and Remote Sensing*, vol. 38, 3, pp. 1242-1252, 2000.
- RAUSTE, Y., HÄME, T., PULLIAINEN, J., HEISKA, K., and HALLIKAINEN, M., "Radar-based forest biomass estimation," *International Journal of Remote Sensing*, vol. 15, 14, pp. 2797-2808, 1994.
- RIBBES, F., LE TOAN, T., BRUNIQUET, J., FLOURY, N., STUSSI, N., LIEW, S. C., and WASRIN, U. R., "Forest mapping in tropical region using multitemporal and interferometric ERS-1/2 data," *Proceedings of Third ERS Symposium on Space at the service of our Environment*, Florence, 14-21 March, pp. 351-356, 1997.
- RICHARDS, J. A., SUN, G., and SIMONETT, D. S., "L-band radar backscatter modeling of forest stands," *IEEE Transactions on Geoscience and Remote Sensing*, vol. GE-25, 4, pp. 487-498, 1987.
- RIGNOT, E., WAY, J., McDONALD, K., VIERECK, L., WILLIAMS, C., ADAMS, P., PAYNE, C., WOOD, W., and SHI, J., "Monitoring of environmental conditions in taiga forests using ERS-1 SAR," *Remote Sensing of Environment*, vol. 49, pp. 145-154, 1994a.
- RIGNOT, E., WAY, J., WILLIAMS, C., and VIERECK, L., "Radar estimates of aboveground biomass in boreal forests of interior Alaska," *IEEE Transactions on Geoscience and Remote Sensing*, vol. 32, 5, pp. 1117-1124, 1994b.
- RODRIGUEZ, E., and MARTIN, J. M., "Theory and design of interferometric synthetic aperture radars," *IEE Proceedings-F*, vol. 139, 2, pp. 147-159, 1992.
- ROSSI, M., ROGRON, B., and MASSONNET, D., "JERS-1 SAR image quality and interferometric potential," *IEEE Transactions on Geoscience and Remote Sensing*, vol. 34, 3, pp. 824-827, 1996.
- RUFINO, G., MOCCIA, A., and ESPOSITO, S., "DEM generation by means of ERS tandem data," *IEEE Transactions on Geoscience and Remote Sensing*, vol. 36, 6, pp. 1905-1912, 1998.
- SAATCHI, S. S., and McDONALD, K. C., "Coherent effects in microwave backscattering models for forest canopies," *IEEE Transactions on Geoscience and Remote Sensing*, vol. 35, 4, pp. 1032-1044, 1997.
- SANDWELL, D. T., and PRICE, E. J., "Phase gradient approach to stacking interferograms," *Journal of Geophysical Research*, vol. 103, B12, pp. 30,183-30,204, 1998.
- SANSOSTI, E., LANARI, R., FORNARO, G., FRANCHSCHETTI, G., TESAURO, M., PUGLISI, G., and COLTELLI, M., "Digital elevation model generation using ascending and descending ERS-1/ERS-2 tandem data," *International Journal of Remote Sensing*, vol. 20, 8, pp. 1527-1547, 1999.
- SANTORO, M., ASKNE, J., DAMMERT, P. B. G., FRANSSON, J. E. S., and SMITH, G., "Retrieval of biomass in boreal forest from multi-temporal ERS-1/2 interferometry,"

Proceedings of 'Fringe 99' Second International Workshop on ERS SAR Interferometry, Liège, 10-12 November, CD-ROM, 1999.

SANTORO, M., ASKNE, J., SMITH, G., DAMMERT, P. B. G., and FRANSSON, J. E. S., "Boreal forest monitoring with ERS coherence," *Proceedings of ERS-Envisat Symposium*, Gothenburg, 16-20 October, CD-ROM, 2000.

SANTORO, M., "Characterisation of Boreal Forests and Urban Areas Using ERS InSAR Coherence," Department of Radio and Space Science, Chalmers University of Technology, Göteborg, Sweden, Technical Report 394L, 2001a.

SANTORO, M., "Analysis of Forests Using Atmosphere-corrected ERS InSAR Phase Imagery," Department of Radio and Space Science, Chalmers University of Technology, Göteborg, Sweden, Research Report 187, 2001b.

SANTORO, M., ASKNE, J., ERIKSSON, L., SCHMULLIUS, C., WIESMANN, A., and FRANSSON, J. E. S., "Seasonal dynamics and stem volume retrieval in boreal forests using JERS-1 backscatter," *Proceedings of SPIE 9th International Symposium on Remote Sensing*, Agia Pelagia, Crete, 22-27 September, pp. 231-242, 2002.

SANTORO, M., ASKNE, J., SMITH, G., and FRANSSON, J. E. S., "Stem Volume Retrieval in Boreal Forests with ERS-1/2 Interferometry," *Remote Sensing of Environment*, vol. 81, 1, pp. 19-35, 2002b.

SARABANDI, K., and LIN, Y.-C., "Simulation of interferometric SAR response for characterizing the scattering phase center statistics of forest canopies," *IEEE Transactions on Geoscience and Remote Sensing*, vol. 38, 1, pp. 115-125, 2000.

SARTI, F., VADON, H., and MASSONNET, D., "A method for the automatic characterization of InSAR atmospheric artifacts by correlation of multiple interferograms over the same site," *Proceedings of IGARSS'99*, Hamburg, 28 June - 2 July, pp. 1937-1939, 1999.

SCHMULLIUS, C., and ROSENQUIST, Å., "Closing the gap - A Siberian boreal forest map with ERS-1/2 and JERS-1," *Proceedings of Third ERS Symposium on Space at the service of our Environment*, Florence, 14-21 March, pp. 1885-1890, 1997.

SCHMULLIUS, C., BAKER, J., BALZTER, H., DAVIDSON, M., ERIKSSON, L., GAVEAU, D., GLUCK, M., HOLZ, A., LETOAN, T., LUCKMAN, A., MARSCHALK, U., MC CALLUM, I., NILSSON, S., ORRMALM, S., QUEGAN, S., RAUSTE, Y., ROTH, A., ROZHKOVA, V., SOKOLOV, V., SHVIDENKO, A., SIRRO, L., SKUDING, V., STROZZI, T., TANSEY, K., UTSI, R., VIETMEIER, J., VOLOSHUK, L., WAGNER, W., WEGMÜLLER, U., WESTIN, T., WIESMANN, A., and YU, J. J., "SIBERIA - SAR Imaging for Boreal Ecology and Radar Interferometry Applications," Friedrich-Schiller-University, Jena, Germany, 2001.

SCHWÄBISCH, M., and GEUDTNER, D., "Improvement of phase and coherence map using azimuth prefiltering: Examples from ERS-1 and X-SAR," *Proceedings of IGARSS'95*, Florence, 10-14 July, pp. 205-207, 1995.

SEYMOUR, M. S., and CUMMING, I. G., "Maximum Likelihood estimation for SAR interferometry," *Proceedings of IGARSS'94*, Pasadena, 8-12 August, pp. 2272-2275, 1994.

- SHINOHARA, H., HOMMA, T., NOHMI, H., HIROSAWA, H., and TAGAWA, T., "Relation between L-band microwave penetration / backscattering characteristics and state of trees," *Proceedings of IGARSS'92*, Houston, 26-29 May, pp. 539-541, 1992.
- SKINNER, L., "Estimating forest parameters from synthetic aperture radar: A case study of Thetford Forest, UK," Department of Geography, University of Wales, Swansea, Ph.D. thesis, 2002.
- SKINNER, L., LUCKMAN, A., and BALZTER, H., "Estimating forest stand height using SAR interferometry: a case study at Thetford forest using spaceborne and airborne interferometric systems," *Proceedings of ForestSAT Symposium*, Edinburgh, 5-9 August, CD-ROM, 2002.
- SMITH, G., DAMMERT, P. B. G., and ASKNE, J., "Decorrelation mechanisms in C-Band SAR interferometry over boreal forest," in *Microwave Sensing and Synthetic Aperture Radar*, Franceschetti, G., Oliver, C. J., Rubertone, F. S., and Tajbakhsh, S., Eds.: Proc. SPIE 2958, pp. 300-310, 1996.
- SMITH, G., "ERS InSAR Coherence for Remote Sensing of Boreal Forests," Department of Radio and Space Science, Chalmers University of Technology, Göteborg, Sweden, Technical Report 300L, 1998.
- SMITH, G., DAMMERT, P. B. G., SANTORO, M., FRANSSON, J. E. S., WEGMÜLLER, U., and ASKNE, J., "Biomass retrieval in boreal forest using ERS and JERS SAR," *Proceedings of Second International Workshop on Retrieval of Bio- and Geophysical Parameters from SAR data for Land Applications*, ESTEC Noordwijk, 21-23 October, pp. 293-300, 1998.
- SMITH, G., "Radar remote sensing of forests using CARABAS and ERS," Department of Radio and Space Science, Chalmers University of Technology, Göteborg, Sweden, Ph.D. thesis, Technical Report, 393, 2000.
- SMITH, G., and ULANDER, L. M. H., "A Model Relating VHF-Band Backscatter to Stem Volume of Coniferous Boreal Forest," *IEEE Transactions on Geoscience and Remote Sensing*, vol. 38, 2, pp. 728-740, 2000.
- SMITH, G., and ASKNE, J., "Clear-cut detection using ERS interferometry," *International Journal of Remote Sensing*, vol. 22, 18, pp. 3651-3664, 2001.
- STOLBOVOI, V., and MCCALLUM, I., "Land Resources of Russia," International Institute for Applied Systems Analysis and the Russian Academy of Science, Laxenburg, Austria, CD-ROM.
- STROZZI, T., WEGMÜLLER, U., and MÄTZLER, C., "Mapping wet snowcovers with SAR interferometry," *International Journal of Remote Sensing*, vol. 20, 12, pp. 2395-2403, 1999.
- STROZZI, T., DAMMERT, P. B. G., WEGMÜLLER, U., MARTINEZ, J.-M., ASKNE, J. I. A., BEAUDOIN, A., and HALLIKAINEN, M. T., "Landuse mapping with ERS SAR interferometry," *IEEE Transactions on Geoscience and Remote Sensing*, vol. 38, 2, pp. 766-775, 2000.
- SUN, G., and SIMONETT, D. S., "Simulation of L-band and HH microwave backscattering from coniferous forest stands. A comparison with SIR-B data," *International Journal of Remote Sensing*, vol. 9, 5, pp. 907-925, 1988.

- SUN, G., SIMONETT, D. S., and STRAHLER, A. H., "A radar backscatter model for discontinuous coniferous forests," *IEEE Transactions on Geoscience and Remote Sensing*, vol. 29, 4, pp. 639-650, 1991.
- TARAYRE, H., and MASSONNET, D., "Atmospheric propagation heterogeneities revealed by ERS-1 interferometry," *Geophysical Research Letters*, vol. 23, 9, pp. 989-992, 1996.
- TÖRMÄ, M., "Classification of tree species using ERS intensity and coherence images," *Proceedings of 'Fringe 99' Second International Workshop on ERS SAR Interferometry*, Liege, 10-12 November, CD-ROM, 1999.
- TOUZI, R., LOPES, A., BRUNIQUEL, J., and VACHON, P. W., "Coherence estimation for SAR imagery," *IEEE Transactions on Geoscience and Remote Sensing*, vol. 37, 1, pp. 135-149, 1999.
- ULABY, F. T., SARABANDI, K., McDONALD, K., WHITT, M., and DOBSON, M. C., "Michigan microwave canopy scattering model," *International Journal of Remote Sensing*, vol. 11, 7, pp. 1223-1253, 1990a.
- ULABY, F. T., WHITT, M. W., and DOBSON, M. C., "Measuring the propagation properties of a forest canopy using a polarimetric scatterometer," *IEEE Transactions on Antennas and Propagation*, vol. 38, 2, pp. 251-258, 1990b.
- ULANDER, L. M. H., DAMMERT, P. B. G., and HAGBERG, J. O., "Measuring tree height using ERS-1 SAR interferometry," *Proceedings of IGARSS'95*, Florence, 10-14 July, pp. 2189-2191, 1995.
- ULANDER, L. M. H., and HAGBERG, J. O., "Radiometric and Interferometric Calibration of ENVISAT-1 ASAR," Department of Radio and Space Science, Chalmers University of Technology, Göteborg, Sweden, Research Report 172, 1995.
- USAI, S., and KLEES, R., "SAR interferometry on a very long time scale: a study of the interferometric characteristics of man-made features," *IEEE Transactions on Geoscience and Remote Sensing*, vol. 37, 4, pp. 2118-2123, 1999.
- VAN DER HOEVEN, A., HANSEN, R. F., and AMBROSIUS, B., "Tropospheric delay estimation and analysis using GPS and SAR interferometry," *Physics and Chemistry of the Earth*, vol. 27, pp. 385-390, 2002.
- WAGNER, W., LUCKMAN, A., VIETMEIER, J., TANSEY, K., BALZTER, H., SCHMULLIUS, C., DAVIDSON, M., GAVEAU, D., GLUCK, M., LE TOAN, T., QUEGAN, S., SHVIDENKO, A., WIESMANN, A., and YU, J. J., "Large-scale mapping of boreal forest in SIBERIA using ERS tandem coherence and JERS backscatter data," *Remote Sensing of Environment*, vol. 85, pp. 125-144, 2003.
- WAY, J., RIGNOT, E. J. M., McDONALD, K. C., OREN, R., KWOK, R., BONAN, G., DOBSON, M. C., VIERECK, L. A., and ROTH, J. E., "Evaluating the type and state of Alaska taiga forests with imaging radar for use in ecosystem models," *IEEE Transactions on Geoscience and Remote Sensing*, vol. 32, 2, pp. 353-370, 1994.
- WAY, J., ZIMMERMANN, R., RIGNOT, E., McDONALD, K., and OREN, R., "Winter and spring thaw as observed with imaging radar at BOREAS," *Journal of Geophysical Research*, vol. 102, D24, pp. 29,673-29,684, 1997.

- WEGMÜLLER, U., and WERNER, C. L., "SAR interferometric signatures of forest," *IEEE Transactions on Geoscience and Remote Sensing*, vol. 33, 5, pp. 1153-1161, 1995.
- WEGMÜLLER, U., WERNER, C., and STROZZI, T., "SAR interferometric and differential interferometric processing," *Proceedings of IGARSS'98*, Seattle, 6-10 July, pp. 1106-1108, 1998.
- WIESMANN, A., WEGMÜLLER, U., and STROZZI, T., "JERS SAR processing for the boreal forest mapping project SIBERIA," *Proceedings of CEOS SAR Workshop*, Toulouse, 26-29 October, pp. 19-23, 1999.
- WILLIAMS, S., BOCK, Y., and FANG, P., "Integrated satellite interferometry: Tropospheric noise, GPS estimates and implications for interferometric synthetic aperture radar products," *Journal of Geophysical Research*, vol. B12, pp. 27,051-27,069, 1998.
- ZEBKER, H. A., and GOLDSTEIN, R. M., "Topographic mapping from interferometric synthetic aperture radar observations," *Journal of Geophysical Research*, vol. 91, B5, pp. 4993-4999, 1986.
- ZEBKER, H. A., MADSEN, S. N., MARTIN, J., WHEELER, K. B., MILLER, T., LOU, Y., ALBERTI, G., VETRELLA, S., and CUCCI, A., "The TOPSAR interferometric radar topographic mapping instrument," *IEEE Transactions on Geoscience and Remote Sensing*, vol. 30, 5, pp. 933-940, 1992.
- ZEBKER, H. A., and VILLASENOR, J., "Decorrelation in interferometric radar echoes," *IEEE Transactions on Geoscience and Remote Sensing*, vol. 30, 5, pp. 950-959, 1992.
- ZEBKER, H. A., ROSEN, P. A., GOLDSTEIN, R. M., and GABRIEL, A., "On the derivation of coseismic displacement field using differential radar interferometry: the Landers earthquake," *Journal of Geophysical Research*, vol. 99, B10, pp. 19617-19634, 1994a.
- ZEBKER, H. A., WERNER, C. L., ROSEN, P. A., and HENSLEY, S., "Accuracy of topographic maps derived from ERS-1 interferometric radar," *IEEE Transactions on Geoscience and Remote Sensing*, vol. 32, 4, pp. 823-836, 1994b.
- ZEBKER, H. A., ROSEN, P. A., and HENSLEY, S., "Atmospheric effects in interferometric synthetic aperture radar surface deformation and topographic maps," *Journal of Geophysical Research*, vol. 102, B4, pp. 7547-7563, 1997.

Appendix A

This Appendix describes the derivation of the second vegetation contribution in Equation (5.12) from Equation (5.11)

If we express the volume decorrelation term in the Eulerian form of a complex number, $Ae^{j\varphi}$, we obtain:

$$\text{Amplitude of } \frac{\alpha}{\alpha - j\omega} \quad \rightarrow \quad A = \frac{1}{\sqrt{1 + \left(\frac{\omega}{\alpha}\right)^2}} \quad (\text{A.1})$$

$$\text{Phase of } \frac{\alpha}{\alpha - j\omega} \quad \rightarrow \quad \varphi = \arctan\left(\frac{\omega}{\alpha}\right) \quad (\text{A.2})$$

The vegetation contribution to the total coherence becomes:

$$\Gamma_{veg} = \eta\gamma_{veg} \frac{\sigma_{veg}^o}{\sigma_{for}^o} \left[\frac{1}{\sqrt{1 + \left(\frac{\omega}{\alpha}\right)^2}} e^{j \cdot \arctan\left(\frac{\omega}{\alpha}\right)} \left(e^{-j\omega h} - e^{-ah} \right) \right] \quad (\text{A.3})$$

which can be rewritten as follows:

$$\Gamma_{veg} = k \cdot e^{-j\left(\omega h - \arctan\left(\frac{\omega}{\alpha}\right)\right)} - k \cdot e^{-ah} \cdot e^{j \cdot \arctan\left(\frac{\omega}{\alpha}\right)} \quad (\text{A.4})$$

where k is a real quantity defined as:

$$k = \eta \gamma_{veg} \frac{\sigma_{veg}^o}{\sigma_{for}^o} \left(\frac{1}{\sqrt{1 + \left(\frac{\omega}{\alpha}\right)^2}} \right) \quad (A.5)$$

Expanding the arctangent in Taylor series:

$$e^{j \cdot \arctan\left(\frac{\omega}{\alpha}\right)} = e^{j \left(\frac{\omega}{\alpha} + \frac{\omega^3}{3\alpha^3} + \frac{\omega^5}{5\alpha^5} + \dots \right)} \quad (A.6)$$

we obtain:

$$\Gamma_{veg} = k \cdot e^{-j\omega(h-\alpha^{-1})} \cdot e^{j \left(\frac{\omega^3}{3\alpha^3} + \frac{\omega^5}{5\alpha^5} + \dots \right)} - k \cdot e^{-ah} \cdot e^{j \cdot \arctan\left(\frac{\omega}{\alpha}\right)} \quad (A.7)$$

If the two-way tree attenuation is strong, the second term can be neglected. Furthermore, if $\omega \ll \alpha$, Equations (A.5) and (A.7) can be finally written as:

$$k = \eta \gamma_{veg} \frac{\sigma_{veg}^o}{\sigma_{for}^o} \quad (A.8)$$

$$\Gamma_{veg} = k \cdot e^{-j\omega(h-\alpha^{-1})} \quad (A.9)$$

List of Publications

Peer-reviewed journal articles

ASKNE, J., SANTORO, M., SMITH, G., and FRANSSON, J. E. S., "Multi-temporal repeat pass SAR interferometry of boreal forests," *IEEE Transactions on Geoscience and Remote Sensing*, vol. 41, 7, pp. 1540-1550, 2003.

ERIKSSON, L. E. B., SANTORO, M., WIESMANN, A., and SCHMULLIUS, C., "Multi-temporal JERS repeat-pass coherence for growing stock volume estimation of Siberian forest," *IEEE Transactions on Geoscience and Remote Sensing*, vol. 41, 7, pp. 1561-1570, 2003.

SANTORO, M., ASKNE, J., SMITH, G., and FRANSSON, J. E. S., "Stem Volume Retrieval in Boreal Forests with ERS-1/2 Interferometry," *Remote Sensing of Environment*, vol. 81, 1, pp. 19-35, 2002.

Conference proceedings

ASKNE, J., SANTORO, M., SMITH, G., and FRANSSON, J., "L-band observations of boreal forest stem volume," *Proceedings of 23rd EARSeL Annual Symposium*, Gent, 2-5 June, in press, 2003.

ASKNE, J., SANTORO, M., SMITH, G., and FRANSSON, J. E. S., "Large area boreal forest investigations using ERS InSAR," *Proceedings of Third International Symposium on Retrieval of Bio- and Geophysical Parameters from SAR Data for Land Applications*, Sheffield, 11-14 September, pp. 39-44, 2001.

ERIKSSON, L., SANTORO, M., WIESMANN, A., and SCHMULLIUS, C., "Multi-seasonal study of the SIBERIA classification procedure," *Proceedings of ForestSAT Symposium*, Edinburgh, 5-9 August, CD-ROM, 2002.

ERIKSSON, L., WIESMANN, A., SCHMULLIUS, C., and SANTORO, M., "The potential of ALOS single polarization InSAR for estimation of growing stock volume in Boreal Forest," *Proceedings of IGARSS 2003*, Toulouse, 21-25 July, CD-ROM, 2003.

FANELLI, A., FERRI, M., SANTORO, M., and VITALE, A., "Analysis of coherence images over urban areas in the extraction of buildings heights," *Proceedings of IEEE/ISPRS joint Workshop on Remote Sensing and Data Fusion over Urban Areas*, Rome, 8-9 November, pp. 69-73, 2001.

FANELLI, A., and SANTORO, M., "Characterization of urban areas using principal component analysis from multitemporal ERS coherence imagery," *Proceedings of SPIE 9th International Symposium on Remote Sensing*, Agia Pelagia, Crete, 22-27 September, pp. 224-232, 2002.

FANELLI, A., SANTORO, M., FERRI, M., and ASKNE, J., "Principal Component Approach to Urban Areas Using ERS Coherence," *Proceedings of Second Symposium Remote Sensing of Urban Areas*, Regensburg, 22-23 June, CD-ROM, 2001.

FANELLI, A., SANTORO, M., VITALE, A., MURINO, P., and ASKNE, J., "Understanding ERS coherence over urban areas," *Proceedings of ERS-Envisat Symposium*, Gothenburg, 16-20 October, CD-ROM, 2000.

LUO, X., ASKNE, J., SMITH, G., SANTORO, M., and FRANSSON, J. E. S., "An analysis of INSAR coherence of boreal forests based on electromagnetic scattering modeling," *Proceedings of ERS-Envisat Symposium*, Gothenburg, 16-20 October, CD-ROM, 2000.

SANTORO, M., ASKNE, J., DAMMERT, P. B. G., FRANSSON, J. E. S., and SMITH, G., "Retrieval of biomass in boreal forest from multi-temporal ERS-1/2 interferometry," *Proceedings of 'Fringe 99' Second International Workshop on ERS SAR Interferometry*, Liège, 10-12 November, CD-ROM, 1999.

SANTORO, M., ASKNE, J., ERIKSSON, L., SCHMULLIUS, C., WIESMANN, A., and FRANSSON, J. E. S., "Seasonal dynamics and stem volume retrieval in boreal forests using JERS-1 backscatter," *Proceedings of SPIE 9th International Symposium on Remote Sensing*, Agia Pelagia, Crete, 22-27 September, pp. 231-242, 2002.

SANTORO, M., ASKNE, J., SMITH, G., DAMMERT, P. B. G., and FRANSSON, J. E. S., "Boreal forest monitoring with ERS coherence," *Proceedings of ERS-Envisat Symposium*, Gothenburg, 16-20 October, CD-ROM, 2000.

SANTORO, M., ERIKSSON, L., SCHMULLIUS, C., and WIESMANN, A., "Seasonal and topographic effects on growing stock volume estimates from JERS-1 backscatter in Siberian forests," *Proceedings of 23rd EARSeL Annual Symposium*, Gent, 2-5 June, in press, 2003.

SANTORO, M., FANELLI, A., ASKNE, J., and MURINO, P., "Urban areas classification with SAR and InSAR signatures," *Proceedings of EUSAR2000, Third European Conference on Synthetic Aperture Radar*, Munich, 23-25 May, pp. 647-650, 2000.

SANTORO, M., FANELLI, A., ASKNE, J., and MURINO, P., "Monitoring urban areas by means of coherence levels," *Proceedings of 'Fringe 99' Second International Workshop on ERS SAR Interferometry*, Liège, 10-12 November, CD-ROM, 1999.

SANTORO, M., SCHMULLIUS, C., ERIKSSON, L., and HESE, S., "The SIBERIA and SIBERIA-II projects: an overview," *Proceedings of SPIE 9th International Symposium on Remote Sensing*, Agia Pelagia, Crete, 22-27 September, pp. 247-256, 2002.

SMITH, G., DAMMERT, P. B. G., SANTORO, M., FRANSSON, J. E. S., WEGMÜLLER, U., and ASKNE, J., "Biomass retrieval in boreal forest using ERS and JERS SAR," *Proceedings of Second International Workshop on Retrieval of Bio- and Geophysical Parameters from SAR data for Land Applications*, ESTEC Noordwijk, 21-23 October, pp. 293-300, 1998.

Thesis and reports

ASKNE, J., WEGMÜLLER, U., SMITH, G., SANTORO, M., and DAMMERT, P., "JERS-1 interferometry of boreal forest," in *JERS-1 Science Program '99 PI Reports*, Shimada, M., Ed.: EORC, National Space Development Agency of Japan, pp. 144-148, 1999.

SANTORO, M., "Estimation of Biophysical Parameters in Boreal Forests from ERS and JERS SAR Interferometry," Department of Geoinformatics, Friedrich-Schiller-University, Jena, Germany, Ph.D. thesis, 2003.

SANTORO, M., "Analysis of Forests Using Atmosphere-corrected ERS InSAR Phase Imagery," Department of Radio and Space Science, Chalmers University of Technology, Göteborg, Sweden, Research Report 187, 2001.

SANTORO, M., "Characterisation of Boreal Forests and Urban Areas Using ERS InSAR Coherence," Department of Radio and Space Science, Chalmers University of Technology, Göteborg, Sweden, Technical Report 394L, 2001.

SANTORO, M., "Spaceborne SAR interferometry: Analysis of coherence over forested areas," Department of Radio and Space Science, Chalmers University of Technology, Gothenburg, Sweden, Internal Report RSG 1998:1, 1998.

Selbständigkeitserklärung

Ich erkläre, dass ich die vorliegende Arbeit selbstständig und unter Verwendung der angegebenen Hilfsmittel, persönlichen Mitteilungen und Quellen angefertigt habe.

Ort, Datum

Unterschrift des Verfassers/der Verfasserin

Tabellarischer Lebenslauf

Name	Santoro, Maurizio
Geburtsdatum	15. Juli 1972
Geburtsort	Neapel, Italien
Bürgerschaft	Deutsche und italienische
Familienstand	Ledig

Januar 2002 – heute	Wissenschaftlicher Mitarbeiter Friedrich-Schiller-Universität Jena, Institut für Geographie, Lehrstuhl für Geoinformatik, Geohydrologie und Modellierung, Abteilung Fernerkundung
7. Juni 2001	„Licentiate of Engineering“ Chalmers University of Technology, Department of Radio and Space Science, Göteborg, Schweden
April 1999 – Dezember 2001	Wissenschaftlicher Mitarbeiter Chalmers University of Technology, Department of Radio and Space Science, Göteborg, Schweden
März 1999	Staatsexamen zum Ingenieurberuf Neapel, Italien
27. Oktober 1998	Hochschulabschluss Dipl. Ing. („summa cum laude“)
Oktober 1990 – Oktober 1998	Diplom Ingenieur- Studium der Flugzeug- und Raumfahrttechnik Universität ”Federico II” Neapel, Italien
Juli 1990	Abitur
September 1985 – Juli 1990	Gymnasium Liceo Classico ”Q. O. Flacco”, Portici, Italien
Jena, 28. April 2003	
Maurizio Santoro	